

**DEVELOPMENT AND EVALUATION OF NIOBIUM  
AND MOLYBDENUM SUBSTITUTED MAGNETITE  
CATALYSTS FOR FENTON-LIKE TREATMENT  
OF RECALCITRANT WASTEWATERS**

**SHIMA RAHIM POURAN**

**THESIS SUBMITTED IN FULFILLMENT  
OF THE REQUIREMENTS FOR THE DEGREE OF  
DOCTOR OF PHILOSOPHY**

**FACULTY OF ENGINEERING  
UNIVERSITY OF MALAYA  
KUALA LUMPUR**

**2016**

**UNIVERSITI MALAYA**  
**ORIGINAL LITERARY WORK DECLARATION**

**Name of Candidate:** Shima Rahim Pouran

**Registration/Matric No:** KHA120010

**Name of Degree:** DOCTOR OF PHILOSOPHY

**Title of Project Paper/Research Report/Dissertation/Thesis ("this Work"):**

DEVELOPMENT AND EVALUATION OF NIOBIUM AND MOLYBDENUM  
SUBSTITUTED MAGNETITE CATALYSTS FOR FENTON-LIKE TREATMENT  
OF RECALCITRANT WASTEWATERS

**Field of Study:** Environmental Engineering

**I do solemnly and sincerely declare that:**

- (1) I am the sole author/writer of this Work;
- (2) This Work is original;
- (3) Any use of any work in which copyright exists was done by way of fair dealing and for permitted purposes and any excerpt or extract from, or reference to or reproduction of any copyright work has been disclosed expressly and sufficiently and the title of the Work and its authorship have been acknowledged in this Work;
- (4) I do not have any actual knowledge nor ought I reasonably to know that the making of this work constitutes an infringement of any copyright work;
- (5) I hereby assign all and every rights in the copyright to this Work to the University of Malaya ("UM"), who henceforth shall be owner of the copyright in this Work and that any reproduction or use in any form or by any means whatsoever is prohibited without the written consent of UM having been first had and obtained;
- (6) I am fully aware that if in the course of making this Work I have infringed any copyright whether intentionally or otherwise, I may be subject to legal action or any other action as may be determined by UM.

**Candidate's Signature**

**Date:** May 2016

**Subscribed and solemnly declared before,**

**Witness's Signature**

**Date:** May 2016

## ABSTRACT

Iron oxides are conventionally used as heterogeneous Fenton catalysts because of their abundance, ease of separation, affordability, and applicability in broad pH range. This is especially reported for magnetite due to the presence of  $\text{Fe}^{2+}$  cations in its structure. However, the magnetite-catalyzed Fenton reaction has lower reaction rate compared with the homogeneous reaction, which led to the introduction of transition metal-substituted magnetites. Previous studies focused mainly on the fourth series transition metals of the periodic table, and there have not been any comprehensive study on the effects of the transition metals from period five on the structure and activity of magnetite in Fenton process. Therefore, the present study synthesized a series of single, and co-doped niobium and/or molybdenum substituted magnetites by co-precipitation method prior to characterization. The amount of Nb and Mo incorporated in the samples were:  $\text{Fe}_{3-x}\text{Nb}_x\text{O}_4$  ( $x = 0.022, 0.049, 0.099, \text{ and } 0.19$ ),  $\text{Fe}_{3-x}\text{Mo}_x\text{O}_4$  ( $x = 0.028, 0.069, 0.13, \text{ and } 0.21$ ) and  $\text{Fe}_{3-x-y}\text{Nb}_x\text{Mo}_y\text{O}_4$  ( $x = 0.025, 0.049, 0.099, 0.149, \text{ and } 0.171$ ;  $y = 0.094, 0.089, 0.073, 0.032, \text{ and } 0.023$ ). All samples maintained the inverse spinel structure and magnetic property. The imported  $\text{Nb}^{4+}$  and  $\text{Mo}^{4+}$  mainly replaced the octahedral  $\text{Fe}^{3+}$  and  $\text{Fe}^{2+}$  cations, respectively. Higher Nb and Mo content decreased the crystal size significantly with concomitant increase in specific surface area, resulting in higher adsorption capacity of the catalysts. Subsequently, the activity of the synthesized samples was tested through the Fenton-like reaction for degradation of a model wastewater (methylene blue solution, MB). The presence of transition metals significantly improved the degradation of MB, especially with higher Nb and Mo contents in which, complete MB removal was achieved within 180 min. This could be attributed to a combination of factors: (i) increased adsorption capacity of the samples evidenced by larger surface area; (ii) participation of thermodynamically favorable  $\text{Nb}^{4+}/\text{Nb}^{5+}$  and  $\text{Mo}^{4+}/\text{Mo}^{6+}$  redox pairs

in regeneration of  $\text{Fe}^{2+}$  and  $\cdot\text{OH}$  radical generation, (iii) presence of oxygen vacancies serves as active sites on the surface of the catalysts, and (iv) direct involvement of peroxo-niobium complexes in MB degradation. Three catalysts,  $\text{Fe}_{2.79}\text{Nb}_{0.19}\text{O}_4$ ,  $\text{Fe}_{2.79}\text{Mo}_{0.13}\text{O}_4$  and  $\text{Fe}_{2.79}\text{Nb}_{0.171}\text{Mo}_{0.023}\text{O}_4$ , with the highest activity in the Fenton reaction were chosen, and used for treatment of MB and methyl orange (MO) solutions through the Fenton-like, UV/Fenton-like and US/Fenton-like reactions. The incorporated Nb and Mo significantly accelerated MB degradation in the US/Fenton followed by the UV-B/Fenton and UV-A/Fenton reactions. However, UV-B/Fenton reaction was more effective in degrading MO compared to the other oxidation systems. Furthermore, MB adsorption on the surface of the samples was well described by pseudo-second-order model kinetics. In addition, MB oxidation through the Fenton reaction catalyzed by the  $\text{Fe}_{3-x}\text{Nb}_x\text{O}_4$ ,  $\text{Fe}_{3-x}\text{Mo}_x\text{O}_4$ , and  $\text{Fe}_{3-x-y}\text{Nb}_x\text{Mo}_y\text{O}_4$  samples was well described by the pseudo-first-order, zero-order, and pseudo-first-order kinetics, respectively. The amount of leached iron and incorporated transition metals were not significant in acidic condition and undetectable in neutral and basic solutions. The samples retained their catalytic efficiency after three recycles in Fenton process. The results proved that niobium and molybdenum substituted magnetites enhanced the Fenton oxidation of organic pollutants. Therefore this highlights the promising potentials for treating recalcitrant effluents.

## ABSTRAK

Oksida besi lazimnya digunakan sebagai mangkin heterogen Fenton kerana kelimpahan, kemudahan pemisahan, kos yang berpatutan dan pengaplikasiannya di dalam julat pH yang luas. Ini yang terutamanya dilaporkan bagi magnetit kerana kehadiran kation  $\text{Fe}^{2+}$  di dalam strukturnya. Walaubagaimanapun, tindakbalas Fenton termangkin magnetit mempunyai kadar tindakbalas yang lebih rendah berbanding tindakbalas homogen, yang membawa kepada pengenalan logam peralihan terganti magnetit. Kajian terdahulu kebanyakannya memfokuskan kepada kajian logam peralihan bagi siri keempat di dalam jadual berkala, dan didapati tiada sebarang kajian yang komprehensif terhadap kesan logam peralihan daripada siri lima bagi struktur dan aktiviti magnetit di dalam proses Fenton. Maka, kajian ini mensistesis siri tunggal, dan Nb terdop bersama dan/atau Mo terganti magnetit melalui kaedah pemendakan bersama sebelum pencirian dijalankan. Jumlah Nb dan Mo yang digabungkan di dalam sampel adalah:  $\text{Fe}_{3-x}\text{Nb}_x\text{O}_4$  ( $x = 0.022, 0.049, 0.099, \text{ dan } 0.19$ ),  $\text{Fe}_{3-x}\text{Mo}_x\text{O}_4$  ( $x = 0.028, 0.069, 0.13, \text{ dan } 0.21$ ) dan  $\text{Fe}_{3-x-y}\text{Nb}_x\text{Mo}_y\text{O}_4$  ( $x = 0.025, 0.049, 0.099, 0.149, \text{ dan } 0.171$ ;  $y = 0.094, 0.089, 0.073, 0.032, \text{ dan } 0.023$ ). Semua sampel mengekalkan struktur spinel songsang dan sifat magnetik.  $\text{Nb}^{4+}$  dan  $\text{Mo}^{4+}$  masing-masing kebanyakannya menggantikan kation oktahedral  $\text{Fe}^{3+}$  and  $\text{Fe}^{2+}$ . Kandungan Nb dan Mo yang tinggi mengurangkan saiz hablur dengan ketara, seiring dengan peningkatan luas permukaan tertentu, menyebabkan peningkatan dalam keupayaan penjerapan mangkin. Seterusnya, aktiviti sampel yang disintesis telah diuji melalui tindakbalas serupa-Fenton bagi penguraian model airsisia (larutan methyl biru, MB). Kehadiran logam peralihan menambahbaik penguraian MB dengan ketara, terutama dengan kandungan Nb dan Mo yang tinggi, di mana penyingkiran MB yang lengkap telah diperolehi dalam masa 180 minit. Ini mungkin disebabkan oleh gabungan beberapa faktor iaitu: (i) peningkatan keupayaan penjerapan sampel yang dibuktikan oleh luas permukaan yang lebih besar; (ii) penglibatan ciri termodinamik yang baik bagi

gabungan pasangan redoks  $\text{Nb}^{4+}/\text{Nb}^{5+}$  dan  $\text{Mo}^{4+}/\text{Mo}^{6+}$  dalam penjanaan semula  $\text{Fe}^{2+}$  dan penjanaan radikal  $\cdot\text{OH}$ .; (iii) kehadiran kekosongan oksigen berfungsi sebagai ruang aktif pada permukaan mangkin; dan (iv) penglibatan langsung peroxo-niobium complexes dalam penguraian MB. Tiga mangkin, iaitu  $\text{Fe}_{2.79}\text{Nb}_{0.19}\text{O}_4$ ,  $\text{Fe}_{2.79}\text{Mo}_{0.13}\text{O}_4$  dan  $\text{Fe}_{2.79}\text{Nb}_{0.171}\text{Mo}_{0.023}\text{O}_4$ , dengan aktiviti yang paling tinggi di dalam tindak balas Fenton telah dipilih, dan digunakan sebagai rawatan bagi MB dan larutan methyl orange (MO) melalui tindakbalas serupa-Fenton, UV/serupa-Fenton dan US/serupa-Fenton. Gabungan Nb dan Mo mempercepatkan penguraian MB dengan ketara di dalam US/Fenton, diikuti tindakbalas UV-B/Fenton dan UV-A/Fenton. Walaubagaimanapun, tindakbalas UV-B/Fenton lebih berkesan dalam penguraian MO, berbanding sistem pengoksidaan yang lain. Selain itu, penyerapan MB pada permukaan sampel telah dinyatakan melalui model kinetik pseudo peringkat kedua. Tambahan, pengoksidaan MB melalui tindakbalas Fenton yang dimungkinkan oleh sampel  $\text{Fe}_{3-x}\text{Nb}_x\text{O}_4$ ,  $\text{Fe}_{3-x}\text{Mo}_x\text{O}_4$  dan  $\text{Fe}_{3-x-y}\text{Nb}_x\text{Mo}_y\text{O}_4$  masing-masing telah dinyatakan melalui model kinetik pseudo peringkat pertama, peringkat sifar dan pseudo peringkat pertama. Jumlah besi terlarutresap dan gabungan logam-logam peralihan adalah tidak ketara di dalam keadaan berasid dan tidak dapat dikesan di dalam larutan asas dan neutral. Kesemua sampel mengekalkan kecekapan pemangkin selepas tiga kitaran semula di dalam proses Fenton. Hasil kajian membuktikan bahawa Ni dan Mo terganti magnetit meningkatkan pengoksidaan Fenton bagi pencemar organik. Maka, ini menonjolkan potensi yang memberangsangkan bagi merawat efluen degil.

*To my beloved family, Abolfazl and Pouya, for their Love, Patience, Understanding and  
Constant support*

*To my loving Mom and the memory of my beloved Dad*

University of Malaya

## ACKNOWLEDGEMENTS

First and foremost, praises and thanks to the God, the Almighty, for His showers of blessings throughout my life and research work.

I would like to express my sincere appreciation to my supervisors Prof. Dr. Abdul Aziz Abdul Raman and Prof. Dr. Wan Mohd Ashri Wan Daud for their support, patience, motivation, constructive criticism and sharing of knowledge. I am grateful for the time they have taken to actively participate in this work.

I am grateful to University of Malaya for the financial support from the High Impact Research Grant (HIR).

My thanks go to all the staff members and laboratory technicians in the Chemical Engineering Department, for extending their help whenever needed.

My sincere gratitude goes to my colleagues especially Dr. Mohammad Saleh Shafeeyan for all the day-to-day support they have provided.

Lastly, many thanks are extended to my beloved brothers and sisters for their never-ending love, support, and encouragement throughout my study overseas.



## TABLE OF CONTENTS

TITLE PAGE.....	i
ORIGINAL LITERARY WORK DECLARATION FORM .....	ii
ABSTRACT .....	iii
ABSTRAK .....	v
ACKNOWLEDGEMENTS .....	viii
TABLE OF CONTENTS .....	ix
LIST OF FIGURES.....	xiv
LIST OF TABLES .....	xviii
LIST OF SYMBOLS AND ABBREVIATIONS .....	xx
<b>CHAPTER 1 INTRODUCTION .....</b>	<b>1</b>
1.1 Background .....	1
1.2 Problem statement .....	4
1.3 Aim.....	5
1.4 Research objectives .....	5
1.5 Scope .....	6
1.6 Thesis organization .....	7
<b>CHAPTER 2 LITERATURE REVIEW .....</b>	<b>10</b>
2.1 Introduction to Advanced Oxidation Processes (AOPs) .....	10
2.2 Effects of the main Fenton treatment conditions .....	18
2.2.1 Contaminant type .....	18
2.2.2 Fenton reagents .....	19
2.2.3 PH of the reaction medium.....	23

2.2.4	Temperature of the reaction medium .....	25
2.2.5	Other factors .....	26
2.3	Homogeneous vs. Heterogeneous Fenton systems .....	32
2.4	Iron minerals as heterogeneous catalysts .....	35
2.4.1	Magnetite (Fe <sub>3</sub> O <sub>4</sub> ) .....	40
2.5	Transition metal substituted iron oxides .....	42
2.5.1	Valence and occupied sites .....	47
2.5.2	Physico-chemical changes.....	49
2.5.3	Adsorption capacity.....	52
2.5.4	Catalytic activity .....	55
2.6	Summary of literature review.....	63
<b>CHAPTER 3 MATERIALS AND METHODS .....</b>		<b>66</b>
3.1	Introduction .....	66
3.2	Materials.....	66
3.3	The application of response surface methodology to optimize the magnetite catalyzed Fenton reaction for treatment of methylene blue aqueous solution .....	66
3.3.1	Experimental design and method of analysis.....	66
3.4	Preparation of magnetite samples .....	69
3.5	Characterization of the samples .....	71
3.5.1	Crystalline phase determination with X-ray diffraction (XRD).....	71
3.5.2	Surface area (Brunauer–Emmett–Teller (BET)) and particle size analyzer.....	72

3.5.3	Transmission electron microscopy (TEM).....	72
3.5.4	Surface characteristics determination (XPS).....	72
3.5.5	Vibrating sample magnetometer (VSM).....	72
3.5.6	PH of Point of zero charge (pHpzc).....	73
3.6	Adsorption experiments .....	73
3.7	Heterogeneous Fenton reactions .....	74
3.8	Stability experiments.....	76
3.9	Kinetic studies .....	76
3.9.1	Kinetic experiments of MB adsorption on the synthesized samples.....	76
3.9.2	Degradation kinetic experiments.....	76
3.9.3	Kinetic models.....	77
3.10	Safety.....	79
<b>CHAPTER 4 RESULTS AND DISCUSSION.....</b>		<b>80</b>
4.1	Introduction .....	80
4.2	Application of RSM to optimize the magnetite catalyzed Fenton reaction for treatment of methylene blue aqueous solution.....	80
4.2.1	ANOVA analysis.....	80
4.2.2	Evaluation of the effects of independent variables on the responses .....	86
4.2.3	Fenton process optimization.....	88
4.3	Niobium Substituted Magnetite ( $\text{Fe}_{3-x}\text{Nb}_x\text{O}_4$ ).....	89
4.3.1	Characterization of $\text{Fe}_{3-x}\text{Nb}_x\text{O}_4$ samples.....	90
4.3.2	Methylene blue adsorption by $\text{Fe}_{3-x}\text{Nb}_x\text{O}_4$ .....	101

4.3.3	Methylene blue degradation by $\text{Fe}_{3-x}\text{Nb}_x\text{O}_4$ .....	104
4.4	Molybdenum Substituted Magnetite ( $\text{Fe}_{3-x}\text{Mo}_x\text{O}_4$ ).....	107
4.4.1	Characterization of $\text{Fe}_{3-x}\text{Mo}_x\text{O}_4$ samples.....	108
4.4.2	Methylene blue adsorption by $\text{Fe}_{3-x}\text{Mo}_x\text{O}_4$ .....	117
4.4.3	Methylene blue degradation and mineralization by $\text{Fe}_{3-x}\text{Mo}_x\text{O}_4$ samples.....	118
4.5	Niobium and Molybdenum co-doped Magnetite ( $\text{Fe}_{3-x-y}\text{Nb}_x\text{Mo}_y\text{O}_4$ ) .....	121
4.5.1	Characterization of $\text{Fe}_{3-x-y}\text{Nb}_x\text{Mo}_y\text{O}_4$ samples .....	122
4.5.2	Adsorption capacity of $\text{Fe}_{3-x-y}\text{Nb}_x\text{Mo}_y\text{O}_4$ samples .....	134
4.5.3	Fenton catalytic activity of $\text{Fe}_{3-x-y}\text{Nb}_x\text{Mo}_y\text{O}_4$ samples.....	138
4.6	Possible explanation for enhanced activities of modified samples in Fenton reaction.....	141
4.7	Fenton oxidation of methyl orange solution .....	146
4.8	Energetically enhanced Fenton activity of the samples .....	148
4.8.1	UV/Fenton catalytic activity of $\text{Fe}_{3-x-y}\text{Nb}_x\text{Mo}_y\text{O}_4$ samples.....	148
4.8.2	US/Fenton catalytic activity of $\text{Fe}_{3-x-y}\text{Nb}_x\text{Mo}_y\text{O}_4$ samples.....	153
4.8.3	Mineralization efficiency of samples in UV/Fenton and US/Fenton reactions.....	155
4.9	Stability of the samples .....	157
4.10	Kinetic studies .....	159
4.10.1	Adsorption kinetics .....	159
4.10.2	Degradation kinetics.....	162

4.11	Single metal vs. co-doped substitutions .....	167
<b>CHAPTER 5 CONCLUSION AND RECOMMANDATIONS .....</b>		<b>169</b>
REFERENCES .....		175
LIST OF APPENDIXES .....		195
Appendix A: LIST OF PUBLICATIONS AND PAPERS PRESENTED.....		195
Appendix B: The response surface plot of the (1) decolorization, (2) COD and (3) TOC removal efficiencies (%).....		205
Appendix C: Hysteresis loops for $\text{Fe}_{3-x}\text{Nb}_x\text{Mo}_y\text{O}_4$ samples.....		214

University of Malaya

## LIST OF FIGURES

Figure 2.1: Literature review content and problem identification process .....	10
Figure 2.2: Oxidation of organic compound by peroxy group on the surface of Nb-iron oxide treated by H <sub>2</sub> O <sub>2</sub> .....	55
Figure 2.3: Proposed mechanism for the participation of Cr in Fenton reaction .....	56
Figure 3.1: Equipment setup and appearance for preparation of modified magnetite samples .....	70
Figure 4.1: XRD patterns for Fe <sub>3-x</sub> Nb <sub>x</sub> O <sub>4</sub> samples	91
Figure 4.2: TEM images of Fe <sub>3-x</sub> Nb <sub>x</sub> O <sub>4</sub> (a) x=0, (b) x=0.049, (c) x=0.099, (d) x=0.19 and particle size distribution in (e) x=0 and (f) x=0.099 samples .....	93
Figure 4.3: Hysteresis loops for (a) magnetite (b) Fe <sub>2.79</sub> Nb <sub>0.19</sub> O <sub>4</sub> .....	95
Figure 4.4: XPS spectra of Fe <sub>3-x</sub> Nb <sub>x</sub> O <sub>4</sub> samples (x = 0 – 0.19) .....	96
Figure 4.5: Deconvolution of the (a) Fe 2p doublet and (b) O 1s of Fe <sub>2.79</sub> Nb <sub>0.19</sub> O <sub>4</sub> sample .....	99
Figure 4.6: XPS spectra for (a) Fe 2p and (b) Nb 3d region for the Fe <sub>3-x</sub> Nb <sub>x</sub> O <sub>4</sub> samples (x = 0 – 0.19). ((a) The arrows show satellite peaks; (b) the binding energies of Nb <sub>2</sub> O <sub>5</sub> and NbO <sub>2</sub> , indicated by vertical lines). .....	100
Figure 4.7: Adsorption of methylene blue on Fe <sub>3-x</sub> Nb <sub>x</sub> O <sub>4</sub> samples (x=0.0-0.2; [MB] 12.5-100 mg/L; Catalyst 1 g/L; pH 7) .....	102
Figure 4.8: The pH of the point of zero charge of Fe <sub>2.79</sub> Nb <sub>0.19</sub> O <sub>4</sub> sample .....	103
Figure 4.9: The effect of pH on MB adsorption on Fe <sub>2.79</sub> Nb <sub>0.19</sub> O <sub>4</sub> sample (1g L <sup>-1</sup> ) .....	103
Figure 4.10: Methylene blue removal through adsorption and Fenton reaction catalyzed by Fe <sub>3-x</sub> Nb <sub>x</sub> O <sub>4</sub> samples ([H <sub>2</sub> O <sub>2</sub> ] 0.2 mol L <sup>-1</sup> ; catalyst 1g L <sup>-1</sup> ; pH 7) .....	104
Figure 4.11: Effect of pH on methylene blue removal through adsorption and Fenton-like reaction catalyzed by Fe <sub>2.79</sub> Nb <sub>0.19</sub> O <sub>4</sub> .....	106

Figure 4.12: Degradation and mineralization of MB solution through Fenton-like reaction using $\text{Fe}_{3-x}\text{Nb}_x\text{O}_4$ catalyst at pH values of 7 and 10 .....	107
Figure 4.13: XRD patterns for $\text{Fe}_{3-x}\text{Mo}_x\text{O}_4$ magnetite samples .....	109
Figure 4.14: TEM images of $\text{Fe}_{3-x}\text{Mo}_x\text{O}_4$ samples (a) A, (b) B, (c) C and (d) D.....	111
Figure 4.15: XPS spectra of $\text{Fe}_{3-x}\text{Mo}_x\text{O}_4$ samples.....	112
Figure 4.16: XPS spectra for Fe 2p region for the $\text{Fe}_{3-x}\text{Mo}_x\text{O}_4$ samples.....	113
Figure 4.17: Deconvolution of the (a) Fe 2p doublet and (b) Mo 3d of $\text{Fe}_{2.62}\text{Mo}_{0.21}\text{O}_4$ sample.....	114
Figure 4.18: Hysteresis loops for (a) magnetite (b) $\text{Fe}_{2.62}\text{Mo}_{0.21}\text{O}_4$ samples.....	116
Figure 4. 19: Effect of pH on the MB adsorption on $\text{Fe}_{3-x-y}\text{Nb}_x\text{Mo}_y\text{O}_4$ samples.....	118
Figure 4. 20: The pH of the point of zero charge of $\text{Fe}_{2.62}\text{Mo}_{0.21}\text{O}_4$ sample .....	118
Figure 4.21: MB removal through adsorption and Fenton oxidation by $\text{Fe}_{3-x}\text{Mo}_x\text{O}_4$ samples.....	119
Figure 4.22: Degradation and mineralization of MB solution through Fenton-like reaction using $\text{Fe}_{3-x}\text{Mo}_x\text{O}_4$ catalysts at pH values of 7 and 10.....	120
Figure 4. 23: TEM image of $\text{Fe}_{3-x-y}\text{Nb}_x\text{Mo}_y\text{O}_4$ sample ( $x = 0.1, y = 0.15$ ); the arrows show $\text{MoO}_3$ orthorhombic phase.....	123
Figure 4.24: XRD patterns of $\text{Fe}_{3-x-y}\text{Nb}_x\text{Mo}_y\text{O}_4$ samples .....	125
Figure 4.25: TEM images of (a) $\text{Fe}_3\text{O}_4$ (b) $\text{Fe}_{2.79}\text{Nb}_{0.0249}\text{Mo}_{0.094}\text{O}_4$ , (c) $\text{Fe}_{2.79}\text{Nb}_{0.049}\text{Mo}_{0.089}\text{O}_4$ , (d) $\text{Fe}_{2.79}\text{Nb}_{0.099}\text{Mo}_{0.073}\text{O}_4$ , (e) $\text{Fe}_{2.79}\text{Nb}_{0.149}\text{Mo}_{0.032}\text{O}_4$ and (f) $\text{Fe}_{2.79}\text{Nb}_{0.171}\text{Mo}_{0.023}\text{O}_4$ samples .....	126
Figure 4.26: XPS spectra of $\text{Fe}_{3-x-y}\text{Nb}_x\text{Mo}_y\text{O}_4$ samples.....	129
Figure 4.27: XPS spectra for Fe 2p of $\text{Fe}_{3-x-y}\text{Nb}_x\text{Mo}_y\text{O}_4$ samples (The arrows show satellite peaks).....	130
Figure 4.28: Deconvolution of the (a) Fe 2p doublet and (b) O 1s of $\text{Fe}_{2.79}\text{Nb}_{0.099}\text{Mo}_{0.073}\text{O}_4$ sample .....	131

Figure 4.29: XPS spectra for (a) Nb 3d and (b) Mo 3d for the $\text{Fe}_{2.79}\text{Nb}_{0.099}\text{Mo}_{0.073}\text{O}_4$ sample.....	133
Figure 4.30: Effect of stirring time on adsorption of MB on samples at $100 \text{ mg L}^{-1}$ (catalyst $1 \text{ g L}^{-1}$ , pH 7, time 120 min).....	135
Figure 4.31: The pH of the point of zero charge of (a) $\text{Fe}_3\text{O}_4$ and (b) $\text{Fe}_{2.79}\text{Nb}_{0.171}\text{Mo}_{0.023}\text{O}_4$ .....	136
Figure 4.32: Effect of pH on adsorption of MB on $\text{Fe}_{3-x-y}\text{Nb}_x\text{Mo}_y\text{O}_4$ samples .....	137
Figure 4.33: Effect of MB initial concentration on adsorption capacity of $\text{Fe}_{3-x-y}\text{Nb}_x\text{Mo}_y\text{O}_4$ samples .....	137
Figure 4.34: Fenton oxidation efficiency of the synthesized samples for (a) $50 \text{ mg L}^{-1}$ and (b) $100 \text{ mg L}^{-1}$ .....	139
Figure 4.35: Effect of MB initial concentration on decolorization efficiency (%) using $\text{Fe}_{3-x-y}\text{Nb}_x\text{Mo}_y\text{O}_4$ samples.....	140
Figure 4.36: The amount of MB removal through adsorption and Fenton oxidation by $\text{Fe}_{3-x-y}\text{Nb}_x\text{Mo}_y\text{O}_4$ samples .....	140
Figure 4.37: Degradation and mineralization of MB solution through Fenton-like reaction using $\text{Fe}_{3-x-y}\text{Nb}_x\text{Mo}_y\text{O}_4$ samples at pH values of 7 and 10 .....	141
Figure 4.38: Radical mechanism for activation of $\text{H}_2\text{O}_2$ by surface cations (proposed by (Magalhães et al., 2007)).....	143
Figure 4.39: Overall action of Nb and Mo in modified magnetite samples in Fenton oxidation of MB .....	145
Figure 4.40: Effect of pH on adsorption and Fenton oxidation efficiency of MO using the synthesized samples at pH 7 (a) and (b) and pH 3 (c) and (d).....	147
Figure 4.41: Fenton oxidation efficiency of the samples for MO .....	148
Figure 4.42: Comparison between (i) dark-Fenton, (ii) UV/ Fenton with $1 \text{ g L}^{-1}$ and (iii) $0.5 \text{ g L}^{-1}$ of the samples for (a) MB and (b) MO ( $365 \text{ nm}$ ; $t=150 \text{ min}$ ) .....	150



Figure 4.43: Effects of UV light intensity on oxidation efficiency of the samples for (a) MB and (b) MO ((i) dark-Fenton, (ii) UV-A and (iii) UV-B/Fenton, [dye] 50 mg L <sup>-1</sup> , [Cat] 0.5 g L <sup>-1</sup> ; [H <sub>2</sub> O <sub>2</sub> ] 0.2 mol L <sup>-1</sup> , UV 365/302 nm; t=120 min) ...	152
Figure 4.44: US/Fenton oxidation efficiency of the samples for (a) MB and (b) MO ([dye] 50 mg L <sup>-1</sup> , [Cat] 0.5 g L <sup>-1</sup> ; [H <sub>2</sub> O <sub>2</sub> ] 0.2 mol L <sup>-1</sup> ) .....	155
Figure 4.45: Mineralization (%) of (a) MB and (b) MO in UV-A/Fenton and US/Fenton reactions .....	157
Figure 4.46: Reuse of Fe <sub>2.79</sub> Nb <sub>0.171</sub> Mo <sub>0.023</sub> O <sub>4</sub> sample .....	158
Figure 4.47: Pseudo-Second-order kinetics for adsorption of MB (100 mg L <sup>-1</sup> ) onto (a) Fe <sub>2.79</sub> Nb <sub>0.0249</sub> Mo <sub>0.094</sub> O <sub>4</sub> , (b) Fe <sub>2.79</sub> Nb <sub>0.049</sub> Mo <sub>0.089</sub> O <sub>4</sub> , (c) Fe <sub>2.79</sub> Nb <sub>0.099</sub> Mo <sub>0.073</sub> O <sub>4</sub> , (d) Fe <sub>2.79</sub> Nb <sub>0.149</sub> Mo <sub>0.032</sub> O <sub>4</sub> and (e) Fe <sub>2.79</sub> Nb <sub>0.171</sub> Mo <sub>0.023</sub> O <sub>4</sub> samples .....	162
Figure 4.48: Pseudo-first order kinetic for MB degradation through heterogeneous Fenton reaction catalyzed by Fe <sub>2.79</sub> Nb <sub>0.19</sub> O <sub>4</sub> samples .....	164
Figure 4.49: Zero order kinetics for MB degradation through heterogeneous Fenton reaction catalyzed by Fe <sub>3-x</sub> Mo <sub>x</sub> O <sub>4</sub> samples .....	165
Figure 4.50: Pseudo-first order kinetic for MB degradation through heterogeneous Fenton reaction catalyzed by Fe <sub>3-x-y</sub> Nb <sub>x</sub> Mo <sub>y</sub> O <sub>4</sub> samples .....	167

## LIST OF TABLES

Table 2.1 Photo-Fenton effectiveness in treatment of some organic compounds in recalcitrant effluents .....	14
Table 2.2: Heterogeneous Fenton catalysis for degradation of recalcitrant organic compounds .....	34
Table 2.3: Fenton degradation of recalcitrant organic compounds catalyzed by iron oxides .....	36
Table 2.4: Preparation method and characteristics of transition metal substituted iron oxide catalysts.....	43
Table 2.5: Oxidation of various organic pollutants through Fenton reactions catalyzed by transition metal substituted iron oxide .....	60
Table 3.1: Independent numerical variables and their levels.....	67
Table 4.1: Experimental design matrix and the outputs.....	81
Table 4.2: Final quadratic models for both categorical factors.....	83
Table 4. 3: Analysis of variance (ANOVA) results for responses .....	85
Table 4.4: Predicted and experimental values of the studied responses at optimum conditions for both the magnetite samples .....	89
Table 4.5: Formula and the amount of oxygen vacancies for the $Fe_{3-x}Nb_xO_4$ samples ..	90
Table 4.6: Surface area, pore size/volume and particle sizes of $Fe_{3-x}Nb_xO_4$ samples.....	92
Table 4.7: Magnetic properties of the synthesized samples.....	95
Table 4.8: The elemental composition and their chemical states on the surface of $Fe_{3-x}Nb_xO_4$ samples .....	97
Table 4.9: Formula and the amount of oxygen vacancies for $Fe_{3-x}Mo_xO_4$ samples.....	108
Table 4.10: Surface area, pore size/volume and particle sizes of $Fe_{3-x}Mo_xO_4$ samples	110
Table 4.11: The elemental composition and their chemical states on the surface of $Fe_{3-x}Mo_xO_4$ samples .....	113

Table 4.12: Magnetic characteristics of $\text{Fe}_{3-x}\text{Mo}_x\text{O}_4$ samples .....	116
Table 4.13: Chemical formula, surface area, pore size/volume and particle size of $\text{Fe}_{3-x-y}\text{Nb}_x\text{Mo}_y\text{O}_4$ samples .....	123
Table 4.14: Magnetic characteristics of $\text{Fe}_{3-x-y}\text{Nb}_x\text{Mo}_y\text{O}_4$ samples.....	127
Table 4.15: Weight (%) of surface Fe cations.....	130
Table 4.16: The calculated parameters of the pseudo-first and pseudo-second order kinetic models with associated $R^2$ and <i>Err</i> (%) for the MB adsorption onto synthesized catalysts at various MB concentrations .....	161
Table 4.17: The calculated parameters of the zero and pseudo-first order kinetic models with associated $R^2$ for Fenton oxidation of MB catalyzed by $\text{Fe}_{2.79}\text{Nb}_{0.19}\text{O}_4$ samples .....	164
Table 4.18: The calculated parameters of the zero and pseudo-first order kinetic models with associated $R^2$ for Fenton oxidation of MB catalyzed by $\text{Fe}_{3-x}\text{Mo}_x\text{O}_4$ samples .....	165
Table 4.19: The calculated parameters of the zero and pseudo-first order kinetic models with associated $R^2$ for Fenton oxidation of MB catalyzed by $\text{Fe}_{3-x-y}\text{Nb}_x\text{Mo}_y\text{O}_4$ samples .....	166

## LIST OF SYMBOLS AND ABBREVIATIONS

<b>Symbols</b>	<b>Description</b>
$b_0$	Constant coefficient
$C$	Total concentration in the bulk phase, $\text{mg L}^{-1}$
$C_0$	Initial concentration, $\text{mg L}^{-1}$
$E_0$	Oxidation potential, V
$\epsilon$	Ecoustic field
€	European Currency Unit, Euro
$e^- - h^+$	Electron-hole pairs
$Err$	Normalized standard deviation, %
$H_{ci}$	Coercivity, G
$k$	kinetic rate constant
$K$	Linear driving force rate coefficient
$K_s$	Pseudo-second-order kinetic rate constant
$m$	Mass, g
$M$	Molecular weight
$Mr$	Remnant magnetism
$Ms$	Saturation magnetism, emu
$q$	Adsorbed concentration
$\bar{q}$	Average adsorbed phase concentration in the micropore
$\bar{q}$	Average concentration in adsorbent particle
$q_e$	Adsorbed concentration in equilibrium with the fluid phase
$q_t$	Adsorbed concentration at time
$\Delta q$	Maximum loading capacity
$R^2$	Regression coefficient
$t$	Time
$V$	Volume, L
$x$	Mole fraction
$y$	Mole fraction
$\lambda$	Wavelength
$\eta$	Effectiveness, %

$\sigma^2$  Residual mean square

### Abbreviations

AC	Aromatic Content
AMKC	Acid Modified Kaolin Clay
AMX	Amoxicillin
ANOVA	Analysis of variance
AO8	Acid Orange 8
AOPs	Advanced Oxidation Processes
AR17	Acid red 17
AS	Activated sludge
AV*	Anion vacancy
BA	Benzoic acid
BET	Brunauer-Emmett-Teller
BOD	Biochemical oxygen demand
BOD <sub>5</sub> /COD	Biodegradability ratio
BPA	2,2-bis-(4-hydroxyphenyl)propane
BTEX	Benzene, toluene, ethylbenzene and Xylene
CA	Chelating agents
CCD	Central composite design
CIP	Ciprofloxacin
CMCD	Carboxymethyl $\beta$ -cyclodextrin
COD	Chemical oxygen demand
DCAA	Dichloroacetic acid
DO	Dissolved Oxygen
DOC	Dissolved organic carbon
DOM	Dissolved organic matter
DZP	Diazepam
EC	Electrocoagulation
EDCs	Endocrine disrupting compounds
EDDS	Ethylenediamine- <i>N,N'</i> -disuccinic acid
EDTA	Ethylenediaminetetraacetic acid
EEC	Electrical energy cost
Fe-Cit	Iron citrate

Fe-Ox	Ferrioxalate
GA	Gallic acid
IAF	Induced air flotation
ICP	Inductively coupled plasma
LCM	Liomycin
MB	Methylene blue
MBR	Membrane bioreactor
MO	Methyl orange
MTX	Mitoxantrone
MV	Methyl Violet
NaDCF	Diclofenac sodium salt
NaMCF	Meclofenamic acid sodium salt
NTA	Nitrilotriacetic acid
NXA	Nalidixic acid
•OH	Hydroxyl radical
Ox	Oxalate
PAM	Polyacrylamide
PCP	Pentachlorophenol
p-CA	p-coumaric acid
ph-F	Photo-Fenton
PREs	Petroleum refinery effluents
PZC	Point of zero charge
RhB	Rhodamine B
SBBGR	Sequencing batch biofilter granular reactor
SBR	Sequencing batch reactor
SDZ	Sulfadiazine
SMX	Sulfamethoxazole
SphF	Solar photo-Fenton
SSA	Surface area per unit mass
SQR	Squareness
SS	Sum of Squares
STZ	sulfathiazole
TBBPA	Tetrabromobis-phenol A
TCP	Trichlorophenol

TDS	Total dissolved solids
TEM	Transmission electron microscopy
TMSIO	Transition metal substituted iron oxide
TMSM	Transition metal substituted magnetite
TNT	Trinitrotoluene
TOC	Total organic carbon
US	Ultrasound
UV-Vis	Ultra violet-visible light
vs.	Versus
VSM	Vibrating sample magnetometer
WWTP	Wastewater treatment plant
XPS	X-ray photoelectron spectroscopy
XRD	X-ray diffraction
2-CP	2-chlorophenol
3-D	3 dimensional

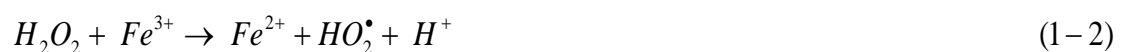
### **Subscript**

<i>adj</i>	Adjusted
<i>cal</i>	Calculated
<i>exp</i>	Experimental
<i>mas</i>	Measured values
<i>max</i>	maximum
<i>mod</i>	Model predicted
<i>pred</i>	predicted
<i>surf</i>	surface

## CHAPTER 1: INTRODUCTION

### 1.1. Background

Water pollution abatement and treatment of wastewaters carrying recalcitrant contaminants has been a major issue for decades. Recalcitrant compounds pose high resistance to microbiological degradation and may not be degraded readily by biological treatment methods (Alexander, 1975). A large number of pharmaceutical and agrochemical compounds are recalcitrant. Discharge of these recalcitrant compounds to the environment even in small quantities may eventually lead to accumulation in ecosystem (Knapp & Bromley-Challoner, 2003). Synthetic dyes are chemically stable organic pollutants that are difficult to be treated using conventional treatment technologies. This contributed to the contaminating water bodies with hundreds of organic dyes that are generally non-biodegradable (Dantas et al., 2006). To prevent their adverse effects, the attempt should encompass minimization of recalcitrant wastewaters from industries as well as improvement in treatment technologies such as Advanced Oxidation Processes (AOPs). Fenton process is a strong advanced oxidation process that has been successfully used for removal of recalcitrant organic contaminants. This process is the reaction between hydrogen peroxide as an oxidant and iron ions as catalyst to produce highly active species, mainly non-selective  $\cdot\text{OH}$  radicals with oxidation potential of 2.8 V, as shown in Eqs. 1-1 and 1-2 (Pignatello et al., 2006):

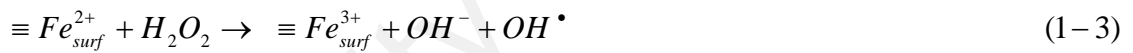




This process offers several advantages over the conventional methods such as simple equipment, high removal efficiency within a short reaction time and complete oxidation and mineralization of pollutants to innocuous byproducts under suitable operating conditions. The Fenton process initiated by heterogeneous  $\text{Fe}^{2+}$  or  $\text{Fe}^{3+}$  compounds or other metals at low oxidation states such as  $\text{Cu}^{2+}$  and  $\text{Co}^{2+}$  is called Fenton-like reaction (Nichela et al., 2013). Fenton-like reaction is of slower rate compared to Fenton reaction ( $42\text{-}79 \text{ L mol}^{-1}\text{S}^{-1}$  vs.  $0.01\text{-}0.002 \text{ L mol}^{-1}\text{S}^{-1}$ ).

Homogeneous Fenton reaction using ferrous or ferric salts as iron source gives rise to rapid oxidation of probe molecules at considerably higher rate, due to unbound transfer of reactants in the reaction medium. The optimum pH value of 3 is accepted for homogeneous Fenton process in which the quantum yield of  $\cdot\text{OH}$  radical generation at this pH is the most (Benkelberg & Warneck, 1995). At higher pH values than optimal value and/or at high concentrations of  $\text{H}_2\text{O}_2$  ( $> 1\%$ ), other non-hydroxyl radicals are also formed. These radicals are less active in oxidation of contaminants when compared to  $\cdot\text{OH}$  radical (Pignatello et al., 2006; Watts & Teel, 2006). Combination of Fenton reaction with external energy sources such as ultraviolet (UV) or ultrasound (US) has attracted great attention. In combined systems, the  $\cdot\text{OH}$  yield is higher than dark Fenton process or the utilized concentrations of Fenton reagents is low (Bagal & Gogate, 2014). On the other hand, there are number of drawbacks that accompanied homogeneous Fenton reaction. These limitations are (i) pH-dependence of the system (2.5-4.0) (Katsumata et al., 2005); (ii) formation of ferric hydroxide sludge at pH values above 4.0, that leads to the decrease of catalyst in the solution (Diya'uddeen et al., 2015), decline in radiation transmission in photo-Fenton process (Faust & Hoigne, 1990; Tamimi et al., 2008) and sludge removal issue; (iii) difficulty in catalyst recovery (Pariante et al., 2008) and (iv) the cost associated with acidification and subsequent neutralization that may limit the use of homogeneous Fenton process at industrial scale.

Therefore, the use of heterogeneous catalysts has been put into perspectives by many researchers as a possible solution to overcome the shortcomings of homogeneous catalysis. In heterogeneous catalysts, iron is stabilized within the interlayer space of the catalyst's structure and can effectively produce hydroxyl radicals from oxidation of hydrogen peroxide. This will enable pollutant mineralization under non-controlled pH condition and for contaminated sites with pH adjustment limitations and without iron hydroxide precipitation (Arora et al., 2010; Garrido-Ramírez et al., 2010; Usman et al., 2012b). The intrinsic convenience of iron minerals such as natural prevalence, simple magnetic separation and low cost, make them valuable candidates for heterogeneous Fenton treatment of recalcitrant wastewaters. Iron oxides can operate at neutral pH without generation of ferric sludge and can be recovered and reused in Fenton reaction (Eq. 1-3):



Amongst iron minerals, magnetite,  $Fe^{II}O \cdot Fe^{III}_2O_3$ , has gained considerable interest in heterogeneous Fenton system due to its structural  $Fe^{2+}$  cations that are important for initiating Fenton reaction. The  $Fe^{2+}$  cations occupy octahedral sites in which the catalytic activity of magnetite is chiefly attributed to the octahedral cations exposed on the surface of catalyst (Ramankutty & Sugunan, 2001b). The efficiency of magnetite catalyzed Fenton process for contaminants removal is less compared to soluble iron ions, because just a small fraction of iron cations are on the surface of catalyst (Xavier et al., 2013). Therefore, several studies put in practice to improve its activity through chemical modifications (Shijian Yang et al., 2009; Zhong et al., 2013). One type of modification is to substitute the iron species of magnetite with other active transition metals. Ever since the concept of transition metal substituted magnetite (TMSM) and

the changes in its physico-chemical properties was studied in 1950s (Bouet et al., 1992; Francombe, 1957; Robbins et al., 1971), their application in Fenton oxidation of recalcitrant organic compounds was frequently reported in the last decade (Costa et al., 2003). This group of catalysts has attracted growing concern due to the stability of the active cations in magnetite structure and relatively simple and inexpensive production method. Therefore, they have the potential to be used for environmental remediation especially treatment of industrial wastewaters through Fenton reaction. Based on the literature reviewed, most of the previous studies on TMSM have dealt with the transition metals of the fourth series of the periodic table (Costa et al., 2006; Liang et al., 2012a; Magalhães et al., 2007; Moura et al., 2005; Nguyen et al., 2011). However, there have not been any comprehensive studies to assess the effects of substituting transition metals from period five on the properties and activity of magnetite in Fenton oxidation process. Additionally, though magnetite samples naturally enclose more than two metals in their structure, the effects of two or more transition metals substitution have rarely reported in literature (Liang et al., 2012b).

## **1.2. Problem statement**

Although, heterogeneous catalysts could solve the pH and reusability limitations of iron ions in homogeneous Fenton system, but their efficiency for contaminants degrading through Fenton reaction is low. Modification in the number of heterogeneous catalysts such as the incorporation of other transition metals into the magnetite, towards high performances in Fenton reaction has been a subject of the recent research. Consequently, several studies is required to develop new transition metal substituted magnetite samples with stable structure and relatively high activity in Fenton reaction compared to pure magnetite while maintaining its magnetic property. In light of this and

considering that the studies on transition metals from period five and for more than one metal substitution are limited, the aim of the present study is defined as follows:

### **1.3. Aim**

The aim of this work is to develop high efficient Fe-based heterogeneous catalysts for enhanced Fenton treatment of recalcitrant contaminants.

### **1.4. Research objectives**

The present work intends to develop a series of heterogeneous catalysts through modification in magnetite structure. The main objective is to achieve higher adsorption capacity and enhanced activity in Fenton treatment of recalcitrant wastewaters. Hence, the objectives of this study are to:

1. Identify, synthesis and characterize a series of heterogeneous catalysts based on niobium and/or molybdenum substituted magnetite, which include:
  - Determining the changes in structure, physico-chemical properties and adsorption capacity of the magnetite.
2. Evaluate the activity of the synthesized catalysts for oxidation of methylene blue through:
  - Heterogeneous Fenton reaction,
  - UV/Fenton-like and US/Fenton-like reactions
3. Evaluate the activity of the selected synthesized catalysts for oxidation of methyl orange through:
  - Heterogeneous Fenton reaction,
  - UV/Fenton-like and US/Fenton-like reactions
4. Determine the degradation kinetics of methylene blue through:
  - Heterogeneous Fenton reaction
  - UV/Fenton-like and US/Fenton-like reactions.

## 1.5. Scope

The scopes of the present project are as below:

1. Two transition metals from the fifth series of the periodic table will be selected based on their similarities in ionic radius and crystal structure to iron species; thus, they can theoretically replaced iron in the magnetite structure.
2. In order to evaluate the effects of small substitutions on magnetite structure and activity, the maximum molar fraction of  $x=0.2$  ( $\text{Fe}_{3-x}\text{M}_x\text{O}_4$ ) will be used for imported transition metal. This is also to prevent the leaching possibility of the incorporated metals to reaction medium or in a bigger scale, to receiving environment.
3. Methylene blue is selected as a probe molecule to evaluate the activity of the synthesized samples through Fenton-like reaction, due to its recalcitrant nature and its application in the similar studies, thus inter-comparisons can be done.
4. Methyl orange is selected to assess the activity of the selected catalysts for degradation of an anionic dye from azo compounds. Therefore, the activity of the samples will be evaluated for two different dyes with different adsorption characteristics.
5. In addition to classic Fenton reaction, the activity of the selected catalysts will be assessed under the influence of UV and US irradiation combined with Fenton reaction.
6. The stability of the synthesized samples will be examined in terms of the amount of leached structural transition metals into the reaction medium. The samples are considered as stable if the amount of leached metal is below 5% of its initial quantity in the structure of the sample.

## **1.6. Thesis organization**

This thesis consists of five chapters dealing with different aspects related to the topic and objectives of the research.

### **CHAPTER 1: INTRODUCTION**

This chapter briefly introduces Fenton oxidation process and the limitations encountered with homogeneous Fenton catalysis. It also gives a concise introduction on a group of heterogeneous catalysts to overcome these limitations. Research problem statement, aim, objectives and scope of the study are also presented.

### **CHAPTER 2: LITERATURE REVIEW**

This chapter presents a review on the Fenton reaction, its application for treatment of recalcitrant wastewaters, exclusively or combined with external energy sources, and the effects of the various treatment conditions on Fenton oxidation efficiency. Subsequently, a review on the synthesized transition metal substituted magnetite (TMSM) catalysts, their properties and applications for degradation of organic pollutants are presented. The valence and occupied sites, changes in physico-chemical properties, adsorption capacity and catalytic activity are discussed in detail in this chapter. Finally, a summary of the reviewed literature is given at the end of this chapter.

### **CHAPTER 3: MATERIALS AND METHODS**

This chapter explains all the experimental and analytical procedures for the synthesis, characterization, and Fenton activity of Nb and/or Mo substituted magnetite samples. Details on raw materials, equipment, and other related procedures are also presented.

## CHAPTER 4: RESULTS AND DISCUSSION

This chapter presents results and data obtained from the laboratory experiments. In this chapter, the results are presented in three parts:

### 4.1. Optimization of the Fenton reaction using Response Surface Methodology

The first part of this chapter investigates the application of response surface methodology in optimizing the magnetite catalyzed Fenton-like oxidation of MB solution. The effects of the main operating parameters, i.e. the concentrations of  $H_2O_2$  and catalyst, reaction pH and time are assessed and optimized to achieve the highest color, COD, and TOC removal efficiencies of MB solution.

### 4.2. Niobium and/or Molybdenum substituted magnetite catalysts: Characteristics and activity

The main characteristics of the  $Fe_{3-x}Nb_xO_4$ ,  $Fe_{3-x}Mo_xO_4$  and  $Fe_{3-x-y}Nb_xMo_yO_4$  samples in terms of crystal structure, surface area, particle size, surface elements, and magnetic property are discussed in Part 2. The results regarding the adsorption capacity and Fenton activity of the synthesized samples for oxidation of MB solution are also presented in this part and the best catalysts with highest activity is accordingly introduced.

### 4.3. Stability evaluation

This part gives data and discussion regarding the stability, durability or reusability of the samples based on the amount of leached transition metals in various pH conditions and under the influence of UV and US irradiations.

#### 4.4. Kinetics studies

The last part of this chapter provides data and discussion on the kinetics of the MB adsorption and degradation through Fenton-like, UV/Fenton and US/Fenton reactions using selected synthesized catalysts.

### CHAPTER 5: CONCLUSION AND RECOMMENDATIONS

This chapter provides a conclusion of the results and findings in this research and subsequently, recommendations are given for possible future research in this area.

University of Malaya



## CHAPTER 2: LITERATURE REVIEW

The relationship between the topics discussed in the literature review, to identify the research problems/gap is summarized in the following diagram.

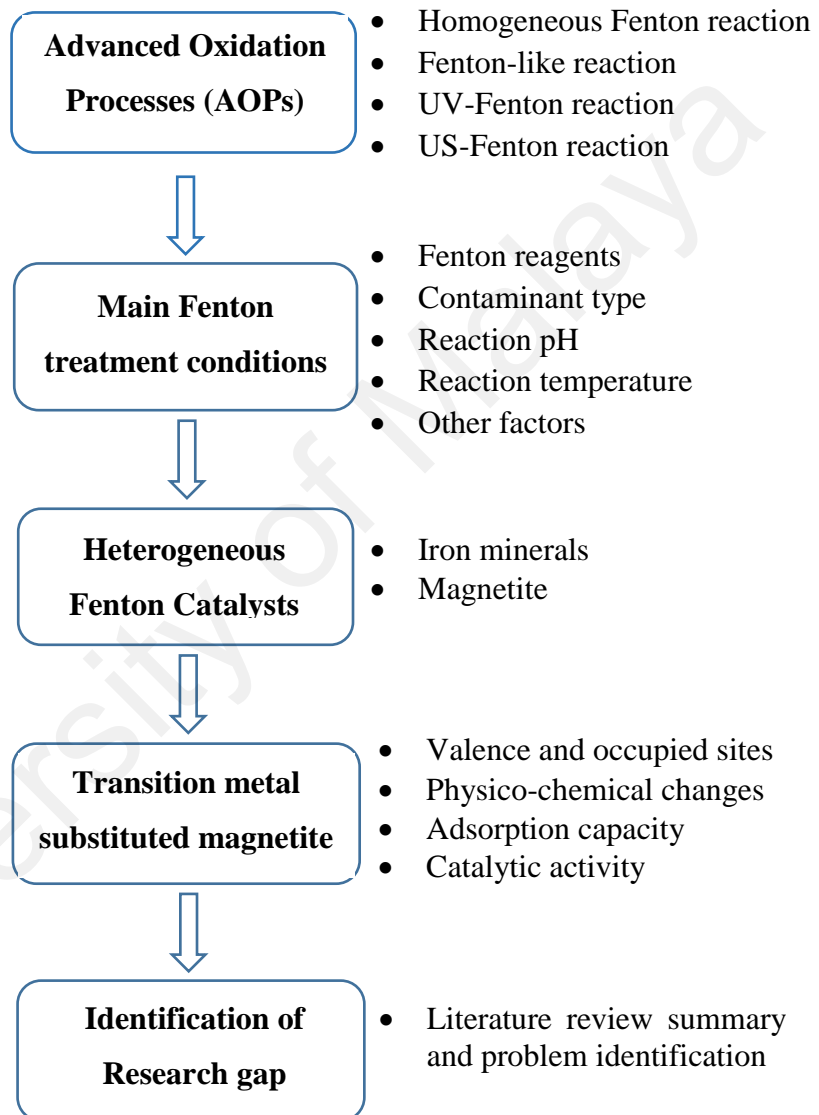


Figure 2.1: Literature review content and problem identification process

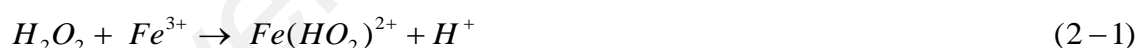
### 2.1. Introduction to Advanced Oxidation Processes (AOPs)

The rapid global economic growth has resulted in clean water crisis and environmental pollution since the industrial revolution. Literature indicates an increasing trend in

generation of wastewaters with recalcitrant characteristics from the many activities of industrial societies (Shukla et al., 2010). In most industries, conventional treatment technologies cannot produce effluents that meet water quality criteria and effluent limitation guidelines for recalcitrant pollutants. Traditional treatment techniques only succeed in contaminants transfer from liquid phase to solid phase (Nitoi et al., 2013; Shukla et al., 2010). Advanced oxidation processes (AOPs) are powerful methods for degradation of pollutants, due to their ability for removing almost any organic contaminant (Comninellis et al., 2008; Klavarioti et al., 2009; Klemenčič et al., 2012 ; Nichela et al., 2013; Nitoi et al., 2013; Wang & Xu, 2011). Glaze et al. (1987) defined AOPs as water treatment processes at near ambient temperature and pressure that produce very active radicals for degradation of pollutants. AOPs generally refer to a group of processes that cover  $O_3$  and  $H_2O_2$  as oxidants with assistance of light, catalyst (e.g.  $Fe^{2+}$ ,  $Fe^{3+}$  and  $TiO_2$ ), ultrasonic insertion and/or thermal input (Gogate & Pandit, 2004). There are several combinations such as Fenton ( $H_2O_2/Fe^{+2}$ ), UV/Fenton ( $H_2O_2/UV/Fe^{+2}$ ), sono/Fenton, peroxidation combined with UV light ( $H_2O_2/UV$ ), peroxone ( $O_3/H_2O_2$ ), peroxone combined with UV light ( $O_3/H_2O_2/UV$ ),  $O_3/UV$  system,  $O_3/TiO_2/H_2O_2$  and  $O_3/TiO_2$ /Electron beam irradiation (Babuponnusami & Muthukumar, 2012; Bobu et al., 2012; Klavarioti et al., 2009; Zhou & Smith, 2002). These oxidation processes are cost-effective technologies and give rise to non-selective active species that oxidize a wide variety of non-biodegradable compounds. Fenton chemistry comprehensively explained in previously published reviews (Malato et al., 2009; Neyens & Baeyens, 2003; Pignatello et al., 2006) and the main equations were presented in introduction section. The existence of  $\cdot OH$  radicals in Fenton reaction was proven using spin-trapping experiments (Jiang et al., 1993). However, possibility of other mechanisms apart from free radical has also proposed because of captured

complexes between iron and H<sub>2</sub>O<sub>2</sub> in Fenton reaction medium using optical absorption measurements (Kremer & Stein, 1959).

Sonolysis is another example of AOPs in which sonochemical degradation of probe molecules occurs due to the released energy from the growth and collapse of cavitation microbubbles (Gong & Hart, 1998). This energy is reported as a possible reason for generation of highly active radicals such as  $\cdot\text{OH}$ ,  $\cdot\text{O}_2\text{H}$  and  $\text{H}\cdot$  in aqueous solutions containing H<sub>2</sub>O<sub>2</sub> (Bagal & Gogate, 2014). On this basis, this technology has been introduced as a mean for degradation of environmental pollutants. However, the degradation efficiency of this method is low when applied alone (Bremner et al., 2008). Therefore, ultrasound (US) combined with other techniques has been established as a tool to increase its efficiency. Several studies have reported US combined Fenton reaction (US/Fenton) for treatment of various range of pollutants (Bagal & Gogate, 2014). In this combination, the generated ferric ion from Fenton reaction (Eq. 1-1) can react with H<sub>2</sub>O<sub>2</sub> and give rise to  $\text{Fe}(\text{HO}_2)^{2+}$  complex that in turn regenerates ferrous ions under acoustic field ( $\epsilon$ ) (Eqs. 2-1 and 2-2):



UV/Fenton reaction is a combination of Fenton reagents and UV-Vis light that brings about additional  $\cdot\text{OH}$  radicals via (i) photo-reduction of ferric ions to ferrous ions ( $\lambda < 580 \text{ nm}$ ) and (ii) hydrogen peroxide photolysis at shorter wavelengths ( $\lambda < 310 \text{ nm}$ ) as shown in Eqs. 2-3 and 2-4 (Pignatello et al., 2006):



The photo-generated ferrous ions enter Fenton reaction to produce supplemental hydroxyl radicals. Consequently, UV/Fenton has higher oxidation rate compared with Fenton process (Ortega-Liébana et al., 2012). In addition to higher oxidation rate, there is a sizable drop in total iron utilization and sludge generation in UV/Fenton compared to Fenton reaction (Hermosilla et al., 2009). Furthermore, UV/Fenton using both solar or UV light, has significant effects on inactivating microorganisms in polluted water-bodies for sustainable reuse for drinking and/or irrigation purpose. However, the efficacy of the process greatly depends on the microorganism present and the type of water under treatment (García-Fernández et al., 2012; Karaolia et al., 2014; Ortega-Gómez et al., 2013; Polo-López et al., 2012). Several studies have been conducted to examine the effectiveness of UV/Fenton for degradation of various recalcitrant compounds. Table 2.1 provides an overview of the recalcitrant compounds degraded by photo-Fenton process and the mineralization efficiency of these chemical pollutants under studied optimum conditions.

Table 2.1 Photo-Fenton effectiveness in treatment of some organic compounds in recalcitrant effluents

Compound	Initial value (mg L <sup>-1</sup> )	Operational condition					Optimal performance	References
		[H <sub>2</sub> O <sub>2</sub> ] (mg L <sup>-1</sup> )	Iron (mg L <sup>-1</sup> )	pH -	[Ox] (mg L <sup>-1</sup> )	T (°C)		
<i>Pharmaceuticals</i>								
Pharmaceutical wastewater	TOC <sub>0</sub> : 125	5250	55	3.0	325	32	84% TOC removal within 115 min at H <sub>2</sub> C <sub>2</sub> O <sub>4</sub> :Fe <sup>III</sup> ratio of 3;	(Monteagudo et al., 2013)
Penicillin G	200	680	55	3.5	-	-	83.3% Pen-G degradation within 30 min,	(Gogate & Pandit, 2004)
Amoxicillin Ampicillin Cloxacillin	104 105 103	H <sub>2</sub> O <sub>2</sub> / COD 1.5	5.2 5.25 5.15	3.0	-	-	Complete degradation within 2 min; COD and DOC removal of 80.8% & 58.4% at 50 min,	(Elmolla & Chaudhuri, 2009)
Amoxicillin Cloxacillin	138 84	H <sub>2</sub> O <sub>2</sub> /COD 2.5	6.9 4.2	3.0	-	-	Complete degradation within 1 min; 89% COD removal & complete nitrification with combined photo-Fenton-SBR	(Elmolla & Chaudhuri, 2011)
lincomycin(LCM) diazepam (DZP)	25 25	170	11.17	-	-	-	DOC removal of 65% for LCM and 80% for DZP within 60 min irradiation.	(Bautitz & Nogueira, 2010)
hospital wastewater		COD:H <sub>2</sub> O <sub>2</sub> :Fe <sup>II</sup> 1:4:0.1		3.0	-	-	Increasing BOD <sub>5</sub> /COD ratio from 0.3 to 0.52 and oxidation degree from -1.14 to +1.58	(Elmolla & Chaudhuri, 2011)
Amoxicillin	50	120	2.8	2.5- 2.8	-	-	73-81% TOC removal after 240 min, AMX removal after 5-15 min using Fe-Ox and FeSO <sub>4</sub> respectively	(Trovo' et al., 2011)
Nalidixic acid	45	300	20	2.6- 2.8	-	-	15% DOC and 100 % NXA removal after 210 min.	(Carla Sirtori et al., 2011)
dichlorodiphenylamine (DCDPA), Diclofenac sodium salt (NaDCF), meclofenamic acid sodium salt (NaMCF),	each 5	10	10	3.5	-	-	99% DCF and MCF and 96% DCDPA degradation within 120 min; rate constant order of k <sub>DCDPA</sub> < k <sub>DCF</sub> < k <sub>MCF</sub> ;	(Miró et al., 2013)

(continued on next page)

'Table 2.1, continued'

Compound	Initial value (mg L <sup>-1</sup> )	Operational condition					Optimal performance	References
		[H <sub>2</sub> O <sub>2</sub> ] (mg L <sup>-1</sup> )	Iron (mg L <sup>-1</sup> )	pH	[Ox] (mg L <sup>-1</sup> )	T (°C)		
<i>Pharmaceuticals</i>								
Sulfamethoxazole [SMX]	200	>300	10	2.8	-	25	98% SMX removal, BOD <sub>5</sub> /COD improvement from 0.0 to 0.3, 2.4-79.9% TOC removal with H <sub>2</sub> O <sub>2</sub> doses from 50-1000 mgL <sup>-1</sup>	(González et al., 2007)
Paracetamol	157.5	200	20	-	-	-	83.33% reduction in reagent cost, 79.11% reduction in costs of reaction time (from 3.4502 \$ /m <sup>3</sup> to 0.7392 \$ /m <sup>3</sup> ).	(Jordá et al., 2011)
sulfadiazine(SDZ) sulfathiazole(STZ)	25 25	170	-	2.5	17.6	-	complete degradation after 8 min irradiation, 92% and 90% mineralization of SDZ and STZ after 42 min of irradiation	(Batista & Nogueira, 2012)
Mitoxantrone (MTX)	31.11	640	30	3.0	47.5	-	60%, 77% and 82% mineralization using Fe <sup>2+</sup> , Fe <sup>3+</sup> and Fe-Ox respectively within 140 min;	(Cavalcante et al., 2013)
<i>Agrochemicals</i>								
Malathion	10	1000	25	3.0	-	-	malathion removal to desired level (0.1 mg L <sup>-1</sup> ) after 135 min,	(Yanming Zhang & Pagilla, 2010)
Diuron & Linuron	TOC <sub>0</sub> : 50	202	15.9	2.8	-	25	herbicides degradation within 60 min irradiation with UVA, 30% TOC removal by UV/Fenton alone & 87% by UV/Fenton- SBR.	(Farré et al., 2006)
Lindane (γ-HCH)	1.01	1000	125	3.0	-	-	95% and 99.91% TOC removal after 2 and 4 h of irradiation.	(Nitoi et al., 2013)
Laition, Metasystox, Sevnol & Ultracid	each 50	100	20	2.8	-	30	Up to 80% mineralization of the mixture after 45 min, 31% DOC removal with only UV/Fenton within 140 min and 90% with UV/Fenton-SBR after 7h.	(Ballesteros Martín et al., 2009)

(continued on next page)

'Table 2.1, continued'

Compound	Initial value (mg L <sup>-1</sup> )	Operational condition					Optimal performance	References
		[H <sub>2</sub> O <sub>2</sub> ] (mg L <sup>-1</sup> )	Iron (mg L <sup>-1</sup> )	pH	[Ox] (mg L <sup>-1</sup> )	T (°C)		
<i>Agrochemicals</i>								
Alachlor, atrazine, chlorfenvinphos, diuron, isoproturon, pentachlorophenol	each 50	100	20	2.8	-	-	Degradation of the all pesticides into intermediates, 90% TOC removal after <15 min.	(Monteagudo et al., 2011)
Methomyl	20	34	28	3.0	-	-	100% methomyl removal within 30 min,	(Tamimi et al., 2008)
linuron	10	13.6	2.2	4.0	-	25	Complete linuron degradation after 20 min, 90% TOC removal after 25 h with formation of chloride, nitrate and ammonium ions.	(Katsumata et al., 2005)
Abamectin	9.0	204	28	2.5	-	-	70% Abamectin degradation within 60 min, 60% mineralization after 180 min,	(de Freitas Matos et al., 2012)
metalaxyl	150	80	2.0	2.8	-	-	96.3% metalaxyl degradation after 180 min,	(A. M. T. Silva et al., 2012)
<i>Petroleum refinery</i>								
oxalates	182	1020	[Fe <sup>2+</sup> ] 280	3.9	-	-	faster degradation of formates than oxalates, <sup>1</sup> EEC <sub>TOC=15</sub> (UV-C) = 1.30 €m <sup>-3</sup> , EEC <sub>TOC=15</sub> (UV-A) = 2.37 €m <sup>-3</sup> ;	(Simunovic et al., 2011)
formates	92		[Fe <sup>3+</sup> ] 447					
Sourwater from refinery plant	-	4000	400	-	-	-	87% DOC removal with UV/Fenton within 60 min,	(Coelho et al., 2006)
diesel oil	-	1700	5.6	3.0	-	-	99% TOC removal within 30 min;	(Galvão et al., 2006)
Petroleum extraction wastewater	1.6	16500	0.93	3.0	-	-	92% and 96% polycyclic aromatic hydrocarbons and aromatic removal within 7 h sunlight exposure,	(da Rocha et al., 2013)
phenol	200	1080	5.0	3.0	10	-	98% COD removal within 120 min, 90% phenol degradation at 10 min,	(Y.-H. Huang et al., 2010)

(continued on next page)

'Table 2.1, continued'

Compound	Initial value (mg L <sup>-1</sup> )	Operational condition					Optimal performance	References
		[H <sub>2</sub> O <sub>2</sub> ] (mg L <sup>-1</sup> )	Iron (mg L <sup>-1</sup> )	pH -	[Ox] (mg L <sup>-1</sup> )	T (°C)		
<i>Pharmaceuticals</i>								
Phenol	100	> 18.2 %	AMKC <sup>2</sup> 2.23 g	5.4	-	-	99.15% phenol degradation within 5 min,	(Ayodele et al., 2012)
Xylene	15	5100	14.5	2.5- 3.0	-	-	94.5% xylene removal after 60 min, 100% TOC removal within 90 min.	(S. S. da Silva et al., 2012)
Phenol	DOC <sub>0</sub> 500	6400	22	3.0	-	-	95.1% DOC removal after 180 min under solar irradiation,	(K. R. B. Nogueira et al., 2008)
<i>p</i> -nitroaniline (PNA)	25	340.15	2.8	3.0	-	20	>98% degradation efficiencies of PNA within 30 min solar irradiation.	(J.-H. Sun et al., 2008)
protocatechuic acid (PCA), <i>p</i> -coumaric acid ( <i>p</i> -CA), gallic acid (GA),	20	400	20	4.0	60	25– 39	100% PCA removal within 4min, 100% <i>p</i> -CA degradation within 2min, 100% GA degradation (within 3min, 94% TOC removal after 194 min.	(Monteagudo et al., 2011)

EEC<sub>TOC=15</sub> : electrical energy costs required to achieve reference value of 15 mg C L<sup>-1</sup>

AMKC: acid modified kaolin clay supported ferric-oxalate catalyst



## **2.2. Effects of the main Fenton treatment conditions**

Amongst various factors that influence the Fenton oxidation effectiveness, the type and concentration of the contaminant, Fenton reagents, pH and temperature of the reaction medium are significant factors. Therefore, optimizing the reaction is very important to achieve better treatment results. In a number of studies, multivariate experimental design based on the response surface methodology, has been used to study the simultaneous effects of experimental variables on the response function (%COD or %TOC removal) instead of expensive and time-consuming classical techniques, (Monteagudo et al., 2013). Some other factors that influence degradation efficiency also reviewed at latter sections.

### **2.2.1. Contaminant type**

The contaminant concentration is one of the important factors in Fenton process. Literature studies have clearly revealed that the increase in concentration of probe molecule has negative effects on its removal efficiency. This is due to the inner filtration effect related to high concentrations of absorbing molecules (Daneshvar et al., 2008). Consequently, it needs longer irradiation time and/or further magnification in Fenton reagents to supply adequate  $\cdot\text{OH}$  radicals into the reaction (Ayodele et al., 2012). For example, the increase in Diclofenac concentration from 10 to 80 mg L<sup>-1</sup> has diminished photo-Fenton reaction rate and extended the mineralization time (Ravina et al., 2002). Similar results reported by Tamimi et al. (2008) for treatment of the agrochemical wastewater (methomyl) and by Ayodele et al. (2012) who conducted photo-Fenton for degradation of phenol using phosphoric acid modified kaolin clay supported ferric-oxalate catalyst. Generally, at low concentrations of probe molecule, the removal efficiency at neutral condition is acceptable. For instance, treating wastewaters containing 15 and 6 emerging contaminants respectively has been carried out at

unchanged pH (Klamerth et al., 2010) or with neutral solar photo-Fenton (Bernabeu et al., 2012). The degrading of 15 emerging contaminants was successful at low concentrations of pollutants and Fenton reagents. Surprisingly, in the wastewater bearing 6 emerging contaminants, the degradation completed within 60 min of irradiation because of the lower concentrations of the pollutants.

In a study by Saghafinia et al. (2011), the increase in initial concentration of Penicillin G in photo-Fenton, initially resulted in the increase in the removal percentage but a decrease in COD removal afterwards. This might be due to the higher amount of  $\text{H}_2\text{O}_2$  in reaction solution at start, which declined as the reaction continued. In another study, the increase in initial concentration of probe molecule from 100 to 250 and 500  $\text{mg L}^{-1}$  altered COD removal from 80.8% to 74.9% and 72.3%, DOC from 58.4% to 47.4% and 33.2% and  $\text{BOD}_5/\text{COD}$  ratio of 0.4 to 0.36 and 0.34 (Elmolla & Chaudhuri, 2009). From the results, the changes in COD removal and biodegradability values were insignificant even with 5 times increase in pollutant concentration due to the correct selection of the  $[\text{H}_2\text{O}_2] / [\text{pollutant}]$  ratio.

### **2.2.2. Fenton reagents**

One of the main steps in Fenton treatment is to estimate the optimum doses of hydrogen peroxide and iron due to their direct effects on the degradation efficacy and operational cost (Heng et al., 2012; Primo et al., 2008). Correspondingly, the presence of both reagents at their most desirable concentrations is essential because of the importance of  $\text{H}_2\text{O}_2$  concentration to determine quantitative degradation and iron dose for reaction kinetics (Chamarro et al., 2000). For example, phenol removal in the absence of  $\text{H}_2\text{O}_2$  was only 2.16% within 60 minutes of irradiation in the study conducted by Ayodele et al. (2012). That is because of the role of hydrogen peroxide in the generation of  $\cdot\text{OH}$  radicals (Batista & Nogueira, 2012; Deng & Englehardt, 2007; Ravina et al., 2002;

Tamimi et al., 2008). Application of solar light exclusively or with iron is also inefficient in degradation process because  $\cdot\text{OH}$  radicals or other active oxidative species are not generated in the absence of  $\text{H}_2\text{O}_2$  (Monteagudo et al., 2011; Monteagudo et al., 2010). On the other hand, addition of iron to the UV/ $\text{H}_2\text{O}_2$  system resulted in complete removal of 3-chloropyridine within 120 min while the removal efficiency was only 7% within 170 min in the absence of iron, in the study conducted by Ortega-Liébana et al. (2012). Accordingly, the stoichiometric oxidation equation of the organic pollutant with  $\text{H}_2\text{O}_2$  to carbon dioxide and water is written and the optimum molar ratio of the  $\text{H}_2\text{O}_2$  dosage to the organic compound concentration is determined. However, the amount of  $[\text{H}_2\text{O}_2]/[\text{organic compound}]$  used in previous studies has often been higher than the stoichiometric value, considering the effect of the other factors on  $\text{H}_2\text{O}_2$  consumption. For instance, the presence of  $\text{Cl}^-$  ions is responsible for higher  $\text{H}_2\text{O}_2$  intake for organic load removal (Carla Sirtori et al., 2011). In addition, chloride radicals ( $\text{Cl}\cdot$  and  $\text{Cl}_2^{\cdot-}$ ) also react with  $\text{H}_2\text{O}_2$  and increase its utilization. Zhang and Pagilla (2010) reported the increase in degradation efficiency from 40% to 73% within 75 min of irradiation when the concentration ratio of  $[\text{H}_2\text{O}_2]: [\text{malathion}]$  increased from 50:1 to 100:1. However, additional concentrations of  $\text{H}_2\text{O}_2$  decreases the removal efficiency mainly through (i) auto-decomposition of  $\text{H}_2\text{O}_2$  to water and oxygen (Eq. 2-5) that is non-productive, and (ii)  $\cdot\text{OH}$  radical scavenging by hydrogen peroxide (Andreozzi et al., 1999) that produces less reactive  $\text{HO}_2\cdot$  ions (Eq. 2-6) and at subsequent reaction with  $\cdot\text{OH}$  radicals, subverts the reaction rate (Eq. 2-7):



Similar assumptions were reported by Zhang and Pagilla (2010) for pesticide degradation, Batista and Nogueira (2012) for pharmaceutical wastewater treatment and Elmolla and Chaudhuri (2009) for degradation of the antibiotics using photo-Fenton system. In light of scavenging effect, successive addition of hydrogen peroxide promotes oxidation efficiency compared to single addition at start time (Primo et al., 2008). Kang and Hwang (2000) used the following equation (Eq. 2-8) to determine the H<sub>2</sub>O<sub>2</sub> effectiveness ( $\eta$ ) for removing COD of landfill leachate:

$$\eta(\%) = \frac{COD_{oxid}}{0.4706 \times [H_2O_2]} \times 100 \quad (2-8)$$

where, the theoretically removable COD value of hydrogen peroxide, 1000 mg/l is 470.6 mg/l, COD<sub>oxid</sub> is the COD removed by oxidation, and [H<sub>2</sub>O<sub>2</sub>] is the concentration of added peroxide. Accordingly, higher COD values require higher H<sub>2</sub>O<sub>2</sub> doses. However, it is better to choose an optimum values, in order to achieve the higher degradation with lower cost. Teixeira et al. (2005) reported that H<sub>2</sub>O<sub>2</sub> at low concentrations (10-50 mmol L<sup>-1</sup>) had negligible effect on degrading agrochemical wastewater using photo-Fenton. However, the effects significantly increased at higher concentrations of H<sub>2</sub>O<sub>2</sub> (500 mmol L<sup>-1</sup>). On the other hand, the increase in H<sub>2</sub>O<sub>2</sub> concentration from 2500 to 10000 mg L<sup>-1</sup> promoted the COD removal from 49% to 78%, while doubled dosages did not enhance COD removal considerably (Primo et al., 2008).

Similarly, the increase in iron concentration contributes to higher organic content removal and process kinetics (Monteagudo et al., 2011; Zaror et al., 2008) considering the catalytic role of iron for H<sub>2</sub>O<sub>2</sub> decomposition. Nonetheless, excess iron dosages brings about a number of difficulties such as higher TDS (Zhang & Pagilla, 2010), iron

sludge generation (Gogate & Pandit, 2004) scavenging of  $\cdot\text{OH}$  radicals (Wailling, 1975) and reduction in color removal efficiency because of possible interference of iron in color assessment (Heng et al., 2012). In a study, the rate constant of methomyl degradation using photo-Fenton increased considerably from 0.0736 to 0.175  $\text{min}^{-1}$  when the amount of  $\text{Fe}^{2+}$  increased ten times (Tamimi et al., 2008). However, at higher dosages than optimum value, degradation rate decreased. That was due to the decline in UV-irradiation intensity caused by the production of  $\text{Fe}(\text{OH})^{2+}$  in acidic medium and its strong UV- light absorption effect.

Different sources of iron are used in Fenton process for different probe compounds (Nogueira et al., 2005); therefore, degradation efficiency varied in different studies. Oliveira et al. (2007) performed preliminary tests to compare ferrous ion ( $\text{Fe}^{2+}$ ), ferric nitrate ( $\text{Fe}^{3+}$ ) and Fe-Ox in photo-Fenton treatment of alkydic resins manufacture wastewater. The resulted COD removal was 40%, 18% and 17%. Bautitz and Nogueira (2010) compared the efficiency of iron nitrate and Fe-Ox in photo-Fenton treatment of pharmaceuticals wastewater. Ferrioxalate (Fe-Ox) yielded higher degradation compared to iron nitrate in all experimental conditions. In another study, although Fe-Ox had a better performance than ferrous sulphate ( $\text{FeSO}_4$ ) for amoxicillin (AMX) degradation by photo-Fenton, the toxicity of the solution increased with Fe-Ox due to the higher toxicity of the generated intermediates (Trovo' et al., 2011). Mitoxantrone ([MTX] 0.07  $\text{mmol L}^{-1}$ ) degradation by photo-Fenton using  $\text{Fe}^{2+}$ ,  $\text{Fe}^{3+}$  or Fe-Ox (0.54  $\text{mmol L}^{-1}$ ) and  $\text{H}_2\text{O}_2$  (18.8  $\text{mmol L}^{-1}$ ) resulted in respectively 60%, 77% and 82% mineralization (Cavalcante et al., 2013). TOC removal of 69.9%, 41.1% and 5% have been reported for ciprofloxacin solution (65  $\mu\text{mol L}^{-1}$ ) within 10 minutes, using Fe-Cit, Fe-Ox and iron nitrate respectively (Perini et al., 2013). Higher performance of Fe-Cit and Fe-Ox could be contributed to their higher quantum yields for  $\text{Fe}^{2+}$  generation at pH 3.0 (Faust & Hoigne, 1990). In addition, Fe-Cit showed lower pH-dependency in relation to other

studied sources in the study. Ferrous sulfate, on the other hand, was reported for better performance in photo-Fenton than ferrous chloride (Ortega-Liébana et al., 2012), due to scavenging effect of chlorine ions. It is noteworthy that the presence of iron in wastewater itself can be advantageous to Fenton oxidation process for wastewater treatment without a new iron addition (Vilar et al., 2012).

In addition, optimum ratio of Fenton reagents, instead of their absolute dosages, has been determined in number of studies. Saghafinia et al. (2011) reported that the  $\text{H}_2\text{O}_2/\text{Fe}^{2+}$  molar ratio of 20 demonstrated higher penicillin G removal percentage (81.2%) with initial concentration of  $200 \text{ mg L}^{-1}$ , where further decrease in the ratio did not enhance the pollutant degradation. This could be from the  $\cdot\text{OH}$  radical scavenging effect of iron at higher concentrations. Elmolla and Chaudhuri (2009) achieved the similar results when they examined different molar ratios of  $\text{H}_2\text{O}_2/\text{Fe}^{2+}$  for the treatment of pharmaceutical wastewater. Primo et al. (2008) obtained the highest COD removal of 83% when they applied a  $\text{Fe}^{2+}/\text{COD}$  mass ratio of 0.33. On the other hand, bigger values decreased the degradation efficiency due to various side reactions.

### **2.2.3. PH of the reaction medium**

The main disadvantage often associated with homogeneous Fenton system is its pH dependency, in order to achieve the best degradation efficiency (Katsumata et al., 2005). This is a challenging issue especially in natural waters or highly buffered wastewaters. There is a concurrence in literature related to optimum pH being 2.8–3.5 (da Silva et al., 2007; Farrokhi et al., 2004; Módenes et al., 2012; Tamimi et al., 2008; V. Kavitha & Palanivelu, 2004). The reason is that at pH values close to 3 the generation of the species with larger light absorption co-efficient and quantum yield for  $\cdot\text{OH}$ -radical production such as  $\text{Fe}(\text{OH})^{2+}(\text{H}_2\text{O})_5$  is high (Benkelberg & Warneck, 1995; Michael et al., 2012; Zhao et al., 2004). Frontistis et al. (2011) performed photo-Fenton initially at

effluent's inherent pH of 8, but the removal efficiency was not satisfactory, pH was therefore altered to 3 in subsequent experiments. Similarly, Trovo' et al. (2011) reported negligible change in AMX initial concentration under photo-Fenton treatment at its natural pH of 6.2 after 360 min irradiation. However, the removal efficiency at pH 2.5 in the absence of light was 64% and 74% after 90 and 330 min respectively. In this study, complete AMX removal was attained after 5 and 15 minutes using Fe-Ox and FeSO<sub>4</sub>, respectively. Interestingly, Luna et al. (2012) obtained desirable results from the degradation of phenolic compounds at neutral or alkaline pH values by photo-Fenton under the influence of high concentrations of chlorine ions (60.0 g/L). This is because at pH 3, the Fe<sup>3+</sup> complexation with chloride ions stabilized the iron species in the solution. Batista and Nogueira (2012) also obtained considerable degradation of sulfonamide antibiotics at pH 6 when they used 0.20 mM Fe-Ox for stabilizing iron species as complex.

Both lower and higher pH values than optimum level affect the process performance negatively. PH values lower than 2.8 causes a considerable decline in the amount of  $\cdot\text{OH}$  radicals due to the scavenging effect of these radicals by H<sup>+</sup> ions (Tang & Huang, 1996) and formation of [Fe(H<sub>2</sub>O)]<sup>2+</sup> ion which reacts with H<sub>2</sub>O<sub>2</sub> at lower rate (Gallared et al., 1998; Shemer et al., 2006). In addition, lower pH prevents the interaction between Fe<sup>3+</sup> and H<sub>2</sub>O<sub>2</sub> (Pignatello, 1992). Another reason is H<sub>2</sub>O<sub>2</sub> stability at pH below 3 via formation of H<sub>3</sub>O<sub>2</sub><sup>+</sup> that impediments the production of  $\cdot\text{OH}$  radicals (Chen et al., 2009). It is noteworthy that in a study conducted by Maldonado et al. (2007), pH adjustment was done at latter step due to lower solubility of probe molecule in acidic solutions. In their study, although a fraction of Fe<sup>2+</sup> was precipitated initially in the form of iron hydroxide, it was stopped by H<sub>2</sub>O<sub>2</sub> addition and further pH adjustment at 3 to achieve higher mineralization efficiency. A decline in initial pH has also been observed in a number of experiments mainly due to the formation of more acidic intermediates from

probe molecule degradation (Farrokhi et al., 2004 ). Therefore, continuous pH adjustment is required in these cases.

On the contrary, higher-than-optimum pH values also disturb Fenton efficiency through (i) prevention of  $\text{H}_2\text{O}_2$  decomposition to generate  $\cdot\text{OH}$  radicals due to the deficiency of  $\text{H}^+$  ions (Wailling, 1975), (ii) accelerated decomposition of  $\text{H}_2\text{O}_2$  to water and oxygen at pH values above 5 (Meeker, 1965), (iii) decline in oxidation potential of  $\cdot\text{OH}$  radicals ( $E_0 = 2.8 - 1.95 \text{ V}$  at  $\text{pH} = 0 - 14$ ) (Kim & Vogelpohl, 1998), (iv) possible generation of more selective ferric species other than  $\cdot\text{OH}$  radicals at pH above 5 (Hug & Leupin, 2003) and (v) development of ferric oxyhydroxide ( $\text{FeOOH}$ ) at pH above 4 that reduces degradation rate (Shemer et al., 2006). At pH values above 4, iron is precipitated as ferric hydroxide (Hermosilla et al., 2009; Katsumata et al., 2005; Nitoi et al., 2013; Tamimi et al., 2008) that leads to the decline in radiation transmission in photo-Fenton process (Faust & Hoigne, 1990). However, recent studies on iron adding strategies have demonstrated that dosing iron at different steps helps to improve reaction rate at neutral pH values to the level obtained at pH 2.8 (Carra et al., 2013). Despite difficulties such as ferric sludge disposal, catalyst depletion in the sludge and negative effects on the environment that are accompanied by the ferric precipitate generation at  $\text{pH} > 4$ , the produced hydroxide was used as flocculent for further COD removal (Xing et al., 2006).

#### **2.2.4. Temperature of the reaction medium**

A large number of studies related to Fenton process carried out at room temperature (González et al., 2007; Hermosilla et al., 2009; Monteagudo et al., 2011; Primo et al., 2008). This is because of the thermal decomposition of  $\text{H}_2\text{O}_2$  at temperatures above  $50^\circ\text{C}$  (Muthukumari et al., 2009; Yip et al., 2005). In addition, due to  $\text{H}_2\text{O}_2$  decomposition acceleration at basic pH values, the increment in temperature brings about a shift in optimum pH towards acidic values (Monteagudo et al., 2011). However, based on the



Arrhenius theory of the rate constants in relation to temperature, it is expected that the increase in temperature leads to higher generation of hydroxyl radicals from the increase in concentration of produced  $\text{Fe}(\text{OH})^{2+}$  (Zapata et al., 2010). For instance, a meaningful change in phenol degradation efficiency from 87.21% to 97.46% was reported by Ayodele et al. (2012) when the temperature increased from 30 °C to 40 °C. In another study, complete mineralization of diclofenac was attained when the experiments were carried out at 50 °C (Ravina et al., 2002). However, the authors did not report any data regarding degradation efficiency at ambient temperature. Teixeira et al. (2005) reported a rapid decrease in COD at 50 °C rather than 30 °C using photo-Fenton that could be resulted from the increase in oxidation reaction rate of the organic pollutants. However, DOC degradation was insignificant at the employed temperature range. Katsumata et al. (2005) reported a slight improvement in linuron degradation efficiency within the temperature range of 10-40 °C. However, in a study conducted by Hermosilla et al. (2009) for treatment of landfill leachate, temperature range of 25-45 °C did not improve COD removal considerably. Although, experimental temperature of 40 °C has been found to be more effective in Fenton process, room temperature (20-25 °C) has often been used because it is practically applicable and able to decrease the operational cost of the system. However, photo-Fenton can be applied without a cooling step in industries generating wastewaters with a temperature ranges between 35-40 °C.

## **2.2.5. Other factors**

### **2.2.5.1. Composition of reaction medium**

Besides the main operational conditions, there are several other factors that affect the efficiency of Fenton process. Amongst them is the composition of the treated water. Inorganic ions such as carbonates, bicarbonates, chlorides, fluoride, bromide,

phosphate, and sulphate may be present in water or generated via degradation process. Some of these ions may alter oxidation rate of Fenton reaction. The extent of the change in reaction kinetic depends on the type of ion and its concentration in the solution through one or combination of the following effects: (i) formation of Fe(III) complexes and lessening of the abundance and activity of iron species, (ii) generation of by-products containing these ions that are in some cases more toxic and recalcitrant than parent compounds, (iii)  $\cdot\text{OH}$ -radical scavenging and generating of less reactive radicals than  $\cdot\text{OH}$ , (iv) reaction of generated radicals with hydrogen peroxide that decreases its availability in solution, (v) competition with organic compounds for active sites on hetero-catalysts, and (vi) effect on ferrous ion recovery (De Laat & Le, 2006; Devi et al., 2011; Klamerth et al., 2010; Luna et al., 2012; Micó et al., 2013; Ortega-Liébana et al., 2012; Sirtori et al., 2011). A comparative study was conducted by Sirtori et al. (2011) to check the effects of the different matrices on efficiency of photo-Fenton process in nalidixic acid (NXA) degradation. In this study, NXA was dissolved in demineralized water, saline water containing  $5 \text{ g L}^{-1}$  of NaCl and simulated industrial effluent. DOC removal of 86%, 73%, and 20% were reported after 92, 107, and 240 min. The difference was probably due to the high concentration of chlorine ions that interfere in the main process through formation of chloride-Fe(III) complexes;  $\cdot\text{OH}$  radical scavenging by chloride ions and generation of other species such as  $\text{ClOH}\cdot^-$ ,  $\text{Cl}\cdot$ ,  $\text{Cl}_2\cdot^-$ . These radicals are of lower oxidation potential compared to  $\cdot\text{OH}$  radicals and decrease the amount of  $\text{H}_2\text{O}_2$  and accordingly,  $\cdot\text{OH}$  generation accordingly (Eqs. 2-9 to 2-13) (De Laat & Le, 2006). However, a considerable difference in NXA degradation at those water matrices has not been observed. That was attributed to the oxidation role of chlorine ions ( $\text{Cl}\cdot$  and  $\text{Cl}_2\cdot^-$ ) with oxidation potential of  $E_0 (\text{Cl}\cdot/\text{Cl}^-) = 2.41 \text{ V}$  and  $E_0 (\text{Cl}_2\cdot^-/2\text{Cl}^-) = 2.09 \text{ V}$  (Sirtori et al., 2009).



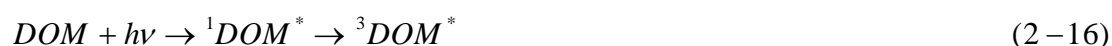
In contrast to the most reported results in literature, photo-Fenton degradation efficiency of a solution containing two pesticides, imidacloprid and methomyl, under high salinity conditions (up to 50 mS cm<sup>-1</sup>) was improved by existing chlorine ions (Micó et al., 2013). However, it dramatically decreased TOC removal efficiency mainly due to the above-mentioned reasons (i and iii). Klamerth et al. (2009) reported that mineralization efficiency of 15 emerging contaminants by photo-Fenton was dependent on the type of water and the presence of CO<sub>3</sub><sup>2-</sup> and HCO<sub>3</sub><sup>-</sup>. This is because carbonate ions fight with contaminants for  $\cdot OH$  radicals. Nonetheless, in their study, the process was independent on the pH of the solution and the initial concentration of utilized H<sub>2</sub>O<sub>2</sub>.

Ortega-Liébaná et al. (2012) examined the influence of chloride, sulphate and phosphate ions on photo-Fenton degradation efficiency of 3-chloropyridine. The effect of chlorine ions was found to be more than sulphate ions. The irradiation time for complete mineralisation of 3-chloropyridine in solutions containing chlorine and sulphate was respectively 170 and 120 min. In the case of phosphate ions, concentration of 2 mg L<sup>-1</sup> decelerated reaction rate; but at higher concentration (1 g L<sup>-1</sup>), insoluble ferric phosphate precipitation appeared within a few minutes of irradiation and prevented the reaction by catalyst removal and a decrease in light penetration into the solution.

Contrarily, increase in the amount of dissolved oxygen (DO) promotes pollutant removal in photo-Fenton system. It can be attributed to the partaking of oxygen in degradation reactions (Huang et al., 2010; Tolman & Barton, 1993). In addition, other oxidative species such as superoxide radical anion ( $O_2^{\bullet-}$ ) and its protonated form, hydroperoxyl radicals ( $HO_2^{\bullet}$ ) are also generated (Eqs. 2-14 and 2-15). However, their oxidation potential is very low compared to  $\bullet OH$  radicals (Miró et al., 2013; Monteagudo et al., 2013). Therefore,  $H_2O_2$  consumption is decreased in higher DO concentrations (Rodríguez et al., 2011). It is noteworthy that DO monitoring during Fenton reaction has been used as an indicator for correcting continuous dosage of  $H_2O_2$ ; in which the increase in DO concentration is a signal for  $H_2O_2$  unproductive decomposition (Eq. 2-5) (Juanes et al., 2011). On the contrary, decontamination rate is decelerated in  $N_2$ -saturated solutions because of the absence of oxygen in the reaction medium (Huang et al., 2010).



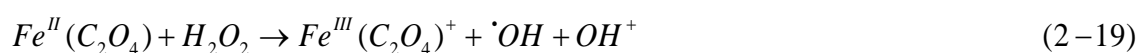
The presence of higher concentrations of dissolved organic matter (DOM) decreases degradation efficacy of probe molecules especially if the contaminants are at lower concentrations than DOM (Michael et al., 2012; Pignatello et al., 2006). This is because DOM competes with micropollutants for degradation and acts as  $\bullet OH$  scavenger. In addition, it decreases the amount of light penetration into the solution in photo-Fenton reaction. However, at lower concentrations, it has been reported that DOM in excited triplet state, indirectly assist photo-degradation of contaminants through production of singlet oxygen in the presence of light (Wenk et al., 2011) based on Eqs. 2-16 and 2-17 (Doll & Frimmel, 2003):



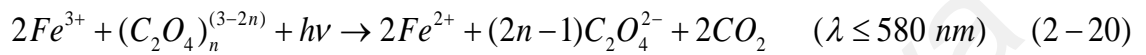
Besides, generation of photoactive and soluble complexes of Fe (III) and carboxylate or polycarboxylate groups in the presence of DOM prevents ferric hydroxide precipitation at neutral pH value (Cruz et al., 2012; Pignatello et al., 2006). However, DOM composition also plays a significant role. For instance, the inhibitory effect of DOM on degradation of endocrine disrupting compounds is higher in the fresh leachate compared to old leachate due to differences in their DOM composition (He et al., 2009).

#### 2.2.5.2. Chelating agents

Despite the fact that Fenton process provides acceptable scores for contaminant degradation in acidic solutions, a large number of recent works have employed several inorganic or organic ligands such as EDTA, EDDS, oxalate, NTA, carboxymethyl  $\beta$ -cyclodextrin (CMCD), tartrate, citrate and succinate, to improve its efficiency and to increase the oxidation rate of probe molecules (An et al., 2013; Huang et al., 2012; Klammer et al., 2013; Xue et al., 2009b). The positive effects of these ions can be attributed to the following aspects: (i) having higher quantum yield of  $\cdot OH$  radical formation compared to other Fe(III)-complexes, (ii) promoting the reduction of ferric ion to ferrous ion and accordingly, regeneration of higher amounts of hydroxyl radical, as shown in Eqs. 2-18 and 2-19 (Duesterberg et al., 2005; Mulazzani et al., 1986):



(iii) Promoting  $H_2O_2$  activation and  $\cdot OH$  radical generation, (iv) enhancing the solubilization of lipophilic organic pollutants, (v) enhancing iron dissolution at neutral pH via photochemical reduction of  $Fe^{3+}$  to  $Fe^{2+}$  (Eq. 2-20), and (vi) being able to operate over wide range of the solar radiation spectrum (An et al., 2013; W. Huang et al., 2012; Panyas et al., 1996; Xue et al., 2009b).



An et al. (2013) compared the degradation efficiency of Methyl Violet ( $[MV]_0$ : 60  $\mu\text{mol/L}$ ) using  $BiFeO_3$  nanoparticles treated with either EDTA or NTA. Removal (%) of MV under various oxidation systems was in an ascending order as follows:  $BiFeO_3/UV\text{-}Vis$  (6% within 90 min) <  $EDTA\text{-}BiFeO_3/H_2O_2$  (25% within 30 sec) <  $EDTA\text{-}BiFeO_3/H_2O_2/UV\text{-}Vis$  (90% within 30 sec). In this study, MV degradation rate constant in ligand-  $BiFeO_3\text{-}H_2O_2\text{-}Vis$  system with EDTA or NTA was respectively 973 or 9.71 times more than Fenton-like reaction ( $BiFeO_3\text{-}H_2O_2$ ), 128 or 1.90 times more than photo-Fenton like system ( $BiFeO_3\text{-}H_2O_2\text{-}Vis$ ) and 136 or 1.75 times more than ligand-Fenton-like system (ligand-  $BiFeO_3\text{-}H_2O_2$ ). It is important to mention that the enhancement in Fenton oxidation rate depends on the initial concentration of the consumed ligand. For instance, oxalate addition at a molar ratio of oxalic acid to ferric ions ( $[Ox]/[Fe^{3+}]$ ) of 2 could improve phenol degradation greatly compared to other ratios (Huang et al., 2010).

Xue et al. (2009b) reported higher degradation efficiencies when they used EDTA in homogeneous Fenton and oxalate in heterogeneous Fenton processes. It should be noted that some of the chelating ions might decrease the degradation efficiency in heterogeneous catalysis using iron minerals. This is due to the strong adsorption of the number of chelating ions such as EDTA to the surface of the catalyst and decrease for

active sites present on the surface for H<sub>2</sub>O<sub>2</sub> degradation. Several researchers have explored this effect (Huang et al., 2013; Xue et al., 2009b). Regardless of this effect, heterogeneous Fenton has shown higher performance compared to conventional Fenton reaction at neutral pH and low concentrations of H<sub>2</sub>O<sub>2</sub> (Huang et al., 2013). This is attributed to higher proportion of O<sub>2</sub><sup>•-</sup> at pH values higher than 6.0 that improves regeneration of ferrous ions (Eqs. 2-21 and 2-22) and increases •OH radical production accordingly (Wang & Xu, 2011).



### 2.3. Homogeneous vs. heterogeneous Fenton systems

Iron species exist in the same phase with reactants in homogeneous Fenton reaction. Therefore, there is no mass transfer limitation. A large number of studies have been conducted successfully using iron salts in Fenton process for treatment of various recalcitrant wastewaters. Despite significant mineralization efficiency of homogeneous Fenton under optimum condition, a number of limitations are associated with the process. The main drawback is the formation of large quantity of ferric-hydroxide sludge at pH values higher than 4.0 (Hermosilla et al., 2009), that poses in adverse effects on the environment and waste disposal issues. In addition, regeneration of catalyst is not only impracticable but also large amount of catalytic metal is misplaced in the sludge. These limitations can be overcome to some extent by application of heterogeneous catalysts. This category of catalysts has gained growing concern in Fenton process as its effectiveness is maintained for wider range of pH. Iron is stabilized within the catalyst structure in heterogeneous catalysts and can effectively activate degradation of recalcitrant compounds without generation of ferric hydroxide

precipitation. Nevertheless, heterogeneous catalysis is of slower oxidation rate compared to homogeneous reaction due to the presence of a small fraction of iron on the catalyst surface (Punzi et al., 2012). On this basis, recent investigations have focused on the development of new hetero-catalysts with larger surface area and higher activities in degradation processes. Three possible mechanisms have been proposed for hetero-catalysts action in Fenton processes: (i) iron leaching to the reaction solution and activating hydrogen peroxide through homogeneous pathway and/or (ii) decomposition of  $H_2O_2$  to  $\cdot OH$  radicals by binding of  $H_2O_2$  with iron species on the surface of catalyst or (iii) chemisorption of probe molecule on the catalyst surface (Arriaga et al., 2010; Punzi et al., 2012).

Numerous heterogeneous catalysts have been used in Fenton reactions. Amongst them are iron minerals that are relatively less priced and can be separated magnetically from the reaction medium (Gonzalez-Olmos et al., 2012). Table 2.2 gives a number of examples on the application of heterogeneous catalysts in UV/Fenton-like reaction. The table exhibits the potential of heterogeneous catalysts for degradation of recalcitrant pollutants in solutions with neutral or unchanged pH values. Finally, it should be pointed out that heterogeneous Fenton-like treatment of highly polluted wastewaters with low transparency is not practically efficient because of inner filtration effects related to large number of absorbing molecules and inhibition of photons absorption by Fe cations (Navalon et al., 2010).



Table 2.2: Heterogeneous Fenton catalysis for degradation of recalcitrant organic compounds

Compound/ Initial amount (mg L <sup>-1</sup> )	Catalyst	Operational condition					Optimal performance	References
		[H <sub>2</sub> O <sub>2</sub> ] (mg L <sup>-1</sup> )	[H <sub>2</sub> O <sub>2</sub> ] (mg L <sup>-1</sup> )	[H <sub>2</sub> O <sub>2</sub> ] (mg L <sup>-1</sup> )	[H <sub>2</sub> O <sub>2</sub> ] (mg L <sup>-1</sup> )	[H <sub>2</sub> O <sub>2</sub> ] (mg L <sup>-1</sup> )		
Methyl Violet (MV)/12.25	BiFeO <sub>3</sub>	680	50	5.0	25	> 420	49.8% MV removal within 120 min in the dark, increased degradation up to 92% within 120 min in presence of light; 3.47 times increase in rate constants in photo-Fenton compared to Fenton.	(An et al., 2013)
Rhodamine B (RhB)/4.8	BiFeO <sub>3</sub>	340	50	5.0	25	> 420	70% RhB removal within 40 min in the dark; 1.95 times increase in rate constants in photo-Fenton compared to Fenton.	(An et al., 2013)
Phenol/50	Fe-zeolites	100	20	7.0	35	>290/765	100 % phenol degradation after 100 min of irradiation; 90% DOC removal after 80 min.	(Gonzalez-Olmos et al., 2012)
Imidacloprid/50	Fe-zeolites	100	20	7.0	35	>290/765	≈98% imidacloprid degradation after 420 min; 43% DOC removal after 800 min.	(Gonzalez-Olmos et al., 2012)
Dichloroacetic acid (DCAA)/50	Fe-zeolites	100	20	7.0	35	>290/765	65% DCAA degradation after 800 min; 63% DOC removal after 800 min.	(Gonzalez-Olmos et al., 2012)
Methylene blue (MB)/100	LiFe(WO <sub>4</sub> ) <sub>2</sub>	170	100	5.0	25	254 / 5	84% decolorization within 60 min.	(Ji et al., 2011)
polyacrylamide (PAM)/100	Fe(III)-SiO <sub>2</sub>	200	100	6.8	-	254/	94% PAM degradation within 90min;70% TOC removal within 180 min.	(Liu et al., 2009)

\*AMKC: acid modified kaolin clay supported ferric-oxalate catalyst

#### 2.4. Iron minerals as heterogeneous catalysts

Iron oxides are abundantly available minerals present in the earth crust. Out of the sixteen known iron minerals (Cornell & Schwertmann, 2003), magnetite ( $\text{Fe}_3\text{O}_4$ ), goethite ( $\alpha\text{FeOOH}$ ), maghemite ( $\gamma\text{Fe}_2\text{O}_3$ ) and hematite ( $\alpha\text{Fe}_2\text{O}_3$ ) are widely used in heterogeneous catalysis processes and have been attractive alternatives for remediation of polluted soil, groundwater and for wastewater treatment as well (Munoz et al., 2015; Yang et al., 2015). Different physico-chemical characteristics of these oxides make them more or less desirable for oxidative reactions. From these features, surface area, pore size/volume, the crystalline structure and surface characteristics have a crucial effect on their activity (Huang et al., 2001; Xue et al., 2009a). Moreover, in Fenton oxidation systems, structural  $\text{Fe}^{2+}$  content is influential (Xue et al., 2009a). These solid catalysts presented powerful potential for degradation of recalcitrant pollutants such as dyes and phenolic compounds (Table 2.3).

Despite the fact that iron oxides provided acceptable scores for contaminant degradation in Fenton-like reactions with uncontrolled pH values, several works have put in practice to improve their efficiency and increase decomposition rate of probe molecules through some modifications in their structure. Thermal treatment of catalyst surface under  $\text{H}_2$  atmosphere, for example, resulted in generation of  $\text{Fe}^{\text{II}}$  sites on the goethite surface and wherefore, enhanced the goethite efficiency significantly in Fenton reaction for quinolone degradation (Guimarães et al., 2008). In this study, pure goethite/ $\text{H}_2\text{O}_2$  system did not perform similarly due to the presence of only  $\text{Fe}^{3+}$  ions on goethite surface and indicates that quinoline degradation occurred chiefly on  $\text{Fe}^{\text{II}}$  sites through  $\cdot\text{OH}$  radical generation route.

Table 2.3: Fenton degradation of recalcitrant organic compounds catalyzed by iron oxides

Compound	Catalyst	Operational condition						Optimal performance	References
		[H <sub>2</sub> O <sub>2</sub> ]	[Cat]	[OX]	pH	T °C	λ nm		
Phenol (0.1 mM)	Magnetite/mesocellular carbon foam (Fe <sub>3</sub> O <sub>4</sub> /MSU-F-C)	0.1 mM	0.1 g L <sup>-1</sup>	-	3.0	25	-	95% phenol degradation within 4 hrs.	(Chun et al., 2012)
Bisphenol A [BPA] 0.01 mM	Magnetite/oxalic acid	0.5 mM	0.15 g L <sup>-1</sup>	0.2 mM	3.0	23– 25	-	Complete removal of BPA within <120 minutes with half-life of ≥ 15 minutes.	(Xue et al., 2009a)
Phenol (0.2 gL <sup>-1</sup> )	Maghemite/ MCM-14 (MSFM)	0,98 mM	5 g L <sup>-1</sup>	-	4.0	40	-	TOC removal of 78% within 2h, decrease in TOC removal to 65% after 3 times recycle reaction.	(Rodríguez et al., 2009)
Methyl red [MR] 50 μM	Quartz/amorphous iron(III) oxide (Q <sub>1</sub> ), quartz/maghemite (Q <sub>2</sub> ), quartz/magnetite (Q <sub>3</sub> ) quartz/goethite (Q <sub>4</sub> )	H <sub>2</sub> O <sub>2</sub> / Fe: 20	-	-	5.0 & 7.0	20	-	Higher oxidation of MR at pH 5.0 than 7.0, > 99% MR sorption on catalyst surface within 2 h, highest degradation rate for Q <sub>4</sub> (min <sup>-1</sup> ) at both pH values.	(Xia et al., 2011)
Methylene blue [MB] 100 mg L <sup>-1</sup> (10 ml)	Niobia/iron oxide composite	2ml/ 10ml	30 mg	-	-	25	-	~90% discoloration using niobia:iron oxide 1:1, 50% discoloration by niobia:iron oxide 1:5 within 120 minutes.	(Hanna et al., 2008)

(continued on next page)

'Table 2.3, continued'

Compound	Catalyst	Operational condition						Optimal performance	References
		[H <sub>2</sub> O <sub>2</sub> ]	[Cat]	[OX]	pH	T °C	λ nm		
Quinolone [Q]10 mg L <sup>-1</sup> (9.9 ml),	Cu <sup>2+</sup> / goethite	-	10 mg	-	-	-	-	Q degradation within 240 min via successive hydroxylations. Higher degradation rate compared to pure goethite.	(Oliveira et al., 2007)
2-chlorophenol [H <sub>2</sub> O <sub>2</sub> ] / [2-CP] 30-50	Goethite	-	0.5 g L <sup>-1</sup>	-	3.0	50	-	2-CP and TOC removal of 99% and 75% respectively within 6 hours.	(Guimaraes et al., 2009)
Pentachlorophenol, [PCP] 0.0375 mM	Goethite and hematite	-	0.4 g L <sup>-1</sup>	1.2 mM	-	-	< 370	68% PCP degradation in the hematite suspension and 83 % in the goethite suspension within 1h, minor PCP degradation under UV light and without oxalic acid,	(Ortiz de la Plata et al., 2008)
Pharmaceuticals [pharma] 420 ml, each 10 mgL <sup>-1</sup> [TOC] 42 mgL <sup>-1</sup>	Immobilized goethite	H <sub>2</sub> O <sub>2</sub> / TOC: 5.8– 2.9	0.05 g L <sup>-1</sup>	-	3.0	25 ± 2	-	100% degradation of the selected pharmaceuticals within 6 h, 12.5% and 21% TOC removal using H <sub>2</sub> O <sub>2</sub> /TOC mass ratio of 2.9 and 5.8 respectively	(Lan et al., 2010)
2,4,6-trinitrotoluene [TNT] 0.11mM	Hematite, ferrihydrite, lepidocrocite, goethite, Magnetite, pyrite, green rust	3% (w/v)	2 g/L	-	7	-	-	60% TNT removal with green rust (38.9% Fe II) followed by pyrite (46.6% Fe II) and magnetite (24.2% Fe II), very low TNT removal with ferrihydrite, lepidocrocite and hematite (Fe III bearing minerals).	(Molina et al., 2012)
2,4,6-trinitrotoluene [TNT] 0.11mM	Magnetite [EDTA] 10 mM [CMCD] 5 mM,	3% (w/v)	5% (w/w)	-	7	-	-	25% TNT removal by magnetite without chelating agent, improved degradation up to 50% and 62% with EDTA and CMCD respectively	(Matta et al., 2008)

(continued on next page)

'Table 2.3, continued'

Compound	Catalyst	Operational condition						Optimal performance	References
		[H <sub>2</sub> O <sub>2</sub> ]	[Cat]	[OX]	pH	T °C	λ nm		
Sulfadiazine [SDZ] 20 mg/L (250ml)	Goethite	0.5 mM	0.4 g L <sup>-1</sup>	4.0 mM	3.5	30	350	3%, 15% and 93% SDZ removal via UV, UV/goethite, UV/goethite/oxalate systems respectively after 40 min of irradiation.	(Matta et al., 2008)
Chlorinated ethylenes (PCE, TCE, cis 1,2-DCE, trans 1,2-DCE, 1,1 DCE) & Benzene, toluene, ethyl benzene in nonaqueous phase liquids (NAPLs) or aqueous phase [HC] 1.0 mM (250ml)	Goethite (α-FeOOH) [HC] 1.0 mM (250ml)	0.01 & 0.5%	0.22 g ~ 4 g L <sup>-1</sup> Fe	4.0 mM	3.5	25 ± 3	-	Removal % of ethyl benzene > toluene > Benzene, Lower removal percentage for compounds with higher water solubility.	(Wang et al., 2010)
Benzoic acids [BA] 50 mgL <sup>-1</sup>	Hematite-SBA-15	162 mgL <sup>-1</sup>	0.6 g L <sup>-1</sup>	-	3.1	27 ± 3	365	100% BA removal and 87.9 % COD removal after 240 min, 93% H <sub>2</sub> O <sub>2</sub> consumption, Efficiency COD <sub>abatement</sub> /H <sub>2</sub> O <sub>2</sub> <sub>consumed</sub> of 0.66.	(Yeh et al., 2008)

Chelating agents (CA), on the other side, can enhance degradation efficiency of iron minerals at near neutral pH (Xue et al., 2009b) via their positive effect on non-reductive/reductive dissolution rate of iron oxide (X. Wang et al., 2008). Xue et al. (2009b) investigated the effect of EDTA, carboxymethyl  $\beta$ -cyclodextrin CMCD, oxalate, tartrate, citrate and succinate as CA with magnetite on pentachlorophenol (PCP) decomposition rate. All CA promoted iron-oxide dissolution amount and PCP oxidation rate. In spite of strong chelating ability of EDTA and its highest oxidation rate to other CA in homogeneous Fenton system, it represented lower efficiency than oxalate in heterogeneous Fenton system due to its strong binding to magnetite surface. Similar results were obtained by Lan et al. (2010) where heterogeneous photo-degradation, dechlorination and detoxification of PCP with goethite or hematite significantly bolstered up with 1.2 mM of oxalate due to the formation of Fe<sup>III</sup> species ( $\text{Fe}(\text{C}_2\text{O}_4)_3^{3-}$ ) and Fe<sup>II</sup> species ( $\text{Fe}(\text{C}_2\text{O}_4)_2^{2-}$ ) with powerful photo-activity in both iron oxides suspensions. Interestingly, photo-degradation of these complexes generated  $1.0 \text{ mgL}^{-1}$  and  $2.4 \text{ mgL}^{-1}$  hydrogen peroxide under the operational conditions of pH 3.5,  $[\text{C}_2\text{O}_4^{2-}]$  1.2 mM and  $0.4 \text{ g L}^{-1}$  catalyst within less than 10 minutes of reaction time in goethite and hematite systems respectively that consequently, increased the PCP degradation through Fenton reaction. However, the oxalate concentrations above 1.2 mM decreased the degradation rate as a consequence of  $\cdot\text{OH}$  ion scavenging by oxalate. In another study, the catalytic performance of magnetite was improved by adding CMCD (Matta et al., 2008). This combination elevated the degradation of 2,4,6-trinitrotoluene TNT) three times more than only magnetite.

Substitution of iron with other transition metal was reported that improves degradation effectiveness of iron oxides. There have been extensive studies on application of transition metal substituted magnetite (TMSM) due to the unique characteristics of the

magnetite. Therefore, this section is aimed to give an account of fundamental aspects of magnetite and its application for wastewater treatment through Fenton reaction in pure or modified form. In terms of transition metal substituted iron oxides (TMSIOs), valence and occupied sites, changes in physico-chemical properties, adsorption capacity and catalytic activity are discussed in detail in the following sections.

#### **2.4.1. Magnetite (Fe<sub>3</sub>O<sub>4</sub>)**

Magnetite is a spinel iron oxide with chemical formula of (Fe<sup>3+</sup>)[Fe<sup>2+</sup>Fe<sup>3+</sup>]O<sub>4</sub> where Fe<sup>3+</sup> cations occupy equally both octahedral and tetrahedral sites and Fe<sup>2+</sup> cations are placed only in octahedral sites. In Fenton process, magnetite has gained considerable attention than other iron oxides due to its unique characteristics; (i) It is the only most abundant iron oxide with Fe<sup>II</sup> in its structure that improves hydroxyl radical production through Fenton reaction, (Munoz et al., 2015; Kwan & Voelker, 2003; Moura et al., 2005), (ii) The presence of octahedral sites in its structure that are mostly at the surface of the crystal and the catalytic activity are chiefly on account of the octahedral cations (Ramankutty & Sugunan, 2001a), (iii) The magnetically easy separation of magnetite catalysts from the reaction system as a result of its magnetic property (Ai et al., 2011; Chun et al., 2012; Costa et al., 2006), (iv) Production of more active systems by the modification in the physico-chemical properties of the magnetite through isostructural substitution of iron by different transition metals (Moura et al., 2005) and (v) Higher dissolution rate of magnetite compared to other iron oxides (Matta et al., 2008) and accordingly, higher electron mobility in its spinel structure (Litter & Blesa, 1992). In consequence, magnetite has been frequently used in contaminant oxidation systems (Ai et al., 2011; Rodríguez et al., 2009; Usman et al., 2012b; Xue et al., 2009a; Yang et al., 2009; Zhong et al., 2012). Usman et al. (2012a) conducted six set of oxidative degradation systems using soluble Fe<sup>2+</sup> with H<sub>2</sub>O<sub>2</sub> (homogeneous Fenton), H<sub>2</sub>O<sub>2</sub> and

magnetite rich sand (heterogeneous Fenton-like), singular  $\text{H}_2\text{O}_2$ , magnetite and sodium persulfate, soluble  $\text{Fe}^{2+}$  and sodium persulfate and singular sodium persulfate to evaluate the effectiveness of magnetite catalysed oxidation system to other combinations in degradation of oil hydrocarbons. The resulted degradation was above 80% by magnetite with both oxidants ending to inconsiderable by-products, while the oxidants represented minor degradation efficiency exclusively or even with homogeneous catalyst (10-15%).

The investigation to compare catalytic activity of amorphous iron (iii) oxide, maghemite, magnetite and goethite mixed with quartz was carried out by Hanna et al. (2008) for methyl red degradation in presence of  $\text{H}_2\text{O}_2$ . The authors believed that the oxidation state of iron in the oxides has been the key parameter as  $\text{Fe}^{\text{II}}$  is superior to  $\text{Fe}^{\text{III}}$  in Fenton-like processes. In this study, magnetite exhibited highest rate constant normalized to surface area per unit mass of oxide (SSA) at neutral pH values and the rate constant according to pseudo-first order kinetic model for goethite was the highest at pH 5. However, their performance in Fenton-like oxidation and also for adsorption of selected dye was pH-dependence and higher at pH 5 than 7.

In many instances, magnetite offered better performance than other iron oxides that might be due to the presence of  $\text{Fe}^{\text{II}}$  cations in its structure (Matta et al., 2008). Nevertheless, the higher  $\text{Fe}^{\text{II}}$  content than stoichiometric ratio in nano-sized magnetite could not increase phenol degradation considerably. The produced catalyst just expedited decomposition of  $\text{H}_2\text{O}_2$  in non-productive manner that could be resulted from the  $\cdot\text{OH}$  radical scavenging by the surface of nanoparticle agglomerates of magnetite (Rusevova et al., 2012).



## 2.5. Transition metal substituted iron oxides

Magnetite is a well-known iron mineral that have been used in synthesis of TMSIOs. Iron in the magnetite structure can be substituted isomorphically by other transition metals. The most common preparation method is co-precipitation of highly pure predetermined amount of ferrous and selected transition metal salts under  $N_2$  atmosphere to avoid the oxidation of ferrous cations (Liang et al., 2012b; Yang et al., 2009) that could be followed by thermal treatment at 400-430 °C (Costa et al., 2003; Costa et al., 2006; Lelis et al., 2004). Yang et al. (2009) presented the following set of reactions (Eqs. 2-23 to 2-26) involved in synthesis of  $Fe_{3-x}Ti_xO_4$  that were proposed by Sugimoto & Matijević (1980):

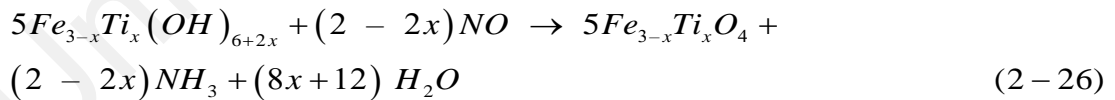
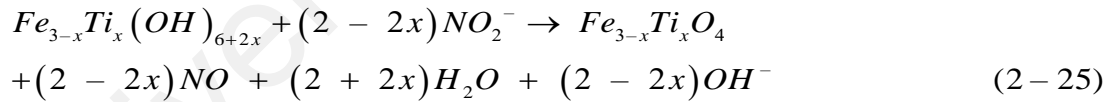
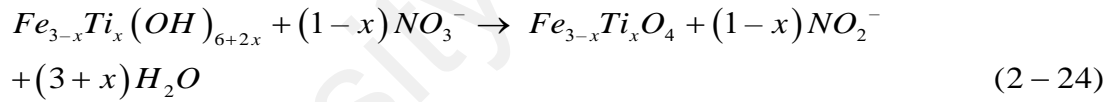


Table 2.4: Preparation method and characteristics of transition metal substituted iron oxide catalysts

Heterogeneous Catalyst	Characteristics	Preparation method	References
$\text{Fe}_{3-x}\text{Cr}_x\text{O}_4$ ( $x = 0.00, 0.07, 0.26, 0.42$ and $0.51$ ) $\text{Fe}_3\text{O}_4$ , $\text{Fe}_{2.93}\text{Cr}_{0.07}\text{O}_4$ , $\text{Fe}_{2.74}\text{Cr}_{0.26}\text{O}_4$ , $\text{Fe}_{2.58}\text{Cr}_{0.42}\text{O}_4$ , $\text{Fe}_{2.49}\text{Cr}_{0.51}\text{O}_4$	Spinel crystalline, replacing of $\text{Cr}^{3+}$ by $\text{Fe}^{3+}_{\text{oct}}$ and for higher Cr contents by $\text{Fe}^{2+}_{\text{oct}}$ and $\text{Fe}^{3+}_{\text{tet}}$ , substitution by $\text{Cr}^{3+}$ decreased the pore diameter from meso- to micropore with a significant increase on the BET surface area.	conventional co-precipitation method	(Magalhães et al., 2007)
$\text{Fe}_{3-x}\text{Ti}_x\text{O}_4$ ( $x = 0.00, 0.20, 0.46, 0.71$ and $0.98$ ) $\text{Fe}_3\text{O}_4$ , $\text{Fe}_{2.80}\text{Ti}_{0.20}\text{O}_4$ , $\text{Fe}_{2.54}\text{Ti}_{0.46}\text{O}_4$ , $\text{Fe}_{2.29}\text{Ti}_{0.71}\text{O}_4$ , $\text{Fe}_{2.02}\text{Ti}_{0.98}\text{O}_4$	well crystallized spinel structure, contains $\text{Ti}^{4+}$ in octahedral sites, hydrophilic surface, Decrease in particle size ( $\approx 82$ nm) and pore diameter plus significant increase in surface area along with the increase in Ti content,	Precipitation-oxidation method	(Zhong et al., 2012)
$\text{Fe}_{3-x}\text{Mn}_x\text{O}_4$ ( $x = 0.21, 0.26$ and $0.53$ ) $\text{Fe}_3\text{O}_4$ , $\text{Fe}_{2.79}\text{Mn}_{0.21}\text{O}_4$ $\text{Fe}_{2.74}\text{Mn}_{0.26}\text{O}_4$ $\text{Fe}_{2.47}\text{Mn}_{0.53}\text{O}_4$	existence of the spinel phase, $\text{Mn}^{2+}$ replacing mainly $\text{Fe}^{2+}$ in the octahedral site, i.e. $[\text{Fe}^{3+}]_{\text{tetrahedral}} [\text{Fe}^{3+}\text{Fe}_{1-x}^{2+}\text{M}_x^{2+}]_{\text{octahedral}}\text{O}_4$ , phase transformation of magnetite to maghemite and hematite due to the presence of Mn.	co-precipitation of the precursor ferric hydroxyl-acetate containing the metals Mn	(Costa et al., 2003; Costa et al., 2006; Oliveira et al., 2000)
$\text{Fe}_{3-x}\text{Co}_x\text{O}_4$ ( $x = 0; 0.19; 0.38$ and $0.75$ ) $\text{Fe}_3\text{O}_4$ , $\text{Fe}_{2.81}\text{Co}_{0.19}\text{O}_4$ , $\text{Fe}_{2.62}\text{Co}_{0.38}\text{O}_4$ , $\text{Fe}_{2.25}\text{Co}_{0.75}\text{O}_4$	Existence of the spinel phase, $\text{Co}^{2+}$ replaces mainly $\text{Fe}^{2+}$ in the octahedral site, , i.e. $[\text{Fe}^{3+}]_{\text{tetrahedral}} [\text{Fe}^{3+}\text{Fe}_{1-x}^{2+}\text{M}_x^{2+}]_{\text{octahedral}}\text{O}_4$ , the increase in hyperfine magnetic field for the octahedral iron with increase in structural Co.	co-precipitation of the precursor ferric hydroxyl-acetate containing the metals Co	(Costa et al., 2003; Costa et al., 2006; Lelis et al., 2004)

(continued on next page)

‘Table 2.4, continued’

Heterogeneous Catalyst	Characteristics	Preparation method	References
$\text{Fe}_{3-x}\text{Ni}_x\text{O}_4$ ( $x = 0; 0.10; 0.28$ and $0.54$ ) $\text{Fe}_3\text{O}_4$ , $\text{Fe}_{2.90}\text{Ni}_{0.10}\text{O}_4$ , $\text{Fe}_{2.72}\text{Ni}_{0.28}\text{O}_4$ , $\text{Fe}_{2.46}\text{Ni}_{0.54}\text{O}_4$ ,	Existence of the spinel phase, $\text{Ni}^{2+}$ replacing mainly $\text{Fe}^{2+}$ in the octahedral site, i.e. $[\text{Fe}^{3+}]_{\text{tetrahedral}} [\text{Fe}^{3+}\text{Fe}_{1-x}^{2+}\text{M}_x^{2+}]_{\text{octahedral}} \text{O}_4$ .	co-precipitation of the precursor ferric hydroxyl-acetate containing the metals Ni	(Costa et al., 2003; Costa et al., 2006)
$\text{Fe}_{3-x-x'}\text{Ti}_x\text{V}_x\text{O}_4$ $(x = 0.00, 0.40, 0.42, 0.54$ and $0.69)$ $(x' = 0.00, 0.03, 0.08, 0.13$ and $0.32)$ $\text{Fe}_3\text{O}_4$ , $\text{Fe}_{2.31}\text{Ti}_{0.69}\text{O}_4$ , $\text{Fe}_{2.43}\text{Ti}_{0.54}\text{V}_{0.03}\text{O}_4$ , $\text{Fe}_{2.50}\text{Ti}_{0.42}\text{V}_{0.08}\text{O}_4$ $\text{Fe}_{2.47}\text{Ti}_{0.40}\text{V}_{0.13}\text{O}_4$ $\text{Fe}_{2.68}\text{V}_{0.32}\text{O}_4$	Well crystallized spinel structure, occupancy of mainly octahedral sites by $\text{Ti}^{4+}$ and $\text{V}^{3+}$ , no apparent effect of Ti-V on the magnetite structure, size: less than 100 nm, magnetic, higher adsorption activity of Ti-V magnetite catalysts than pure magnetite (more dependent on Ti than V), increase in specific surface area compared to $\text{Fe}_3\text{O}_4$ .	co-precipitation method	(Liang et al., 2012b)
$\text{Fe}_{3-x}\text{Ti}_x\text{O}_4$ ( $x = 0.00, 0.17, 0.23, 0.37, 0.50, 0.78$ ) $\text{Fe}_3\text{O}_4$ , $\text{Fe}_{2.83}\text{Ti}_{0.17}\text{O}_4$ , $\text{Fe}_{2.77}\text{Ti}_{0.23}\text{O}_4$ , $\text{Fe}_{2.63}\text{Ti}_{0.37}\text{O}_4$ , $\text{Fe}_{2.50}\text{Ti}_{0.50}\text{O}_4$ , $\text{Fe}_{2.22}\text{Ti}_{0.78}\text{O}_4$ ,	spinel structure, bigger lattice parameter than magnetite, average diameters of 120 nm, $\text{Ti}^{4+}$ replacing mainly $\text{Fe}^{3+}$ in the octahedral site, Simultaneous increase in oxidation and transition temperature by increase in Ti content, increase in surface area from $6.65 \text{ m}^2 \text{ g}^{-1}$ of pure magnetite to $20.7 \text{ m}^2 \text{ g}^{-1}$ in titanomagnetite.	new soft chemical method	(Yang et al., 2009; Yang et al., 2009)
$\text{Fe}_{3-x}\text{V}_x\text{O}_4$ ( $x = 0.00, 0.16, 0.26, 0.34$ ) $\text{Fe}_{2+0.61}\text{Fe}_{3+2.39}\text{O}_4$ $\text{Fe}_{2+0.45}\text{Fe}_{3+2.39}\text{V}_{0.16}\text{O}_4$ $\text{Fe}_{2+0.70}\text{Fe}_{3+2.04}\text{V}_{0.26}\text{O}_4$ $\text{Fe}_{2+0.73}\text{Fe}_{3+1.93}\text{V}_{0.34}\text{O}_4$	$\text{V}^{3+}$ mainly occupies the octahedral site (chiefly replaced $\text{Fe}^{3+}$ ), the increase in vanadium content cause a decrease in the total Fe and $\text{Fe}^{3+}$ content, no apparent change in the average crystal size and surface area, increase in the superficial hydroxyl groups and a decrease in the temperature of maghemite-hematite phase transformation.	precipitation-oxidation method	(Liang et al., 2010)

(continued on next page)

‘Table 2.4, continued’

Heterogeneous Catalyst	Characteristics	Preparation method	References
$\text{Fe}_{3-x}\text{Al}_x\text{O}_4$ ( $x=0.00, 1.48, 2.14, 5.49, 8.07$ mol %) $\text{Fe}_3\text{O}_4$ , $\text{Fe}_{2.83}\text{Al}_{0.17}\text{O}_4$ , $\text{Fe}_{2.77}\text{Al}_{0.23}\text{O}_4$ , $\text{Fe}_{2.63}\text{Al}_{0.37}\text{O}_4$ , $\text{Fe}_{2.50}\text{Al}_{0.50}\text{O}_4$ ,	$\text{Al}^{3+}$ replacing mainly $\text{Fe}^{3+}$ , the increase in aluminum content cause a decrease in the particle size, no obvious change in porosity of the particles and their surface area, samples containing greater amounts of aluminum were overall less reactive than undoped samples,	Co-precipitation method	(Jentzsch et al., 2007)
$\text{Cu}_x\text{Fe}_{3-x}\text{O}_4$ ( $x = 0.00, 0.2, 0.3$ ) $\text{Fe}_3\text{O}_4$ $\text{Cu}_{0.2}\text{Fe}_{2.8}\text{O}_4$ $\text{Cu}_{0.3}\text{Fe}_{2.7}\text{O}_4$	A single-phase cubic spinel structure of $\text{Cu}_{0.2}\text{Fe}_{2.8}\text{O}_4$ in magnetite and $\text{Cu}_{0.3}\text{Fe}_{2.7}\text{O}_4$ , consists of a cubic spinel structure in magnetite and a hexagonal structure in hematite,	mechanical alloying	(Lee & Joe, 2010)
$\text{Fe}_{2-x}\text{Nb}_x\text{O}_3$ (% Nb = 0.00, 1.49, 5.00, 9.24) % Nb = 0.00 pure Hm, % Nb = 1.49: Hm-Nb2, % Nb = 5.00: Hm-Nb5, % Nb = 9.24: Hm-Nb10,	Crystalline phase, partial replacement of $\text{Fe}^{3+}$ by $\text{Nb}^{5+}$ , increase in the surface area with increase in $\text{Nb}^{5+}$ content, decrease in hyperfine field value in Hm-Nb2, production of superparamagnetic hematite with smaller particle size by increase in Nb content.	conventional co-precipitation method	(Silva et al., 2009)
Nb-hematite-maghemite $(\alpha\text{-Fe}_2\text{O}_3)\text{-}(\gamma\text{-Fe}_2\text{O}_3)\text{-FeNb}_2\text{O}_6$ Nb-NCBT: Nb- nanocomposite before $\text{H}_2\text{O}_2$ treatment Nb-NCAT: Nb- nanocomposite after $\text{H}_2\text{O}_2$ treatment	Nb-NCBT : mainly constituted by maghemite, isomorphic replacement of $\text{Fe}^{3+}$ by $\text{Nb}^{5+}$ , high value of saturation magnetization, lower value of the hyperfine field due to Nb substitution, retarding of maghemite transformation to hematite at 500 °C. Nb-NCAT: significant structural disorder due to $\text{H}_2\text{O}_2$ treatment, mainly constituted by hematite, increase in hyperfine field value, decrease in particle size, decrease in saturation magnetization.	Co-precipitation method	(Silva et al., 2011)

(continued on next page)

'Table 2.4, continued'

Heterogeneous Catalyst	Characteristics	Preparation method	References
Si-FeOOH Si/Fe (0.0, 0.1, 0.2, 0.33)	amorphous structure, Fe-Si complex formation, decrease in particle size and increase in uniformity and surface area, formation of decentralized fibrous structure in the spherical surface of catalyst, higher stability of the catalyst at Si/Fe:0.2,	Not mentioned	(Yuan et al., 2011)
Nb-goethite % Nb= 4,7 &11) % Nb = 0.00 pure Gt, % Nb = 4.0: Hm-Nb4, % Nb = 7.00: Hm-Nb7, % Nb = 11.0: Hm-Nb11,	existence of a hexagonal crystalline phase in Gt and Nb4,increase in surface area and pore size along with decrease in particle size and magnetic order and loss of crystallinity in the goethite by increase in Nb content,	Co-precipitation followed by thermal treatment at 60 °C (72h)	(Oliveira et al., 2008)
Fe <sub>1-x</sub> Ni <sub>x</sub> OOH %Ni (0.1-10)	hexagonal crystalline phase of goethite, decrease in the goethite to magnetite and metallic iron reduction temperature and increase in the specific surface area and pore diameter by increase in Ni <sup>2+</sup> content.	Co-precipitation followed by thermal treatment at 60 °C (72 h)	(de Souza et al., 2010)

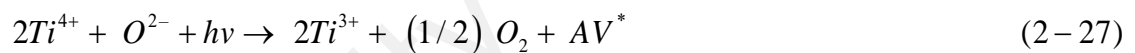
TMSIOs of other iron oxides were often prepared under air atmosphere (Alvarez et al., 2006; Santos et al., 2001; Guimaraes et al., 2009) since they contain only Fe<sup>III</sup> species. Meanwhile, the type and the amount of loaded transition metal, preparation method and the range of temperature affect the characteristics of the produced TMSIO (Table 2.4). Development of several catalysts through the incorporation of transition metal/metals into the magnetite structure has been well-documented. A large number of studies were reported the incorporation of the period 4 transition metals such as Ti (Liang et al., 2012b; Yang et al., 2009; Zhong et al., 2012), V (Liang et al., 2012b; Liang et al., 2010), Cr (Magalhães et al., 2007), Mn (Coker et al., 2008; Costa et al., 2003; Costa et al., 2006; Oliveira et al., 2000), Co (Coker et al., 2008; Costa et al., 2003; Costa et al., 2006; Lelis et al., 2004), Ni (Coker et al., 2008; Costa et al., 2003; Costa et al., 2006), Cu (Lee & Joe, 2010), Zn (Coker et al., 2008) and other metals like Al (Jentzsch et al., 2007) into the magnetite structure. The investigation on the recent studies indicates that such catalysts can be considered as modern promising heterogeneous catalysts capable of activating Fenton oxidation of recalcitrant compounds with or without the illumination of UV-Vis light.

Hence, in relation to TMSIOs, the main aspects that are important to be considered are the valence and occupied site, the physical-chemical changes arisen from the incorporation, the changes in adsorption capacity of the catalyst and its catalytic activity for the target organic contaminant removal.

### **2.5.1. Valence and occupied sites**

In most TMSMs, the structural iron species is replaced isomorphically with introduced cation. If so, the oxidation state of the imported transition metal is similar to the exchanged iron species or has one or two unit difference, in addition to having similar ionic radius. For instance, the substitution of octahedral Fe<sup>3+</sup> by Cr<sup>3+</sup> in Fe<sub>3-x</sub>Cr<sub>x</sub>O<sub>4</sub> with

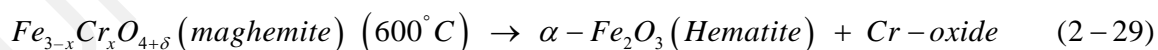
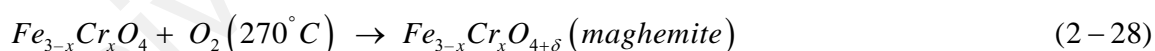
similar ionic radius (64.5 vs. 61.5 pm) (Magalhães et al., 2007), Fe<sup>3+</sup> by Nb<sup>5+</sup> with the same ionic radius (64pm) (Oliveira et al., 2008), Fe<sup>2+</sup> by Co<sup>2+</sup>, Ni<sup>2+</sup> and Mn<sup>2+</sup> (78 vs. 74.5, 69 and 83 pm respectively) (Costa et al., 2006) or Fe<sup>3+</sup> by Ti<sup>4+</sup> and V<sup>3+</sup> in Fe<sub>3-x</sub>·Ti<sub>x</sub>V<sub>x</sub>·O<sub>4</sub> (64.5 vs. 60.5 and 64 pm) (Liang et al., 2012). Regarding those substitutions with unequal charges, as reported for Ti<sup>4+</sup> (Zhong et al., 2012), Fe<sup>3+</sup> replacement by Ti<sup>4+</sup> has been responsible for the reduction of the same amount of Fe<sup>3+</sup> to Fe<sup>2+</sup> on the basis of electrovalence equilibrium (Pearce et al., 2010). For the replacements in the absence of reduction, the structural dislocations would be adjusted by inducing oxygen vacancy (Moura et al., 2006) that is believed to be the active site for hydroxyl radical generation in Fenton oxidation reactions. However, the presence of UV irradiation also simulated the generation of anion vacancies (AV<sup>\*</sup>) through the reduction of Ti<sup>4+</sup> to Ti<sup>3+</sup> (Eq. 2-27) (Zhong et al., 2012):



As reported (Jacobs et al., 1994), the cations of octahedral sites are chiefly responsible for the catalytic activity and are about totally located on the surface of the crystal in the spinel structures. In TMSM, the imported cations are mostly located in octahedral sites (Costa et al., 2003; Costa et al., 2006; Liang et al., 2012b; Zhong et al., 2012) and in tetrahedral sites only if the concentration of imported active cation was very high (Magalhães et al., 2007). In a study conducted by Lelis et al. (2004), the imported Co<sup>2+</sup> cations occupied Fe<sup>2+</sup> station not only at octahedral sites of magnetite spinel structure but it also octahedral coordination sites. In other iron oxides, the incorporated transition metal replaced Fe<sup>III</sup> cations (Silva et al., 2011; Silva et al., 2009). For non-metal incorporations, the ion forms a complex with structural iron as reported by Yuan et al. (2011) for Si-goethite.

### 2.5.2. Physico-chemical changes

The imported transition metal may bring about remarkable changes in iron oxide physical-chemical properties such as the increase in surface area and/or a decrease in particle size in which are desirable for catalytic activities (Magalhães et al., 2007; Zhong et al., 2012). Table 2.4 gives data regarding the structural changes of various developed TMSIOs. The extent of the changes are found to be dependent on the preparation technique, type and the amount of the introduced metal and the nature of the occupied site (Costa et al., 2003; Costa et al., 2006; Lee et al., 2008; Lelis et al., 2004; Liang et al., 2013b; Liang et al., 2012b; Magalhães et al., 2007; Oliveira et al., 2000; Ramankutty et al., 2002; Zhong et al., 2012). However, the main structural phase of the iron oxide such as the spinel structure of magnetite is often kept unchanged after the incorporation. On the other hand, the change in oxidation temperature could have resulted in magnetite transformation to maghemite or hematite respectively at 270 °C and 600 °C of which at 600 °C the substituted metal was ejected from the hexagonal structure of the produced hematite in the form of a separate phase as summarized in Eqs. 2-28 and 2-29 (Magalhães et al., 2007):



Although Magalhães et al. (2007) reported a remarkable decrease in the discoloration rate and TOC removal by the increment in the amount of introduced Cr from Cr<sub>0.07</sub> to Cr<sub>0.51</sub>, higher content of Cr resulted in thermal stabilization of the maghemite cubic structure. Oliveira et al. (2008) reported a raise in the temperature range for goethite to hematite transformation concurrent increasing in Nb content (218 °C to 251 °C and



271 °C in Nb7% and Nb11%). Similarly, Nb-hematite reduction at 500 °C resulted in the formation of magnetite but at higher temperatures, Nb was expelled from the structure; whereas the pure hematite reduced to metallic iron at 900 °C (Silva et al., 2009).

Frequent reports from the characterization studies of this category of heterogeneous catalysts using Brunauer-Emmett-Teller (BET) surface area analysis represented a significant increase in surface area (Souza et al., 2010; Liang et al., 2012b; Magalhães et al., 2007; Oliveira et al., 2008; Silva et al., 2009; Zhong et al., 2012) that could be due to the decline in their particle size and/or pore diameter (Silva et al., 2009). For instance, Fe<sup>3+</sup> substitution by Cr<sup>3+</sup> in Fe<sub>3-x</sub>Cr<sub>x</sub>O<sub>4</sub> decreased the pore diameter from meso to micro-size resulted in a significant increase in surface area (Magalhães et al., 2007). Furthermore, the values of surface area for pure hematite and Fe<sub>2-x</sub>Nb<sub>x</sub>O<sub>3</sub> with %Nb of 1.49, 5.00 and 9.24 were obtained respectively 11, 17, 34 and 42 m<sup>2</sup>g<sup>-1</sup> (Silva et al., 2009) and in Nb-goethite, it changed from 70 m<sup>2</sup> g<sup>-1</sup> for pure goethite to 78, 99, and 136 m<sup>2</sup> g<sup>-1</sup> in Nb4%, Nb7% and Nb11%, respectively (Oliveira et al., 2008). However, in non-transition metals, Jentsch et al. (2007) reported an unclear change in the surface area and porosity of the Al-magnetite particles.

Apart from the catalytic characteristics, preserving the magnetic property after incorporation of a foreign-ion was also studied for its facile recovery from the reaction medium (Liang et al., 2012b). This is important especially for their practical applications in wastewater treatment at industrial scale. The magnetic property of magnetite is affected by the cationic pattern in tetrahedral and octahedral sites as well as the synthesis conditions (Lelis et al., 2004). In addition, the descent in particle size could also result in a rise in the magnetic order on the surface of the particles (Haneda & Morrish, 1988). As reported (Cornell & Schwertmann, 2003) the magnetic hyperfine field was affected by the isomorphically replacement of iron with other cations. It was observed that The Fe<sup>2+</sup> replacement with Co<sup>2+</sup> on octahedral sites resulted in an increase

in the internal hyperfine magnetic field of the site from 46.2 T of pure magnetite to 47.4 T in  $\text{Fe}_{2.24}\text{Co}_{0.75}\square_{0.01}\text{O}_4$  along with increment in Co content but it stayed almost unaltered in tetrahedral sites (Lelis et al., 2004). Silva et al. (2009) reported a decrease in hyperfine field value in the hematite with Nb% of 1.49 due to the replacement of magnetic ion with non-magnetic one and disbalance in the electronic charges between  $\text{Fe}^{3+}$  and  $\text{Nb}^{5+}$  that came about vacancies in the catalyst structure. Moreover, higher concentrations of Nb (%Nb = 5 and 9.24) resulted in smaller sized superparamagnetic hematites. Similarly, substitution of iron in goethite with non-magnetic Nb resulted in the decrease in magnetic order of the catalyst by increase in the Nb content (Oliveira et al., 2008).

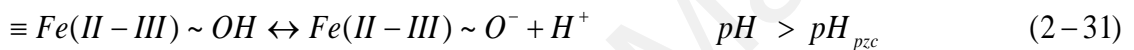
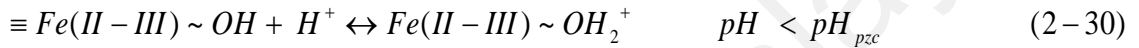
In heterogeneous Fenton system using TMSIOs, the stability of the catalyst is a prominent factor from catalytic, environmental and economic viewpoints (Yang et al., 2009). The stability is often measured by the magnitude of iron and incorporated ions leaching in the reaction medium. In stable catalysts, the concentration of dissolved iron and introduced ion/ions in the solution is below 5% concerning the initial iron content or is not detectable with iron measuring devices (Pariante et al., 2008). In this condition, the involvement of homogeneous Fenton process in the oxidation of organic pollutants is negligible (Costa et al., 2006) and the catalyst can be run for several times with insignificant decrease in its efficacy (Silva et al., 2009; Zhong et al., 2012). In addition, the incorporated transition metal is required to be stable in the cation leaching test to prevent probable pollution from their entrance to environment. Accordingly, iron-leaching promoters are of concern for its effective action. Numerous factors control this rate, such as pH, temperature, irradiation source and intensity, contact time, type and concentration of oxidant and presence of other molecules in the reaction medium like carboxylic acids (Rodríguez et al., 2009; Rodríguez et al., 2009). The reaction between iron species and number of carboxylic acids produce ferricarboxylate complexes that

initiate oxidation process by adsorbing UV-A radiation with high quantum yield (Franch et al., 2004; Rodríguez et al., 2009). For example, carboxylate complexes of tartaric, malic, oxalic and citric acids are active in UV-A region but malonic acid complexes adsorb light under 320 nm. Moreover, succinic and maleic acids do not produce ferricarboxylate complexes and consequently, they do not have positive effect on contaminant oxidation (Rodríguez et al., 2009). Rodríguez et al. (2009) reported that oxalic acid was the most effective carboxylic acid for iron leaching when compared with malic, citric and tartaric acids. The authors found that this effect was higher for magnetite in contrast to hematite. In addition, the UV-A/iron oxide/oxalic acid/H<sub>2</sub>O<sub>2</sub>/TiO<sub>2</sub> oxidation system represented higher bisphenol A removal than other studied oxidation systems.

### **2.5.3. Adsorption capacity**

Surface properties of hetero-catalysts determine their activity in the solution. The electrostatic interaction between the surface of the catalyst and the probe molecule is a very important factor and removal of probe molecule from reaction solution is mainly accounted by its adsorption on the surface of catalyst (Yang et al., 2009). Several factors such as pH, contact time, chemical properties, and initial concentration of contaminant affect the adsorption capacity of the catalyst (Ai et al., 2011; Hanna et al., 2008; Liang et al., 2012b; Yang et al., 2009; Yuan et al., 2011). Amongst surface properties, basicity is an important factor that derives from the presence of hydroxyl groups on the catalyst surface. The completion of the ligand shell of surface Fe atoms results in Fe-OH groups on catalysts surface in which the surface adsorption is mainly governed by these groups (Sun et al., 1998). Accordingly, pH plays a significant role in catalytic behavior of iron oxides. One of the main parameters is the pH of point of zero charge (PZC), which is the pH that the surface charge of the iron oxide is zero or the

amount of  $\text{FeOH}_2^+$  and  $\text{FeO}^-$  groups on catalyst surface is the same. Determination of the  $\text{pH}_{\text{pzc}}$  is essential for understanding the effect of pH of the reaction solution on catalysts surface charge and consequently on its interaction with probe molecule. In magnetite, the main reactions that take place on the surface are protonation and deprotonation reactions (Eqs. 2-30 to 2-32). At pH values less than  $\text{pH}_{\text{pzc}}$ , the surface of magnetite is positively charged and at higher pH values, it is negative (Petrova et al., 2011):

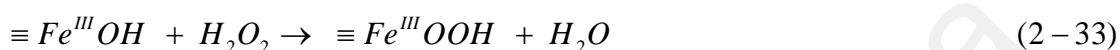


The  $\text{pH}_{\text{pzc}}$  of magnetite varies between 6.0 – 6.8 in an aqueous medium and at room temperature in which the surface charge is of about neutral at this range (Cornell & Schwertmann, 2003; Sun et al., 1998).

To achieve adsorption equilibrium, the organic contaminant and the heterogeneous iron catalyst are stirred together for a period of time (1-3 h) (Hanna et al., 2008). In a study, Liang et al. (2012b) conducted a set of experiments to develop two-metals-substituted magnetites with exertion of  $\text{Ti}^{4+}$  and  $\text{V}^{3+}$  cations to its spinel structure by co-precipitation method. This incorporation improved the adsorption activity of magnetite in which all the  $\text{Fe}_{3-x-x'}\text{Ti}_x\text{V}_x\text{O}_4$  samples had higher saturated adsorbed amount than  $\text{Fe}_3\text{O}_4$  with greater dependence on  $\text{Ti}^{4+}$  content than  $\text{V}^{3+}$ .

In UV/Si-FeOOH/  $\text{H}_2\text{O}_2$  system (Yuan et al., 2011), the surface charge of the catalyst and dimethyl phthalate (DMP) hydrolysis was found to be pH-dependence. Electron-

donating groups in DMP induces negative charge to DMP at pH values higher than zero potential charge of Si-FeOOH (8.4) and on the other side, at pH<8.4, the surface of the catalyst is positively charged that is desirable for DMP adsorption. In this study, pH=5 improved DMP removal by 10-15%. Eqs. 2-33 to 2-36 summarized the reactions involved in DMP degradation under UV irradiation:



Under the influence of UV irradiation, both produced holes from Si-FeOOH semiconductor and the electron-hole pairs ( $e^- - h^+$ ) could react with adsorbed hydrogen peroxide or  $\cdot OH$  anion and yield  $\cdot OH$  radicals. Moreover, other strong oxidizing species such as  $\cdot O_2^-$  also were produced from the reduction of adsorbed  $O_2$  on the catalyst surface over conduction band electrons (Yuan et al., 2011).

Yang et al. (2009) measured element C in the reaction solution to determine the total amount of the adsorbed probe molecule to the surface of Ti-magnetite catalyst. The amount of element C was utmost at time zero of the reaction. After degradation of adsorbed MB on the Ti-magnetite by  $H_2O_2$ , the degradation products desorbed from the catalyst. That was due to their lower electrostatic interaction at neutral pH values and consequently, the concentration of element C in the solution decreased. The results exhibited that the MB degradation with Ti-magnetite was pH-dependent and was low at neutral pH values. In this study, both adsorption and degradation could result in contaminant removal.

Silva et al. (2011) investigated the effect of pre-activating of the catalyst with  $H_2O_2$  in its efficiency in Fenton reaction. In this study,  $H_2O_2$ -treated Nb-doped iron oxide catalyst, mainly comprised of hematite, maghemite and  $FeNb_2O_6$ , was characterized by peroxy groups (Nb-O-O) on its surface derived from the presence of Nb (Esteves et al., 2008) that relatively promoted methylene blue discoloration (Silva et al., 2011). For non-treated catalyst, there was an aging time or delay in the degradation due to catalyst hydroxylation step (Fig. 2.2) (Ramalho et al., 2009).

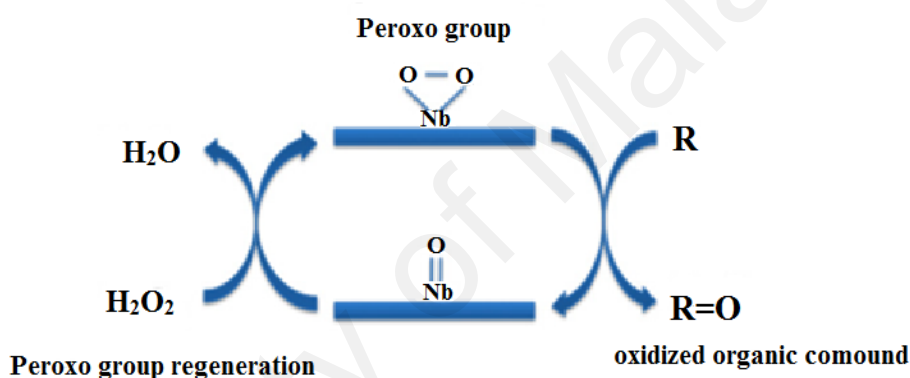


Figure 2.2: Oxidation of organic compound by peroxy group on the surface of Nb-iron oxide treated by  $H_2O_2$

#### 2.5.4. Catalytic activity

Review of the literature clearly revealed that the introduced active cation/cations changed the characteristics of the catalyst with respect to the active sites for enhanced pollutant degradation. Furthermore, the incorporated cations, directly involved in oxidation process via the conjugation of redox pairs and their efficient role in generation of active species. For instance, the presence of Cr in magnetite,  $Fe_{2.93}Cr_{0.07}O_4$ , did not affect the catalyst's surface area and size. Whereas, it improved the discoloration and oxidation rate considerably mainly because of the participation of  $Fe^{3+}/Fe^{2+}$  and  $Cr^{2+}/Cr^{3+}$  pairs in  $H_2O_2$  oxidation cycle (Fig. 2.3) (Magalhães et al., 2007).

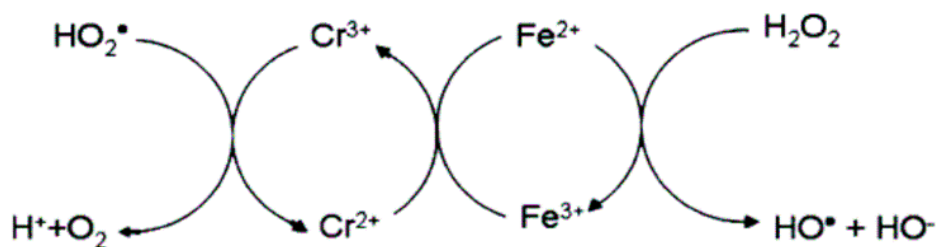


Figure 2.3: Proposed mechanism for the participation of Cr in Fenton reaction (Magalhães et al., 2007).

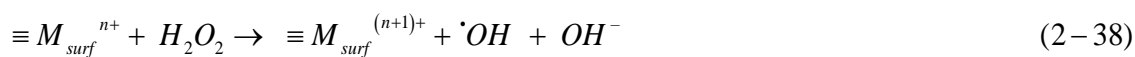
The activity of TMSIO catalyst was evaluated by measuring the generated oxygen through hydrogen peroxide decomposition (Eq. 2-37), and/or oxidation of organic pollutants (Wie et al., 2015; Costa et al., 2006; Guimaraes et al., 2009; Hanna et al., 2008; Liang et al., 2012b; Magalhães et al., 2007; Moura et al., 2005; Oliveira et al., 2007; Yang et al., 2009; Zhong et al., 2012).



Not all the introduced transition metals intensify the activity of the catalyst. The incorporated  $Ni^{2+}$  species generally replaced  $Fe^{2+}$  cations in magnetite structure that are accountable for Fenton initiating step. On the other hand,  $Ni^{2+}$  ions are stable and cannot start the radical reaction; for that reason, its occupancy in magnetite structure had an inhibitory effect on  $H_2O_2$  decomposition and methylene blue degradation reactions (Costa et al., 2006).

#### 2.5.4.1. $H_2O_2$ Decomposition

In Fenton oxidation system, decontamination process commonly starts by generation of hydroxyl radicals through hydrogen peroxide decomposition on the surface of the TMSIOs catalyst as is for iron oxides (Eq. 2-38):



On the other side, the occurrence of mechanisms other than radical generation comes into play when the presence of radical scavengers such as phenol, hydroquinone or ascorbic acid does not affect the rate of  $H_2O_2$  decomposition (Oliveira et al., 2008). This may result from the rivalry between organic compound and active sites (Costa et al., 2003). If so, Oliveira et al. (2008) and Costa et al. (2003) proposed the role of oxygen vacancies in production of  $O_2$  from  $H_2O_2$  as Eqs. 2-39 and 2-40:



Higher  $H_2O_2$  decomposition rates over TMSIOs demonstrates higher activity of the catalyst and consequently, higher Fenton oxidation efficiency for organic contaminant removal (Xue et al., 2009a). Guimaraes et al. (2009) reported that  $H_2O_2$  decomposition rate was significantly high over the surface of cu-doped goethite catalyst, containing both copper and iron active cations in contrast with pure goethite holding solely  $Fe^{3+}$  species. The results indicated that  $Cu^{2+}$  inclusion into the structure of goethite accelerated  $H_2O_2$  decomposition on the surface of the catalyst and resulted in generation of hydroxylation compounds as main by-products. Costa et al. (2003) compared the catalytic activity of pure magnetite ( $Fe_3O_4$ ) and cobalt oxide. Although  $Co_3O_4$  represented higher activity to some degree, but it was distinctly less in relation to cobalt substituted magnetite catalyst. Furthermore, Silva et al. observed that a significant methylene blue removal by Nb-containing hematite was started with 25 min delay, the time in which the catalyst surface was activated by  $Fe^{3+}$  reduction for higher  $H_2O_2$



decomposition. The authors reported that the presence of other organic compound in the reaction medium prevented  $\text{H}_2\text{O}_2$  decomposition forcibly due to the competition between organic compounds and  $\text{H}_2\text{O}_2$  for active sites and they proposed radical mechanism for oxidation reactions (Silva et al., 2009).

#### **2.5.4.2. Organic contaminant degradation**

Amongst various organic compounds that are used for activity evaluation of TMSIOs, the dye methylene blue (MB) has been studied frequently due to its recalcitrant nature, wide application in textile industry, powerful adsorption onto the surface of hetero-catalysts, dissolution in water and easy spectrophotometric measurement (Silva et al., 2011). Table 2.5 summarized the data on the degradation of recalcitrant organic compounds using TMSIOs in Fenton reactions. The studies for MB degradation/discoloration at concentrations of 50-100  $\text{mg L}^{-1}$  and at neutral pH show that its discoloration rate has been generally higher with TMSIOs than of pure iron oxide (Costa et al., 2006; Liang et al., 2010; Oliveira et al., 2008; Silva et al., 2009). In addition, the catalytic efficiency increased simultaneously by increasing the imported transition metal content (Liang et al., 2012b; Liang et al., 2010; Oliveira et al., 2008; Silva et al., 2009). Although, Magalhães et al. (2007) reported a higher MB degradation at lower Cr content in  $\text{Fe}_{3x}\text{Cr}_x\text{O}_4$  ( $x = 0.00, 0.07, 0.26, 0.42, \text{ and } 0.51$ ) and higher Cr content was desirable for hydrogen peroxide decomposition to oxygen. However, being thermodynamically unfavorable for  $\text{Fe}^{3+}$  reduction to  $\text{Fe}^{2+}$  in Fenton reaction,  $\text{Fe}_{2.46}\text{Ni}_{0.54}\text{O}_4$  could remove only 10  $\text{mg L}^{-1}$  of MB with initial concentration of 100  $\text{mg L}^{-1}$  within 50 min. Besides, complete discoloration of the solution was achieved using  $\text{Fe}_{2.47}\text{Mn}_{0.53}\text{O}_4$  and  $\text{Fe}_{2.25}\text{Co}_{0.75}\text{O}_4$  within 5 and 10 min due to their desirable effect on the rate of  $\text{Fe}^{2+}$  regeneration (Costa et al., 2003).

On the other side, the higher activity of  $\text{Fe}_2\text{NiO}_4$  catalyst towards hydroxyl radical generation in UV/Fenton-like reaction and its effective degradation of tetrabromobisphenol A (TBBPA) was ascribed based on the lower oxidation potential of  $\text{Ni}^{2+}/\text{Ni}^{3+}$  redox pair on the catalyst surface compared to  $\text{H}_2\text{O}_2$  (-1.74 V vs. 1.776 V) (Zhong et al., 2013). In the same study, although the oxidation potential of  $\text{Co}^{2+}/\text{Co}^{3+}$  was higher than that of  $\text{H}_2\text{O}_2$  (1.81 V vs. 1.776 V), it enhanced the catalytic activity of the respective TMSIO that could be due to the domination of other mechanism. The likely mechanism is the role of these ions in prohibition of the recombination of photo-generated electrons ( $e^-$ ) and holes ( $h^+$ ) on catalyst surface (Büchler et al., 1998) and extending the existence time of charge carriers. Accordingly, the catalytic activity of magnetite was improved in the order of  $\text{Cr} > \text{Ni} \approx \text{Ti} > \text{Mn} > \text{Co}$ .

Table 2.5: Oxidation of various organic pollutants through Fenton reactions catalyzed by transition metal substituted iron oxide

Compound (mg L <sup>-1</sup> )	Catalyst	Operational condition				Optimal performance	References
		[H <sub>2</sub> O <sub>2</sub> ]	pH	T (°C)	λ (nm)		
Methylene blue [MB] 50	Cr-magnetite Fe <sub>3-x</sub> Cr <sub>x</sub> O <sub>4</sub> (15 mg)	0.3 mg L <sup>-1</sup>	6.0	25	-	Higher degradation rate at lower Cr content, decrease in discoloration rate and TOC removal by increase in Cr content mainly due to the decrease in Fe <sup>2+</sup> .	(Magalhães et al., 2007)
Tetrabromobis-phenol A [TBBPA], 20	Titanomagnetite Fe <sub>2.02</sub> Ti <sub>0.98</sub> O <sub>4</sub> 0.125 g L <sup>-1</sup>	10 mmol L <sup>-1</sup>	6.5	25	-	>97% TBBPA degradation in UV/Fe <sub>2.02</sub> Ti <sub>0.98</sub> O <sub>4</sub> /H <sub>2</sub> O <sub>2</sub> system, ≈75% in UV/H <sub>2</sub> O <sub>2</sub> system within 240 min of UV irradiation.	(Zhong et al., 2012)
Methylene blue [MB], 100	Fe <sub>2.46</sub> Ni <sub>0.54</sub> O <sub>4</sub> Fe <sub>2.47</sub> Mn <sub>0.53</sub> O <sub>4</sub> Fe <sub>2.25</sub> Co <sub>0.75</sub> O <sub>4</sub> (30 mg)	2.5 molL <sup>-1</sup>	-	25	633	10 % color removal within 50 min using Fe <sub>2.46</sub> Ni <sub>0.54</sub> O <sub>4</sub> , complete discoloration of the solution in 5 and 10 min using Fe <sub>2.47</sub> Mn <sub>0.53</sub> O <sub>4</sub> and Fe <sub>2.25</sub> Co <sub>0.75</sub> O <sub>4</sub> respectively.	(Costa et al., 2003)
Chlorobenzene [CBZ] 30 mg L <sup>-1</sup>	Mn-magnetite Fe <sub>3-x</sub> Mn <sub>x</sub> O <sub>4</sub> (30 mg)	2.5 molL <sup>-1</sup>	-	25	-	14, 7, 5 and <1% Chlorobenzene degradation for the reactions using Fe <sub>2.47</sub> Mn <sub>0.53</sub> O <sub>4</sub> , Fe <sub>2.74</sub> Mn <sub>0.26</sub> O <sub>4</sub> , Fe <sub>2.79</sub> Mn <sub>0.21</sub> O <sub>4</sub> and Fe <sub>3</sub> O <sub>4</sub> , respectively.	(Costa et al., 2003; Oliveira et al., 2000)
Methylene blue [MB] 100 mg L <sup>-1</sup>	γ-Fe <sub>2</sub> O <sub>3</sub> α- Fe <sub>2</sub> O <sub>3</sub> Fe <sub>3-x</sub> M <sub>x</sub> O <sub>4</sub> (M = Co & Mn) (30 mg)	0.3 molL <sup>-1</sup> (10 ml)	5- 6.5	25	-	Not remarkable discoloration with Fe <sub>2</sub> O <sub>3</sub> oxides, complete color removal and higher oxidation by Fe <sub>3-x</sub> M <sub>x</sub> O <sub>4</sub> within 5-10 min.	(Costa et al., 2006)
Chlorobenzene [CBZ] 20 mg L <sup>-1</sup>	Mn-magnetite Fe <sub>3-x</sub> Mn <sub>x</sub> O <sub>4</sub> (30 mg)	0.3 molL <sup>-1</sup>	-	25	-	1, 5, 7 and 14% CBZ removal using Fe <sub>3</sub> O <sub>4</sub> , Fe <sub>2.79</sub> Mn <sub>0.21</sub> O <sub>4</sub> , Fe <sub>2.74</sub> Mn <sub>0.26</sub> O <sub>4</sub> and Fe <sub>2.47</sub> Mn <sub>0.53</sub> O <sub>4</sub> respectively within 30 min,	(Costa et al., 2006)

(continued on next page)

'Table 2.5, continued'

Compound	Catalyst	Operational condition				Optimal performance	References
		[H <sub>2</sub> O <sub>2</sub> ]	pH	T (°C)	λ (nm)		
Methylene blue UV [MB] 0.2 mmol L <sup>-1</sup> (500ml)	Ti-V- magnetite Fe <sub>3-x</sub> Ti <sub>x</sub> V <sub>x</sub> O <sub>4</sub> (1.0 g L <sup>-1</sup> )	10 mmol L <sup>-1</sup>	7.0	25	365	Increase in MB discoloration from 48% to 96% by increase in Ti content from x=0.0 to x=0.69 after 120min,	(Liang et al., 2012b)
Methylene blue [MB] 100 mg L <sup>-1</sup> (400 mL)	Titanomagnetite Fe <sub>3-x</sub> Ti <sub>x</sub> O <sub>4</sub> (1.0 g L <sup>-1</sup> )	0.30 molL <sup>-1</sup>	6.8	30	-	Higher activity for Ti-magnetite than pure magnetite, Decrease in residual MB with the increase in Ti content.	(Yang et al., 2009; Yang et al., 2009)
Methylene blue [MB] 0.2 mmol L <sup>-1</sup> (200mL)	V-magnetite Fe <sub>3-x</sub> V <sub>x</sub> O <sub>4</sub> 0≤x≤0.34 (1.0 g L <sup>-1</sup> )	100 mmol L <sup>-1</sup>	10.0	25	-	Colour removal of 41, 60, 81 and 93% of MB within 11 h using Fe <sub>3</sub> O <sub>4</sub> , Fe <sub>2.84</sub> V <sub>0.16</sub> O <sub>4</sub> , Fe <sub>2.74</sub> V <sub>0.26</sub> O <sub>4</sub> and Fe <sub>2.66</sub> V <sub>0.34</sub> O <sub>4</sub> , respectively.	(Liang et al., 2010)
Methylene blue [MB] 50 mg L <sup>-1</sup> (10mL)	Nb-Hematite Fe <sub>2-x</sub> Nb <sub>x</sub> O <sub>3</sub> (10 g L <sup>-1</sup> )	0.3 molL <sup>-1</sup>	6.0	25	-	Low discoloration with pure hematite and Hm-Nb2, 70% color removal and 25% TOC removal after 60 min with Hm-Nb10.	(Silva et al., 2009)
Methylene blue [MB] 50 mg L <sup>-1</sup> (10mL)	Nb-hematite-maghemite treated by H <sub>2</sub> O <sub>2</sub> (1 g L <sup>-1</sup> )	8.0 mM 30% v/v	6.0	25	-	73% MB removal using treated catalyst compared to 30% MB removal by non-treated samples within 60 min.	(Silva et al., 2011)
Bromophenol Blue, Chicago Sky Blue, Evans Blue and Naphthol Blue Black [dye] 50 mg L <sup>-1</sup>	FeO-Fe <sub>2</sub> O <sub>3</sub> (25 mg mL <sup>-1</sup> )	100 mmol L <sup>-1</sup>	6.6	30	-	90% color removal within 24hours, the fast decomposition rate at first hour.	(Baldrian et al., 2006)

(continued on next page)

'Table 2.5, continued'

Compound	Catalyst	Operational condition				Optimal performance	References
		[H <sub>2</sub> O <sub>2</sub> ]	pH	T (°C)	λ (nm)		
Naphthol Blue Black [NBB] 500 mg L <sup>-1</sup> , COD <sub>0</sub> 1.80	MO-Fe <sub>2</sub> O <sub>3</sub> , (M: Mn,Co, Cu,Fe) 25 mg mL <sup>-1</sup>	100 mmol L <sup>-1</sup>	6.0-6.6	30	-	COD removal of 97%, 92%, 88% & 75% and color removal of 85%, 67%, 53% & 58% using the catalysts of Cu, Co, Fe & Mn respectively.	(Baldrian et al., 2006)
Dimethyl phthalate [DMP] 7.7 mgL <sup>-1</sup> (100ml)	Si-FeOOH 0.5 g L <sup>-1</sup>	2 mmol L <sup>-1</sup>	5.0	25	365	97% DMP degradation within 30 minutes.	(Yuan et al., 2011)
Methylene blue [MB] 50 mg L <sup>-1</sup>	Nb-FeOOH (11% Nb) 1 g L <sup>-1</sup>	0.3 molL <sup>-1</sup>	6.0	25	-	15% discoloration after 120 min by pure goethite, ≈ 85% color removal using Nb11-FeOOH within 120 min.	(Oliveira et al., 2008)
Quinoline [Q] 10 mg L <sup>-1</sup>	Ni-FeOOH 1 g L <sup>-1</sup>	0.1 ml 5% v/v	6.0	25	-	28% Q removal after 5h by pure goethite, 70% Q removal within 5h.	(de Souza et al., 2010)

The optimum ratio of incorporated active cation to iron species drives higher activities and the concentration above this value may not affect the activity remarkably. For example, (Yuan et al., 2011) observed that the amount of degraded dimethyl phthalate (DMP) by Si=FeOOH was the highest at Si/Fe ratio of 0.2 and both higher and lower values than 0.2 decreased degradation percentages. This is attributed to the decrease in UV transmission into the solution caused by the formation of suspended indigent catalyst particles at lower ratios; and at higher values, the active sites were covered with high concentrations of SiO<sub>2</sub> and resulted in lower  $\cdot$ OH radical generation from H<sub>2</sub>O<sub>2</sub>. Nevertheless, the increase in the amount of incorporated Mn and Co resulted in a considerable increase in the activity of the produced catalyst where Fe<sub>3</sub>O<sub>4</sub> (pure magnetite) showed lower activity compared to the Fe<sub>3-x</sub>Mn<sub>x</sub>O<sub>4</sub> and Fe<sub>3-x</sub>Co<sub>x</sub>O<sub>4</sub> catalysts and amongst them, Fe<sub>2.47</sub>Mn<sub>0.53</sub>O<sub>4</sub> and Fe<sub>2.25</sub>Co<sub>0.75</sub>O<sub>4</sub> represented the highest activity for the above mentioned reactions (Costa et al., 2003).

A mixture of natural niobia (Nb<sub>2</sub>O<sub>5</sub>) and iron oxides resulted in formation of a composite catalyst containing goethite ( $\alpha$ -FeOOH) and maghemite ( $\gamma$ -Fe<sub>2</sub>O<sub>3</sub>) as main constitutive iron oxides in its structure (Oliveira et al., 2007). The amount of Niobia in the composite affected the discoloration rate significantly when niobia/iron oxides of 1:5 could remove only 50% of the color of methylene blue solution while it increased up to 90% in ratio of 1:1.

## **2.6. Summary of literature review**

Fenton process, as a strong oxidation system amongst advanced oxidation processes, has been successfully applied for removal of recalcitrant compounds. However, a number of shortcomings such as pH limitations, catalyst recovery problem and formation of ferric hydroxide sludge are encountered in homogeneous systems. Several studies have reported the heterogeneous Fenton oxidation process as one of the possible

solutions to overcome these limitations (Munoz et al., 2015; Garrido-Ramírez et al., 2010). In a heterogeneous catalyst, iron is stabilized in the catalyst structure and can be used under neutral and unchanged pH conditions. Amongst them are iron oxides that are abundant on the earth crust, which has shown significant efficiency for organic pollutant removal. Magnetite, the Fe<sup>2+</sup>-Fe<sup>3+</sup> iron oxide, has been largely used as a heterogeneous catalyst, either pure or in a modified form. Recently, transition metal substituted magnetites (TMSMs) have received growing interest in treatment of wastewaters using Fenton reaction due to their higher adsorption capacity and reactivity in the reaction solution compared to pure magnetite. The changes in catalytic activity of modified magnetite samples have been reported to be due to the existence of thermodynamically favorable redox pairs of the imported cations on the surface of the catalysts. These redox pairs enhance Fenton degradation of probe molecule via (i) direct involvement in Fenton oxidation cycle and generation of <sup>•</sup>OH radicals through Haber-Weiss mechanism; (ii) regeneration of Fe<sup>+2</sup> cations and (iii) acceleration of electron transfer during the oxidation reaction in the magnetite structure. Generation of oxygen vacancies due to adjustments for unequal charge replacements or cationic deficiency in the structure of modified iron oxide was proposed by Costa et al. (2006) as another possible reason for enhanced activities (Costa et al., 2006). These vacancies act as active sites for direct involvement in degradation of probe molecules or indirectly in decomposition of H<sub>2</sub>O<sub>2</sub> (Magalhães et al., 2007). Other factors such as enlarged surface area and accordingly, higher concentrations of OH groups on the surface of the catalysts are also reported in number of studies (Liang et al., 2012a).

The reported studies have mainly focused on substitution of transition metals from the fourth row of the periodic table with single ion incorporation and in a few cases, two metals substitution have been studied. However, data related to incorporation of fifth period transition metals into magnetite and their subsequent application in Fenton

reaction, especially for co-doped ions, has not been reported. Therefore, this study will identify, synthesize and characterize TMSMs from period five using established methods and evaluate their effectiveness in Fenton oxidation of recalcitrant effluents.

University of Malaya



### 3. CHAPTER 3: MATERIALS AND METHODS

#### 3.1. Introduction

The following sections provide explanation and information about the materials and the procedures used in developing efficient heterogeneous catalysts for Fenton treatment of organic pollutants. Details of Fenton reaction optimization, modified magnetite preparation, characterization, evaluation of their oxidation performance, and kinetic studies are described here.

#### 3.2. Materials

All the chemicals were of reagent grade and used as received without further purification. All the solutions were prepared with deionized water. Methylene blue (MB), methyl orange (MO), hydrogen peroxide ( $H_2O_2$ , 30% w/w), potassium iodide (KI), sodium hydroxide (NaOH), sulfuric acid ( $H_2SO_4$ ), hydrochloric acid (HCl) and sodium chloride (NaCl) were purchased from Merck. Iron (II) chloride tetrahydrate ( $FeCl_2 \cdot 4H_2O$ ), ammonium niobate (V) oxalate hydrate ( $C_4H_4NNbO_9 \cdot xH_2O$ ), molybdenum (V) chloride ( $MoCl_5$ ), hydrazine, sodium sulfite ( $Na_2SO_3$ ), and sodium dihydrogen phosphate ( $NaH_2PO_4 \cdot H_2O$ ) were purchased from Sigma Aldrich. Sigma Aldrich also supplied commercial magnetite samples used in this research for optimization of the reaction.

#### 3.3. The application of response surface methodology to optimize the magnetite catalyzed Fenton reaction for treatment of methylene blue aqueous solution

##### 3.3.1. Experimental design and method of analysis

Response surface methodology (RSM) is suitable for fitting a quadratic surface with a minimum number of experiments and to analyse the interactions amongst the parameters. The software Design Expert 8.0.7.1 was used for the experimental design,

statistical analysis of data, development of regression models and optimization of Fenton-like reaction conditions. Here, RSM was used to assess the individual and interactive effects of five Factors (four numeric and one categorical) on the colour, COD and TOC removal efficiencies of Fenton reaction using methylene blue as probe molecule and two magnetite samples as catalyst. Central composite design (CCD) combined with RSM, was employed to optimize the independent variables in order to get the maximum values for the dependent variables. The ranges and the levels of the numerical independent variables are given in Table 3.1 that were chosen based on the preliminary studies and the literatures. For statistical calculations, Eq. 3-1 was used to convert actual values to their coded form (Aleboyeh et al., 2008):

$$x_i = \frac{(X_i - X_0)}{\delta X} \quad (3-1)$$

where  $x_i$ ,  $X_i$ ,  $X_0$  and  $\delta X$  are respectively the coded value of  $i^{\text{th}}$  independent variable, actual value, actual value at the centre point and the step change of the  $i^{\text{th}}$  variable. The coded values  $\pm 1$  give the relevant values of each factor in respect to the selected unit variation intervals for each factor (Khataee et al., 2010).

Table 3.1: Independent numerical variables and their levels

Independent numerical Variables	Symbol	Variable levels				
		-1	-0.5	0	0.5	+1
H <sub>2</sub> O <sub>2</sub> concentration (mol/L)	A	0.05	0.1	0.15	0.2	0.25
Catalyst concentration (g/L)	B	0.5	1.0	1.5	2.0	2.5
pH	C	2.5	4.0	5.5	7.0	8.5
Reaction time (h)	D	0.5	1.0	1.5	2.0	2.5

A total of 60 experiments were performed for both categorical variables in which 12 replications were at center points: H<sub>2</sub>O<sub>2</sub> concentration: 0.15 M, Catalyst concentration: 1.5 g/L, pH value: 5.5 and reaction time of 1.5 h, to determine the experimental error. In this design, Fenton efficiencies (%) for colour (Y<sub>MB</sub>), COD (Y<sub>COD</sub>) and TOC (Y<sub>TOC</sub>) removal were chosen as the responses. The following second order polynomial equation (Eq. 3-2) was used to predict the chosen responses as a function of independent variables and the interaction amongst them:

$$Y = b_0 + \sum_{i=1}^k b_i X_i + \sum_{i=1}^k b_{ii} X_i^2 + \sum_{i=1}^k \sum_{j=1}^k b_{ij} X_i X_j + \varepsilon \quad (3-2)$$

where, Y is the predicted dependent variable, b<sub>0</sub> is constant coefficient, b<sub>i</sub>, b<sub>ii</sub> and b<sub>ij</sub> are regression coefficients, i and j are index numbers, k is number of patterns, X<sub>i</sub>'s are independent variables and ε is the random error. The analysis of variance (ANOVA) was applied to test the significance and adequacy of the model. The fitness of the polynomial models was expressed by the coefficients of determination, R<sup>2</sup>, R<sup>2</sup><sub>adj</sub> and R<sup>2</sup><sub>pred</sub>. The main indicators that were used to show the significance of the model were Fisher variation ratio (F-value), probability value (*Prob* > *F*) with 95% confidence level and adequate precision using Eqs. 3-3 and 3-4 (Beltran Huarac):

$$Adequate\ Precision = \frac{\max(Y) - \min(Y)}{\sqrt{\bar{V}(Y)}} \quad (3-3)$$

$$\bar{V}(Y) = \frac{1}{n} \sum_{i=1}^n \bar{V}(Y) = \frac{p\sigma^2}{n} \quad (3-4)$$

In these equations,  $Y$  is predicted response,  $p$  and  $n$  are the number of model parameters and experiments and  $\sigma^2$  is the residual mean square. The final models for each categorical variable were obtained after elimination of insignificant terms ( $p > 0.05$ ) after F-test and the 3-D plots were presented for the corresponding responses based on the effects of four numerical factors (concentrations of  $\text{H}_2\text{O}_2$  and catalyst, pH and reaction time). Furthermore, the optimum values for independent variables were identified and additional experiments were performed to verify the regression models.

### 3.4. Preparation of magnetite samples

Figure 3.1 shows the equipment setup and appearance for preparation of magnetite samples by co-precipitation method. Prior to use, all water samples and solutions were deoxygenated by nitrogen bubbling. A modified work reported by Liang et al. (2012b) was used for samples preparation. For the synthesis of  $\text{Fe}_3\text{O}_4$ ,  $0.90 \text{ mol L}^{-1}$  of  $\text{FeCl}_2 \cdot 4\text{H}_2\text{O}$  dissolved in an HCl solution. 1.0 mL of hydrazine was added to prevent  $\text{Fe}^{2+}$  oxidation, and the pH was set below 1.0 to prevent  $\text{Fe}^{2+}$  oxidation, and hydroxide precipitation. This solution was heated to 90–100 °C. Equal volume of a solution containing  $4.0 \text{ mol L}^{-1}$  NaOH and  $0.90 \text{ mol L}^{-1}$   $\text{NaNO}_3$  was added drop-wise ( $10 \text{ mL min}^{-1}$ ) into the heated iron solution and the reaction was maintained at 90 °C for 2 h, while mechanically stirring at a rate of 500 rpm. Then the solution was cooled down to room temperature. During the reaction,  $\text{N}_2$  flux was passed through to prevent  $\text{Fe}^{2+}$  oxidation. The particles were then separated by centrifugation at 3500 rpm for 5 min and washed with boiling deionized water, followed by an additional centrifugation. After 3–4 washings, the particles were collected and dried in a vacuum oven at 100 °C for 24 h. The preparation of  $\text{Fe}_{3-x}\text{Nb}_x\text{O}_4$  ( $x=0.025, 0.05, 0.1, \text{ and } 0.2$ ) or  $\text{Fe}_{3-x}\text{Mo}_x\text{O}_4$  ( $x=0.5, 0.1, 0.2, \text{ and } 0.3$ ) samples also followed the above procedure, except for dissolving predetermined amount of  $\text{MoCl}_5$  in HCl solution with  $\text{FeCl}_2 \cdot 4\text{H}_2\text{O}$  or

$C_4H_8N_2NbO_{11}$  in basic solution. For the preparation of  $Fe_{3-x-y}Nb_xMo_yO_4$  ( $x=0.025, 0.05, 0.1, 0.15, \text{ and } 0.175, x+y=0.2$ ) samples, predetermined amount of  $MoCl_5$  is dissolved in HCl and Nb in basic solution and followed the same procedure. All the samples were grounded and passed through a 200 mesh screen.

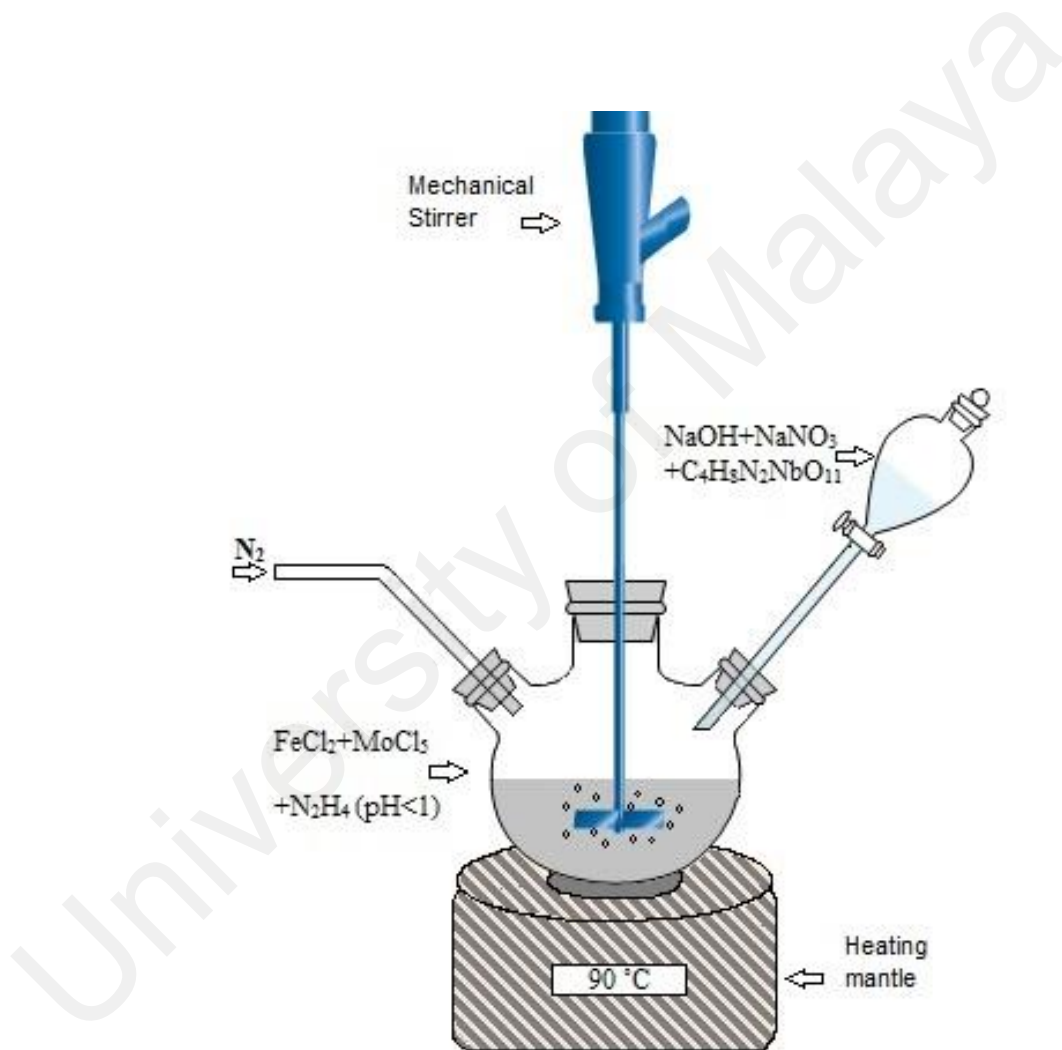


Figure 3.1: Equipment setup and appearance for preparation of modified magnetite samples

### **3.5. Characterization of the samples**

The main physico-chemical characteristics of the synthesized catalysts were determined for better understanding of their activities in Fenton oxidation of selected dye solutions. Accordingly, the following techniques and methods used to characterize the samples in terms of durability, crystalline phase, morphology, size, surface area, and composition and magnetic property.

#### **3.5.1. Crystalline phase determination with X-ray diffraction (XRD)**

The X-ray diffraction or XRD gives information regarding crystalline phase and the constituents of the cell of the studied solid samples. This method is based on the principles of the diffracted light over a sample bombarded by short wavelength X-rays. The magnetite samples were analyzed with powder X-ray diffraction (XRD) to determine the crystalline phase of them using a PANalytical Empyrean (DY 1032) diffractometer with Cu K $\alpha$  radiation ( $\lambda = 0.15418$  nm). The XRD data were collected from  $20^\circ$  to  $80^\circ$  ( $2\theta$ ).

#### **3.5.2. Surface area (Brunauer–Emmett–Teller (BET)) and particle size analyzer**

In heterogeneous catalysis, determination of the surface area of the catalyst is very important because the activity of a catalyst directly related to the available surface area. The surface area of the samples was determined using Brunauer–Emmett–Teller BET-surface area method (Micromeritics, tristar II 3020). BET technique is generally based on the physical adsorption of nitrogen at low temperature in which the gas uptake is measured under increasing the nitrogen partial pressure in contact with the powder sample and the desorption of nitrogen (Garriga I Cabo 2007). The pore volumes and pore sizes were also measured.

Malvern, Zetasizer Nano-range, particle size analyzer was used to measure the particle size of the synthesized samples.

### **3.5.3. Transmission electron microscopy (TEM)**

Transmission electron microscopy (TEM) used to investigate surface morphology and particle sizes of the samples. The TEM micrographs were obtained on a Hitachi H-7100 electron microscope (Veleta).

### **3.5.4. X-ray photoelectron spectroscopy (XPS)**

X-ray photoelectron spectroscopy (XPS) is a surface characterization technique especially for determination of the oxidation states of the elements present on the surface or near surface of the sample. The XPS measurements were performed with a CLAM II-VG electron analyzer and a non-monochromatic Al K $\alpha$  (1486.6 eV) source. The C 1s line of spurious carbon located at the binding energy of 284.6 eV used as a reference to correct binding energies for the charge shift.

### **3.5.5. Vibrating sample magnetometer (VSM)**

Vibrating sample magnetometer (VSM) (Lakeshore VSM, 7400 Series) was used to study the magnetic properties of the prepared samples. The powder sample was placed in a glass ampoule (measuring cap) mounted in VSM and was fixed in paraffin in order to exclude the motion of powder. Moment Vs field measurement for 40-45 mg of the samples was taken at room temperature and applied Field Range of  $\pm 10000$  G. When the sample was placed in that magnetic field B, a magnetic moment 'm' or magnetization 'M' (magnetic moment per unit volume) was induced which related to B. The magnetic moment vs. Magnetization curve plotted for each sample and the magnetization variations were studied. The hysteresis parameters such as saturation magnetization ( $M_s$ ), coercivity ( $H_{ci}$ ) and remnant magnetism ( $M_r$ ) were measured.

### 3.5.6. PH of point of zero charge (pH<sub>pzc</sub>)

The point of zero charge (pH<sub>PZC</sub>) of the samples was determined by the solid addition method. To a series of 250 mL conical flasks, 45 mL of 0.1 mol L<sup>-1</sup> NaCl solution was transferred. The initial pH values (pH<sub>i</sub>) of the solution were adjusted from 4.0 to 11.0 by adding either 0.1 mol L<sup>-1</sup> HCl or 0.1 mol L<sup>-1</sup> NaOH. The total volume of the solution in each flask was made exactly to 50 mL by adding the NaCl solution. Then, 0.05 g of each sample was added to each flask and the mixtures were agitated at 170 rpm. After 24 h, the final pH values (pH<sub>f</sub>) of the solutions were measured. The difference between the initial and final pH values (\*pH = pH<sub>i</sub> - pH<sub>f</sub>) was plotted against the pH<sub>i</sub>. The point of intersection of the resulting curve with abscissa, at which \*pH=0, gave the pH<sub>PZC</sub> (Ai et al., 2011).

### 3.6. Adsorption experiments

MB and MO adsorption studies on the modified magnetite samples were carried out in batch system at 25 °C. The initial pH of dye solution was adjusted to desired value by H<sub>2</sub>SO<sub>4</sub> or NaOH solutions. To assess the effects of initial dye concentration on adsorption efficiency, 1 g L<sup>-1</sup> of each sample was added to varying concentrations of dye solution (12.5, 50, 75, and 100 mg L<sup>-1</sup>) and constantly stirred mechanically at 170 rpm for 120 min, to achieve sorption equilibrium. Then the adsorbent was separated by centrifugation at 3500 rpm for 5 min and the equilibrium concentration of MB or MO was determined by UV-vis spectrophotometer (Spectroquant® Pharo 300) at λ<sub>max</sub> 664 and 462 nm, respectively. Prior to the measurement, a calibration curve was obtained using standard MB or MO solutions with the known concentrations that shows a liner relationship between absorbance and MB/MO concentrations. The amount of MB/MO adsorbed per unit mass of magnetite samples were calculated using the following equation (Eq. 3-5):



$$q_e = \frac{(C_0 - C_e)V}{m} \quad (3-5)$$

where  $C_0$  and  $C_e$  are the initial and equilibrium concentrations of MB/MO ( $\text{mg L}^{-1}$ ) in liquid phase,  $m$  is the mass of dry magnetite sample (g), and  $V$  is the volume of solution (L).

Adsorption experiments versus pH were performed with a single initial solute concentration in a 200 mL reaction vessel at varying pH values (4.0, 7.0, 8.0, and 10) and  $25^\circ\text{C}$  temperature. The pH was controlled by adding HCl or NaOH to the stock solid suspensions.

Prior to UV/Fenton and US/Fenton reactions, the amount of adsorbed MB and MO on the selected catalysts was investigated using  $0.5 \text{ g L}^{-1}$  of each sample into  $50 \text{ mg L}^{-1}$  of the studied dye solutions and stirred mechanically for 2 h at 170 rpm to achieve adsorption equilibrium.

### **3.7. Heterogeneous Fenton reactions**

All dye oxidation experiments were carried out in batch systems using 250 ml Pyrex beakers with a solution volume of 100 ml of the studied dye solution (50 or 100 ppm) at room temperature. First, the pH of the solution was adjusted at selected value by sodium hydroxide (NaOH, 0.1 M) or sulphuric acid ( $\text{H}_2\text{SO}_4$ , 0.1 M) using pH-meter (EUTECH, CyberScan pH 300). Then, the selected amount of each synthesized sample is added to the dye solution and is stirred mechanically for 2 h at 170 rpm to achieve adsorption equilibrium. The Fenton reaction was initiated by the addition of  $\text{H}_2\text{O}_2$  and continued for additional 180 minutes. Then, the sample was centrifuged for 5 minutes at 3500 rpm and supernatant was filtered through  $0.20 \mu\text{m}$  (nylon, Whatman) filters to remove catalyst particles. Dye concentration was immediately measured using UV-Vis

spectrophotometer (Spec-troquant ® Pharo 300) at  $\lambda_{\max}$  664 nm for MB and 462 nm for MO.

Heterogeneous UV/Fenton treatment of the studied dye solutions was carried out in batch using a lab-scale photo-reactor at two wavelengths of 365 nm (UV-A) and 302 nm (UV-B). In US/Fenton reaction, a 24 kHz commercial ultrasonic processor (Ultrasonic Processor model UP400S; Dr. Hielscher GmbH, Stuttgart, Germany) was used in a power of 100 W. In a typical run, the probe was immersed in a 150 mL cylindrical glass vessel containing 100 ml of MB or MO (50 mg/L). Reaction was timed as soon as the ultrasonicator was turned on.

In order to measure the amount of TOC, a stopping reagent with no carbon-containing compound, comprising of  $\text{Na}_2\text{SO}_3$  (0.1 M),  $\text{NaH}_2\text{PO}_4$  (0.1 M), KI (0.1 M) and NaOH (0.05 M) was added to the sample solutions, right after filtration and in a volume ratio of 1:1. Thereafter, the TOC values were obtained by a TOC analyzer (Shimadzu TOC-L CPH CN 200, Japan) equipped with an auto-sampler. All experimental runs were performed at room temperature and in the absence of light. The measurements were done at least twice and the results were expressed as a mean value of the measurements with an experimental error below 5%. The following equation (Eq. 3-6) was used to calculate the percentages of colour and TOC removals:

$$\text{removal}(\%) = \frac{(X_0 - X_i)}{X_0} \times 100 \quad (3-6)$$

here,  $X_0$  is the initial values of Colour or TOC and  $X_i$  is the measured values of Colour, or TOC after defined reaction time.

### **3.8. Stability experiments**

The stability of magnetite samples and the possibility of homogeneous Fenton oxidation route were investigated through leaching of iron, molybdenum and/or niobium from magnetite samples, at studied pH values using a modified procedure (Ai et al., 2011). 0.02 g of magnetite samples were dispersed in 100 mL aqueous solution with known pH values (4, 7, 8, and 10) and agitated in a temperature-controlled shaker for 3 h. In US/Fenton and UV/Fenton-like reactions, the stability was examined by measuring iron, niobium and molybdenum dissolved in the medium after the reactions. The leached Fe, Nb and Mo concentrations in supernatant were determined by Optical Emission Spectrometer (ICP-OES Perkin Elmer, Optima 7000 DV).

### **3.9. Kinetic studies**

The following sections provide information about the procedures used to study the adsorption and degradation of MB using synthesized samples and through Fenton-like reaction.

#### **3.9.1. Kinetic experiments of MB adsorption on the synthesized samples**

Batch kinetic experiments of MB adsorption were carried out by mixing 1 g L<sup>-1</sup> of a synthesized sample to MB solution with a known initial concentration at neutral pH condition and agitated in a shaker at 25 °C for different time interval (10–120 min). The concentration of MB left in the supernatant solution was analyzed using UV–Vis spectrophotometer (Spec-troquant ® Pharo 300) at  $\lambda_{\max}$  664 nm.

#### **3.9.2. Degradation kinetic experiments**

Batch kinetic experiments were carried out by mixing 1 g L<sup>-1</sup> in dark-Fenton and 0.5 g L<sup>-1</sup> in UV/Fenton and US/Fenton reactions to MB solution with a known initial concentration (12.5, 25, 50, and 100 mg L<sup>-1</sup>) at pH value of 7 and agitated in a shaker at

25 °C for different time interval (10–180 min). The concentration of MB left in the supernatant solution was analyzed using Eq. (3-6).

For US and UV assisted Fenton oxidation of MB, kinetic studies were carried out by mixing 0.5 g L<sup>-1</sup> of magnetite sample into MB solution (50 mg L<sup>-1</sup>) at pH 7 and agitated in a shaker at 25 °C for different time intervals (10–200 min). The concentration of MB left in the supernatant solution was determined using Eq. (3-6).

### 3.9.3. Kinetic models

Large number of kinetic models with diverse degrees of complexity have been established to describe the adsorption and degradation processes quantitatively. Because of this complexity, the experimental results are commonly fitted to a number of conventional kinetic models and the model with the best fit is selected (Loganathan et al., 2014; Guerrero & Sayari, 2010). Consequently, three of the most common kinetic models, zero-order, pseudo-first-order and pseudo-second-order models, that have been previously employed in the similar studies to define the adsorption or degradation rate behaviors were used in the present study.

Two commonly reported models for adsorption kinetics in the literature are pseudo-first-order and pseudo-second-order models. The linear forms of these models are as follows:

$$\log(q_e - q_t) = \frac{\log q_e - k_1 t}{2.303} \quad (3-7)$$

$$\frac{1}{q_t} = \frac{1}{K_2 q_e^2} + \frac{1}{q_e t} \quad (3-8)$$

where  $q_t$  and  $q_e$  ( $\text{mg g}^{-1}$ ) are the amounts of MB adsorbed at time  $t$  (min) and equilibrium, respectively.  $k_1$  ( $\text{min}^{-1}$ ) and  $k_2$  ( $\text{g mg}^{-1} \text{min}^{-1}$ ) are respectively the pseudo-first-order and the pseudo-second-order rate constants.

Zero-order and pseudo-first-order models are the most reported kinetic models in the literature for MB degradation through Fenton reaction using transition metal substituted magnetite catalysts. The following equations are the linear forms of zero-order (Eq. 3-9) and pseudo-first-order (Eq. 3-10) models:

$$C_0 - C_t = k_0 t \quad (3-9)$$

$$-\ln\left(\frac{C_t}{C_0}\right) = k_1 t \quad (3-10)$$

where  $C_0$  and  $C_t$  are the MB concentrations ( $\text{mg L}^{-1}$ ) at the initial time and reaction time  $t$ ,  $k_0$  and  $k_1$  are zero-order rate constant ( $\text{mg L}^{-1} \text{min}^{-1}$ ) and pseudo-first-order rate constant ( $\text{min}^{-1}$ ). The  $k_0$  and  $k_1$  constants were obtained from the slope of the straight lines by plotting  $C_0 - C_t$  and  $-\ln(C_t/C_0)$  as a function of time  $t$ , through regression.

Subsequently, the experimental data were fitted to these kinetic models in order to determine the parameters of each set of the kinetic models. In this study, a linear regression analysis using the Marquardt-Levenberg algorithm implemented in SigmaPlot software version 12.0 (Systat Software Inc., USA) was used. Then, two different error functions, the linear regression coefficient ( $R^2$ ) and the normalized standard deviation ( $Err$  (%)) were estimated to compare the goodness of fit of the experimental results with the kinetic models:

The regression coefficient ( $R^2$ ) was calculated using the following equation (Stevens et al., 2013):

$$R^2 = 1 - \left( \frac{\sum_{i=1}^n (q_{t(mes)} - q_{t(mod)})^2}{\sum_{i=1}^n (q_{t(mes)} - \overline{q_{t(mes)}})^2} \right) \cdot \left( \frac{n-1}{n-p} \right) \quad (3-11)$$

where  $n$  is the number of experimental adsorption points of the kinetic curves, the subscripts “*mod*” and “*mes*” refer to the model predicted and measured values of the amount adsorbed, respectively,  $\overline{q_{t(mes)}}$  is the average of the experimental data, and  $p$  is the number of parameters of the model.

The normalized standard deviation, which is the deviation between the experimental results and the values predicted by the kinetic models, was calculated by Eq. 3-12 (Vargas et al., 2011):

$$Err (\%) = 1 / N \sum_{i=1}^N \left| \frac{(q_{cal} - q_{exp})}{q_{exp}} \right| \times 100 \quad (3-12)$$

where, the subscripts “*exp*” and “*cal*” are the experimental and calculated values of  $q$ , respectively and  $N$  is the number of data points.

### 3.10. Safety

Throughout the experiments, care was taken to prevent the health, fire, reactivity, and contact hazards associated with all the chemicals and hazards associated with all the equipment and instruments (including ultrasound and UV radiation) used in the research project. Besides, normal laboratory safety precaution procedures including the use of appropriate personal protective equipment and use of standard operating procedures and waste disposal system is followed to eliminate and minimize the risk.

## CHAPTER 4: RESULTS AND DISCUSSION

### 4.1. Introduction

Transition metal substituted iron oxides have been introduced as promising Fenton catalysts for treatment of recalcitrant wastewaters. Most existing literature focused on magnetite due to the presence of  $\text{Fe}^{\text{II}}$  and octahedral sites in its structure that are the key reasons for higher activity of magnetite. In this category of catalysts, iron is substituted isomorphically by other transition metal/metals such as Cr, Co, Ti, V and Mn in magnetite sites (octahedral and/or tetrahedral). Based on the articles reviewed, the previous studies are primarily concentrated on the transition metals from forth series of the periodic table. Accordingly, two transition metals from fifth series of periodic table, niobium (Nb) and molybdenum (Mo), were chosen in this study. Consequently, their influence was investigated on the physico-chemical properties and activity of magnetite in Fenton treatment of methylene blue (MB) solution. At first, Fenton oxidation of MB optimized by response surface methodology (RSM) using unmodified magnetite samples. It was to compare the changes in the activity of the modified samples with pure magnetite under the same operational conditions. Subsequently, two commercial magnetite samples (M and N) with different particle sizes were used to consider the effects surface area on the activity of magnetite and in optimizing process.

### 4.2. Application of RSM to optimize the magnetite catalyzed Fenton reaction for treatment of methylene blue aqueous solution

#### 4.2.1. ANOVA analysis

The results obtained from Fenton-like experiments for the studied dependent variables using either magnetite sample M or N presented in Table 4.1. A series of mathematical

models suggested with the CCD analysis, based on the experimental results. The color ( $Y_{MB}$ ), COD ( $Y_{COD}$ ) and TOC ( $Y_{TOC}$ ) removal efficiencies (%) were assessed as a function of the concentrations of  $H_2O_2$  (A) and magnetite (B), the initial pH (C) and reaction time (D). The developed equations are sum of a constant value, linear terms and interaction effects with quadratic terms as shown in Eq. 3-2.

Table 4.1: Experimental design matrix and the outputs

Run No.	Experimental design					Results (removal (%))		
	$H_2O_2$ (A) (mol L <sup>-1</sup> )	Fe (B) (g L <sup>-1</sup> )	pH (C)	Time (D) (h)	$X_5$ (E)	Color	COD	TOC
1	0.1	2	7	1	N	48	36	26
2	0.15	1.5	5.5	1.5	M	55	44	32
3	0.1	1	4	2	N	28	21	11
4	0.1	1	4	1	N	27	19	12
5	0.15	1.5	5.5	0.5	M	22	14	8
6	0.2	2	4	2	M	73	62	44
7	0.1	2	4	2	N	49	37	27
8	0.2	1	4	2	M	74	63	44
9	0.2	1	7	2	N	80	71	47
10	0.15	2.5	5.5	1.5	N	54	43	29
11	0.1	2	7	2	N	56	45	32
12	0.2	2	4	2	N	75	63	43
13	0.2	2	4	1	M	66	55	39
14	0.2	2	7	1	M	67	56	40
15	0.2	1	7	1	N	77	66	45
16	0.15	0.5	5.5	1.5	N	30	22	14
17	0.1	2	7	1	M	20	13	6
18	0.15	1.5	5.5	1.5	N	65	55	38
19	0.15	1.5	5.5	2.5	N	71	59	42
20	0.2	1	7	1	M	68	57	40
21	0.2	2	7	2	M	74	62	41
22	0.05	1.5	5.5	1.5	M	8	2	1
23	0.2	2	4	1	N	70	58	42
24	0.2	1	7	2	M	74	62	45
25	0.25	1.5	5.5	1.5	M	77	64.79	45.04
26	0.1	1	7	2	N	55	43.54	31.72
27	0.15	1.5	5.5	1.5	M	57	45.92	30.11
28	0.1	2	7	2	M	42	32.32	23.03
29	0.15	1.5	5.5	1.5	M	58	48.29	32.82
30	0.15	1.5	8.5	1.5	N	26	14.97	12.16
31	0.2	1	4	2	N	77	65.31	45.32
32	0.1	1	7	2	M	52	40.48	28.94
33	0.15	2.5	5.5	1.5	M	32	23.81	14.73
34	0.15	1.5	5.5	0.5	N	35	25	17

(continued on next page)



‘Table 4.1, continued’

Run No.	Experimental design					Results (removal (%))		
	H <sub>2</sub> O <sub>2</sub> (A) (mol L <sup>-1</sup> )	Fe (B) (g L <sup>-1</sup> )	pH (C)	Time (D) (h)	X <sub>5</sub> (E)	Color	COD	TOC
35	0.15	1.5	5.5	1.5	M	61	49	34
36	0.15	1.5	5.5	1.5	N	64	54	38
37	0.15	0.5	5.5	1.5	M	21	13	8
38	0.1	1	7	1	N	30	22	13
39	0.15	1.5	8.5	1.5	M	18	10	4
40	0.15	1.5	5.5	1.5	N	65	55	37
41	0.1	1	4	1	M	19	11	4
42	0.15	1.5	5.5	1.5	M	57	45	33
43	0.15	1.5	2.5	1.5	M	11	5	2
44	0.15	1.5	5.5	1.5	M	58	47	33
45	0.25	1.5	5.5	1.5	N	79	69	47
46	0.15	1.5	5.5	2.5	M	65	55	38
47	0.15	1.5	5.5	1.5	N	64	53	39
48	0.1	1	7	1	M	22	14	6
49	0.2	2	7	2	N	78	66	46
50	0.1	1	4	2	M	36	27	17
51	0.1	2	4	1	M	9	3	1
52	0.1	2	4	1	N	19	12	5
53	0.2	1	4	1	M	65	55	38
54	0.2	1	4	1	N	68	57	40
55	0.15	1.5	5.5	1.5	N	62	51	36
56	0.1	2	4	2	M	32	23	16
57	0.15	1.5	5.5	1.5	N	63	53	36
58	0.05	1.5	5.5	1.5	N	14	5	3
59	0.15	1.5	2.5	1.5	N	22	14	8
60	0.2	2	7	1	N	73	61.56	43.78

To assess the “goodness of Fit” of the model, the obtained results were analysed by ANOVA. The statistically significant model terms ( $p < 0.05$ ) were included in the models and the rest were eliminated manually to improve the regression model (Shafeeyan et al., 2012). For instance, the term BC was insignificant to the  $Y_{TOC}$  whereas it was significant to  $Y_{MB}$  and  $Y_{COD}$  and the interaction between the variables B and D were insignificant model term in all the responses. The final models (Eqs. 4–1 to 4–6) in terms of actual values, for both categorical factors, presented in Table 4.2.

Table 4.2: Final quadratic models for both categorical factors

Sample	Response	Equation	Eq.
M	Y <sub>Color</sub>	$-213.44966 + 947.13200 A + 37.98612 B + 44.77312 C + 2.49128 D - 17.17500 AB - 70.84167 AC - 34.07500 AD + 1.00083 BC + 1.66750 CD - 516.67610 A^2 - 12.77676 B^2 - 3.19575 C^2 + 3.00131 D^2$	4-1
	Y <sub>COD</sub>	$-215.02688 + 937.04811 A + 36.43106 B + 41.96307 C + 3.97461 D - 64.91667 AC - 42.50000 AD + 0.86417 BC + 1.55750 CD - 633.16038 A^2 - 12.73660 B^2 - 3.00934 C^2 + 3.00302 D^2$	4-2
	Y <sub>TOC</sub>	$-177.79715 + 744.58660 A + 30.83199 B + 33.54394 C + 5.92035 D - 14.08750 AB - 70.84167 AC - 34.07500 AD + 1.00083 BC + 1.66750 CD - 516.67610 A^2 - 12.77676 B^2 - 3.19575 C^2 + 3.00131 D^2$	4-3
N	Y <sub>Color</sub>	$-200.88506 + 947.13200 A + 37.98612 B + 46.19701 C - 5.63616 D - 17.17500 AB - 70.84167 AC - 34.07500 AD + 1.00083 BC + 1.66750 CD - 516.67610 A^2 - 12.77676 B^2 - 3.19575 C^2 + 3.00131 D^2$	4-4
	Y <sub>COD</sub>	$-198.35721 + 919.84811 A + 35.13606 B + 43.36752 C - 3.85164 D - 64.91667 AC - 42.50000 AD + 0.86417 BC + 1.55750 CD - 633.16038 A^2 - 12.73660 B^2 - 3.00934 C^2 + 3.00302 D^2$	4-5
	Y <sub>TOC</sub>	$-161.75894 + 720.11160 A + 29.94449 B + 34.45644 C - 0.71669 D - 14.08750 AB - 52.02917 A - 39.23750 AD + 0.97042 CD - 463.87893 A^2 - 8.68379 B^2 - 2.27903 C^2 + 1.99770 D^2$	4-6

The negative and positive signs in the equations indicate antagonistic or synergistic effects respectively. An ANOVA analysis was carried out for each dependent variable and the results were given in Table (4-3). From the results, the  $p$ -values for all responses were less than 0.05 ( $< 0.0001$  in all cases) that shows the models are significant for prediction of response values. Accordingly, the quality of the developed equations was evaluated based on regression coefficients,  $R^2$ ,  $R_{adj}^2$  and  $R_{pred}^2$ . The  $R_{adj}^2$  shows the total variation of the responses that can be explained with the developed models and are 86.73%, 86.37% and 86.06% for the responses  $Y_{MB}$ ,  $Y_{COD}$  and  $Y_{TOC}$  respectively. The proportion of the total variation in the predicted response is given by  $R^2$  coefficient. The  $R^2$  value close to 1.0 is desirable and shows the acceptable adjustment of the suggested model with experimental data. In this study, the results were found in good agreement where the difference between adjusted  $R^2$  and predicted  $R^2$  were close to each other and less than 0.2 (Arami-Niya et al., 2012). The adequate precision measures the signal to noise ratio and the ratio greater than 4.0 is desirable. The adequate precision values derived from the analysis were 20.81, 19.64 and 19.86 ( $\gg 4$ ) for the studied responses, indicating an adequate signal and shows that the models can be used to navigate the design space.

Table 4. 3: Analysis of variance (ANOVA) results for responses

Response	Final equation in terms of coded values	PE <sup>1</sup>	LOF <sup>2</sup>	R <sup>2</sup>	R <sub>adj</sub> <sup>2</sup>	R <sub>pred</sub> <sup>2</sup>	AP <sup>3</sup>	S.D <sup>4</sup>	CV (%)	PRESS
Y <sub>MB</sub>	+ 61.44 + 16.28A + 1.29B + 5.56C + 5.75D + 4.10E - 0.43AB - 5.31AC - 0.85AD + 0.75BC + 1.25CD + 1.07CE - 2.03 DE - 1.29A <sup>2</sup> - 3.19B <sup>2</sup> - 7.19C <sup>2</sup> + 0.75D <sup>2</sup>	<0.0001	47.42	0.9033	0.8673	0.7829	20.809	7.31	13.94	5159.51
Y <sub>COD</sub>	+ 50.68 + 15.89A + 1.16B + 5.19C + 5.63D + 4.07E - 4.87AC - 1.06AD - 0.43 AE + 0.65 BC - 0.32BE + 1.17 CD + 1.05 CE - 1.96DE - 1.58A <sup>2</sup> - 3.18B <sup>2</sup> - 6.77C <sup>2</sup> + 0.75D <sup>2</sup>	<0.0001	43.20	0.9030	0.8637	0.7625	19.639	7.17	17.16	5288.42
Y <sub>TOC</sub>	35.22 + 11.35A + 1.11B + 3.87C + 4.02D + 3.05E - 0.35AB - 3.90AC - 0.98AD - 0.61AE - 0.22BE + 0.73CD - 0.22BE + 0.73CD + 0.68 CE - 1.66 DE - 1.16A <sup>2</sup> - 2.17B <sup>2</sup> - 5.13C <sup>2</sup> + 0.50D <sup>2</sup>	<0.0001	30.75	0.9008	0.8606	0.7572	19.859	5.29	18.48	2879.82

1.P value, Prob>F; 2. Lack of fit value; 3. Adequate precision; 4. Standard deviation

## 4.2.2. Evaluation of the effects of independent variables on the responses

### 4.2.2.1. Effects of Fenton reagents

From the response surface analysis, it can be seen that the variables were involved directly and indirectly in methylene blue decolorization, degradation and mineralization via Fenton-like oxidation system. In order to assess the effects of the variables on the removal efficiencies, 3-D graphs were developed. Figures (A.B1<sub>a-f</sub>), (A.B2<sub>a-f</sub>) and (A.B3<sub>a-f</sub>) illustrate the response surface plots of decolorization ( $Y_{MB}$ ), COD ( $Y_{COD}$ ) and TOC ( $Y_{TOC}$ ) removal efficiencies as a function of the combined synergistic or antagonistic effects of significant terms in the regression models. In general, the combined effects of the variables represented a similar trend in all the studied responses. The results imply that  $H_2O_2$  concentration had the highest effect on the oxidation of methylene blue. From the figures, it can be seen that the removal efficiencies (%) increased significantly with the raise in the concentration of  $H_2O_2$  from 0.05 to 0.2 M, whereas, further increase from 0.2 to 0.25 M did not contribute to significant change in oxidation results. This can be explained by the hydroxyl radical scavenging effects of hydrogen peroxide at higher concentrations ( $K_{OH,H_2O_2} = 1.2\text{--}4.5 \times 10^7 \text{ M}^{-1} \text{ s}^{-1}$ ) (Sun et al., 2013).

On the other hand, the catalyst also played a vital role in the process. It can be observed that the catalyst concentration of  $\approx 2.0 \text{ g L}^{-1}$  in synergistic interaction with higher levels of  $H_2O_2$  (0.2 M) and at the solution's neutral pH lead to maximum Fenton efficiency for methylene blue oxidation within 2 h of reaction. The oxidation efficiency was significantly decreased when the catalyst concentration increased to above  $2.0 \text{ g L}^{-1}$ . For instance, reaction conditions of  $H_2O_2$ : 0.15 M, Cat:  $1.5 \text{ g L}^{-1}$ , pH: 5.5 and time: 1.5 h, brought about 65.32 %, 54.76 % and 37.96 % removal of color, COD and TOC of the

methylene blue solution respectively; whereas the responses decreased dramatically to 49.68 %, 37.29 % and 27.29 % when the catalyst concentration was almost doubled. This can be attributed to the scavenging of  $\cdot\text{OH}$  radicals over the surface of catalyst. The results display that the Fenton efficiency is greatly affected by catalyst concentration in presence of sufficient hydrogen peroxide (Mitsika et al., 2013). In addition, it can be observed that over 40 % of the oxidation occurred within 30 minutes and it rise to above 60% at the first hour of the reaction. The optimum reaction time of the 2 h was suggested with the software, to maintain higher performance efficiencies over the optimum concentrations of Fenton reagents.

#### **4.2.2.2. Effect of the solution pH**

As explained earlier, the pH of the point of zero charge of the catalyst plays a significant role in adsorption of the probe molecule in reaction medium. In this study, the initial pH also had significant effect on Fenton-like efficacy for oxidation of MB over the studied range of variables. The activity of the catalyst increased at neutral pH compared to acidic solutions. This can be ascribed based on PZC of the magnetite that is about 6.0-6.8 (Cornell and Schwertmann, 2003; Sun et al., 1998). Since MB is a cationic dye, its adsorption onto the magnetite surface is increased at pH values higher than  $\text{pH}_{\text{pzc}}$  ( $\text{pH} > 6.0$ ) and at  $\text{pH} < 6.0$  will be decreased due to the charge repulsion. From the results, the higher removal efficiencies have been obtained over neutral pH values. Opposite to the results that were generally obtained for homogeneous Fenton treatment of contaminants in literature, acidic condition did not result in higher degradation of MB over magnetite samples. In addition to elimination of acidification and subsequent neutralization step with magnetite, it should be pointed out that magnetite have demonstrated acceptable scores over wide pH values due to the stability of iron species inside the catalyst structure. Similar results were obtained with Sun et al.

(2014) when they studied the application of nano-Fe<sub>3</sub>O<sub>4</sub> for degradation of carbamazepine over the pH range: 5.0 to 9.0. Accordingly, the pH value of 7.0 was chosen as target value in optimization process.

#### **4.2.3. Fenton process optimization**

The optimum conditions were determined based on the best combination of factor levels to obtain maximum amounts for the studied dependent variables, using the optimization function in the DOE software. In addition, this would help to conclude which catalyst represents better removal efficiency in the studied process. The chosen criteria for optimization purpose were as “maximize” for responses (Color, COD and TOC removal %), “within the range” for Fenton reagents and reaction time and “target” pH value of 7.0. In the next step, these targets applied to find the optimum conditions with the higher desirability. The identified optimal conditions for the sample N and M were H<sub>2</sub>O<sub>2</sub>: 2.0 mol L<sup>-1</sup>, catalyst: 1.6 g L<sup>-1</sup>, pH: 7.0 and reaction time: 2.00 h with the peak desirability values: 97.3 % and 92.5 %. The values of color % removal: 73.43 and 79.71, COD % removal: 62.59 and 67.92, and TOC % removal: 43.17 and 46.01 were predicted at optimum points for the samples M and N respectively. Six additional experiments conducted under the CCD-predicted optimum conditions to confirm the validity of the procedure and the accuracy of the quadratic models. The mean values of the experimental results and the predicted values by the regression models are given in Table 4.4. As can be seen in the table, the deviation errors between the all experimental and predicted values were less than 5% and in a close agreement with one another. It indicates that the developed CCD models can correlate the reaction factors to studied responses with high accuracy. It is evident from the both experimental results and developed models that magnetite sample N performed well in Fenton process with respect to decolorization, degradation and mineralization of methylene blue solution.

This indicates that the differences in physical properties, especially in surface area, of the magnetite samples in the studied conditions have significant effects on their activity in Fenton-like reaction.

Table 4.4: Predicted and experimental values of the studied responses at optimum conditions for both the magnetite samples

Response	Experimental results		Predicted values		Error (%)	
	M	N	M	N	M	N
Colour removal efficiency (%)	73.62	78.06	73.43	79.71	0.26	2.07
COD removal efficiency (%)	62.92	68.14	62.59	67.92	0.52	0.32
TOC removal efficiency (%)	44.28	47.16	43.17	46.01	2.51	2.44

Based on the obtained results in this step and the preliminary experiments, the conditions of  $[H_2O_2]_0$ : 2.0 mol L<sup>-1</sup>, catalyst: 1.0 g L<sup>-1</sup>, reaction time: 3 h and neutral pH were chosen as Fenton optimal conditions for the subsequent experiments using synthesized magnetite samples.

### 4.3. Niobium-substituted-magnetite (Fe<sub>3-x</sub>Nb<sub>x</sub>O<sub>4</sub>)

Niobium (previously columbium) is a transition metal with atomic number of 41 and one electron in its last electron shell. Its main application is in the field of superconductivity in alloy with Ti and Al (Kneisel et al., 2015). This metal was chosen in this study for some reasons: (i) No comprehensive study on the effects of Nb incorporation on physico-chemical characteristics of magnetite and its application in Fenton reaction (ii) the similar ionic radius of Nb to iron species (Nb<sup>+4</sup> (68 pm) and Nb<sup>+5</sup> (64 pm) vs. Fe<sup>2+</sup> (61 pm) Fe<sup>+3</sup> (55 pm)); therefore, it can theoretically replace iron in magnetite structure (isomorphic); (iii) the same crystal structure of Nb as Fe (body centered cubic structure) and (iv) its paramagnetic characteristic, thus can be attracted to



external magnetic field. One of the main study objectives was to assess the effects of the changes in magnetite using a very small amount of Nb. On this basis,  $x=0.2$  was chosen as the maximum value of incorporated Nb. Subsequently, a series of  $\text{Fe}_{3-x}\text{Nb}_x\text{O}_4$  samples were prepared by using the stoichiometric amount of the elements at  $x=0.0-0.2$ . Details regarding the characteristics of the synthesized Nb substituted magnetite samples is given in the following chapters.

#### 4.3.1. Characterization of $\text{Fe}_{3-x}\text{Nb}_x\text{O}_4$ samples

The main elemental ratio of the synthesized Nb substituted magnetite samples was obtained by Inductively Coupled Plasma (ICP) analysis and the amount of oxygen vacancy in each sample was calculated (Table 4.5). The Nb content of the synthesized samples was between 0.022 and 0.19 and vacancy concentrations of 0.001, 0.008, 0.02 and a significantly high value of 0.251 in  $\text{Fe}_{2.65}\text{Nb}_{0.099}\text{O}_4$  sample were obtained that were mainly generated due to the cationic deficiency in its structure (Pearce et al., 2015).

Table 4.5: Formula and the amount of oxygen vacancies for the  $\text{Fe}_{3-x}\text{Nb}_x\text{O}_4$  samples

Sample	Formula	Oxygen vacancy
$\text{Fe}_3\text{O}_4$	$\text{Fe}_{2.999}\text{O}_4$	□ <sub>0.001</sub>
$\text{Fe}_{3-x}\text{Nb}_x\text{O}_4$ ( $x = 0.025$ )	$\text{Fe}_{2.97}\text{Nb}_{0.022}\text{O}_4$	□ <sub>0.008</sub>
$\text{Fe}_{3-x}\text{Nb}_x\text{O}_4$ ( $x = 0.05$ )	$\text{Fe}_{2.95}\text{Nb}_{0.049}\text{O}_4$	□ <sub>0.001</sub>
$\text{Fe}_{3-x}\text{Nb}_x\text{O}_4$ ( $x = 0.1$ )	$\text{Fe}_{2.65}\text{Nb}_{0.099}\text{O}_4$	□ <sub>0.251</sub>
$\text{Fe}_{3-x}\text{Nb}_x\text{O}_4$ ( $x = 0.2$ )	$\text{Fe}_{2.79}\text{Nb}_{0.19}\text{O}_4$	□ <sub>0.02</sub>

The XRD patterns of  $\text{Fe}_{3-x}\text{Nb}_x\text{O}_4$  ( $x \approx 0.022 - 0.19$ ) samples are shown in Fig. 4.1. All the main characteristic peaks of magnetite were observed in the recorded data and fit well with the data of standard magnetite cards numbers 98-015-8744, 98-002-9129 and 98-016-3306. The d-spacing values of all magnetite samples matched the lines 111,

220, 311, 222, 400, 422, 511, 440, and 533, which verified the presence of crystalline magnetite phases. The diffractograms of all samples were similar with varying intensity of the peaks attributed to their differences in particle size.

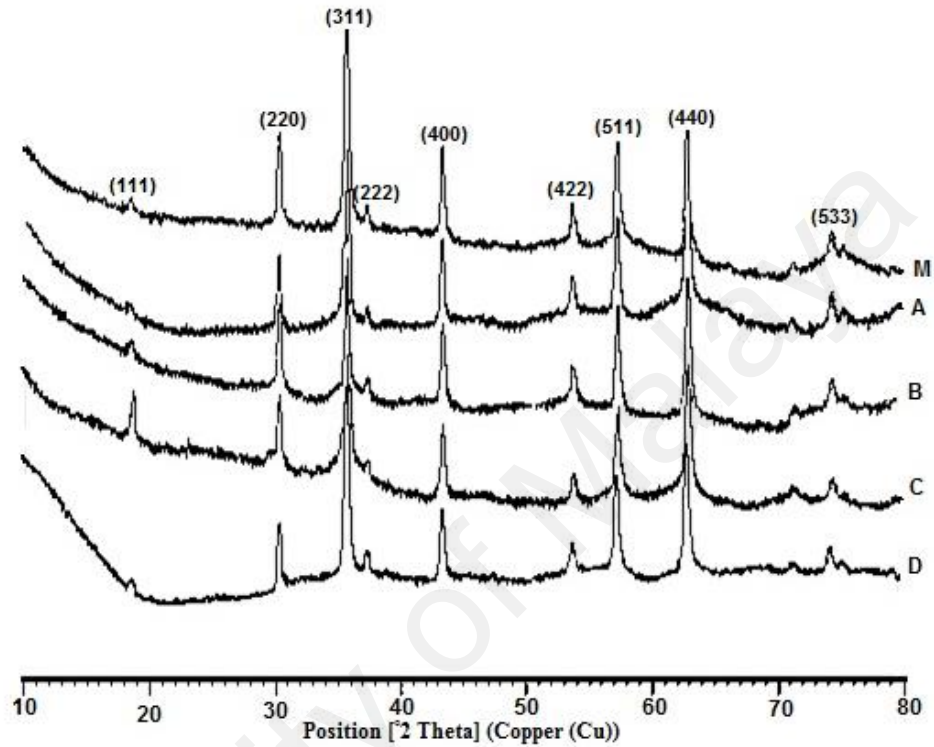


Figure 4.1: XRD patterns for  $\text{Fe}_{3-x}\text{Nb}_x\text{O}_4$  samples

BET surface area, total pore volume and pore size distribution were obtained at physisorption capacity of 77.35 K using Micromeritics (tristar 3020) instrument. All the synthesized samples were degassed at 90 °C for 1 h and then at 303° K/min for 4 h before the test. Data on the surface properties obtained with BET method and particle size analyzer were summarized in Table 4.6. The surface area of the modified samples increased significantly with Nb content up to  $x \approx 0.1$ , resulted from the decrease in pore diameter. The surface area of the  $\text{Fe}_{2.65}\text{Nb}_{0.099}\square_{0.025}\text{O}_4$  sample was three times larger than that of pure magnetite, possibly attributed to cationic deficiency in its structure. However, in  $\text{Fe}_{2.79}\text{Nb}_{0.19}\text{O}_4$  sample, a decrease in surface area compared to  $\text{Fe}_{2.65}\text{Nb}_{0.099}\square_{0.025}\text{O}_4$  was observed that could be related to occupied sites of the imported

Nb<sup>5+</sup> ions. As it may be, in this group, the imported Nb<sup>5+</sup> ions were initially substituted by octahedral Fe<sup>3+</sup> cations that are mainly exposed on the surface and contributed in the increment in surface area primarily due to reduction in pore size of the particles. When the amount of incorporated Nb was doubled, Nb<sup>4+</sup> replaced tetrahedral Fe<sup>3+</sup> cations in the crystalline structure that led to increase in particle size due to larger ionic radius of Nb<sup>4+</sup> (68 pm) compared to Fe<sup>3+</sup> (55 pm) and consequently, decrease in surface area (Lide, 2005; Ok et al., 1978; Robbins et al., 1971).

Table 4.6: Surface area, pore size/volume and particle sizes of Fe<sub>3-x</sub>Nb<sub>x</sub>O<sub>4</sub> samples

Sample	BET Surface area (m <sup>2</sup> /g)	Pore size (Å)	Pore volume (× 10 <sup>-2</sup> cm <sup>3</sup> /g)	Particle size distribution (nm)
Fe <sub>3</sub> O <sub>4</sub>	29.9804	157.7447	11.8231	90.9
Fe <sub>2.97</sub> Nb <sub>0.022</sub> O <sub>4</sub>	30.2216	157.3319	7.9538	87
Fe <sub>2.95</sub> Nb <sub>0.049</sub> O <sub>4</sub>	36.4067	144.9385	9.5684	70
Fe <sub>2.65</sub> Nb <sub>0.099</sub> O <sub>4</sub>	109.7218	55.9164	15.3381	55.1
Fe <sub>2.79</sub> Nb <sub>0.19</sub> O <sub>4</sub>	43.2054	134.1628	18.5257	57.0

Transmission electron microscopy (TEM) was used to investigate the morphology and size of the samples. The images obtained from TEM are presented in Fig. (4.2<sub>a-f</sub>). The micrographs show the particles of characteristic shape of magnetite (octahedral) in all the synthesized samples. The particles had a diameter ranging between 50 and 100 nm and they appeared smaller when concentrations of Nb were higher (Fig. 4.2<sub>e-f</sub>).

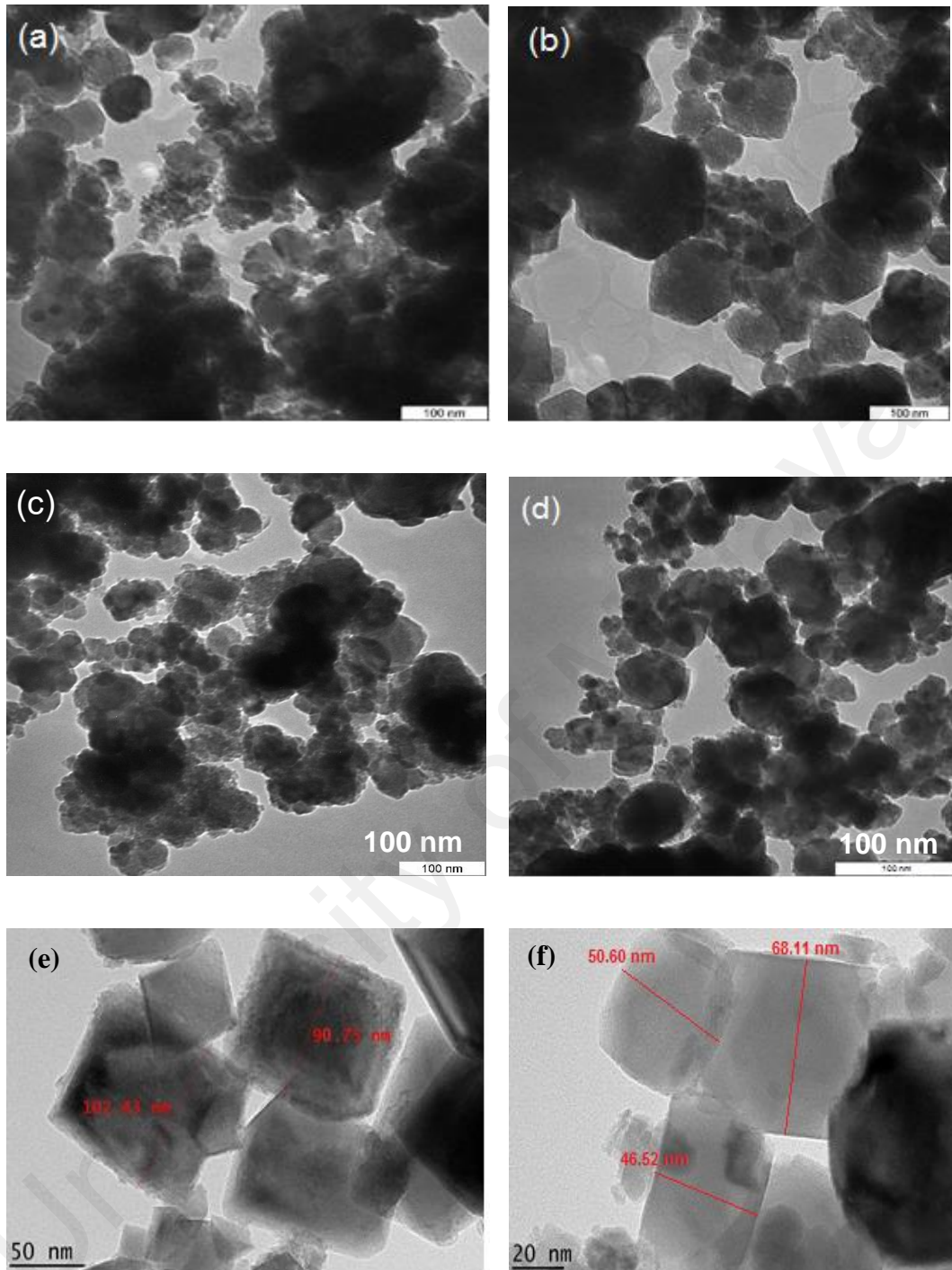
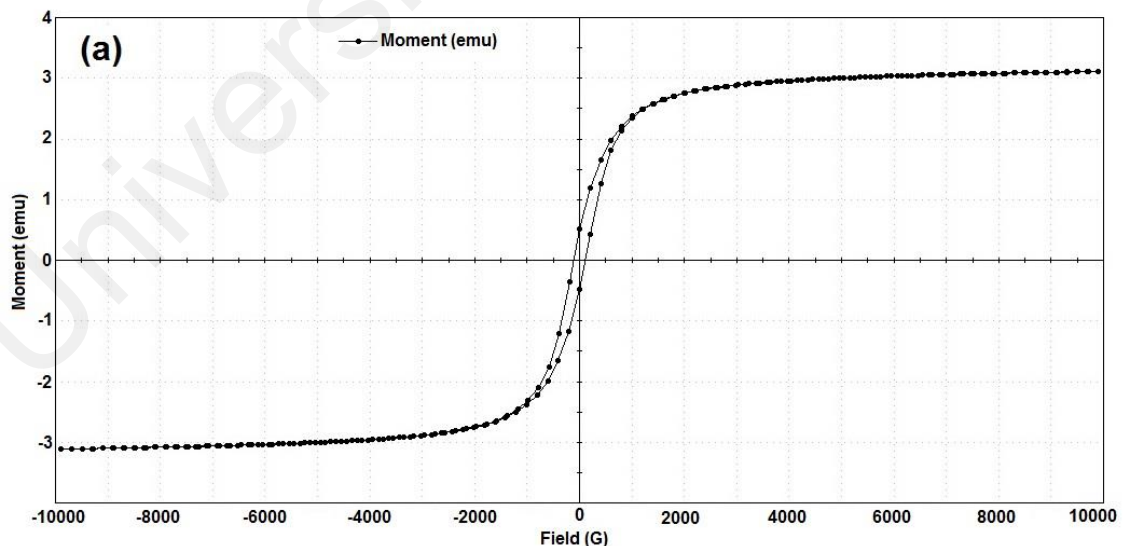


Figure 4.2: TEM images of  $\text{Fe}_{3-x}\text{Nb}_x\text{O}_4$  (a)  $x=0$ , (b)  $x=0.049$ , (c)  $x=0.099$ , (d)  $x=0.19$  and particle size distribution in (e)  $x=0$  and (f)  $x=0.099$  samples

The magnetic behavior of Nb substituted magnetite samples was investigated by VSM. All samples showed good magnetic property that is required for their easy separation from the reaction solution. Table 4.7 gives the data extracted from the hysteresis loops (Fig. 4.3) of the samples. The main parameters that used for characterization of

magnetic properties of the samples were the coercivity ( $H_{ci}$ : is the field needed to decrease the magnetization to zero after saturation), saturation magnetization ( $M_s$ ), the remanence ( $M_r$  and the squareness ratio ( $SQR = M_r/M_s$ ). A large SQR (measures the squareness of the hysteresis loop) value is desired for memory devices but in the case of magnetic materials, it should be as low as possible and close to zero (Stoner & Wohlfarth, 1948). As can be seen, all samples showed similar SQR values of about 0.15 that shows a minor change in magnetic properties of the synthesized samples compared to pure magnetite. The obtained hysteresis loops showed the characteristic graphs of ferromagnetic materials. The slim magnetic hysteresis loops showed high magnetic saturation (up to 100 emu/g) and minor amounts of residual magnetism (0.6 emu) that is a characteristic of soft magnetic materials such as iron. They can be easily magnetized and demagnetized due to the need for small coercive force to overcome residual magnetism.



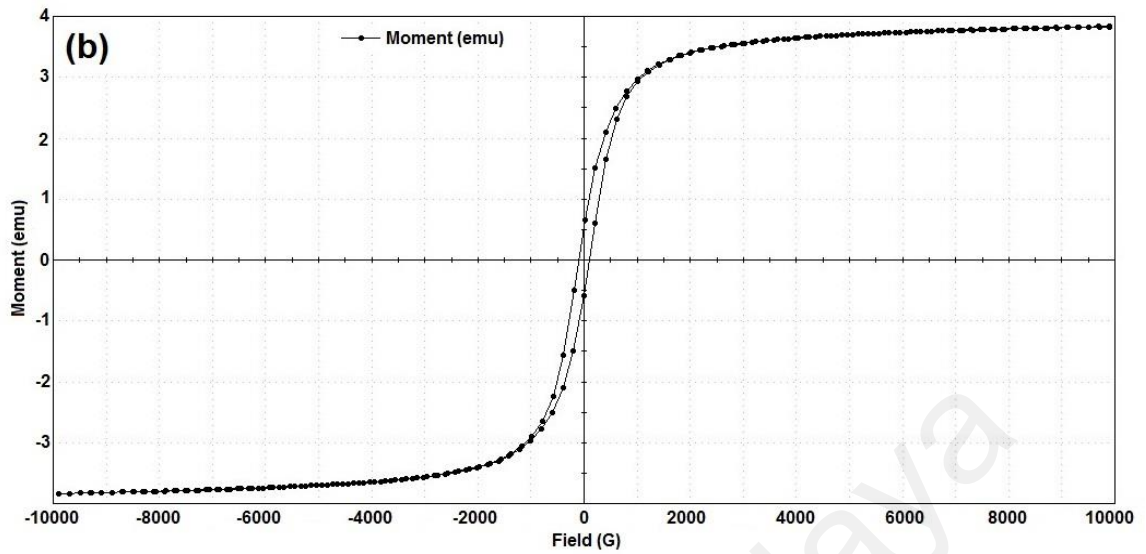


Figure 4.3: Hysteresis loops for (a) magnetite (b)  $\text{Fe}_{2.79}\text{Nb}_{0.19}\text{O}_4$

Table 4.7: Magnetic properties of the synthesized samples

Samples	$H_{ci}$ (G)	Magnetization	$SQR$
		$M_s$ (emu/g)	( $M_r/M_s$ )
$\text{Fe}_3\text{O}_4$	108.39	68.93	0.15
$\text{Fe}_{2.97}\text{Nb}_{0.022}\text{O}_4$	107.15	85.29	0.15
$\text{Fe}_{2.95}\text{Nb}_{0.049}\text{O}_4$	106.16	98.43	0.15
$\text{Fe}_{2.65}\text{Nb}_{0.099}\text{O}_4$	104.88	78.77	0.15
$\text{Fe}_{2.79}\text{Nb}_{0.19}\text{O}_4$	103.24	95.63	0.16

The spectrum derived from the XPS analysis was used to get information on elemental composition and chemical states of the active surface ions. However, the accuracy of the results depends on the analytical procedure where there is an overlapping of peaks of various species in a sample. For the  $\text{Fe}_{3-x}\text{Nb}_x\text{O}_4$  samples, the spectral regions of interest were B.E: 700-740 eV, 520-550 eV, 278-298 eV, and 197-217 eV for Fe 2p, O 1s, C 1s, and Nb 3d, respectively. In order to determine the chemical species present on the surface, a complete XPS survey spectrum of the samples were acquired (Fig. 4.4).

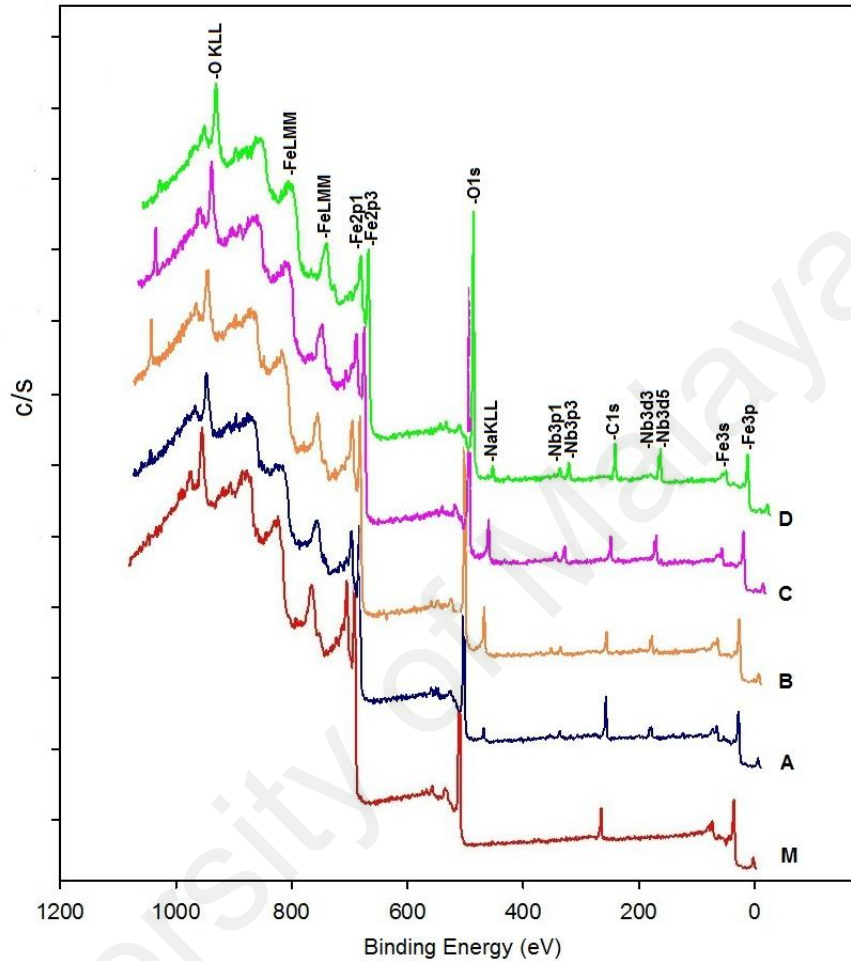


Figure 4.4: XPS spectra of  $\text{Fe}_{3-x}\text{Nb}_x\text{O}_4$  samples ( $x = 0 - 0.19$ )

Table 4.8 presents the composition of the elements and the corresponding percentage of each chemical state. The  $\text{Fe}^{2+}/\text{Fe}^{3+}$  ratio increased with Nb content of the magnetite indicating that  $\text{Fe}^{3+}$  cations replaced by Nb ions.

Table 4.8: The elemental composition and their chemical states on the surface of  $\text{Fe}_{3-x}\text{Nb}_x\text{O}_4$  samples

ID	Samples	Weight Fe (%)				Weight O (%)		Weight Nb (%)	
		FeO	Fe <sub>2</sub> O <sub>3</sub>	Fe(II) satellite	Fe III satellite	FeO/Fe <sub>2</sub> O <sub>3</sub>	NbO <sub>2</sub> /Nb <sub>2</sub> O <sub>5</sub>	NbO <sub>2</sub>	Nb <sub>2</sub> O <sub>5</sub>
M	Fe <sub>3</sub> O <sub>4</sub>	29.25	45.14	9.10	16.50	62.96/29.28	-	-	-
A	Fe <sub>2.97</sub> Nb <sub>0.022</sub> O <sub>4</sub>	34.62	38.52	9.30	17.563	69.97	30.03	65.50	34.5
B	Fe <sub>2.95</sub> Nb <sub>0.049</sub> O <sub>4</sub>	36.02	35.73	13.01	15.24	59.43	35.83	54.59	45.41
C	Fe <sub>2.65</sub> Nb <sub>0.099</sub> O <sub>4</sub>	39.13	32.20	12.37	16.29	62.08	33.65	55.85	44.15
D	Fe <sub>2.79</sub> Nb <sub>0.19</sub> O <sub>4</sub>	47.64	30.25	10.77	11.34	67.22	29.82	63.53	36.47



The exposed surfaces of the Nb-substituted magnetite samples host various species. The narrow scan of the elements of interest, iron (Fe), niobium (Nb) and oxygen (O) were recorded and deconvolution of peak shape was carried out to identify the chemical states of the surface ions. Figure 4.5a shows the narrow scanned Fe 2p spectra of the  $\text{Fe}_{3-x}\text{Nb}_x\text{O}_4$  samples. The peak position of Fe 2p<sub>1/2</sub> and Fe 2p<sub>3/2</sub> was used for qualitative determination of the ionic states of Fe (Yamashita & Hayes, 2008). The Fe 2p peaks were positioned between B.E. of 709.9 eV and 711.5 eV. By comparing the results obtained in this study with the reference data, the peaks are characteristic of Fe<sup>2+</sup> and Fe<sup>3+</sup> cations in the samples (Magalhães et al., 2007). In addition, the satellite peaks at the low kinetic energy side of the main peaks are also characteristic of Fe<sup>2+</sup> and Fe<sup>3+</sup>. The satellite peaks of Fe<sup>2+</sup> and Fe<sup>3+</sup> cations are clear in this figure. These peaks are caused mainly by configuration interaction resulted from valence electrons relaxation. It is worth to mention that the satellite peaks intensity cannot be ignored in order to have an accurate measurement of the amount of surface iron species (Paparazzo, 2006).

Deconvolution of the O1s of  $\text{Fe}_{2.79}\text{Nb}_{0.19}\text{O}_4$  sample is shown in Fig. 4.5b. It was observed that the oxygen present in the form of FeO/Fe<sub>2</sub>O<sub>3</sub> situated at B.E. 529.7 eV and NbO<sub>2</sub>/Nb<sub>2</sub>O<sub>5</sub> situated at B.E. 530.9 eV. The graph shows the considerable amount of surface Nb when compared to Fe species.

In this study, it was especially important to validate the presence of Nb on the surface of the modified magnetite samples and its valence state. XPS is an ideal tool to study the surface Nb of the samples in which different oxidation states of Nb can be easily distinguished (Maximova, 2008). The results (Fig. 4.6) showed the presence of Nb<sup>+5</sup> with the Nb 3d core level situated between 207.7 eV and 206 eV that is related to NbO<sub>2</sub> and Nb<sub>2</sub>O<sub>5</sub> respectively. Figure represents the evolution of Nb 3d peaks with the growth in Nb content of the samples. In addition, the results indicated that Nb was not in a pure +5 oxidation state but presented in both +4 and +5 oxidation states (Table 4.8). The high

Nb/Fe ratio of the samples ( $x= 0.099$  and  $0.19$ ) indicated niobium enrichment of the surface of these modified samples.

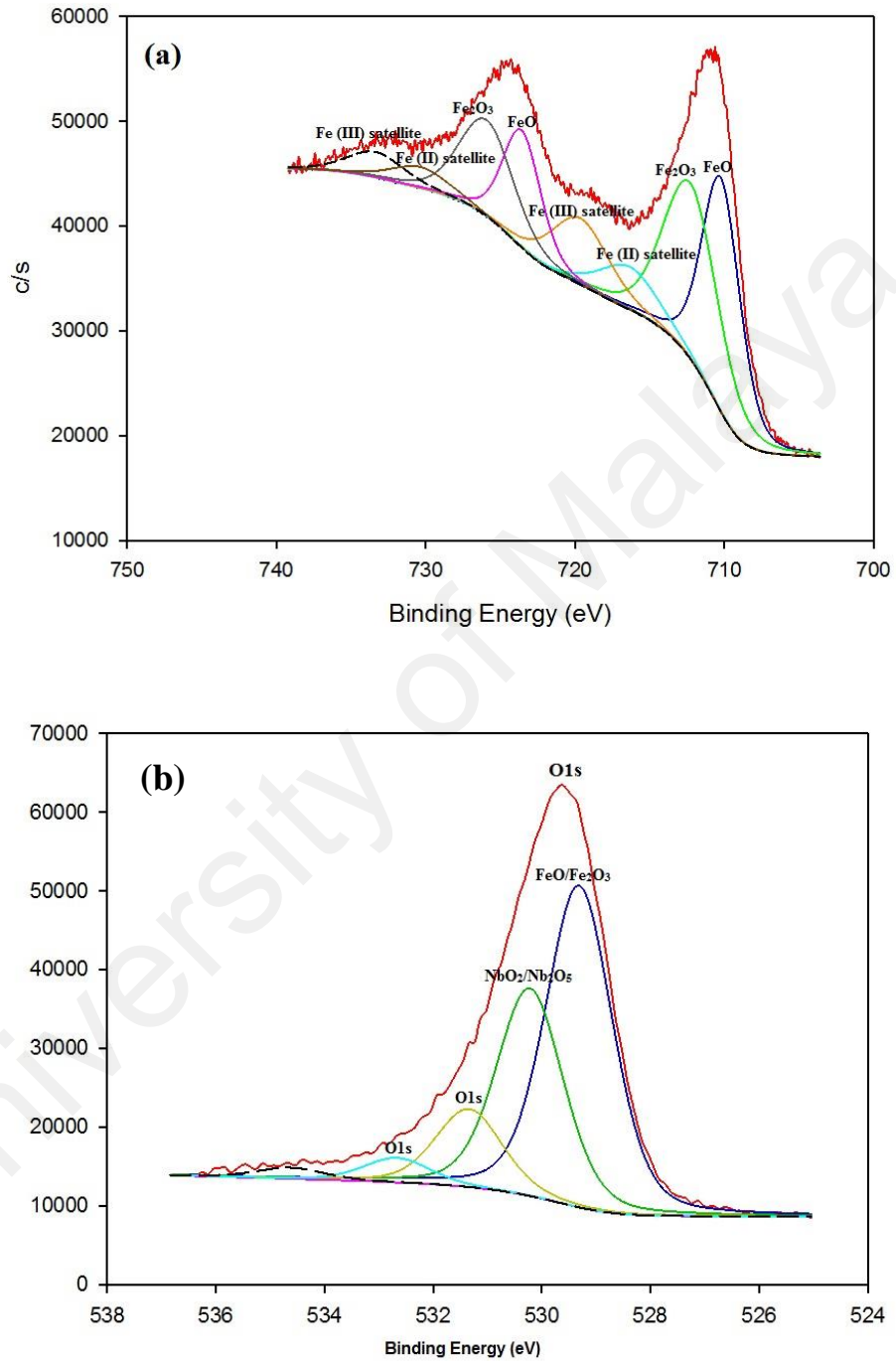


Figure 4.5: Deconvolution of the (a) Fe 2p doublet and (b) O 1s of  $\text{Fe}_{2.79}\text{Nb}_{0.19}\text{O}_4$  sample

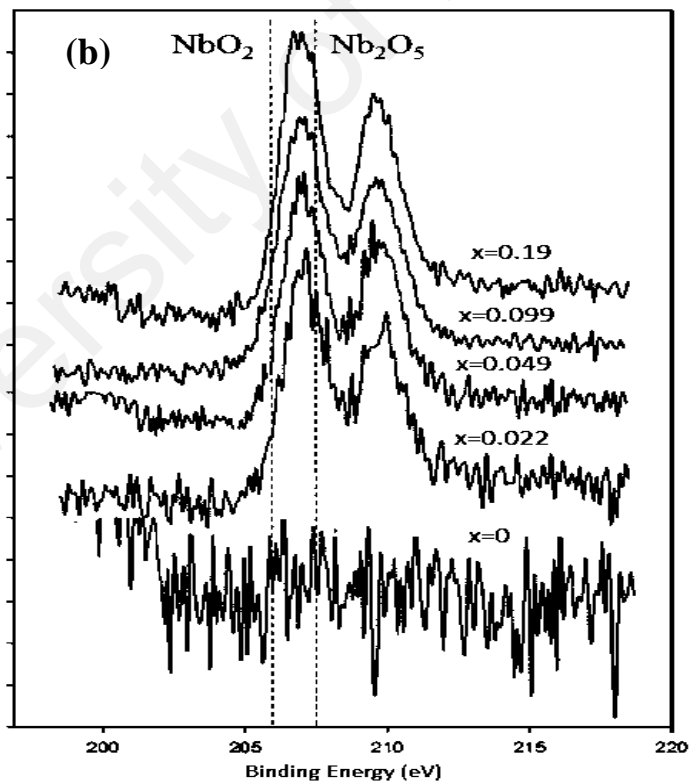
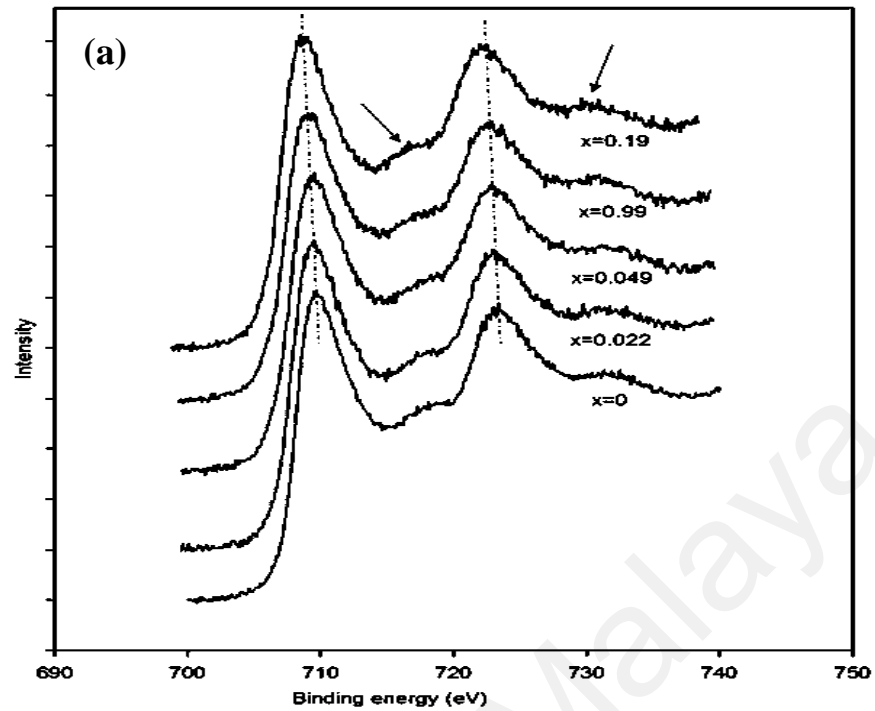


Figure 4.6: XPS spectra for (a) Fe 2p and (b) Nb 3d region for the  $\text{Fe}_{3-x}\text{Nb}_x\text{O}_4$  samples ( $x = 0 - 0.19$ ). ((a) The arrows show satellite peaks; (b) the binding energies of  $\text{Nb}_2\text{O}_5$  and  $\text{NbO}_2$ , indicated by vertical lines).

### 4.3.2. Methylene blue adsorption by $\text{Fe}_{3-x}\text{Nb}_x\text{O}_4$

Figure 4.7 shows the adsorption of different concentrations of MB ( $\text{mg g}^{-1}$ ) on  $\text{Fe}_{3-x}\text{Nb}_x\text{O}_4$  samples at pH 7. It was observed that  $q_e$  of all the synthesized samples were bigger than that of pure magnetite, indicating that niobium incorporation had a positive effect on MB adsorption. The corresponding BET surface area values of the Nb-magnetite samples are also given in the figure. The highest BET value ( $109.7 \text{ m}^2 \text{ g}^{-1}$ ) amongst this series was for the  $\text{Fe}_{2.65}\text{Nb}_{0.099}\text{O}_4$  sample and the adsorption capacity of this sample was the highest, as shown in the figure.

The adsorption capacity of MB on  $\text{Fe}_{2.97}\text{Nb}_{0.022}\text{O}_4$ ,  $\text{Fe}_{2.95}\text{Nb}_{0.049}\text{O}_4$ ,  $\text{Fe}_{2.65}\text{Nb}_{0.099}\text{O}_4$ , and  $\text{Fe}_{2.79}\text{Nb}_{0.19}\text{O}_4$  samples were 21.3%, 31.14%, 47.8%, and 41.7%, respectively which were significantly higher compared to unmodified magnetite which only achieved 17.9% of MB removal through adsorption. From the results, the adsorption capacity of the samples increased with Nb content of the samples up to  $x = 0.1$ . This can be attributed to the increase in the specific surface areas of the samples caused by incorporation of Nb ions (Liang et al., 2013). However, adsorption of MB on  $\text{Fe}_{3-x}\text{Nb}_x\text{O}_4$  samples is mainly corresponding to their surface charge. Based on the  $\text{pH}_{\text{pzc}}$  values (Fig. 4.8) of the synthesized samples, at  $\text{pH} > \text{pH}_{\text{pzc}}$ , the surface of the samples was negatively charged which is favored for adsorption of cationic dye (MB) based on electrostatic interaction. This finding is in agreement with the other studies. Liang et al. (2012a) reported that MB removal through Fenton reaction catalyzed by Cr substituted magnetite were mainly relied on its adsorption on the surface of the samples at neutral pH value while the samples showed no adsorption to acid orange II and the degradation of the studied dyes followed different removal mechanisms. Figure 4.9 shows the effects of solution pH on the adsorption of MB on  $\text{Fe}_{2.79}\text{Nb}_{0.19}\text{O}_4$ . The amount of adsorption was significantly affected by the initial pH of the solution. The negligible adsorption was resulted at pH 4.0 due to repulsion between cationic dye molecules and

positively charged catalyst surface. Therefore,  $\text{pH} > \text{pH}_{\text{pzc}}$  increased the adsorption accordingly. The highest MB adsorption was obtained at  $\text{pH}=10$  that could be associated with the higher amount of surface  $-\text{OH}$  groups of the samples (Liang et al., 2012a). The higher adsorption capacity of the modified samples compared to pure magnetite did not only depend to pollutant's characteristics but the surface characteristics of the samples. Although, the high adsorption could be one of the main reasons for improved catalytic activity of the samples, but it should be mentioned that for the pollutants with low adsorption on surface but enhanced Fenton degradation, such as acid orange II as anionic dye, other degradation mechanism has been suggested (Liang et al., 2013).

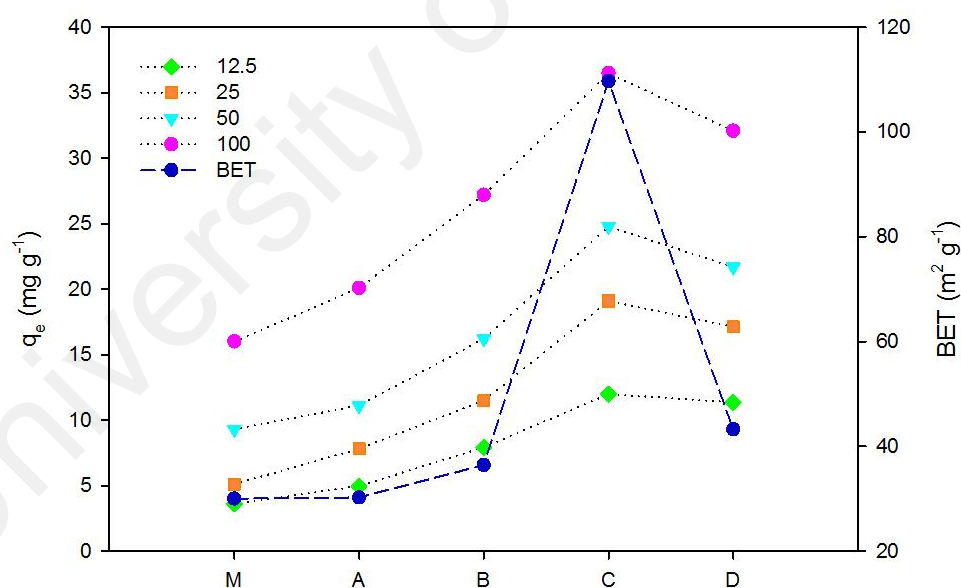


Figure 4.7: Adsorption of methylene blue on (M)  $\text{Fe}_3\text{O}_4$ , (A)  $\text{Fe}_{2.97}\text{Nb}_{0.022}\text{O}_4$ , (B)  $\text{Fe}_{2.95}\text{Nb}_{0.049}\text{O}_4$ , (c)  $\text{Fe}_{2.65}\text{Nb}_{0.099}\text{O}_4$ , and (D)  $\text{Fe}_{2.79}\text{Nb}_{0.19}\text{O}_4$  samples ( $[\text{MB}]$  12.5-100 mg/L; Catalyst 1 g/L;  $\text{pH}$  7,  $t = 2$  h)

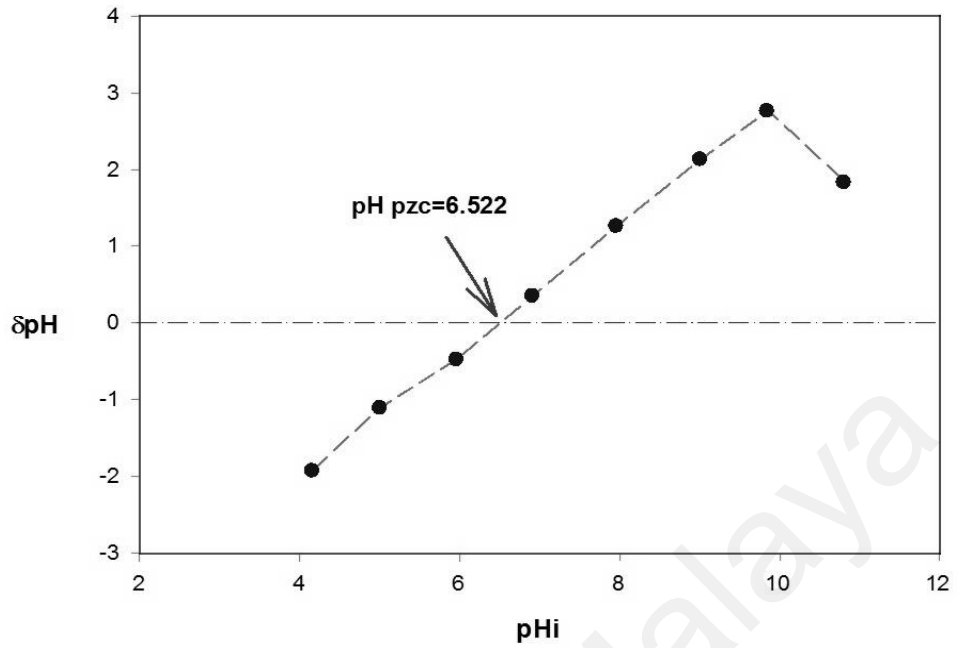


Figure 4.8: The pH of the point of zero charge of  $\text{Fe}_{2.79}\text{Nb}_{0.19}\text{O}_4$  sample

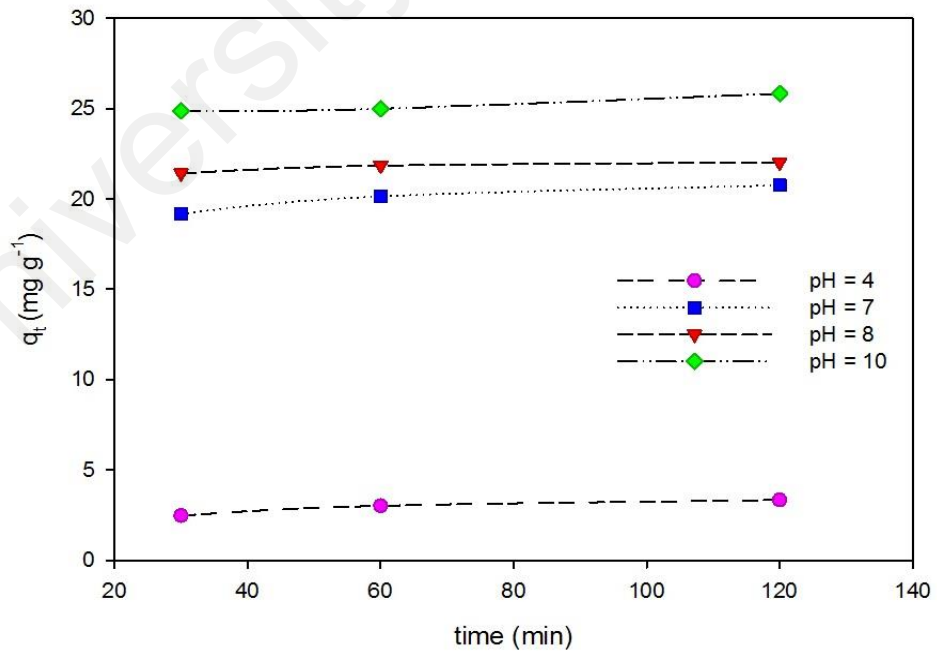


Figure 4.9: The effect of pH on MB adsorption on  $\text{Fe}_{2.79}\text{Nb}_{0.19}\text{O}_4$  sample ( $1\text{g L}^{-1}$ )

### 4.3.3. Methylene blue degradation by $\text{Fe}_{3-x}\text{Nb}_x\text{O}_4$

Methylene blue removal was initiated by its adsorption on the catalyst surface before  $\text{H}_2\text{O}_2$  addition and starting Fenton reaction. Figure 4.10 shows MB removal ( $C_t/C_0$ ) through adsorption on the  $\text{Fe}_{3-x}\text{Nb}_x\text{O}_4$  samples at 120 min of agitation and Fenton-like reaction at neutral pH over additional 180 minutes.

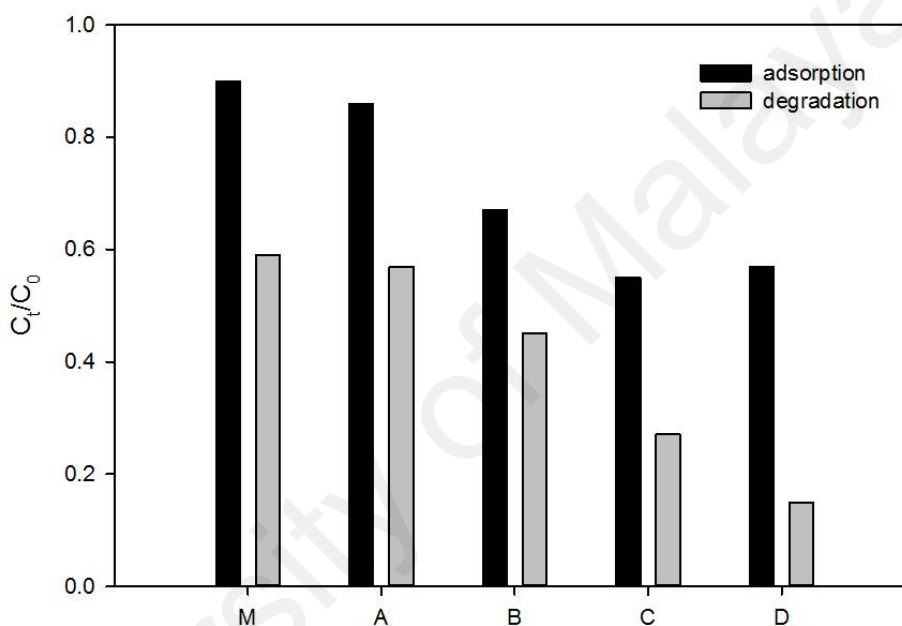


Figure 4.10: Methylene blue removal through adsorption and Fenton reaction catalyzed by  $\text{Fe}_{3-x}\text{Nb}_x\text{O}_4$  samples ( $[\text{H}_2\text{O}_2]$   $0.2 \text{ mol L}^{-1}$ ; catalyst  $1 \text{ g L}^{-1}$ ; pH 7;  $t_{\text{ads}} = 2 \text{ h}$ ;  $t_{\text{Fenton}} = 3 \text{ h}$ )

By adding  $\text{H}_2\text{O}_2$ , MB degradation was enhanced through heterogeneous Fenton reaction. After 180 min, MB oxidation was increased through Fenton-like reaction. The oxidation rate was improved concurrent with pH rising from 4 to 10 (Fig. 4.11). The amount of MB adsorbed on  $\text{Fe}_{2.79}\text{Nb}_{0.19}\text{O}_4$  sample was negligible because pH of the solution was less than  $\text{pH}_{\text{pzc}}$  of the catalyst. Accordingly, Fenton removal efficiency was relatively low. The resulted decolorization at pH 4 might be caused through the homogeneous Fenton route due to the slight leaching of Nb into the solution. Figure 4.12

shows the MB and TOC removal efficacies of the synthesized samples at pH 7 and 10. Degradation and mineralization of MB were significantly higher at pH 10 and improved by increasing the amount of Nb incorporated into catalysts. During the reaction, the concentration of leached Fe and Nb ions were very low indicating that degradation mainly occurred through a heterogeneous route and leaching of ions into the solution had negligible role in the oxidation of MB. Based on the findings of previous studies (Liang et al., 2012a; Lin & Gurol, 1998), enhanced MB oxidation is not only related to the specific surface area of the samples but also the concentration of hydroxyl radicals on the surface of hetero-catalysts resulted from decomposition of H<sub>2</sub>O<sub>2</sub>. On the other hand, the role of Nb<sup>4+</sup>/ Nb<sup>5+</sup> cations that were substituted in place of octahedral Fe<sup>3+</sup> cations in transfer of electrons in spinel structure to generate Fe<sup>2+</sup> cations in Fenton-like reaction and decomposition of H<sub>2</sub>O<sub>2</sub> is critical. In the Fe<sub>3-x</sub>Nb<sub>x</sub>O<sub>4</sub> series, the catalytic activity of the samples was greatly enhanced by the increase in Nb-content of the magnetite samples, ranging from 0 to 0.19, in which total MB removal was obtained under the studied conditions. It can be ascribed to difference in adsorption capacity of the samples. However, for Fe<sub>2.79</sub>Nb<sub>0.19</sub>O<sub>4</sub> sample, which had lower change in its BET and adsorption than Fe<sub>2.65</sub>Nb<sub>0.099</sub>O<sub>4</sub>, its peak activity might be associated with other factors such as oxygen vacancies as active sites on the surface, higher electron transfer and subsequently higher H<sub>2</sub>O<sub>2</sub> decomposition (Costa et al., 2003). In the similar studies, it was reported that the increment in imported ion generally lead to higher removal efficacies. Nevertheless, it should be beared in mind that the concentration of Fenton reagents, type and the amount of probe molecule, reaction condition and duration and especially the elemental ratio of the imported transition metal play significant role and have crucial effects on the degradation effectiveness. For instance, in a study reported by Costa et al. (2006), although MB (50 ppm) removal was attained within 10 minutes, higher H<sub>2</sub>O<sub>2</sub> concentrations (0.3 M) and Mn (x=0.53) and Co (x=0.75) contents were



the main reasons for the short reaction time. In another study, Liang et al. (Liang et al., 2012a) reported that 59.3% of MB ( $\approx 64 \text{ mg L}^{-1}$ ) was removed from the solution using  $\text{Fe}_{2.82}\text{Cr}_{0.18}\text{O}_4 / \text{H}_2\text{O}_2$  (0.08 M) within 4 hours. Whereas,  $\text{Fe}_{2.33}\text{Cr}_{0.67}\text{O}_4 / \text{H}_2\text{O}_2$  resulted in 95% decolorization at studied reaction time. On the other hand, a long reaction time of 11 h was taken to degrade  $> 90\%$  of MB ( $70 \text{ mg g}^{-1}$  of  $\text{Fe}_{2.66}\text{V}_{0.34}\text{O}_4$  at pH 10 (Liang et al., 2013a). Therefore, the studied  $\text{Fe}_{3-x}\text{Nb}_x\text{O}_4$  sample with relatively lower Nb content ( $x = 0.19$ ) and shorter reaction time showed significantly improved performance in Fenton degradation of MB solution.

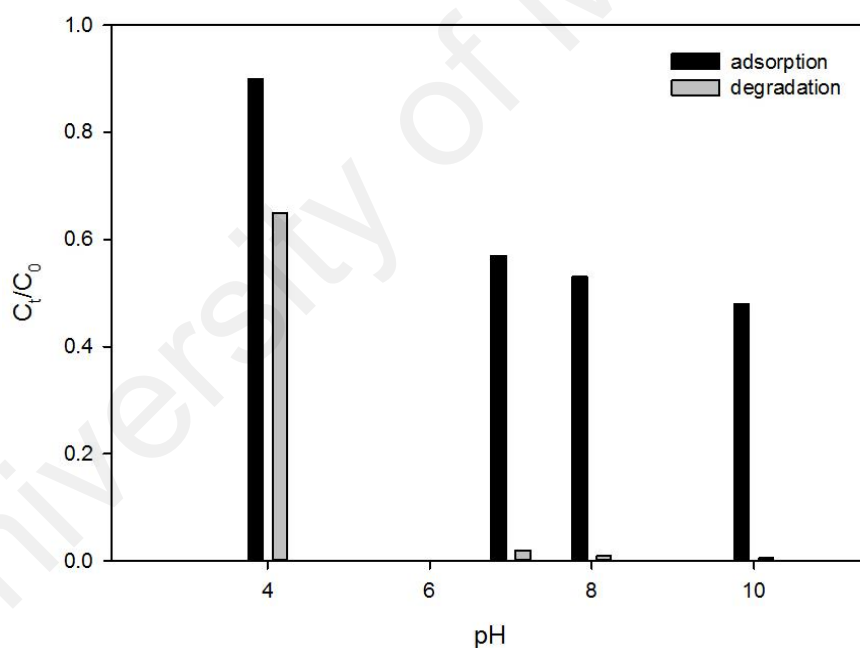


Figure 4.11: Effect of pH on methylene blue removal through adsorption and Fenton-like reaction catalyzed by  $\text{Fe}_{2.79}\text{Nb}_{0.19}\text{O}_4$

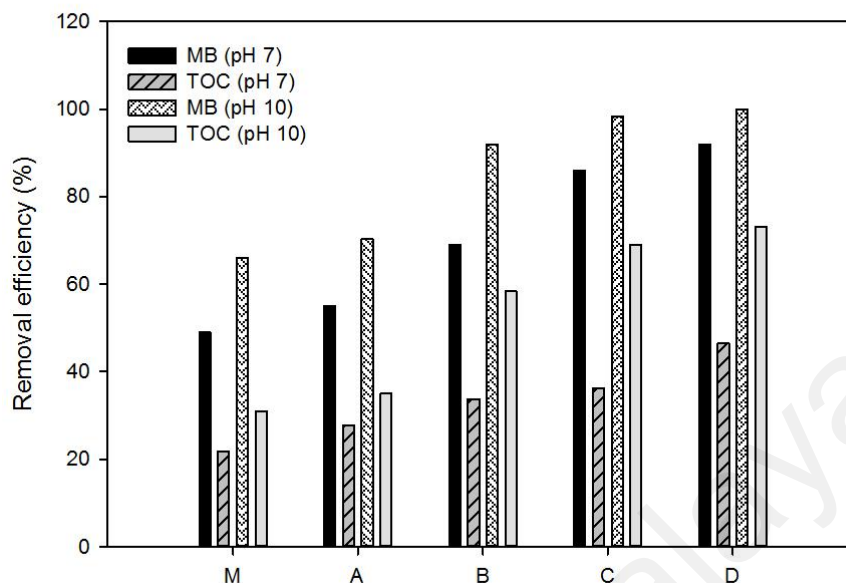


Figure 4.12: Degradation and mineralization of MB solution through Fenton-like reaction using  $\text{Fe}_{3-x}\text{Nb}_x\text{O}_4$  catalyst at pH values of 7 and 10

From the results,  $x=0.2$  was found as the optimal value in the  $\text{Fe}_{3-x}\text{Nb}_x\text{O}_4$  series that showed the highest activity in Fenton oxidation of MB solution. Following this experiments, Mo was used instead of Nb to explore the changes derived from this substitution in magnetite structure and activity in Fenton-like reaction.

#### 4.4. Molybdenum-substituted-magnetite ( $\text{Fe}_{3-x}\text{Mo}_x\text{O}_4$ )

Molybdenum (Mo) is a transition metal from fifth series of periodic table with atomic number of 42. The main industrial applications of this element are as catalyst and pigment (Platanitis et al., 2016). Similar to Nb, it has one electron in its last electron shell. In addition, the crystal structure of Mo is also body centered cubic structure and it is paramagnetic. From the isomorphic substitution viewpoint, Mo has similar ionic radius to iron species ( $\text{Mo}^{+4}$  (65 pm) and  $\text{Mo}^{+6}$  (59 pm) vs.  $\text{Fe}^{2+}$  (61 pm)  $\text{Fe}^{+3}$  (55 pm)). As a result, Mo could theoretically replace iron in magnetite structure. The following sections gives data regarding a number of the main physico-chemical characteristics of

Mo substituted magnetite samples ( $\text{Fe}_{3-x}\text{Nb}_x\text{Mo}_y\text{O}_4$ ) and their activity in Fenton-like reaction.

#### 4.4.1. Characterization of $\text{Fe}_{3-x}\text{Mo}_x\text{O}_4$ samples

The chemical formula of the synthesized  $\text{Fe}_{3-x}\text{Mo}_x\text{O}_4$  samples was obtained using Inductively Coupled Plasma (ICP) analysis and the amount of oxygen vacancy in each sample was calculated subsequently. Table 4.9 shows the actual amount of Mo entered the lattice structure of magnetite. The results showed lower incorporation maxima of Mo when compared to Nb. The amount of Mo in the sample using the ratio of  $x=0.025$  was negligible; therefore, it was not used in this study. On the other hand, the amount of incorporated Mo in other samples compared to initial value was about 56% ( $x=0.05$ ), 69% ( $x=0.1$ ) and 65% ( $x=0.2$ ). Because of this, a sample with  $x=0.3$  of Mo was also prepared in which the amount of incorporated Mo to magnetite was about 70% of initially utilized value. Accordingly, the amount of oxygen vacancies improved concurrent with increase in the utilized Mo in the modified magnetite samples. This was mainly because of the cationic deficiency in the structure of the samples.

Table 4.9: Formula and the amount of oxygen vacancies for  $\text{Fe}_{3-x}\text{Mo}_x\text{O}_4$  samples

Sample	Formula	Oxygen vacancy
$\text{Fe}_3\text{O}_4$	$\text{Fe}_{2.999}\text{O}_4$	$\square_{0.001}$
$\text{Fe}_{3-x}\text{Mo}_x\text{O}_4$ ( $x = 0.05$ )	$\text{Fe}_{2.94}\text{Mo}_{0.028}\text{O}_4$	$\square_{0.0224}$
$\text{Fe}_{3-x}\text{Mo}_x\text{O}_4$ ( $x = 0.1$ )	$\text{Fe}_{2.89}\text{Mo}_{0.069}\text{O}_4$	$\square_{0.0319}$
$\text{Fe}_{3-x}\text{Mo}_x\text{O}_4$ ( $x = 0.2$ )	$\text{Fe}_{2.79}\text{Mo}_{0.13}\text{O}_4$	$\square_{0.0733}$
$\text{Fe}_{3-x}\text{Mo}_x\text{O}_4$ ( $x = 0.3$ )	$\text{Fe}_{2.62}\text{Mo}_{0.21}\text{O}_4$	$\square_{0.17}$

The XRD patterns of  $\text{Fe}_{3-x}\text{Mo}_x\text{O}_4$  samples ( $x \approx 0.028 - 0.21$ ) are shown in Fig. 4.13. The main signature peaks of  $2\theta \approx 18.3^\circ$  (111),  $30.2^\circ$  (220),  $35.6^\circ$  (311),  $37^\circ$  (222),  $43.3^\circ$  (400),  $53.7^\circ$  (422),  $57.2^\circ$  (511),  $62.8^\circ$  (440) and  $74.4^\circ$  (533) were observed in the recorded data and fitted well with the data of standard magnetite card numbers (JCPDS no.) 98-009-8087, 98-015-8745, 98-007-7589 and 98-015-7651. This certifies the conservation of the magnetite spinel structure in synthesized samples. In this group, the replacement of  $\text{Fe}^{2+}$  (61 pm) with  $\text{Mo}^{4+}$  (65 pm) and  $\text{Mo}^{6+}$  (59 pm) altered the lattice parameters from  $8.394 \text{ \AA}$  for the unmodified magnetite to 8.378, 8.358 and 8.344. A slight difference in the intensity of the diffractograms of the samples was resulted mainly from the differences in the particle sizes of the samples.

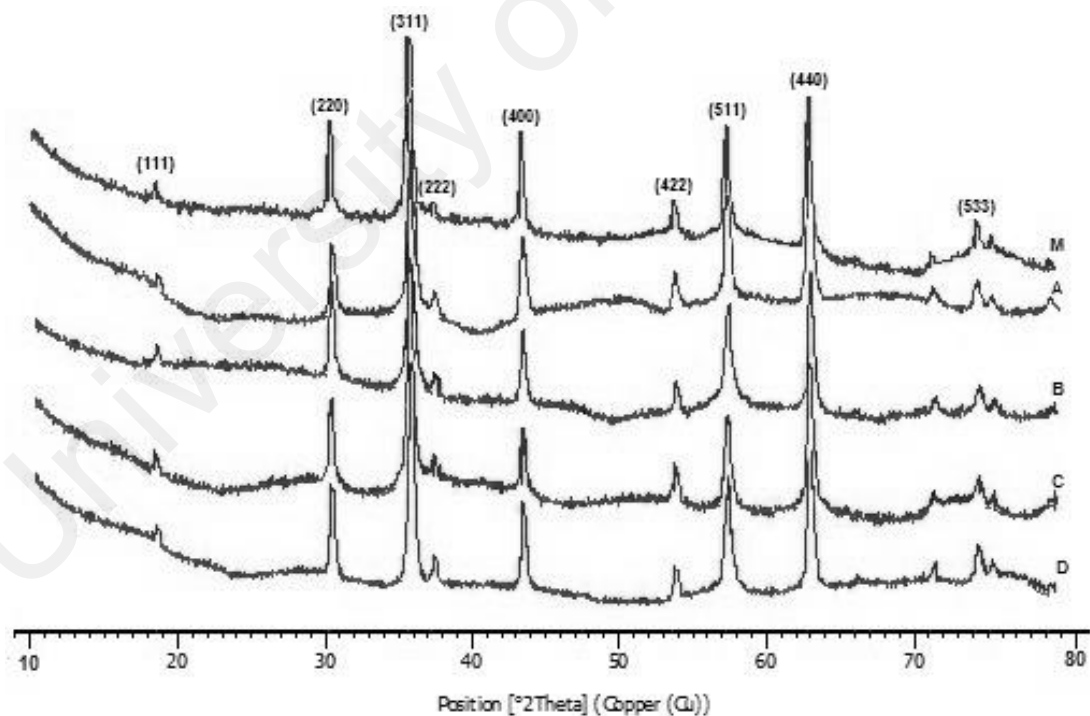


Figure 4.13: XRD patterns for  $\text{Fe}_{3-x}\text{Mo}_x\text{O}_4$  magnetite samples

Table 4.10 gives the data obtained from BET method and particle size analyzer. From the table, it can be seen that the size of the particles was decreased with the increased structural Mo in the samples. Subsequently, the amount of the specific surface area of the samples was also increased by increment in Mo content. The corresponding pore sizes and pore volumes of the samples is also given in the table.

Table 4.10: Surface area, pore size/volume and particle sizes of  $\text{Fe}_{3-x}\text{Mo}_x\text{O}_4$  samples

ID	Sample	BET Surface area ( $\text{m}^2/\text{g}$ )	Pore size ( $\text{Å}$ )	Pore volume ( $\times 10^{-2}\text{cm}^3/\text{g}$ )	Particle size distribution (nm)
M	$\text{Fe}_3\text{O}_4$	29.9804	157.7447	11.8231	90.9
A	$\text{Fe}_{2.94}\text{Mo}_{0.028}\text{O}_4$	39.7167	103.7773	10.0137	75.6
B	$\text{Fe}_{2.89}\text{Mo}_{0.069}\text{O}_4$	61.0534	106.2230	18.8688	61.2
C	$\text{Fe}_{2.79}\text{Mo}_{0.13}\text{O}_4$	69.4753	89.9683	17.8757	55.5
D	$\text{Fe}_{2.62}\text{Mo}_{0.21}\text{O}_4$	100.4605	64.9741	16.3183	22.1

Transmission electron microscopy (TEM) revealed the morphology, shape and size of the  $\text{Fe}_{3-x}\text{Mo}_x\text{O}_4$  samples. The micrographs show the characteristic morphology of well-crystallized magnetite in which all the samples grew well in octahedral form (Fig. 4.14). Furthermore, the size of the samples decreased parallel with the growth in Mo content of the samples.

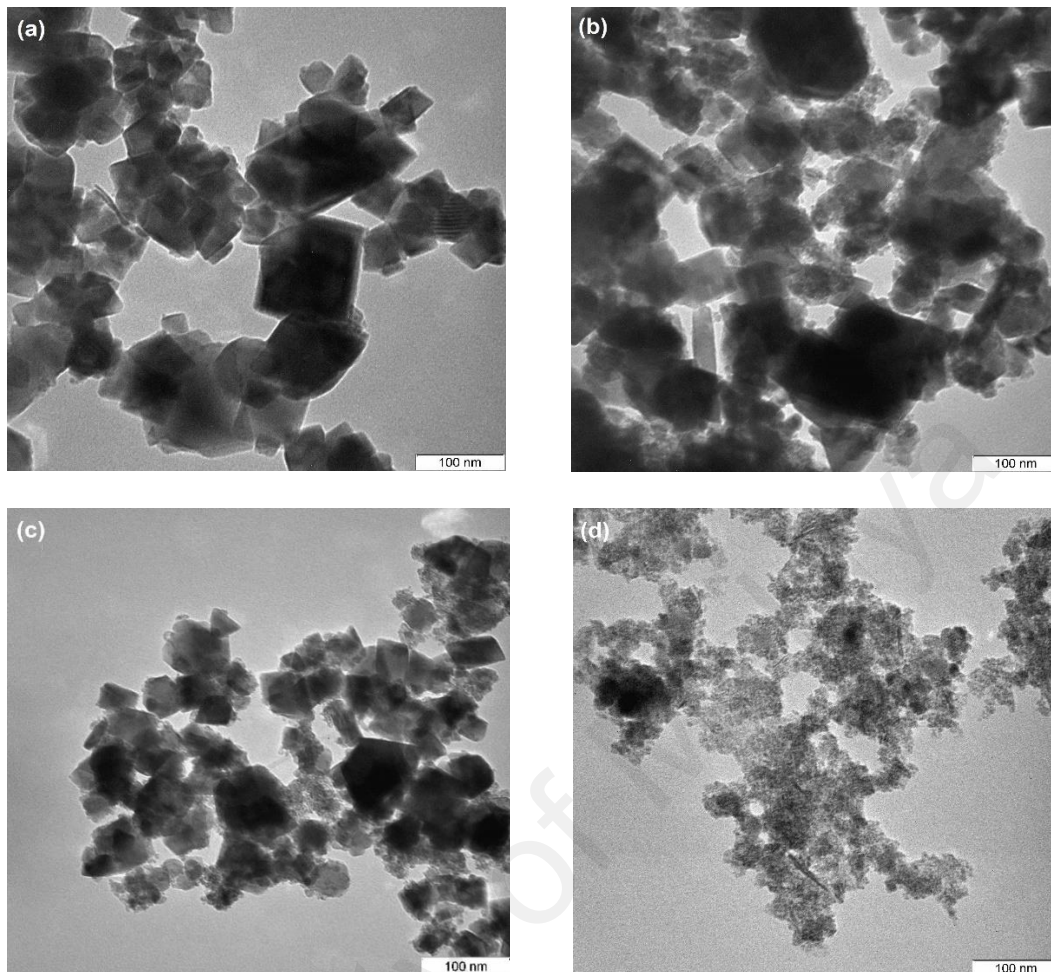


Figure 4.14: TEM images of  $\text{Fe}_{3-x}\text{Mo}_x\text{O}_4$  samples (a) A, (b) B, (c) C and (d) D

X-ray photoelectron spectroscopy (XPS) used to identify the elements present on the surface of the  $\text{Fe}_{3-x}\text{Mo}_x\text{O}_4$  samples. This is mainly to prove the presence of incorporated Mo on the surface of the samples and to determine its chemical state. On this basis, a complete XPS survey spectrum of the samples helped for determination of the elemental composition of the samples (Fig. 4.15). Subsequently, narrow scanning of the elements of interest carried out and peak deconvolution processed to detect the chemical states of the elements in the samples. The spectral regions of B.E: 700-740 eV, 520-550 eV, 278-298 eV and 222-242 eV for Fe 2p, O 1s, C 1s and Mo 3d used for narrow scanning respectively.

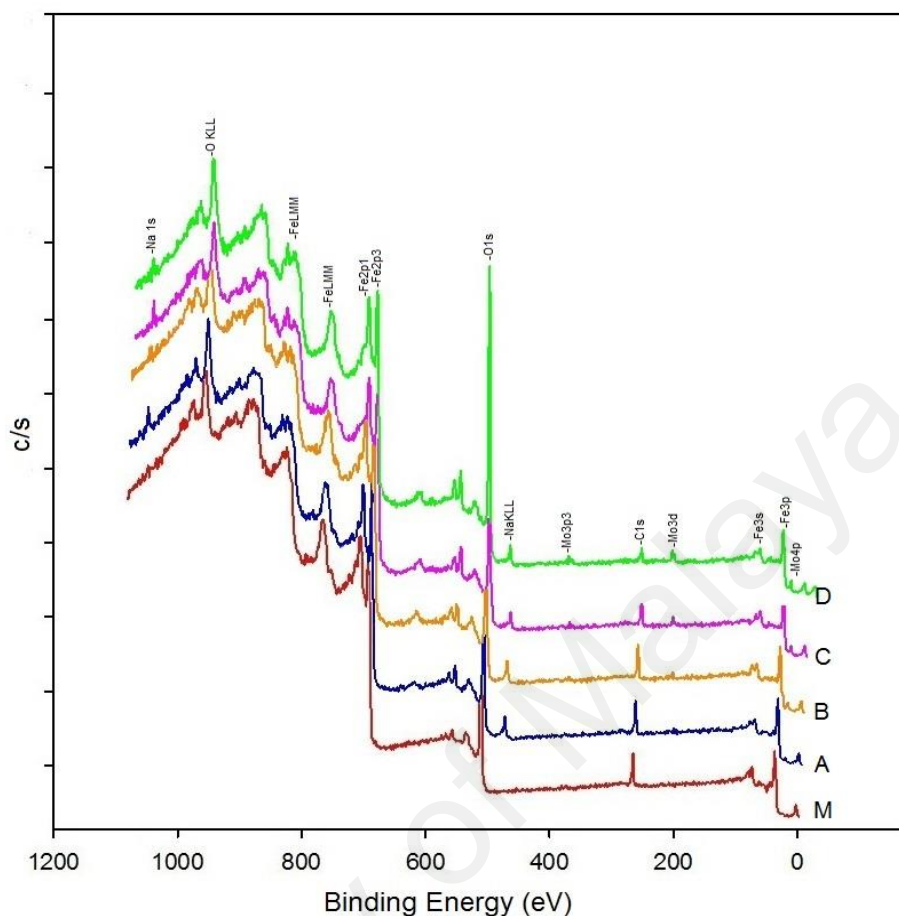


Figure 4.15: XPS spectra of  $\text{Fe}_{3-x}\text{Mo}_x\text{O}_4$  samples

Figure 4.16 shows the narrow scanned Fe 2p spectra of the  $\text{Fe}_{3-x}\text{Mo}_x\text{O}_4$  samples. The peak position of Fe 2p<sub>1/2</sub> and Fe 2p<sub>3/2</sub> located between B.E. of 709.9 eV and 7110.5 eV used to determine the chemical states of Fe (Yamashita & Hayes, 2008).

The obtained results matched well with reference data for  $\text{Fe}^{2+}$  and  $\text{Fe}^{3+}$  cations (Magalhães et al., 2007). Furthermore, the satellite peaks at the side of the main peaks were also the characteristic of  $\text{Fe}^{2+}$  and  $\text{Fe}^{3+}$ . The configuration interaction of valence electrons relaxation is the main reason for generation of the satellite peaks (Paparazzo, 2006). Table 4.11 gives data regarding the weight (%) of Fe species on the surface of the samples. The  $\text{Fe}^{2+}$  cations decreased in the samples by the growth in Mo content that was evident from the Fe (II)/Fe (III) ratio values. This indicates the incorporated  $\text{Mo}^{4+}$  cations placed Fe (II) cations in octahedral sites of the magnetite. The data for satellite

Fe (II) and Fe (III) also presented in the table, which is important for precise quantification of the surface iron species.

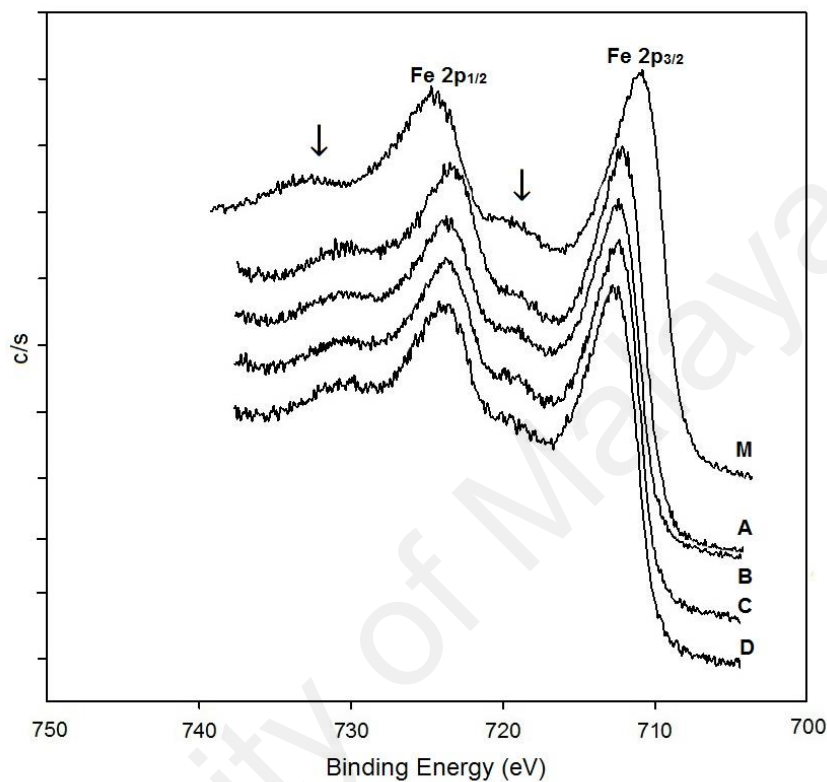


Figure 4.16: XPS spectra for Fe 2p region for the  $\text{Fe}_{3-x}\text{Mo}_x\text{O}_4$  samples (The arrows show satellite peaks)

Table 4.11: The elemental composition and their chemical states on the surface of  $\text{Fe}_{3-x}\text{Mo}_x\text{O}_4$  samples

Samples	Weight Fe (%)				$\text{Fe}^{\text{II}}/\text{Fe}^{\text{III}}$
	FeO	$\text{Fe}_2\text{O}_3$	Fe(II) satellite	Fe III satellite	
$\text{Fe}_{2.94}\text{Mo}_{0.028}\text{O}_4$	30.76	44.28	12.41	12.55	0.695
$\text{Fe}_{2.89}\text{Mo}_{0.069}\text{O}_4$	29.24	45.17	12.58	13.01	0.647
$\text{Fe}_{2.79}\text{Mo}_{0.13}\text{O}_4$	27.64	45.43	12.60	14.33	0.608
$\text{Fe}_{2.62}\text{Mo}_{0.21}\text{O}_4$	25.92	47.43	10.93	15.72	0.546



Details of peak position and corresponding chemical states of Fe species in the samples obtained via deconvolution of the Fe 2p spectra of  $\text{Fe}_{2.62}\text{Mo}_{0.21}\text{O}_4$  sample (Figure 4.17a).

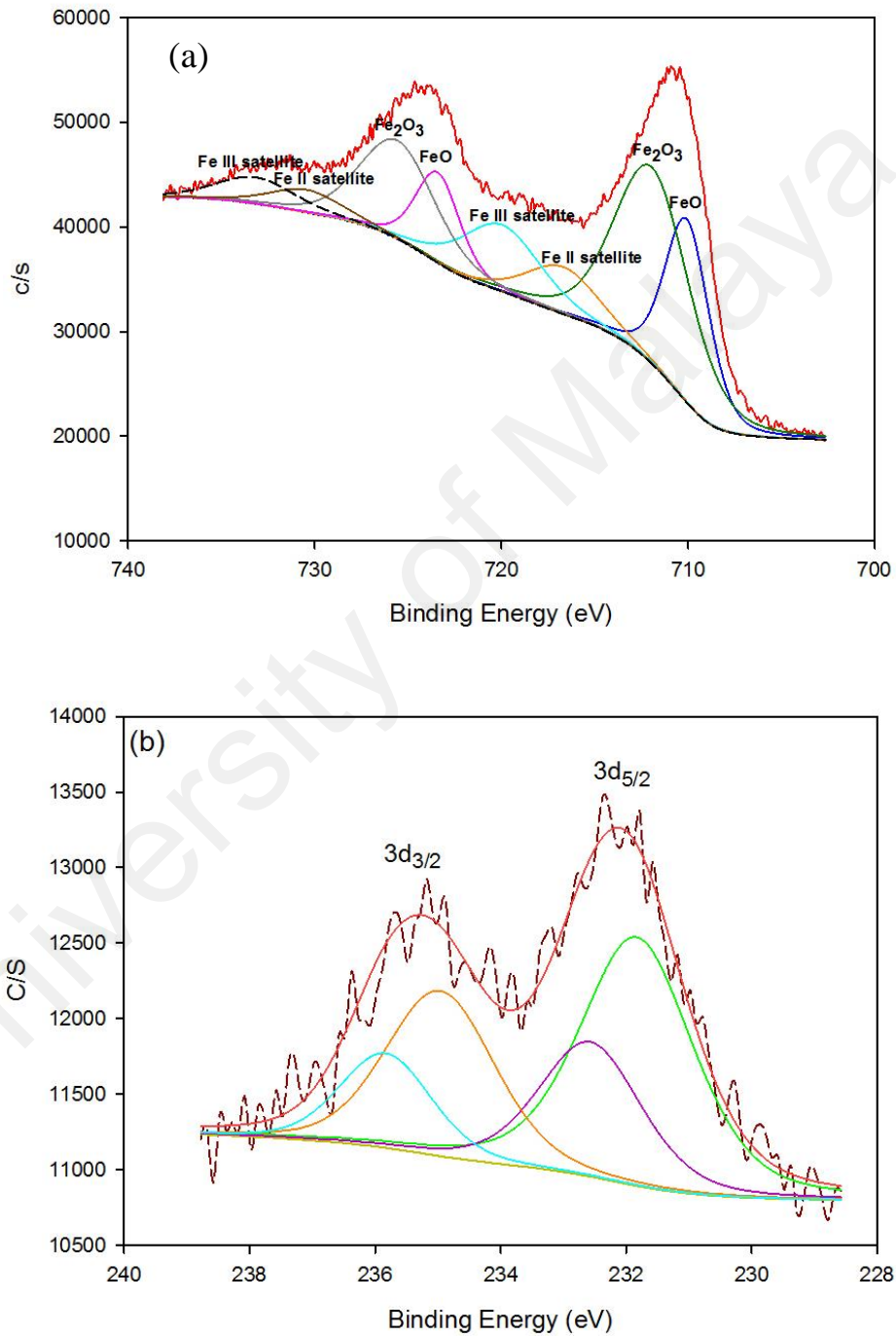


Figure 4.17: Deconvolution of the (a) Fe 2p doublet and (b) Mo 3d of  $\text{Fe}_{2.62}\text{Mo}_{0.21}\text{O}_4$  sample

The XPS analysis validated the presence of Mo on the surface of the synthesized samples. Figure (4.17b) shows the XPS spectra of Mo 3d for the  $\text{Fe}_{2.62}\text{Mo}_{0.21}\text{O}_4$  sample. The Mo 3d data matched well to that of Mo (IV) and Mo (VI) by the peaks at binding energies of 232.2 and 235.6, which ascribed to Mo  $3d_{5/2}$  and Mo  $3d_{3/2}$  respectively.

The magnetic properties of the  $\text{Fe}_{3-x}\text{Mo}_x\text{O}_4$  samples obtained using vibrating sample magnetometer (VSM). The main parameters extracted from the hysteresis loops were coercivity ( $H_{ci}$ ), saturation magnetization ( $M_s$ ), remanence ( $M_r$ ) and squareness ratio ( $\text{SQR} = M_r/M_s$ ) (Figure 4.18). The above-mentioned parameters used to assess the magnetic characteristics of the samples (Table 4.12).

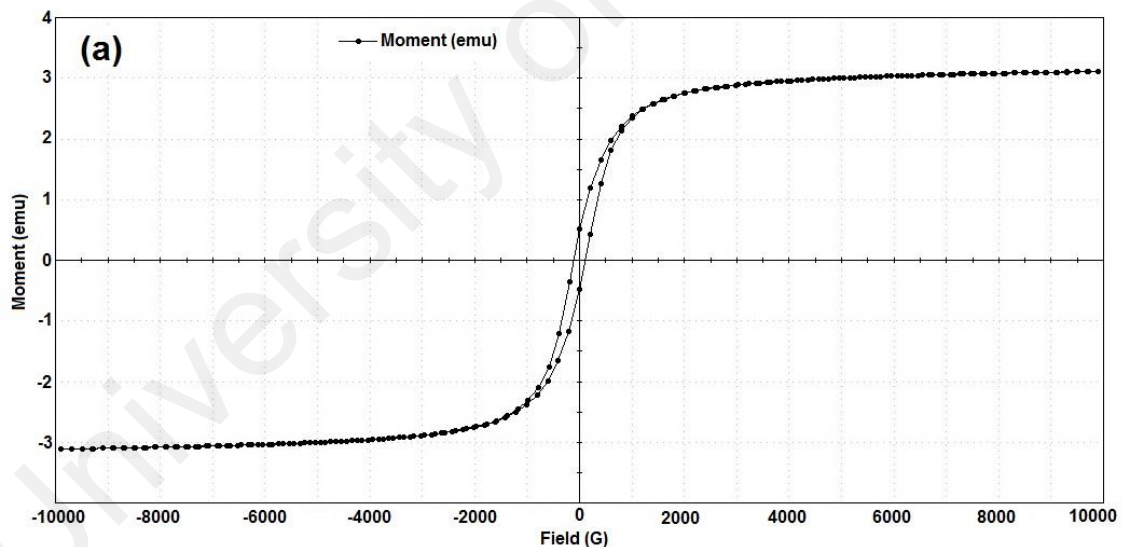


Figure 4.18a: Hysteresis loops for magnetite sample

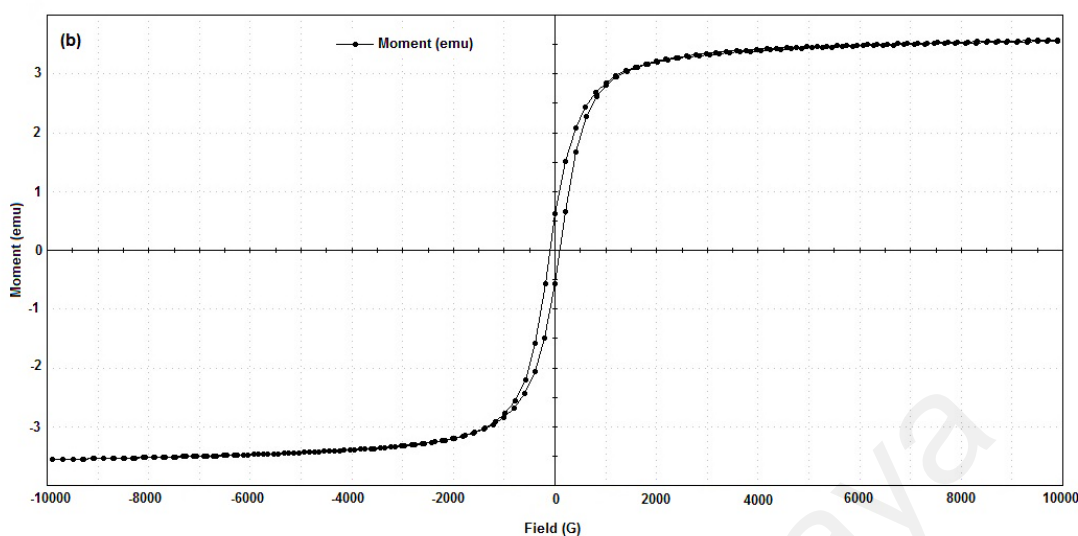


Figure 4.19b: Hysteresis loops for  $\text{Fe}_{2.62}\text{Mo}_{0.21}\text{O}_4$  sample

The slim hysteresis loop (low SQR values) is the characteristic property of the ferromagnetic materials that resulted from the high magnetic saturation ( $M_s$ ) and low residual magnetism ( $M_r$ ) of the samples. From the results, the magnetic property of magnetite maintained in all the modified samples and helped for magnetically separation of the samples from the reaction medium.

Table 4.12: Magnetic characteristics of  $\text{Fe}_{3-x}\text{Mo}_x\text{O}_4$  samples

Samples	H <sub>ci</sub> (G)	Magnetization M <sub>s</sub> (emu g <sup>-1</sup> )	SQR (M <sub>r</sub> /M <sub>s</sub> )
$\text{Fe}_3\text{O}_4$	108.39	68.93	0.1544
$\text{Fe}_{2.94}\text{Mo}_{0.028}\text{O}_4$	105.15	91.154	0.1547
$\text{Fe}_{2.89}\text{Mo}_{0.069}\text{O}_4$	107.24	80.06	0.1535
$\text{Fe}_{2.79}\text{Mo}_{0.13}\text{O}_4$	96.513	85.94	0.1559
$\text{Fe}_{2.62}\text{Mo}_{0.21}\text{O}_4$	96.468	89.23	0.1521

#### 4.4.2. Methylene blue adsorption by $\text{Fe}_{3-x}\text{Mo}_x\text{O}_4$

Figure 4.19 shows the quantity of MB adsorbed on the  $\text{Fe}_{3-x}\text{Mo}_x\text{O}_4$  samples at the state of equilibrium after 120 minutes of stirring. The value of MB adsorbed increased significantly in Mo substituted magnetite samples compared with pure magnetite. The rise in  $q_e$  was parallel with the increase in Mo content of the samples. A substantial MB removal of about 40% achieved through adsorption on  $\text{Fe}_{2.62}\text{Mo}_{0.21}\text{O}_4$  sample. This could be attributed to its large specific surface area (Liang et al., 2013). As explained earlier, the surface area of the  $\text{Fe}_{3-x}\text{Mo}_x\text{O}_4$  samples increased as the introduced Mo into the magnetite structure increased. Therefore, the available site for MB adsorption increased. This indicates the Mo substitution significantly improved the surface characteristics of magnetite towards enhanced adsorption capacity.

On the other hand, the surface charge of the samples also played a key role in MB adsorption. Being a cationic dye, MB adsorbs on the negatively charged surface of the catalyst. Based on the  $\text{pH}_{\text{pzc}}$  values of  $\text{Fe}_{3-x}\text{Mo}_x\text{O}_4$  samples that are below 7 (Figure 4.20), the surface of the samples was negatively charged at neutral condition. Therefore, MB adsorption took place under the studied condition. The adsorption experiments repeated at pH 10, to evaluate the effects of pH on the adsorption capacity of the samples. The MB adsorbed at pH 10 after 120 min of agitation improved significantly. This could be attributed to the increase in the surface hydroxyl groups of the samples at basic conditions (Liang et al., 2012a). The results indicated that both surface properties of hetero-catalyst and probe molecule characteristics have had crucial effects on the adsorption capacity of the samples.

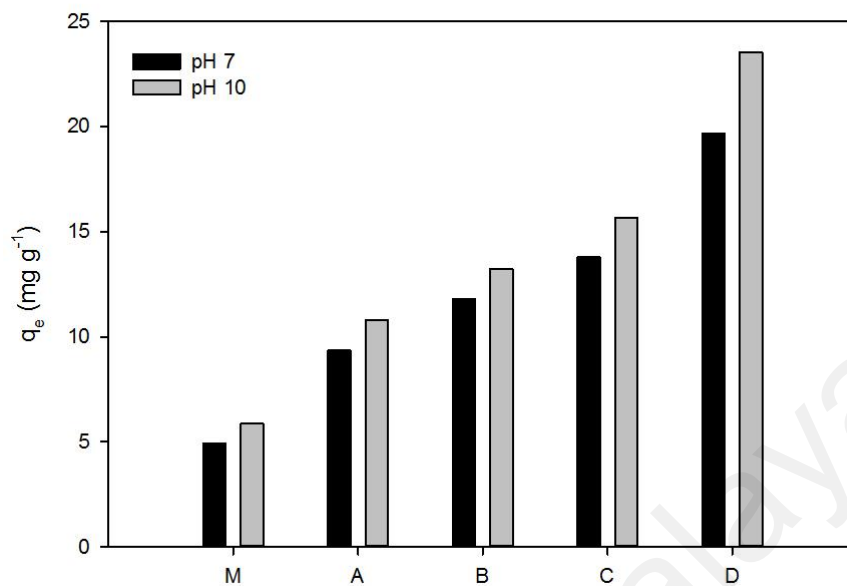


Figure 4. 20: Effect of pH on the MB adsorption on  $\text{Fe}_{3-x-y}\text{Nb}_x\text{Mo}_y\text{O}_4$  samples

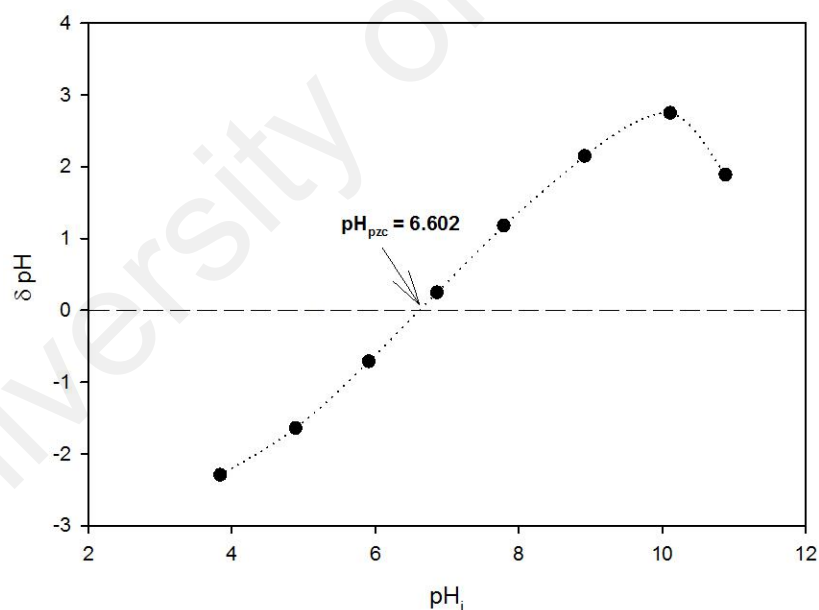


Figure 4. 21: The pH of the point of zero charge of  $\text{Fe}_{2.62}\text{Mo}_{0.21}\text{O}_4$  sample

#### 4.4.3. Methylene blue degradation and mineralization by $\text{Fe}_{3-x}\text{Mo}_x\text{O}_4$ samples

The activity of the synthesized samples investigated through MB oxidation in Fenton reaction. Fenton degradation of MB solution started after MB adsorption on the surface of the samples by mechanical stirring of the catalyst in MB solution. After attaining the

adsorption equilibrium, MB degradation process initiated after  $H_2O_2$  addition to the system. Figure 4.21 shows the MB removal ( $C_t/C_0$ ) through adsorption and Fenton reaction. All Mo substituted magnetite samples showed remarkable activity in Fenton decolorization of MB solution in comparison to pure magnetite. The MB removal efficiency using  $Fe_{2.94}Mo_{0.028}O_4$ ,  $Fe_{2.89}Mo_{0.069}O_4$ ,  $Fe_{2.79}Mo_{0.13}O_4$  and  $Fe_{2.62}Mo_{0.21}O_4$  samples was about 48%, 52%, 56% and 63% more than pure magnetite within the reaction duration of 150 min. However, MB decolorization rate significantly improved to about 10 to 25 % when the pH of the solution increased to 10 (Fig. 4.22). The enhancement in degradation efficiency at pH 10 was mainly because of the large number of surface OH<sup>-</sup> groups on the samples compared with neutral pH and accordingly, higher adsorption capacity of the samples.

However, there are reports on some anionic dyes with low adsorption on the surface of a modified magnetite. Degrading these anionic dyes through Fenton reaction was via some other oxidation mechanisms (Liang et al., 2013).

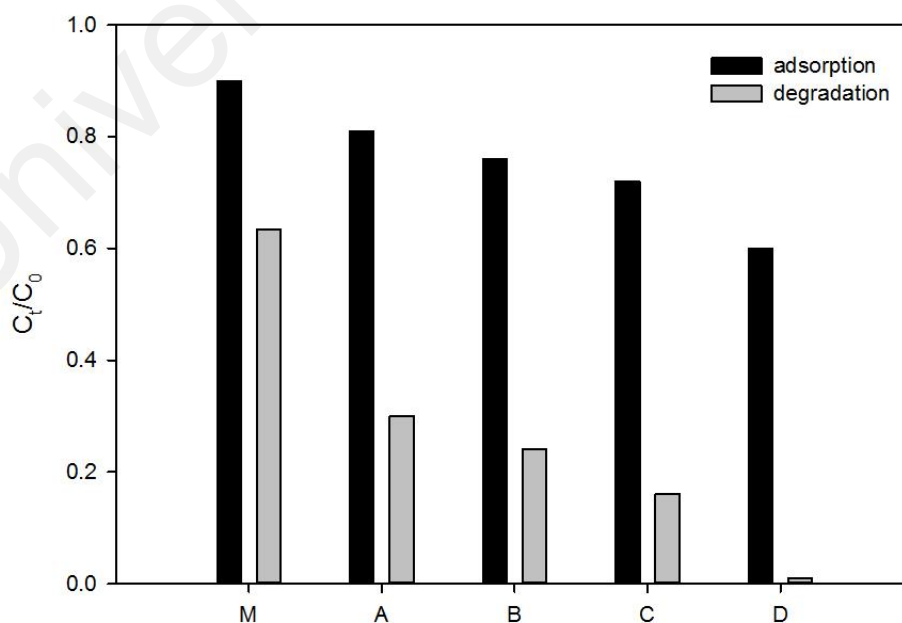


Figure 4.22: MB removal through adsorption and Fenton oxidation by  $Fe_{3-x}Mo_xO_4$  samples

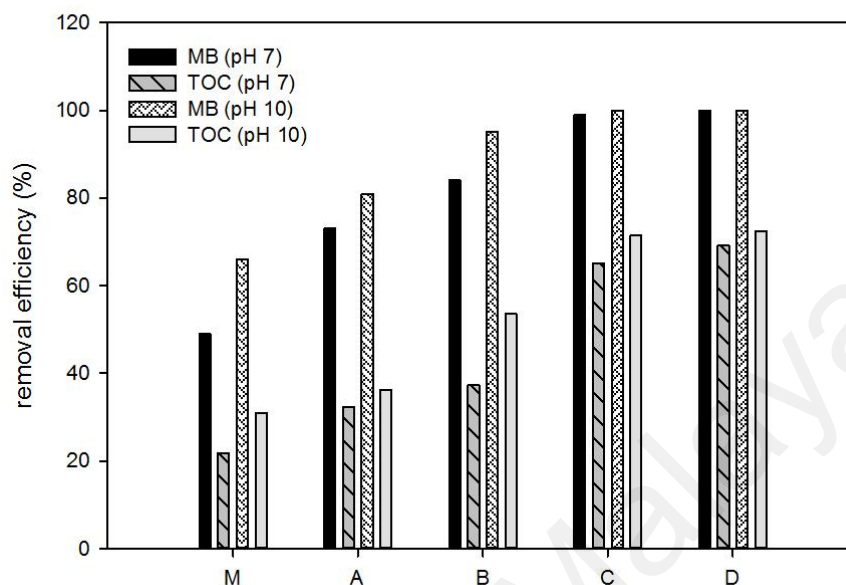


Figure 4.23: Degradation and mineralization of MB solution through Fenton-like reaction using  $\text{Fe}_{3-x}\text{Mo}_x\text{O}_4$  catalysts at pH values of 7 and 10

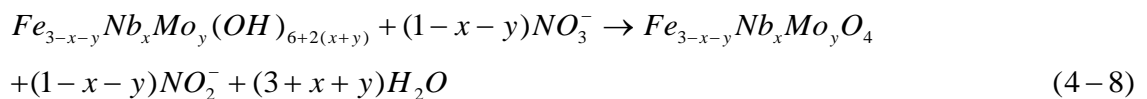
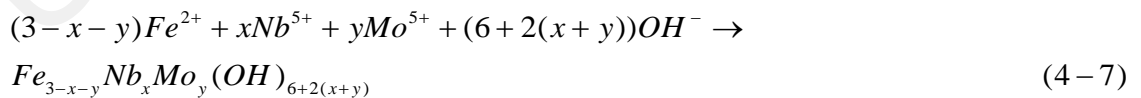
The MB mineralization effectiveness of  $\text{Fe}_{3-x}\text{Mo}_x\text{O}_4$  samples is also shown in Fig. 4.23. The degree of mineralization meaningfully improved by modified samples. It was about 34%, 42%, 66% and 68% higher than unmodified magnetite using  $\text{Fe}_{2.94}\text{Mo}_{0.028}\text{O}_4$ ,  $\text{Fe}_{2.89}\text{Mo}_{0.069}\text{O}_4$ ,  $\text{Fe}_{2.79}\text{Mo}_{0.13}\text{O}_4$  and  $\text{Fe}_{2.62}\text{Mo}_{0.21}\text{O}_4$  samples. The differences in TOC removal significantly increased when the pH of the solution altered to 10. A significant TOC removal efficiency of 71.5% and 72.4% obtained using  $\text{Fe}_{2.79}\text{Mo}_{0.13}\text{O}_4$  and  $\text{Fe}_{2.62}\text{Mo}_{0.21}\text{O}_4$  samples at pH 10.

The results strongly proved that Mo substitution improved the characteristics of magnetite towards higher adsorption capacity and activity in Fenton oxidation of MB. A distinct enhancement specially observed using  $\text{Fe}_{2.79}\text{Mo}_{0.13}\text{O}_4$  and  $\text{Fe}_{2.62}\text{Mo}_{0.21}\text{O}_4$  samples with the highest values of Mo in their structure. In  $\text{Fe}_{2.62}\text{Mo}_{0.21}\text{O}_4$  sample, though the stoichiometric value of  $x=0.3$  was initially used but the actual structural

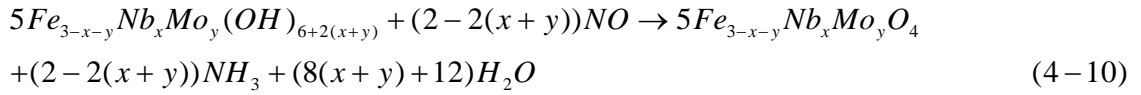
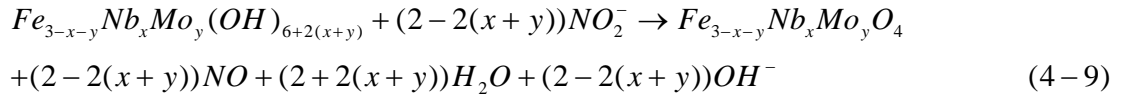
value was  $x=0.21$ . Therefore, similar to Nb substituted magnetite series, the ratio of  $x=0.2$  found as optimal value amongst  $Fe_{3-x}Mo_xO_4$  samples. Afterwards, the value of  $x=0.2$  used as a sum amount to prepare co-doped (Nb + Mo) substituted magnetite samples. The aim was to investigate the effects of co-precipitation of Nb and Mo on magnetite adsorption capacity and activity and to assess the prominence of one metal over another. The characteristics and activity of co-doped samples is discussed in detail in the following sections.

#### 4.5. Niobium and molybdenum co-doped magnetite ( $Fe_{3-x-y}Nb_xMo_yO_4$ )

In previous studied series,  $Fe_{3-x}Nb_xO_4$  and  $Fe_{3-x}Mo_xO_4$ ,  $x = 0.2$  was the optimal value to achieve a high removal efficiency. Accordingly, the molar value of 0.2 was chosen for the sum of  $x$  and  $y$  for co-doped samples. It was to investigate the effects of combined Nb+Mo incorporation versus singular substitution of Nb or Mo and the prominence of one over another metal. Five  $Fe_{3-x-y}Nb_xMo_yO_4$  samples ( $x = 0.025, 0.05, 0.1, 0.15, 0.175$  and  $y = 0.2 - x$ ) were prepared based on the stoichiometric amount of each element. The following set of the reactions (Eqs. 4-7 to 4-10) proposed by Sugimoto and Matijević (1980), used to show the synthesis of  $Fe_{3-x-y}Nb_xMo_yO_4$  samples and possible intermediate steps:







#### 4.5.1. Characterization of $Fe_{3-x-y}Nb_xMo_yO_4$ samples

The chemical formula of the synthesized samples was determined using ICP analysis and the amount of oxygen vacancy for each sample was calculated (Table 4.13). The results showed that negligible amount of Fe (0.002-0.05%) and Nb (0.01-0.05%) remained unreacted, while in the case of Mo, it was very high (6-46%) which showed that the incorporation maxima of Mo into magnetite was much less than Nb. The maxima incorporation value for number of transition metals from fourth row of periodic table has been determined (Klas et al., 2011), but in the case of other transition metals has been poorly addressed in literature. The generated oxygen vacancies in the samples were mainly from the cationic deficiency in their structure and adjustments for structural dislocations (Pearce et al., 2015).

Table 4.13: Chemical formula, surface area, pore size/volume and particle size of  $\text{Fe}_{3-x-y}\text{Nb}_x\text{Mo}_y\text{O}_4$  samples

ID	Formula from analysis	OV*	BET Surface area ( $\text{m}^2/\text{g}$ )	Pore size ( $\text{\AA}$ )	Pore volume ( $\times 10^{-2}\text{cm}^3/\text{g}$ )	Particle size (nm)
M	$\text{Fe}_{2.999}\text{O}_4$	0.001	29.980	157.745	11.823	90.9
A	$\text{Fe}_{2.79}\text{Nb}_{0.0249}\text{Mo}_{0.094}\text{O}_4$	0.082	55.121	113.467	12.793	48.7
B	$\text{Fe}_{2.79}\text{Nb}_{0.049}\text{Mo}_{0.089}\text{O}_4$	0.062	56.213	110.264	14.793	45.9
C	$\text{Fe}_{2.79}\text{Nb}_{0.099}\text{Mo}_{0.073}\text{O}_4$	0.027	57.645	106.548	15.756	45.2
D	$\text{Fe}_{2.79}\text{Nb}_{0.149}\text{Mo}_{0.032}\text{O}_4$	0.018	62.845	103.122	15.183	44.2
E	$\text{Fe}_{2.79}\text{Nb}_{0.171}\text{Mo}_{0.023}\text{O}_4$	0.006	79.665	90.055	18.753	31.3

In order to investigate the amount of incorporation maxima of Mo, a  $\text{Fe}_{3-x-y}\text{Nb}_x\text{Mo}_y\text{O}_4$  sample with higher Mo content than stoichiometric value ( $\text{Fe}_{2.8}\text{Nb}_{0.1}\text{Mo}_{0.15}\text{O}_4$ ) was prepared and characterized by XRD and TEM. The results showed that the crystal structure of the sample was not purely magnetite and a fraction of orthorhombic phase was observed in the TEM images of the sample (Fig. 4.24).

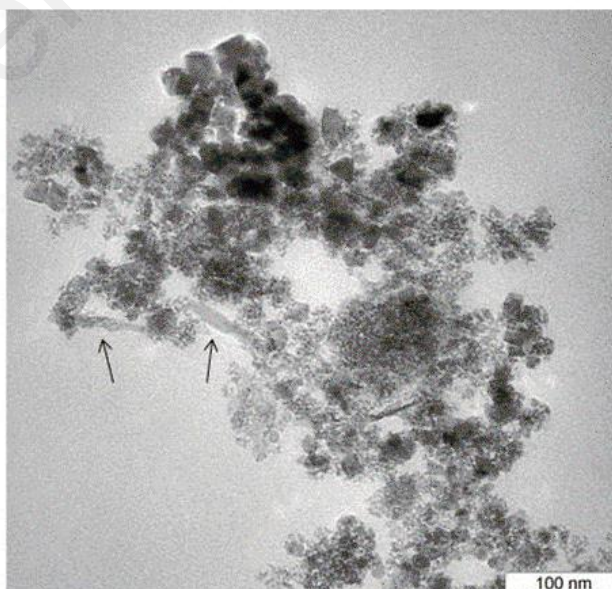


Figure 4. 24: TEM image of  $\text{Fe}_{3-x-y}\text{Nb}_x\text{Mo}_y\text{O}_4$  sample ( $x = 0.1, y = 0.15$ ); the arrows show the orthorhombic phase

BET surface area, total pore volume and pore size distribution were obtained at physisorption capacity of 77.35 K using Micromeritics instrument (tristar 3020). All the synthesized samples were degassed at 90°C for 1h and then at 303° K/min for 4 h before the test. The chemical formula and data on BET surface properties and particle size of the samples are summarized in Table 4.14. The results presented in the table show that the increment in total Nb+Mo content of the samples ranging from 0.1189 to 0.194 was followed by the decrease in particle size or increase in surface area. The difference observed between the surface area values of the Nb+Mo substituted magnetite samples and pure magnetite could be justified considering the decrease in pore size of the samples.

Figure 4.25 shows the XRD patterns for co-precipitated Nb and Mo magnetite samples. All the diffraction peaks of five  $\text{Fe}_{3-x-y}\text{Nb}_x\text{Mo}_y\text{O}_4$  samples corresponded well to the magnetite crystal structure of the standard cards numbered: 98-007-7589, 98-002-9129, 98-015-7651 and 98-015-8743. The peaks at  $2\theta$  values of 18.3° (111), 30.2° (220), 35.6° (311), 37° (222), 43.3° (400), 53.7° (422), 57.2° (511), 62.8° (440) and 74.4° (533) were observed, which are consistent with the standard XRD data for magnetite.

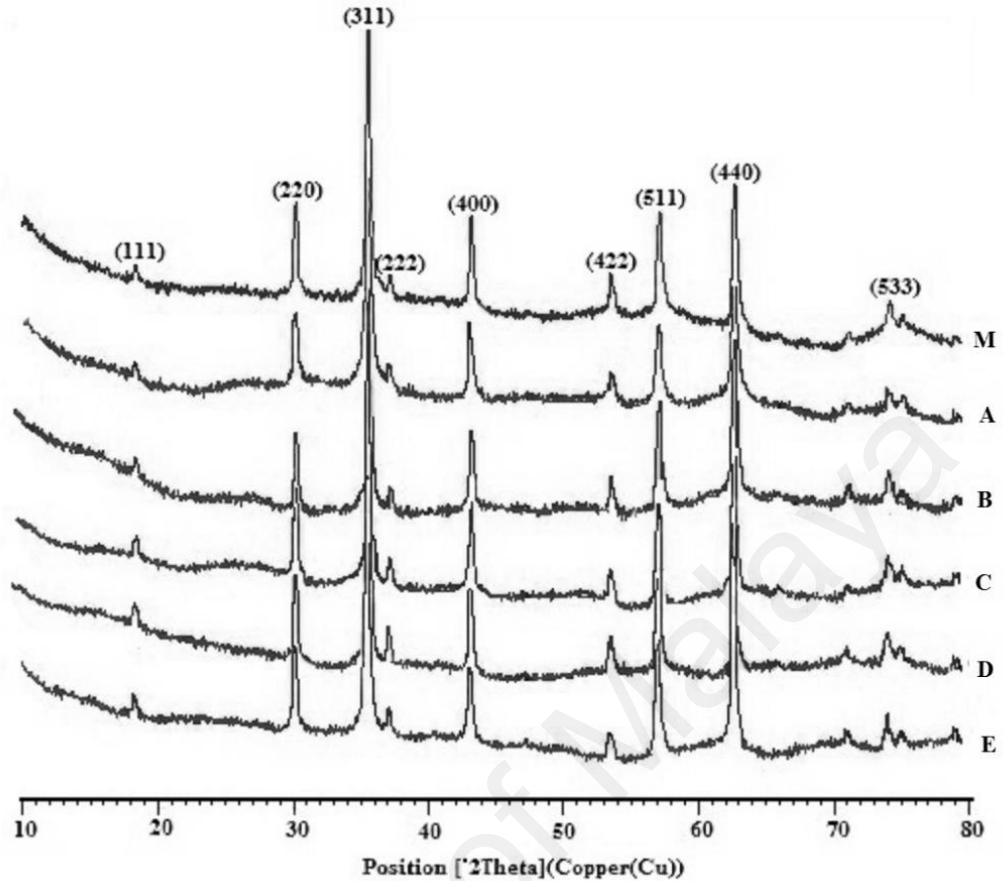


Figure 4.25: XRD patterns of  $\text{Fe}_{3-x-y}\text{Nb}_x\text{Mo}_y\text{O}_4$  samples

The size, shape, dispersity and morphology of the samples were analyzed by TEM. Figure (4.26b-f) show the TEM images of the co-doped samples in comparison to pure magnetite (Fig. 4.26a). The average size of the particles of each sample was determined from the obtained images. It can be seen from the micrographs of the samples that the particles grew well in octahedral form which is a characteristic morphology of well-crystallized magnetite (Liang et al., 2012b). The diameters of the particles were less than 50 nm that decreased with growth in the amount of incorporated metals.

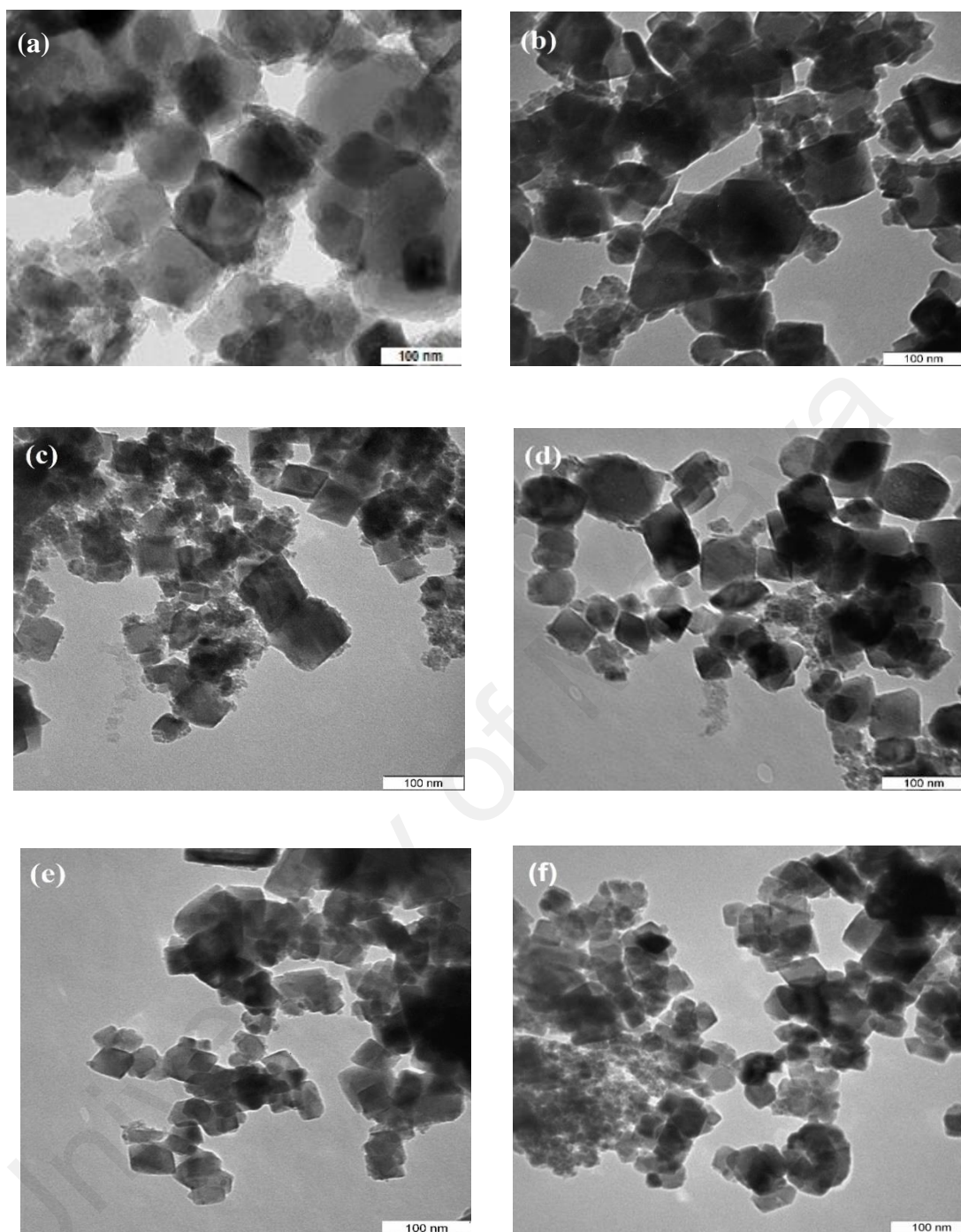


Figure 4.26: TEM images of (a)  $\text{Fe}_3\text{O}_4$  (b)  $\text{Fe}_{2.79}\text{Nb}_{0.0249}\text{Mo}_{0.094}\text{O}_4$ , (c)  $\text{Fe}_{2.79}\text{Nb}_{0.049}\text{Mo}_{0.089}\text{O}_4$ , (d)  $\text{Fe}_{2.79}\text{Nb}_{0.099}\text{Mo}_{0.073}\text{O}_4$ , (e)  $\text{Fe}_{2.79}\text{Nb}_{0.149}\text{Mo}_{0.032}\text{O}_4$  and (f)  $\text{Fe}_{2.79}\text{Nb}_{0.171}\text{Mo}_{0.023}\text{O}_4$  samples

Vibrating sample magnetometer (VSM) was used to study the magnetic behavior of the samples. This property was a key factor for easy separation of the synthesized catalysts from the reaction medium. The coercivity ( $H_{ci}$ ), saturation magnetization ( $M_s$ ),

remanence ( $M_r$ ) and squareness ratio ( $SQR = M_r/M_s$ ) were the main parameters that were used to assess the magnetic characteristics of the samples. Table 4.14 shows the data acquired from the hysteresis loops generated from the VSM analysis (Fig. A.C<sub>a-f</sub>). The resulted slim hysteresis loops are the characteristic feature of the ferromagnetic materials that came from the high magnetic saturation ( $M_s$ ) and low residual magnetism ( $M_r$ ) of the samples. Accordingly, the SQR values ( $\approx 0.15$ ) were very small and close to zero that is characteristic of magnetic materials.

Table 4.14: Magnetic characteristics of  $Fe_{3-x}Nb_xMo_yO_4$  samples

Samples	H <sub>ci</sub> (G)	Magnetization M <sub>s</sub> (emu g <sup>-1</sup> )	SQR (M <sub>r</sub> /M <sub>s</sub> )
Fe <sub>3</sub> O <sub>4</sub>	108.39	68.93	0.1544
Fe <sub>2.79</sub> Nb <sub>0.0249</sub> Mo <sub>0.094</sub> O <sub>4</sub>	87.312	66.46	0.1526
Fe <sub>2.79</sub> Nb <sub>0.049</sub> Mo <sub>0.089</sub> O <sub>4</sub>	88.94	64.77	0.1556
Fe <sub>2.79</sub> Nb <sub>0.099</sub> Mo <sub>0.073</sub> O <sub>4</sub>	84.362	64.26	0.1538
Fe <sub>2.79</sub> Nb <sub>0.149</sub> Mo <sub>0.032</sub> O <sub>4</sub>	83.973	65.6	0.1547
Fe <sub>2.79</sub> Nb <sub>0.171</sub> Mo <sub>0.023</sub> O <sub>4</sub>	77.038	67.48	0.1513

X-ray photoelectron spectroscopy (XPS) was used to determine the elemental composition, corresponding oxidation states and relative distribution of the imported transition metals located on the surface or near-surface of the synthesized samples. The required information was acquired by analyzing the XPS spectrum of the samples through a complete XPS spectrum (survey scan) and the narrow scan of the interested elements. The narrow scans were completed on the spectral regions of 700–740, 520–550, 278–298, 222–242 and 197–217 eV for Fe 2p, O 1s, C 1s, Mo 3d and Nb 3d respectively.

Fig. 4.27 shows the XPS survey spectrum of the samples. The strong Nb/Mo position peaks supported the incorporation of these elements into the magnetite structure and their presence on the surface of the catalysts. This was noticeable especially in the case of Nb cations in which the intensity of Nb3p and Nb3d increased gradually with the imported Nb. However, the amount of Mo on the surface of the samples was less in comparison with Nb.

To identify the chemical states of the surface ions of interest, the narrow scan of iron (Fe), niobium (Nb), molybdenum (Mo) and oxygen (O) were recorded and deconvolution of peak shape was carried out. Figure 4.28 presents the XPS spectra for Fe 2p of the  $\text{Fe}_{3-x-y}\text{Nb}_x\text{Mo}_y\text{O}_4$  samples. The satellite peaks were observed at the side of the main peaks with low kinetic energy. These satellite peaks are characteristics of  $\text{Fe}^{2+}$  and  $\text{Fe}^{3+}$  species, which are generated due to configuration interaction caused by relaxation of valence electrons.

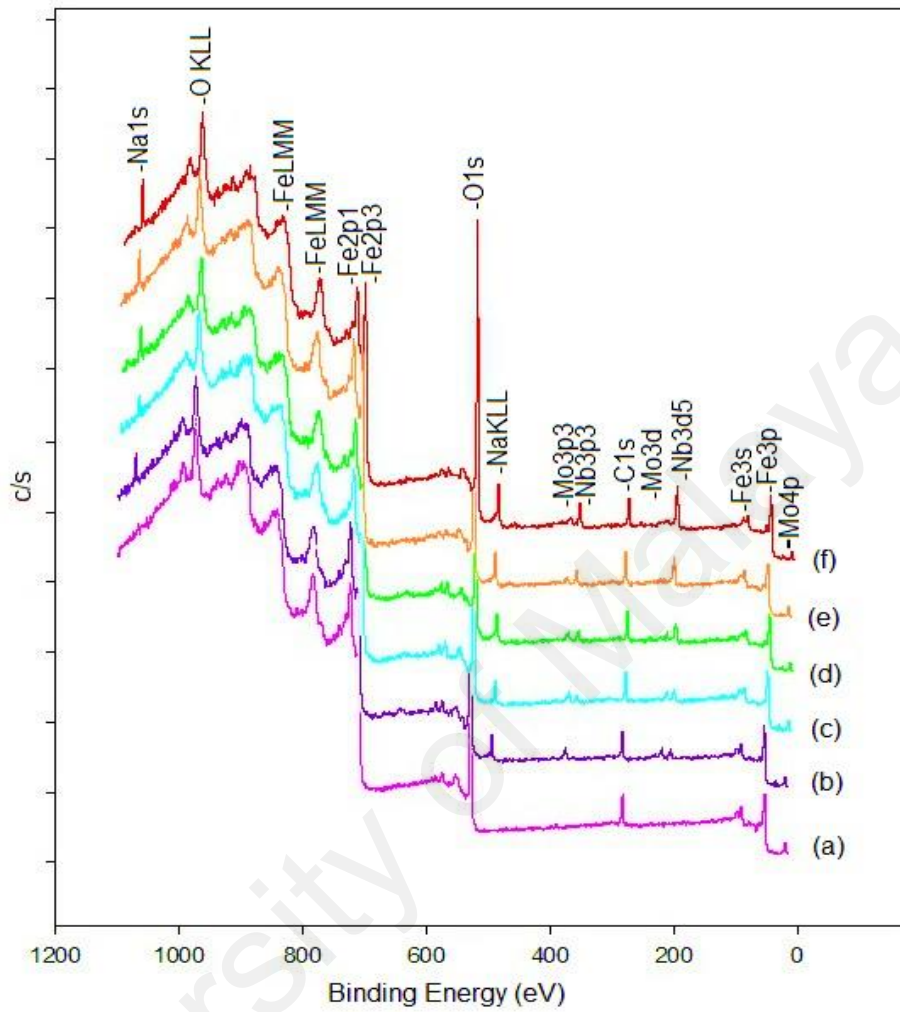


Figure 4.27: XPS spectra of Fe<sub>3-x-y</sub>Nb<sub>x</sub>Mo<sub>y</sub>O<sub>4</sub> samples



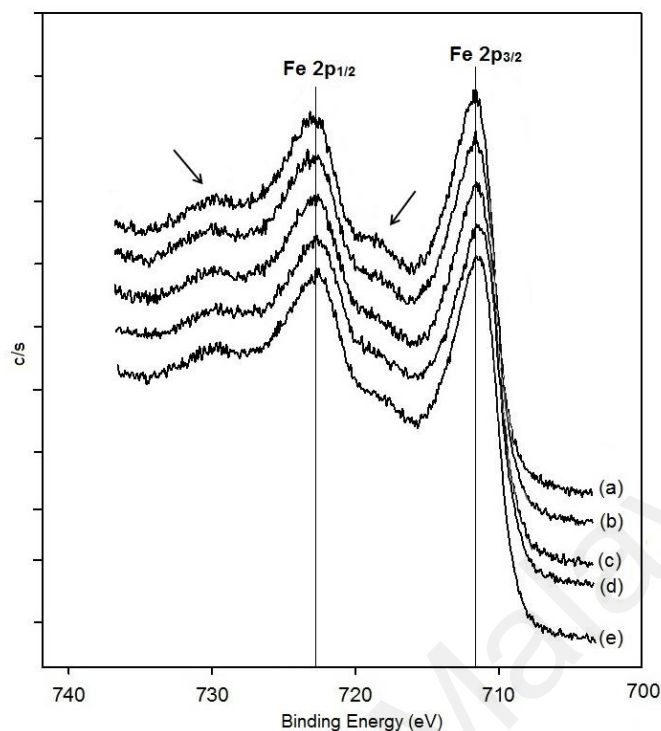


Figure 4.28: XPS spectra for Fe 2p of  $\text{Fe}_{3-x-y}\text{Nb}_x\text{Mo}_y\text{O}_4$  samples (The arrows show satellite peaks)

Table 4.15 shows data on relative weight (%) of each oxidation state of Fe. From the table, the increased  $\text{Fe}^{2+}/\text{Fe}^{3+}$  ratios indicated that the  $\text{Fe}^{3+}$  cations were replaced by imported Nb and Mo ions of which the total Nb+Mo content of the samples increased with incorporated Nb, as explained earlier. In addition, the table gives the concentrations of satellite Fe (II) and Fe (III) to show the accurate magnitude of the surface iron species.

Table 4.15: Weight (%) of surface Fe cations

Sample	Weight (%)			
	FeO	Fe <sub>2</sub> O <sub>3</sub>	Fe (II) Sat.	Fe (III) Sat.
$\text{Fe}_{2.79}\text{Nb}_{0.0249}\text{Mo}_{0.094}\text{O}_4$	26.29	48.48	10.73	14.49
$\text{Fe}_{2.79}\text{Nb}_{0.049}\text{Mo}_{0.089}\text{O}_4$	28.29	48.62	11.59	11.49
$\text{Fe}_{2.79}\text{Nb}_{0.099}\text{Mo}_{0.073}\text{O}_4$	28.97	46.73	11.37	12.93
$\text{Fe}_{2.79}\text{Nb}_{0.149}\text{Mo}_{0.032}\text{O}_4$	29.71	46.22	11.50	12.56
$\text{Fe}_{2.79}\text{Nb}_{0.171}\text{Mo}_{0.023}\text{O}_4$	29.96	45.90	12.69	11.45

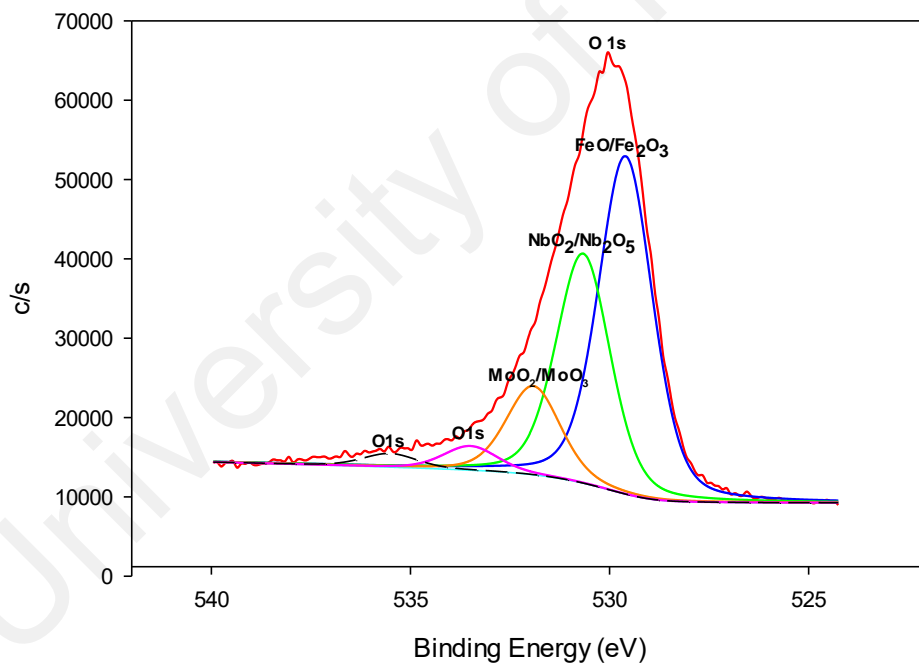
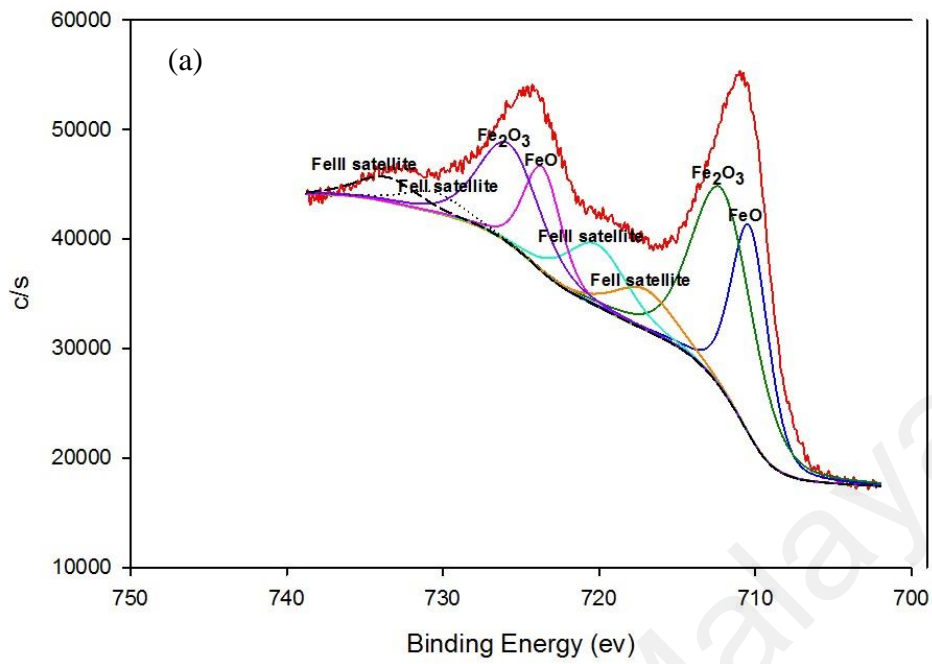
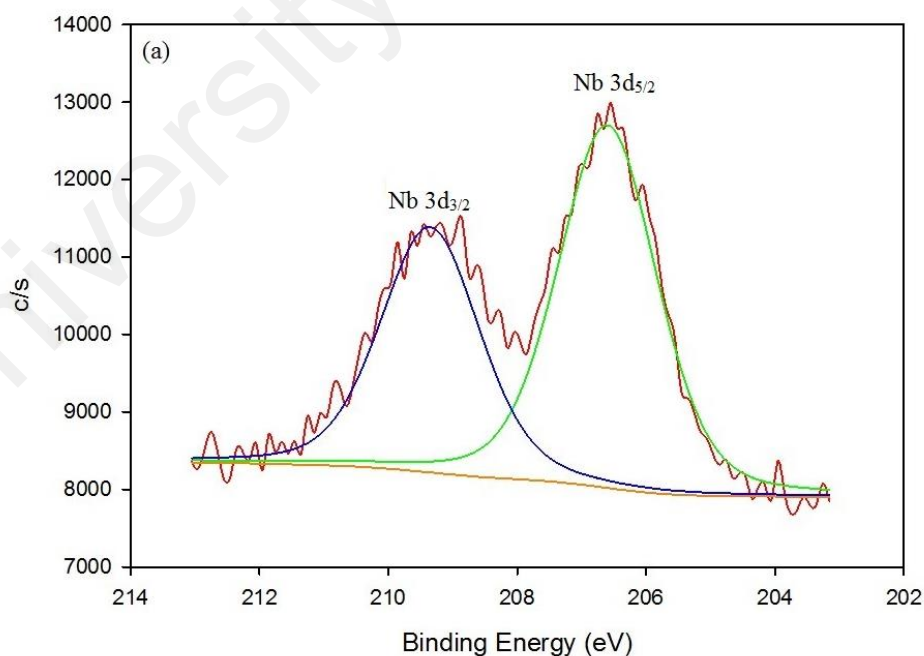


Figure 4.29: Deconvolution of the (a) Fe 2p doublet and (b) O 1s of



Figure 4.29<sub>a</sub> shows the deconvolution of the Fe 2p related to Fe<sub>2.79</sub>Nb<sub>0.099</sub>Mo<sub>0.073</sub>O<sub>4</sub> sample. It was observed that the Fe 2p peaks were located at B.E. of 709.9 and 7110.5 eV that are characteristic of Fe<sup>2+</sup> and Fe<sup>3+</sup> cations based on the referred data.

Deconvolution of O1s is presented in Fig. 4.29<sub>b</sub>. The O 1s spectrum could be deconvoluted into three main individual component peaks, which originated from overlapping of the peaks of FeO/Fe<sub>2</sub>O<sub>3</sub>, NbO<sub>2</sub>/Nb<sub>2</sub>O<sub>5</sub> and MoO<sub>2</sub>/MoO<sub>3</sub> on each other. The peaks at binding energies of 529.7, 530.9 and 531.4 are representing oxygen in the forms of FeO/Fe<sub>2</sub>O<sub>3</sub>, NbO<sub>2</sub>/Nb<sub>2</sub>O<sub>5</sub> and MoO<sub>2</sub>/MoO<sub>3</sub> respectively. The atomic concentration (%) of Nb-O and Mo-O varied between 9.52 to 34.94 and 5.04 to 14.06 respectively. This also supports the fact that the amount of surface Mo was relatively lower than surface Nb.



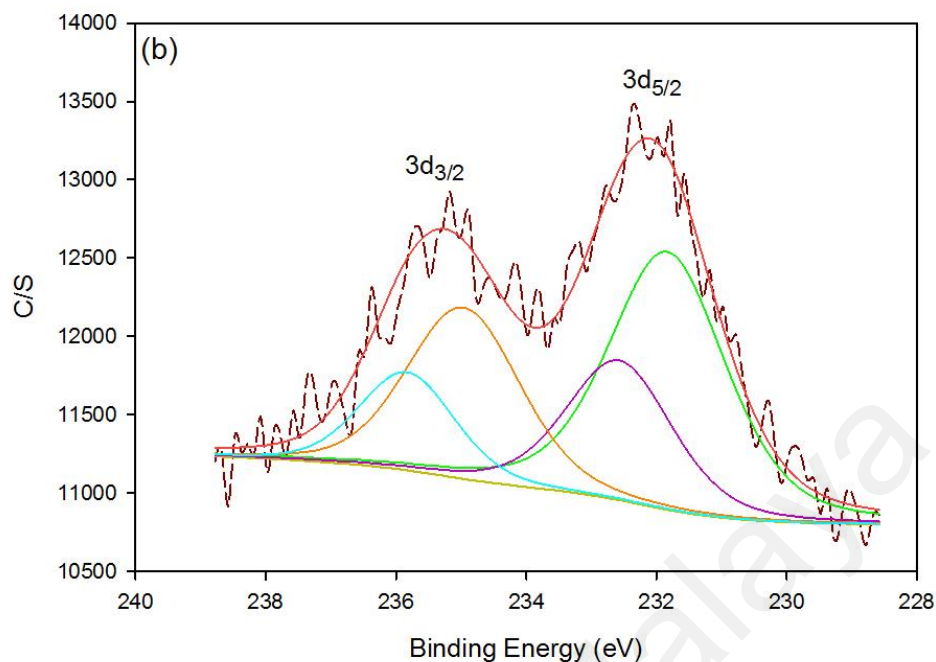


Figure 4.30: XPS spectra for (a) Nb 3d and (b) Mo 3d for the  $\text{Fe}_{2.79}\text{Nb}_{0.099}\text{Mo}_{0.073}\text{O}_4$  sample

The fundamental goal of XPS analysis was to confirm the presence of the incorporated Nb and Mo on the surface of the synthesized samples and to distinguish the corresponding oxidation states of these elements. From the data obtained, the surface atomic concentration ratios of Nb/Fe and Mo/Fe varied at 0.018-0.098 and 0.008-0.043 respectively, representing the higher concentrations of Nb on the surface compared to Mo. Figs. 4.30<sub>a-b</sub> illustrates the XPS spectra of Nb 3d and Mo 3d for the  $\text{Fe}_{2.79}\text{Nb}_{0.099}\text{Mo}_{0.073}\text{O}_4$  sample. The Nb 3d and Mo 3d data matched well to that of Nb (IV) and Nb (V) and Mo (IV) and Mo (VI). From the figures, the peaks at binding energies of 206.3 and 209.8 eV could be assigned to Nb  $3d_{5/2}$  and Nb  $3d_{3/2}$  and the peaks at binding energies of 232.2 and 235.6 eV was ascribed to Mo  $3d_{5/2}$  and Mo  $3d_{3/2}$  respectively. In this study, the incorporation of Nb and Mo into the magnetite brought about a shift in valence electrons from Nb and Mo to oxygen and accordingly, a difference in their electronic structure of inner shells. However, this change was not very obvious but was detected by XPS based on the variation in bonding energies. In

fact, when the bonds between Nb-O and Mo-O forms the valence electrons transfer from Nb and Mo to O. Consequently, a shift in 3d5/2 to higher energy level and O 1s to lower energy level takes place.

#### **4.5.2. Adsorption capacity of $\text{Fe}_{3-x-y}\text{Nb}_x\text{Mo}_y\text{O}_4$ samples**

The amount of MB adsorbed on the synthesized samples over 2 h of stirring time for 100 mg L<sup>-1</sup> of MB is shown in Fig. 4.31. The maximum adsorption was achieved in the first hour and it continued at slower rate to reach the state of equilibrium at 120 min. This could be attributed to the large number of available adsorption sites on the surface of catalysts at initial time that were occupied rapidly. Then, the adsorption rate decreased due to decrease in vacant sites and repulsion force between the MB molecules on the surface of catalysts. Furthermore, the amount of adsorbed MB on Nb-Mo-magnetite samples was significantly higher than pure magnetite and it increased with total Nb+Mo content of the samples. The  $\text{Fe}_{2.52}\text{Nb}_{0.155}\text{Mo}_{0.016}\text{O}_4$  sample showed the highest adsorption capacity that was about 80% more than the pure magnetite. The results clearly indicated that incorporation of Nb and Mo had a positive effect on the adsorption capacity of magnetite, mainly due to the increase in specific surface area of the samples.

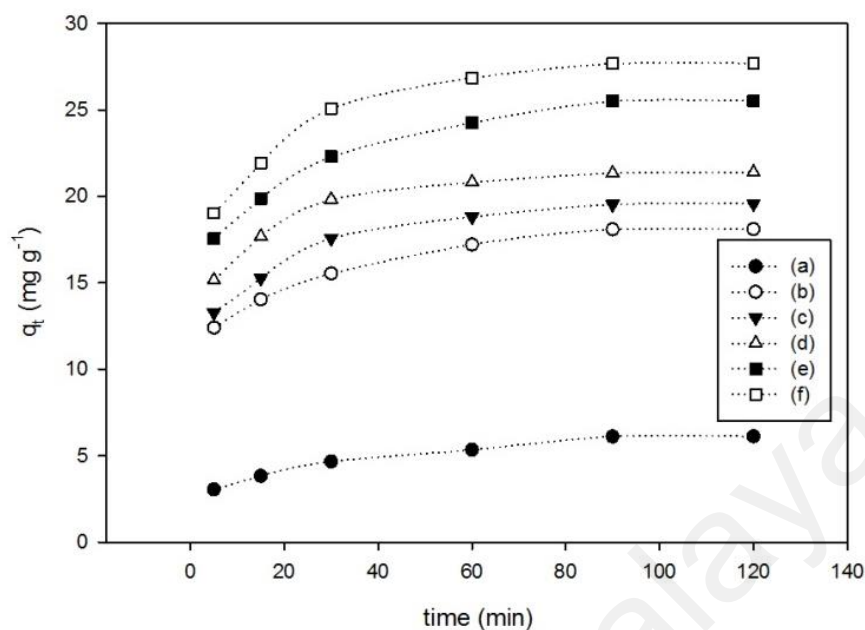


Figure 4.31: Effect of stirring time on adsorption of MB on samples at  $100 \text{ mg L}^{-1}$  (catalyst  $1 \text{ g L}^{-1}$ , pH 7, time 120 min)

It is noteworthy that pH of the solution played an important role for MB adsorption on the surface of the catalysts. Based on the pH of the point of zero charge of the samples ( $\text{pH}_{\text{pzc}}$ ), that were laid between 6.6 – 6.9 (Fig. 4.32), the surface of the samples were negatively charged at neutral pH ( $> \text{pH}_{\text{pzc}}$ ) and it was ideal for adsorption of MB as cationic dye due to electrostatic interaction. Since, the  $\text{pH}_{\text{pzc}}$  of the samples was smaller for higher Nb+Mo content than unmodified magnetite; the high basicity could be a possible fraction in more adsorption of MB on the surface of the samples at pH 7.

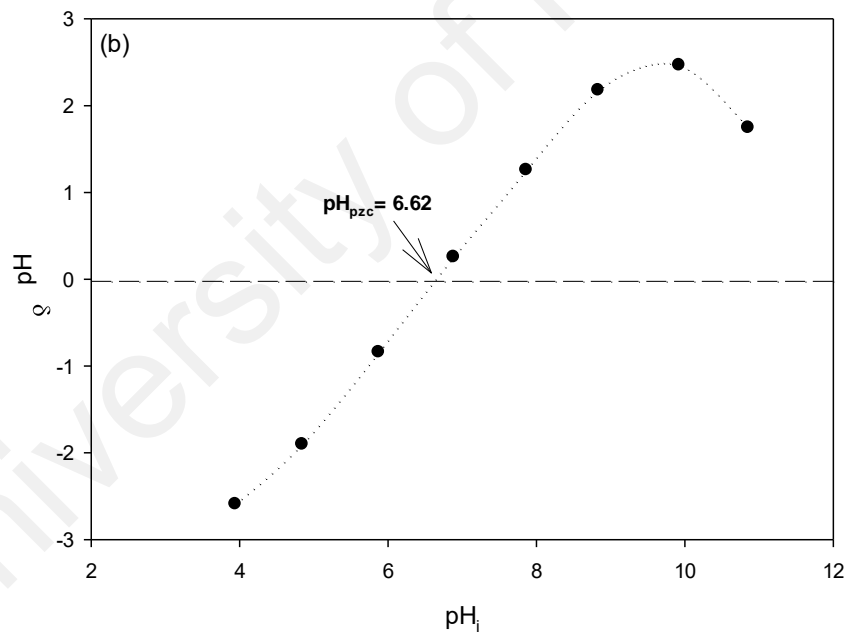
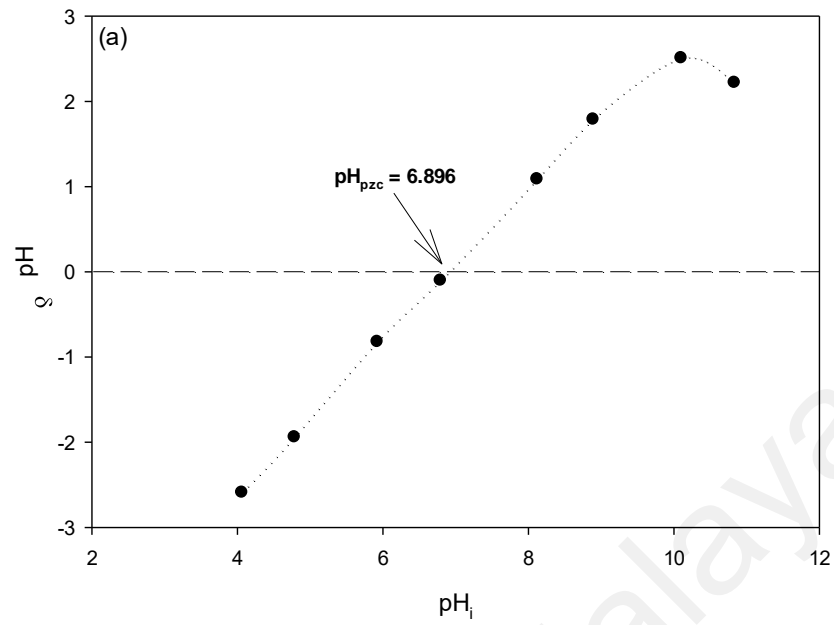


Figure 4.32: The pH of the point of zero charge of (a)  $Fe_3O_4$  and (b)  $Fe_{2.79}Nb_{0.171}Mo_{0.023}O_4$

Figure 4.33 shows the amount of adsorbed MB on the samples at pH 7 and 10. As explained earlier, the adsorption capacity of the samples significantly increased at basic

solution of pH 10 due to the large number of  $-OH$  groups on the surface of the samples (Liang et al., 2012a; Zhang et al., 2005).

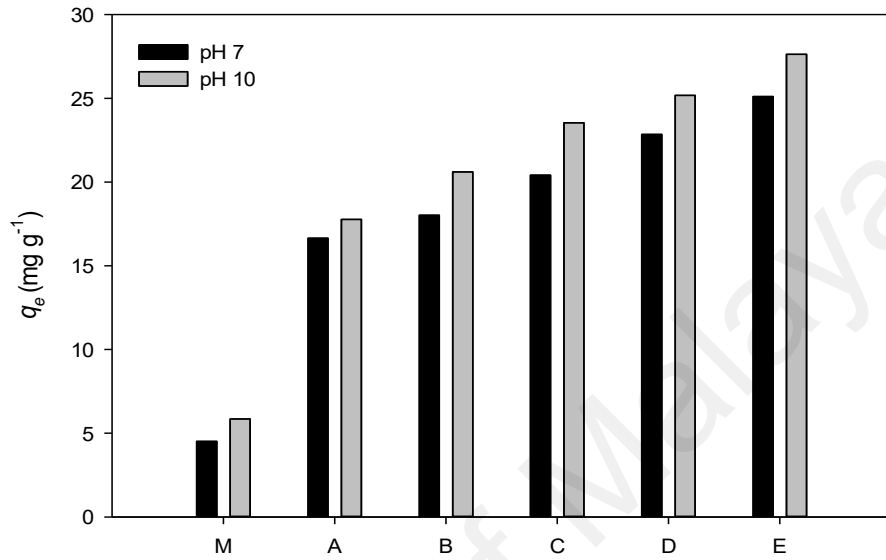


Figure 4.33: Effect of pH on adsorption of MB on  $Fe_{3-x-y}Nb_xMo_yO_4$  samples

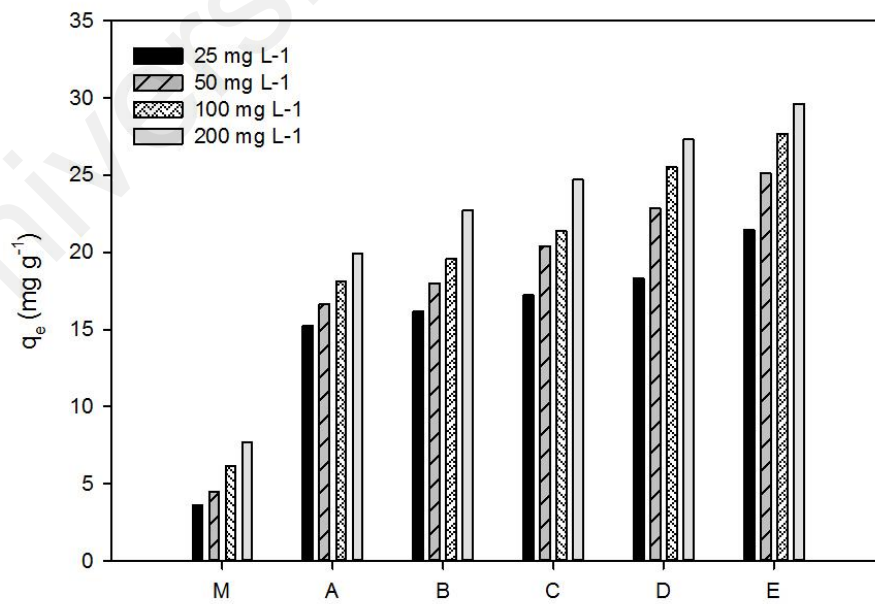


Figure 4.34: Effect of MB initial concentration on adsorption capacity of  $Fe_{3-x-y}Nb_xMo_yO_4$  samples



Fig. 4.34 shows the effects of initial MB concentration on the adsorption capacity of the samples. The amount of adsorbed MB increased at higher MB concentrations. This discrepancy was attributed to domination on mass transfer limitation of MB between the bulk solution (aqueous phase) and catalysts surface (solid phase) at high concentrations. Additionally, different dye concentrations showed similar adsorption trend in which the adsorption increased with Nb+Mo content and the difference in adsorption was more significant at lower MB concentrations.

#### **4.5.3. Fenton catalytic activity of $\text{Fe}_{3-x-y}\text{Nb}_x\text{Mo}_y\text{O}_4$ samples**

The catalytic activity of  $\text{Fe}_{3-x-y}\text{Nb}_x\text{Mo}_y\text{O}_4$  samples for MB degradation was assessed through Fenton reaction at neutral and basic conditions. Accordingly, MB degradation was monitored in the presence of Nb-Mo-magnetite samples as the catalyst and  $\text{H}_2\text{O}_2$  as the oxidant. The degradation process was initiated by adsorption of dye molecules on the surface of catalyst by agitation for 120 min before adding  $\text{H}_2\text{O}_2$ . All the synthesized samples showed exceptional performance compared to unmodified magnetite at neutral condition for both 50 and 100  $\text{mg L}^{-1}$  of MB (Fig. 4.35). As displayed in Fig. (4.35<sub>a</sub>), the total color removal for  $[\text{MB}]_0$  50  $\text{mg L}^{-1}$  using Nb+Mo substituted magnetite samples was completed within 180 min; whereas, pure magnetite showed only 40% decolorization under the same operating conditions. The effects were more pronounced for  $\text{Fe}_{2.79}\text{Nb}_{0.149}\text{Mo}_{0.032}\text{O}_4$  and  $\text{Fe}_{2.79}\text{Nb}_{0.171}\text{Mo}_{0.023}\text{O}_4$  samples in which more than 90% of MB was removed after 150 min. Similarly, above 70% MB (100  $\text{mg L}^{-1}$ ) was removed by the synthesized catalysts while the removal was only 30% using pure magnetite catalyzed Fenton reaction within 180 min (Fig 4.35<sub>b</sub>). The results obviously indicated that the incorporation of Nb and Mo in the magnetite structure significantly enhanced its activity for MB oxidation.

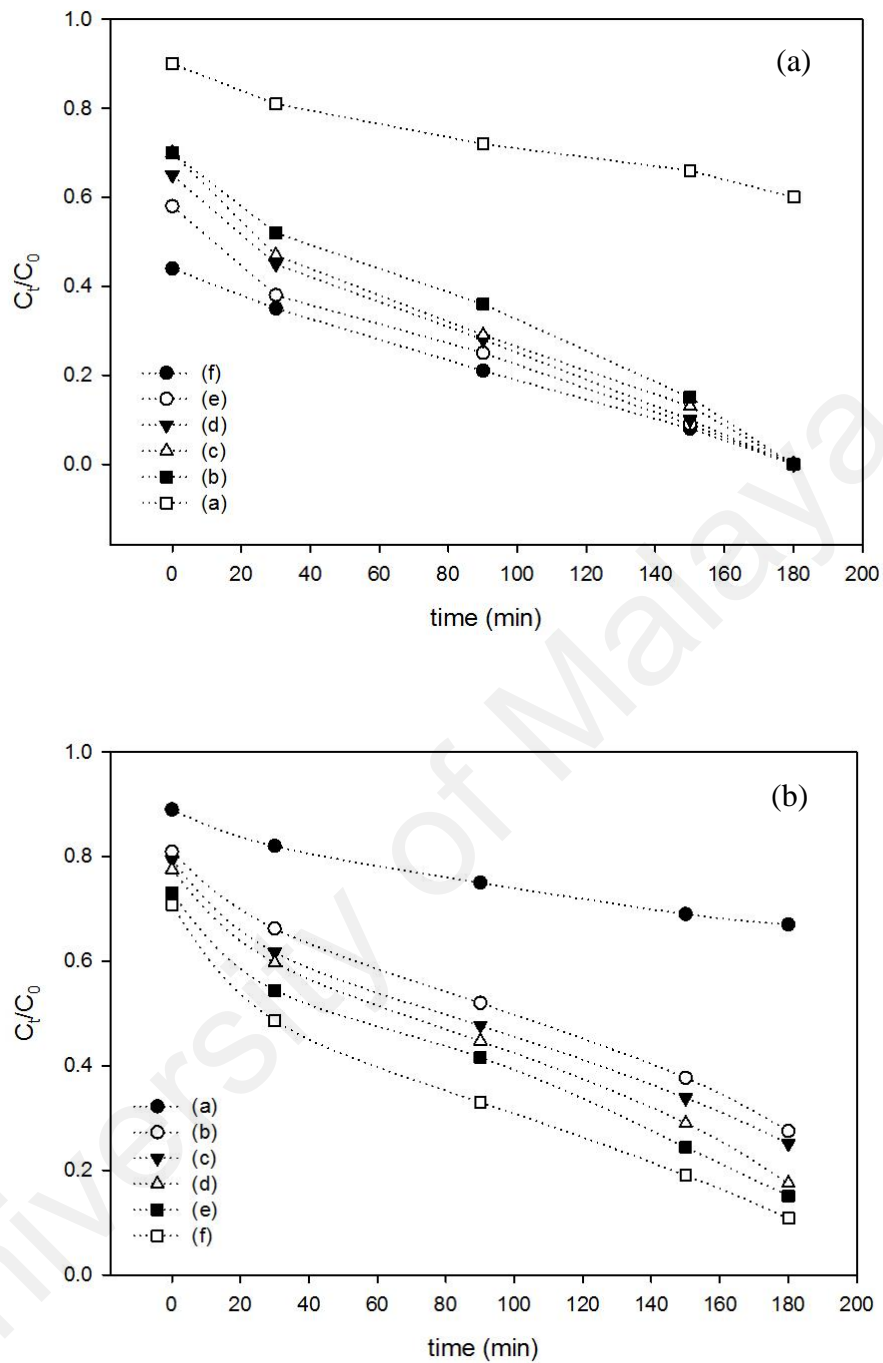


Figure 4.35: Fenton oxidation efficiency of the synthesized samples for (a)  $50 \text{ mg L}^{-1}$  and (b)  $100 \text{ mg L}^{-1}$

The influence of MB initial concentration on Fenton oxidation efficiency was assessed for MB solutions of  $25\text{-}200 \text{ mg L}^{-1}$  (Fig. 4.36). Though the amount of adsorption increased at higher concentrations of MB due to overcome on mass transfer limitation, the efficiency of Fenton oxidation decreased by increasing the initial concentration of

MB. This could be attributed to a large number of probe molecules at higher concentrations of MB that compete with  $\cdot\text{OH}$  radicals.

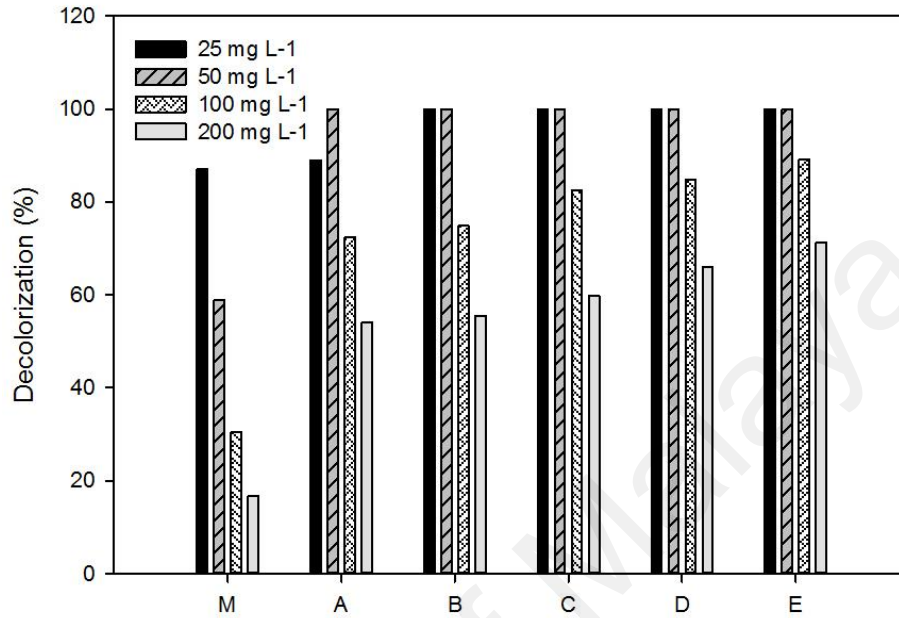


Figure 4.36: Effect of MB initial concentration on decolorization efficiency (%) using  $\text{Fe}_{3-x-y}\text{Nb}_x\text{Mo}_y\text{O}_4$  samples

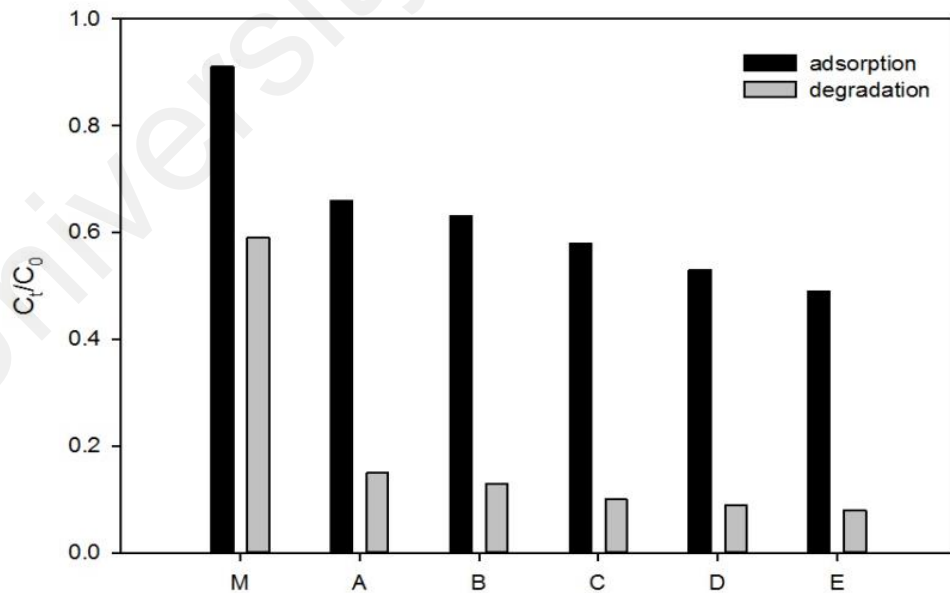


Figure 4.37: The amount of MB removal through adsorption and Fenton oxidation by  $\text{Fe}_{3-x-y}\text{Nb}_x\text{Mo}_y\text{O}_4$  samples

Degradation and mineralization effectiveness of  $\text{Fe}_{3-x-y}\text{Nb}_x\text{Mo}_y\text{O}_4$  samples at pH 7 and 10 are shown in Fig. 4.38. The figure provides an insight into their efficacy toward enhanced treatment of dye solution. The samples exhibited great activity for mineralization of MB solution ( $100 \text{ mg L}^{-1}$ ) in comparison to pure magnetite where more than 55% of TOC was removed by  $\text{Fe}_{2.79}\text{Nb}_{0.171}\text{Mo}_{0.023}\text{O}_4$  sample within 180 min. In all cases, TOC removal (%) was enhanced at basic condition and higher dosages of Nb+Mo. For example, the amount of mineralization through Fenton reaction catalyzed by  $\text{Fe}_{2.79}\text{Nb}_{0.171}\text{Mo}_{0.023}\text{O}_4$  sample was 70% and 75% higher than  $\text{Fe}_3\text{O}_4$  and 32% and 40% higher than  $\text{Fe}_{2.79}\text{Nb}_{0.0249}\text{Mo}_{0.094}\text{O}_4$  at pH 7 and 10, respectively.

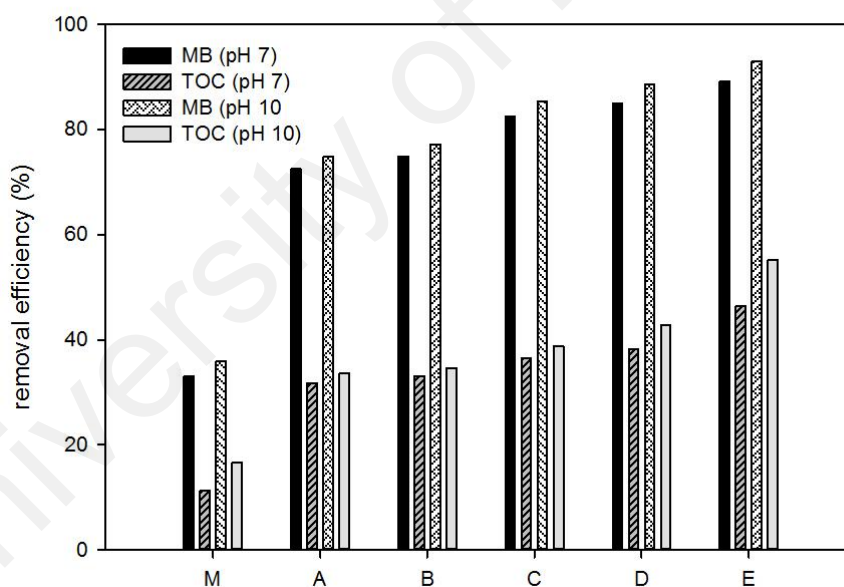
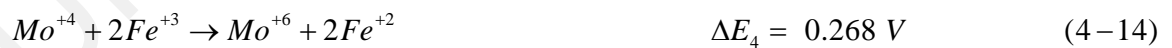
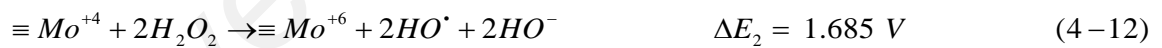


Figure 4.38: Degradation and mineralization of MB solution through Fenton-like reaction using  $\text{Fe}_{3-x-y}\text{Nb}_x\text{Mo}_y\text{O}_4$  samples at pH values of 7 and 10

#### 4.6. Possible explanation for enhanced activities of modified samples in Fenton reaction

The improved MB degradation could be mainly attributed to a number of factors. The primary reason was the enhancement in the adsorption capacity of the samples due to

increase in specific surface area or precisely the increase in surface OH of Nb and/or Mo substituted magnetite samples. In addition to the effects of physical changes, the results showed that the introduced Nb and/or Mo not only affected the adsorption capacity of magnetite but also were directly involved in the degradation mechanism. From the XPS analysis, niobium and molybdenum ions were chiefly placed Fe<sup>3+</sup> and Fe<sup>2+</sup> cations, respectively and the surface concentration of these species increased with the sum of introduced Nb+Mo. Based on Magalhães et al. (2007), the Nb<sup>+4</sup>/Nb<sup>+5</sup> and Mo<sup>+4</sup>/Mo<sup>+6</sup> redox pairs can play similar roles as Fe<sup>+2</sup>/Fe<sup>+3</sup> on the surface of the catalysts. The surface Nb<sup>+4</sup> and Mo<sup>+4</sup> enter the Fenton oxidation cycle and participate in Haber-Weiss mechanism to produce  $\cdot$ OH radicals and quickened electron transfer in the magnetite spinel structure during the oxidation reaction (Eqs. 4-11 and 4-12). In addition, regeneration of Fe<sup>+2</sup> cations accelerated through oxidation of surface Nb<sup>+4</sup> and Mo<sup>+4</sup> to Nb<sup>+5</sup> and Mo<sup>+6</sup> (Fig. 4.39) according to Eqs. 4-13 and 4-14:



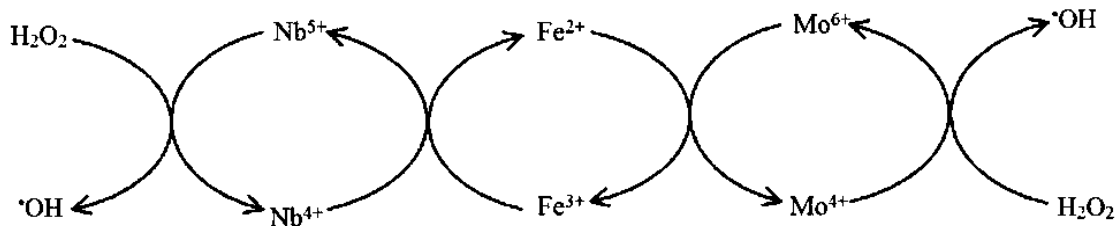


Figure 4.39: Radical mechanism for activation of  $H_2O_2$  by surface cations (proposed by Magalhães et al. (2007))

In view of the reduction potentials of  $Nb^{5+}/Nb^{4+}$  (-1.5 V),  $Mo^{4+}/Mo^{6+}$  (-0.818 V) and  $H_2O_2/HO^-$  (0.867 V) redox pairs, the Fenton reactions catalyzed by Nb and Mo were also thermodynamically favorable. Furthermore, the reduction potential of both redox pairs is smaller than that of  $Fe^{2+}/Fe^{3+}$  (-0.55). This implied that the imported Nb and Mo could accelerate the regeneration of  $Fe^{2+}$  cations from reduction of  $Fe^{3+}$  and accordingly, increase the oxidation efficiency of Fenton reaction.

On the other hand, the pronounced activity of the co-doped samples compared to single Nb or Mo substituted magnetite samples implied that there were mechanisms other than Fenton reaction involved in degradation process. One possible mechanism as reported by Silva et al. (2011) could be the formation of peroxo-niobium complexes ( $\equiv NbO_2$ ) on the surface of catalysts from the reaction of surface NbO and  $H_2O_2$  and direct participation of these complexes in MB oxidation (Eq. 4-15 and 4-16):



In addition to the above-mentioned factors, the generated oxygen vacancies in the structure of the synthesized samples also had positive effects on the degradation

efficiency of the system. The vacancies were mainly the results of the adjustments for unequal charge substitutions and cationic deficiency in the structure of the samples. It is believed that the vacancies are mainly located on the surface of the catalyst and act as active sites for oxidation of probe molecules. The following equations (Eq. 4-17 and 4-18) are suggested for the action of oxygen vacancies ( $V^*$ ) in oxidation reaction (Costa et al., 2003):

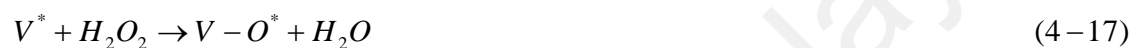


Figure 4.40 shows the overall action of the incorporated Nb and Mo in Fenton reaction for MB oxidation:

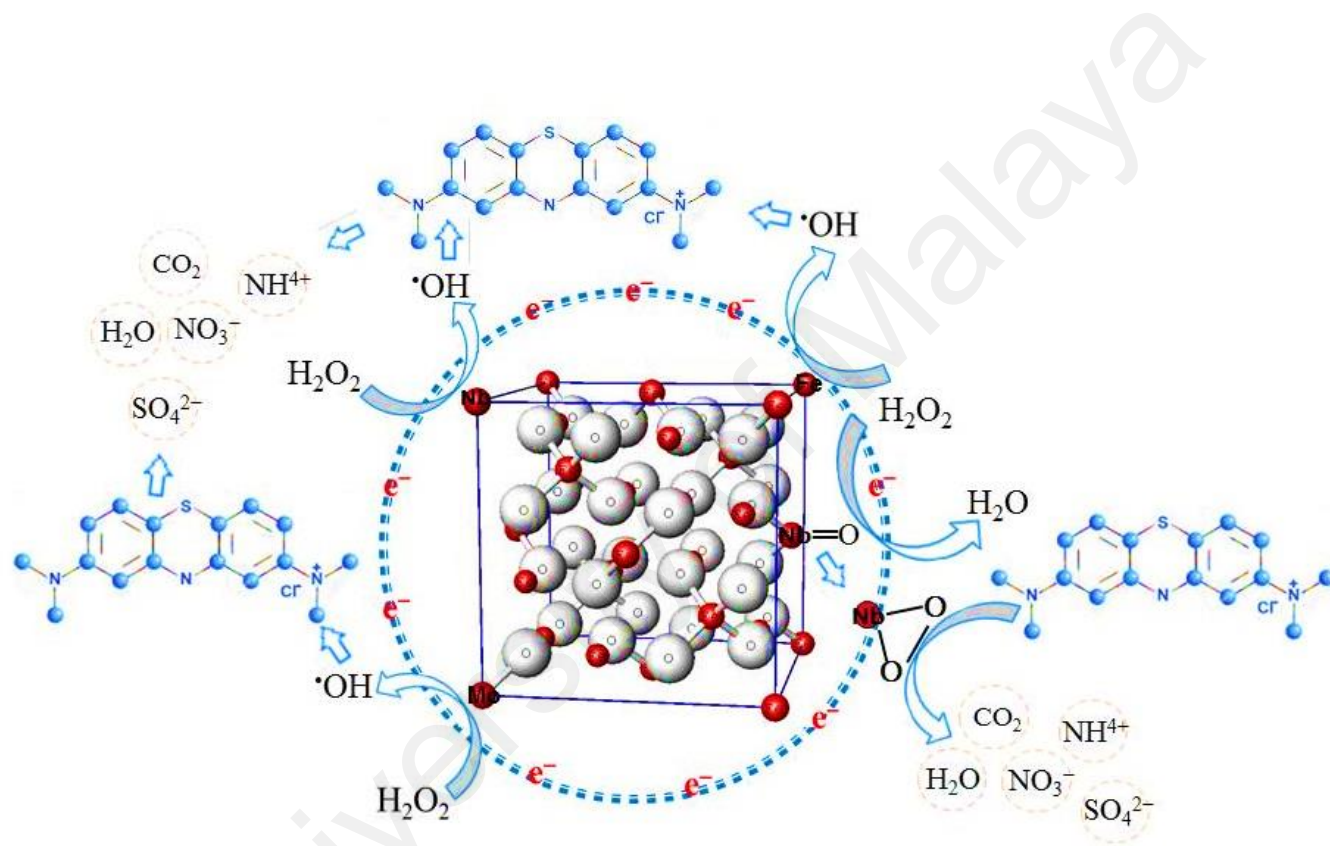


Figure 4.40: Overall action of Nb and Mo in modified magnetite samples in Fenton oxidation of MB



#### 4.7. Fenton oxidation of methyl orange solution

Among the studied synthesized samples, three catalysts,  $\text{Fe}_{2.79}\text{Mo}_{0.13}\text{O}_4$ ,  $\text{Fe}_{2.79}\text{Nb}_{0.19}\text{O}_4$ , and  $\text{Fe}_{2.79}\text{Nb}_{0.171}\text{Mo}_{0.023}\text{O}_4$ , showed higher activities in the corresponding groups in degradation of MB through the Fenton reaction. Here, in addition to MB, methyl orange (MO), which belongs to azo compounds was also selected as an anionic model dye to assess the activity of the selected catalysts for degradation of two different dyes with different adsorption characteristics. On this basis, the degradation of each dye ( $50 \text{ mg L}^{-1}$ ) was carried out through Fenton reaction in the presence of selected catalysts and  $\text{H}_2\text{O}_2$ . The same optimal conditions as previous studies were used here for inter-comparisons of the results. Prior to  $\text{H}_2\text{O}_2$  addition, the adsorption process was initiated by agitation of the dye in the presence of catalyst for 2 h to reach the state of equilibrium ( $q_e$ ). The adsorption behavior of MO was evaluated under neutral and acidic conditions. Being an anionic dye, MO adsorption on the surface of the studied catalysts was negligible at neutral condition because of the repulsive force between the negatively charged surface and anionic dye. However, the amount of adsorbed MO increased significantly when the reaction medium acidified (Fig. 4.41). Therefore, all the Fenton reactions performed at pH 3 to fulfill the adsorption equilibrium of MO on the studied catalysts. The selected modified magnetite samples exhibited remarkable performance in comparison to unmodified magnetite for MO degradation.

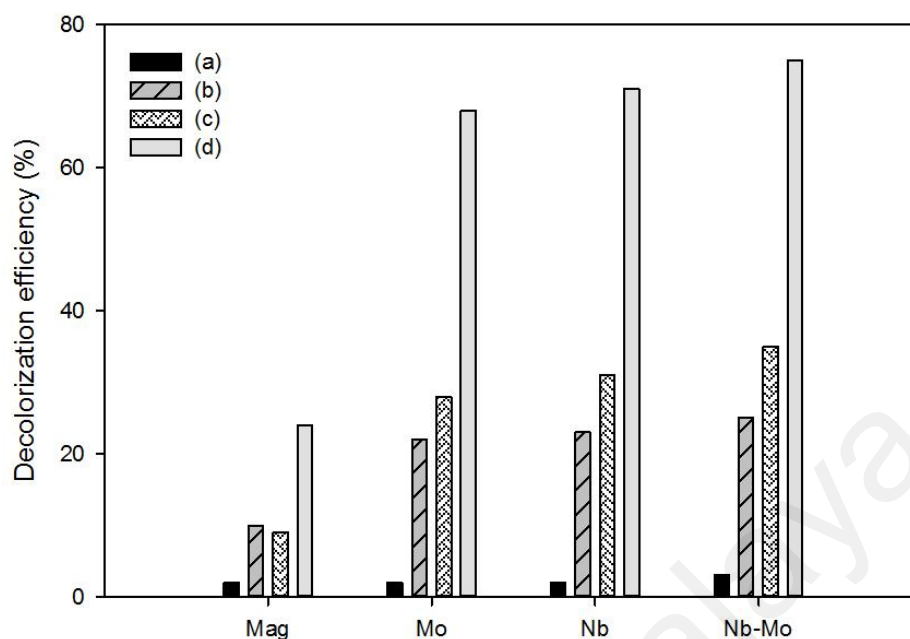


Figure 4.41: Effect of pH on adsorption and Fenton oxidation efficiency of MO using the synthesized samples at pH 7 (a) adsorption and (b) oxidation and pH 3 (c) adsorption and (d) oxidation

The amount of MO adsorbed on the samples at pH 3 was 9% for pure magnetite (Mag), 28% for  $\text{Fe}_{2.79}\text{Mo}_{0.13}\text{O}_4$  (Mo-), 31% for  $\text{Fe}_{2.79}\text{Nb}_{0.19}\text{O}_4$  (Nb-), and 35% for  $\text{Fe}_{2.79}\text{Nb}_{0.171}\text{Mo}_{0.023}\text{O}_4$  (Nb-Mo). However, its degradation was not completed within 3 h of the reaction time using any of the selected catalysts. The MO decolorization was only 24% under magnetite catalyzed Fenton reaction and improved up to 68%, 71%, and 75% with Mo-, Nb-, and Nb-Mo catalysts (Figs. 4.42). This signified that MO structure was more refractory to be degraded under the same amount of Fenton reagents to MB. This could be due to the presence of  $-\text{N}=\text{N}-$  functional group joined with two aryl groups that makes a very stable structure.

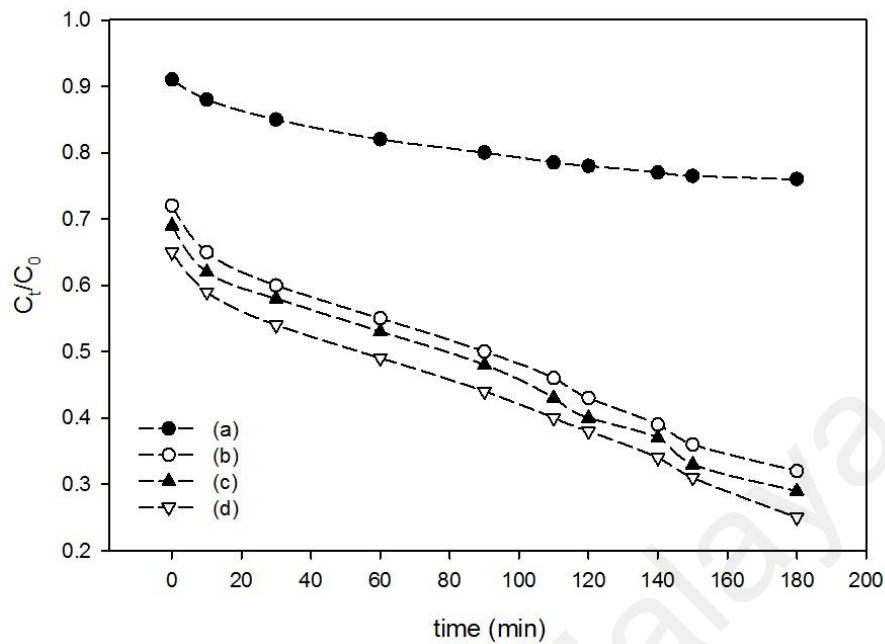


Figure 4.42: Fenton oxidation efficiency of the samples for MO

#### 4.8. Energetically enhanced Fenton activity of the samples

In previous experiments, the activity of the synthesized Nb and/or Mo substituted magnetite samples were evaluated through dark-Fenton oxidation of MB and MO solutions. Here, a combination of UV light or ultrasound (US) energy with Fenton reaction was also used to assess the activity of the samples in energetically enhanced Fenton reactions and evaluate the degradation efficiency of the applied dye solutions under various oxidation conditions.

##### 4.8.1. UV/Fenton catalytic activity of $\text{Fe}_{3-x-y}\text{Nb}_x\text{Mo}_y\text{O}_4$ samples

The catalytic performance of the selected catalysts,  $\text{Fe}_{2.79}\text{Mo}_{0.13}\text{O}_4$  (Mo-),  $\text{Fe}_{2.79}\text{Nb}_{0.19}\text{O}_4$  (Nb-), and  $\text{Fe}_{2.79}\text{Nb}_{0.171}\text{Mo}_{0.023}\text{O}_4$  (Nb-Mo), was also evaluated via photo-Fenton-like reaction. The same amount of Fenton reagents as previous studies was initially used to assess the effects of UV light induction on the system. Concerning additional  $\cdot\text{OH}$

radical generation via photo-reduction of  $\text{Fe}^{3+}$  to  $\text{Fe}^{2+}$ , it was expected to significantly increase the MB degradation rate. Nonetheless, the degradation efficacy was not considerable after introduction of UV-A irradiation (Fig. 4.43). The insignificant improvement in this degradation system might be due to two possible reasons: (i) scavenging effects caused by high concentrations of  $\text{H}_2\text{O}_2$  and/or catalyst, and (ii) the turbidity caused by higher concentration of the catalysts, which interfered UV light penetration. For this, two additional sets of experiments were performed for each dye to identify the main reason and optimize the reaction parameters. Reduction in  $\text{H}_2\text{O}_2$  concentration from 0.2 M to 0.15 M diminished degradation efficacy significantly (data not presented) while the reduction in the catalyst concentration to  $0.5 \text{ g L}^{-1}$  resulted in considerable enhancement in the decolorization rate in both the studied dyes solutions (Fig. 4.43). It was recognized that the inner-filtration of light due to high concentration of catalyst particles in the solution was the main reason. Under lower catalyst concentrations, the introduced light could activate the reaction mainly through photo reduction of surface  $\text{Fe}^{3+}$  to  $\text{Fe}^{2+}$ , which in turn entered the Fenton cycle and yielded more  $\cdot\text{OH}$  radicals.

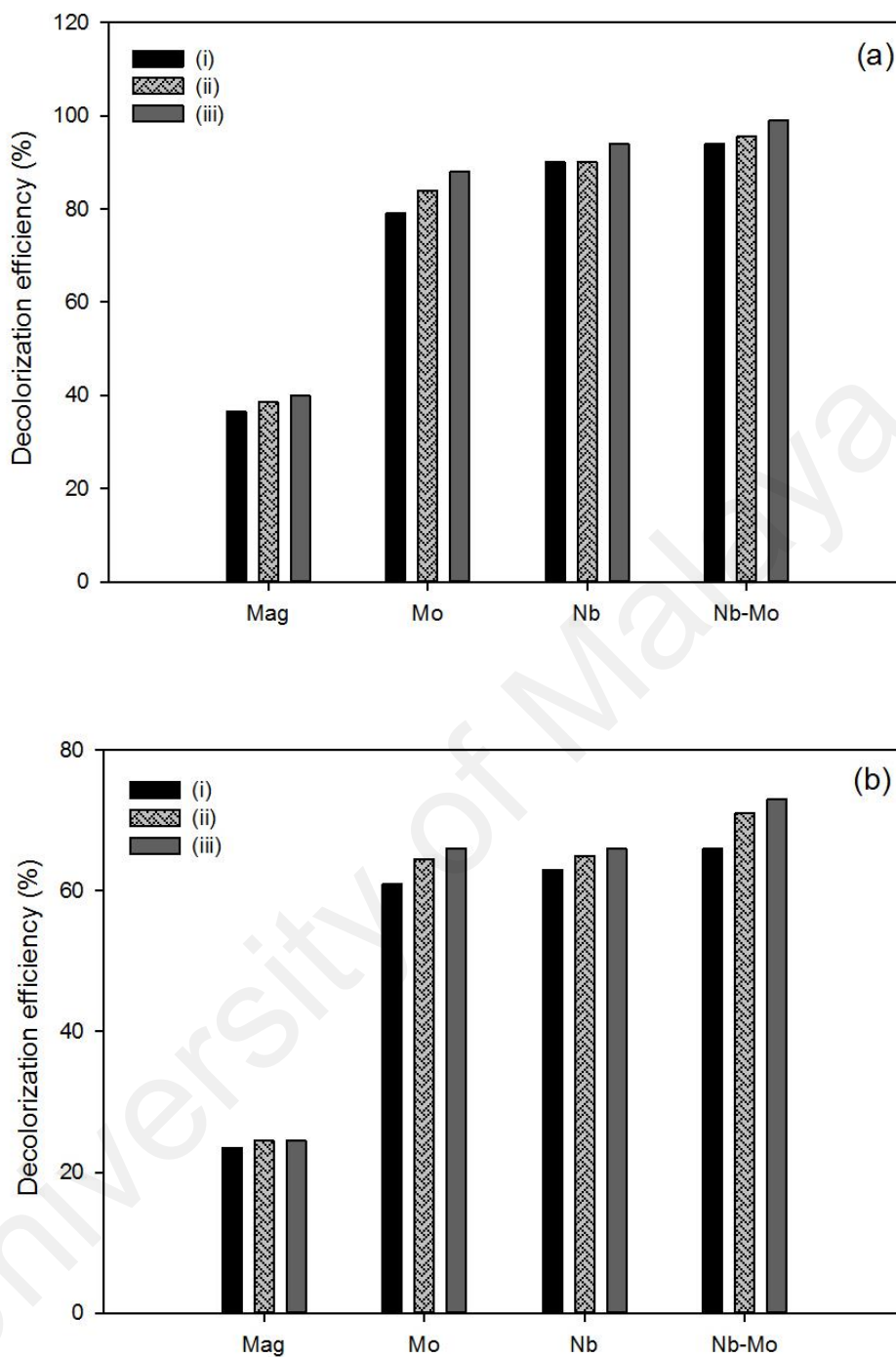


Figure 4.43: Comparison between (i) dark-Fenton, (ii) UV/ Fenton with 1 g L<sup>-1</sup> and (iii) 0.5 g L<sup>-1</sup> of the samples for (a) MB and (b) MO (365 nm; t=150 min)

In order to assess the effects of light intensity on the oxidation of MB and MO, the degradation experiments through the photo-Fenton like reaction was carried out at 302 nm using the UV-B irradiation. The UV-B radiation was sufficiently energetic to break down H<sub>2</sub>O<sub>2</sub> molecules and generate <sup>•</sup>OH radicals. Decolorization of both the studied dye

solutions was accelerated in this condition with considerably shorter reaction time (Fig. 4.44<sub>a-b</sub>). For example, switching dark Fenton to UV/Fenton at 302 nm increased the MB removal by about 39%, 25%, and 26% within 120 minutes using Mo-, Nb-, and Nb-Mo-substituted magnetite samples, respectively. Besides the additionally produced  $\cdot\text{OH}$  radicals through  $\text{H}_2\text{O}_2$  decomposition, the  $\text{Nb}^{+4}/\text{Nb}^{+5}$  and  $\text{Mo}^{+4}/\text{Mo}^{+6}$  redox pairs also played important roles on the surface of the catalysts. The introduced energy increased the reduction of  $\text{Nb}^{+5}$  and  $\text{Mo}^{+6}$  to  $\text{Nb}^{+4}$  and  $\text{Mo}^{+4}$  which in turn entered to the Haber-Weiss mechanism and produced additional  $\cdot\text{OH}$  radicals (Magalhães et al., 2007). Furthermore, the presence of dopants improved the photocatalytic activity of magnetite via (i) reduction in the band gap energy (ii) creation of the hole-electron pair under UV-light and (iii) prohibiting the recombination of photo-generated electrons ( $e^-$ ) and holes ( $h^+$ ) on the catalyst surface that led to  $\cdot\text{OH}$  radical generation and effective degradation of the organic dyes (Liang et al., 2012b; Zhong et al., 2013). Remarkable enhancement in the photo-catalytic activity of magnetite after structural changes caused by transition metal incorporation has been reported in several studies. The presence of 1% Mn in the magnetite structure improved the photo/Fenton degradation of MB up to 12% within 5h of reaction time (Carvalho et al., 2014); while the degradation enhancement was two-times more via 23% Fe replacement by Ti in the magnetite structure and within a reaction duration of 2 h (Liang et al., 2012b). Zhong et al (2014) reported the similar results for Cr (III), Ti (VI) and Mn (II); whereas Ni (II) and Co (II) did not affect the magnetite activity in the UV/Fenton reaction.

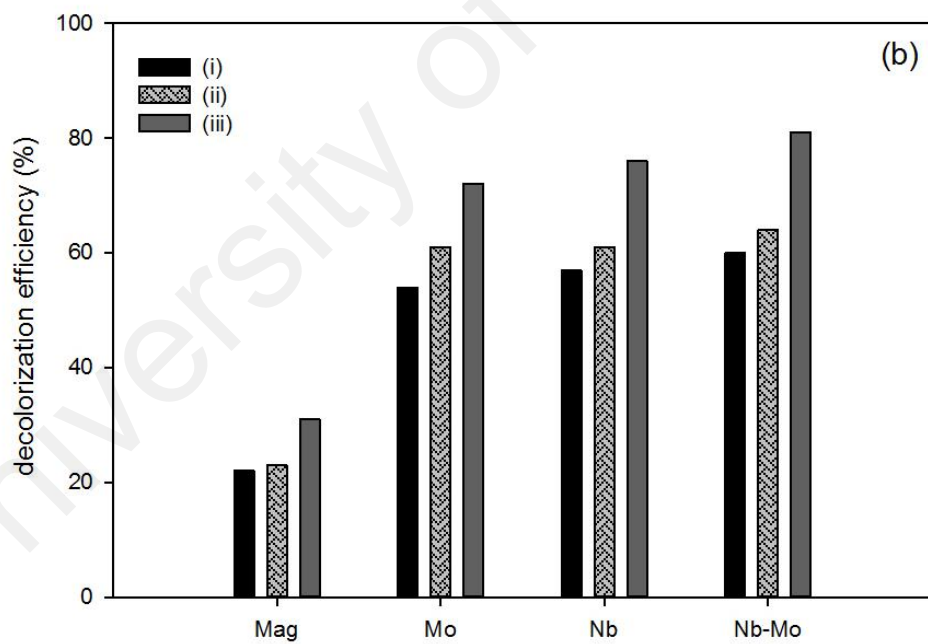
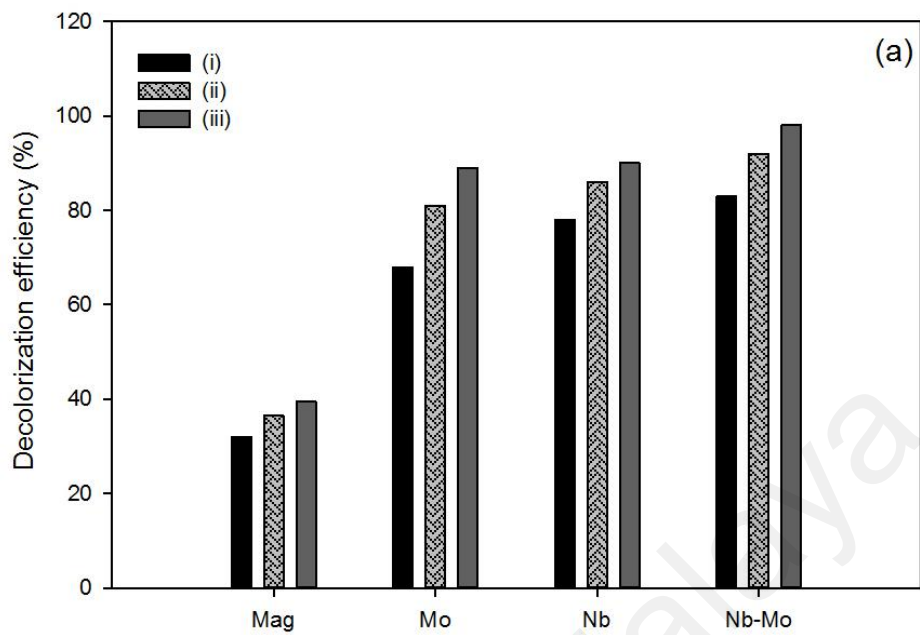


Figure 4.44: Effects of UV light intensity on oxidation efficiency of the samples for (a) MB and (b) MO ((i) dark-Fenton, (ii) UV-A and (iii) UV-B/Fenton, [dye]  $50 \text{ mg L}^{-1}$ , [Cat]  $0.5 \text{ g L}^{-1}$ ;  $[\text{H}_2\text{O}_2]$   $0.2 \text{ mol L}^{-1}$ , UV 365/302 nm;  $t=120 \text{ min}$ )

#### 4.8.2. US/Fenton catalytic activity of $\text{Fe}_{3-x-y}\text{Nb}_x\text{Mo}_y\text{O}_4$ samples

Combination of ultrasound induced cavitation with Fenton process has been established as an effective tool for enhanced treatment of recalcitrant wastewaters. In this study, the US/Fenton process presented an exceptional performance for decolorization of MB compared to other oxidation systems (Fig. 4.45). All employed catalysts were competent at the studied operating condition and the degradation process was almost completed within 2.5 hours. The MB decolorization removal efficiency in the US/Fenton process was almost 1.4 and 1.15-fold more in comparison to the dark Fenton and UV/Fenton reactions. In addition to the homogenizing effects of the US and its role in increasing reactivity in liquid–solid systems, sonochemical cavitation produced by the US irradiation brought about strong chemical and mechanical effects on the species engaged in the oxidation system (Suslick et al., 1999). Generally, under the US irradiation, the ionic pathway switches to radical pathway (Leong et al., 2011). The central effect caused by the US irradiation was generation of highly active species mainly  $\cdot\text{OH}$  radicals (Bagal & Gogate, 2014). The strong oxidation of dye molecules in this system was the evidence for aggressively attacked dye molecules by  $\cdot\text{OH}$  radicals. The other reason for effective degradation of MB could be direct contribution of cavitation in degradation of dye molecules through various routes ("Acoustic cavitation and its chemical consequences,"). For the studied hetero-catalysts, the following reactions (Eqs. 4-19 to 4.21) occurred in the US/Fenton reaction (Dükkancı et al., 2014):





Where, M represents the surface Fe, Nb or Mo. The generated  $M^{n+}$  in turn, reacts with  $H_2O_2$  and generates Higher  ${}^{\bullet}OH$  radicals.

Figure 4.45b shows the efficiency of the employed catalysts for degradation of MO. The US/Fenton system enhanced MO decolorization significantly when compared to the dark Fenton system, but its efficiency was close to that of the UV-B/Fenton process. The results showed that MO molecules were more instable under UV-B irradiation than US influence. Amongst the studied samples,  $Fe_{2.79}Nb_{0.171}Mo_{0.023}O_4$  showed the highest activity in all the studied systems followed by  $Fe_{2.79}Nb_{0.19}O_4$  and  $Fe_{2.79}Mo_{0.13}O_4$  samples. The synergistic contribution of Nb and Mo in magnetite was the reason for higher activity of co-doped sample. The main reasons were: (i) larger surface area and accordingly, higher adsorption capacity, (ii) the presence of both the  $Nb^{+4}/Nb^{+5}$  and  $Mo^{+4}/Mo^{+6}$  redox pairs in the magnetite structure that increased the electron mobility in the crystal structure and participated in the  $H_2O_2$  decomposition and Haber–Weiss reactions. Nb-substituted magnetite also showed better activities in all systems compared to the Mo-magnetite sample. This could be due to direct participation of Nb in dye molecules degradation and higher incorporation maxima of Nb compared to Mo.

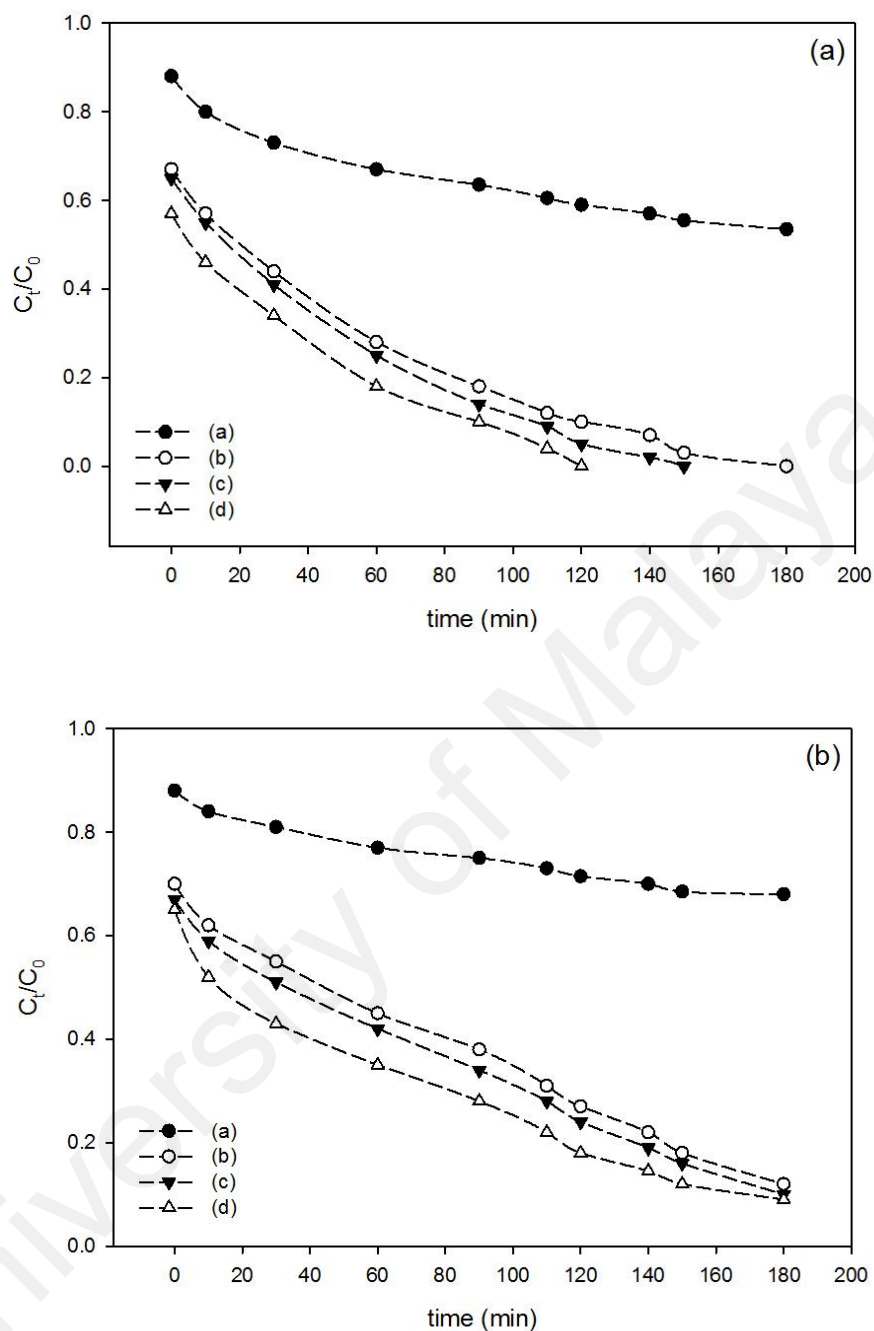
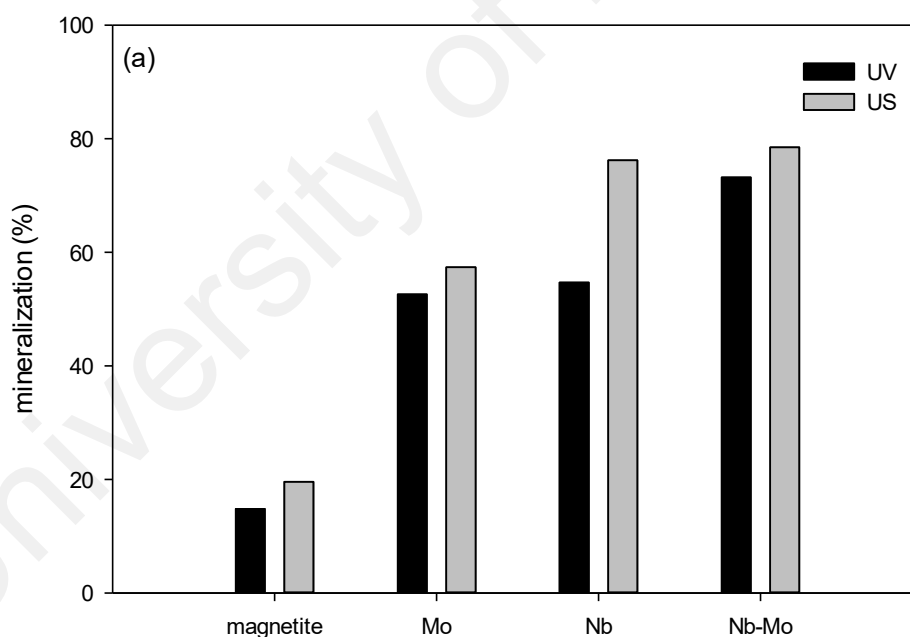


Figure 4.45: US/Fenton oxidation efficiency of the samples for (a) MB and (b) MO ([dye] 50 mg L<sup>-1</sup>, [Cat] 0.5 g L<sup>-1</sup>; [H<sub>2</sub>O<sub>2</sub>] 0.2 mol L<sup>-1</sup>)

### 4.8.3. Mineralization efficiency of samples in UV/Fenton and US/Fenton reactions

Figure 4.46 shows the mineralization efficiency of Fe<sub>2.79</sub>Mo<sub>0.13</sub>O<sub>4</sub>, Fe<sub>2.79</sub>Nb<sub>0.19</sub>O<sub>4</sub> and Fe<sub>2.79</sub>Nb<sub>0.171</sub>Mo<sub>0.023</sub>O<sub>4</sub> samples under the various oxidation conditions for aqueous MB

and MO solutions. The mineralization degree of both the dyes improved effectively under the UV- and US-illuminated Fenton systems. The studied samples showed significantly enhanced activity for mineralization of MB and MO. The MB mineralization compared to pure magnetite was 72 %, 73 % and 80% in the UV/Fenton and 66 %, 74% and 75% in the US/Fenton using  $\text{Fe}_{2.79}\text{Mo}_{0.13}\text{O}_4$ ,  $\text{Fe}_{2.79}\text{Nb}_{0.19}\text{O}_4$  and  $\text{Fe}_{2.79}\text{Nb}_{0.171}\text{Mo}_{0.023}\text{O}_4$  samples. Similarly, the mineralization efficiency was 72%, 73% and 76 % in the UV/Fenton process and 68%, 69% and 75% in the US/Fenton process for MO mineralization. It was evident from the results that the modified samples could effectively activate the Fenton systems towards pronounced mineralization efficiency.



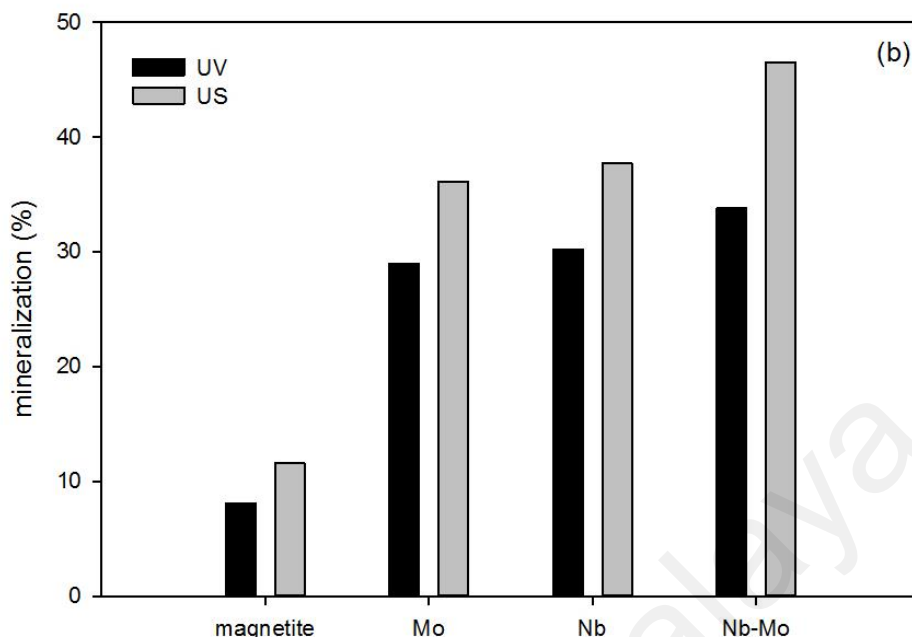


Figure 4.46: Mineralization (%) of (a) MB and (b) MO in UV-A/Fenton and US/Fenton reactions

#### 4.9. Stability of the samples

The stability and durability of the synthesized catalysts under various experimental conditions is essential to preserve their effectiveness over several applications and for abatement of environmental pollution via the utilized transition metals. Accordingly, a number of leaching experiments were carried out at the studied conditions. Based on the results obtained from the leaching experiments, there was not a detectable leached Fe into the solutions at all studied experimental conditions using the synthesized samples. On the other hand, the amount of leached Nb in  $\text{Fe}_{3-x}\text{Nb}_x\text{O}_4$  series, at acidic condition, was 0.002% and 0.003% of the amount of Nb in catalyst (0.057 mg/L for sample  $\text{Fe}_{2.65}\text{Nb}_{0.099}\text{O}_4$  and 0.154 mg/L for  $\text{Fe}_{2.79}\text{Nb}_{0.19}\text{O}_4$  sample). In addition, the amount of leached Nb was about 0.002–0.004 wt% of structural Nb of the  $\text{Fe}_{3-x-y}\text{Nb}_x\text{Mo}_y\text{O}_4$  samples. However, Nb leached was not detectable in neutral and basic conditions. Surprisingly, the amount of Mo leached was not detectable at all studied conditions,

though its tendency for incorporation was relatively lower than Nb. The  $\text{Fe}_{2.79}\text{Nb}_{0.19}\text{O}_4$  catalyst was reused four times without a significant decrease in its catalytic activity showing that it is durable and can be reused for several times. The  $\text{Fe}_{2.79}\text{Nb}_{0.171}\text{Mo}_{0.023}\text{O}_4$  sample reused three times to evaluate its performance after repeated applications. The decrease in catalytic activity of the studied sample was not remarkable in which the amount of MB ( $100 \text{ mg L}^{-1}$ ) removed at three runs was about 89%, 85% and 82%, within 180 min (Fig. 4.47). The decrease in catalytic activity of the sample was not only related to the loss of the structural transition metals but some other factors such as incomplete removal of reactants and/or by-products from the catalysts surface. However, further research is required to explore and prevent the main causes of catalyst deactivation for effective treatment of pollutants.

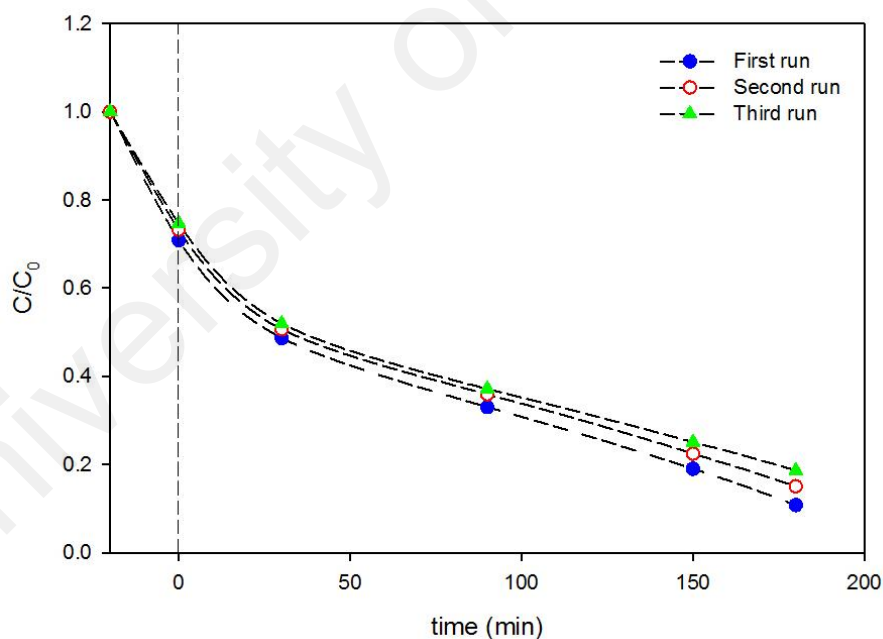


Figure 4.47: Reusability of  $\text{Fe}_{2.79}\text{Nb}_{0.171}\text{Mo}_{0.023}\text{O}_4$  sample

Lastly, a number of leaching experiments were carried out for both the dyes under the US and UV irradiation and in the studied pH conditions. Although the amount of leached Nb was relatively higher than that of the classic Fenton reaction, the samples showed acceptable scores at three consecutive experiments. Similar to earlier findings,

the amount of leached Mo and Fe into the reaction solution was not detectable at all studied conditions. On the other hand, the amount of structural Nb leached from the  $\text{Fe}_{2.79}\text{Nb}_{0.19}\text{O}_4$  and  $\text{Fe}_{2.79}\text{Nb}_{0.171}\text{Mo}_{0.023}\text{O}_4$  samples at pH 3 was 0.008 and 0.006 wt% under the UV and 0.006 and 0.005 wt% under the US influence. However, the leaching did not affect the performance of the catalysts considerably over three consecutive experiments. The results proved good durability of the samples for their practical applications in environmental purification and decomposition of toxic and organic pollutants.

#### **4.10. Kinetic studies**

The Kinetics of the adsorption of MB on the  $\text{Fe}_{3-x-y}\text{Nb}_x\text{Mo}_y\text{O}_4$  samples and its degradation through Fenton reaction were studied to predict the behavior of the samples in adsorption and degradation processes.

##### **4.10.1. Adsorption kinetics**

The rate or kinetics of MB adsorption onto the  $\text{Fe}_{3-x-y}\text{Nb}_x\text{Mo}_y\text{O}_4$  samples was studied to further understand the properties of the adsorption process and determine the required stirring time to achieve adsorption equilibrium. In light of this, a number of adsorption kinetic models have been developed to describe the adsorption processes quantitatively and identify the adsorption mechanism. It is a common approach to fit experimental data with a series of popular models and find the most suitable one, which provides the best fit. In this study, the pseudo-first-order and pseudo-second-order kinetic models were chosen from the similar studies and used to fit the data obtained from the adsorption experiments and the relative errors, *Err (%)*, were calculated.

The linear forms of the pseudo-first-order and pseudo-second-order kinetic models are as follows:

$$\log(q_e - q_t) = \frac{\log q_e - k_1 t}{2.303} \quad (4-23)$$

$$\frac{1}{q_t} = \frac{1}{K_2 q_e^2} + \frac{1}{q_e t} \quad (4-24)$$

where  $q_t$  and  $q_e$  ( $\text{mg g}^{-1}$ ) are the amounts of MB adsorbed at time  $t$  (min) and equilibrium, respectively. The  $k_1$  ( $\text{min}^{-1}$ ) and  $k_2$  ( $\text{g mg}^{-1} \text{min}^{-1}$ ) are the pseudo-first-order and pseudo-second-order rate constants, respectively. The kinetic parameters ( $k_1$ ,  $k_2$ , and  $q_{e,\text{cal}}$ ), correlation coefficient ( $R^2$ ) and error (%) of all synthesized catalysts at 25, 50, 100, and 200  $\text{mg L}^{-1}$  of MB for both models are given in Table (4.16). Although, the calculated  $q_e$  values for both models were adjacent to the experimental values, the  $R^2$  values of pseudo-second-order kinetic model ( $> 0.99$ ) were higher than pseudo-first-order kinetic model. In addition, *Err* (%) values for pseudo-second-order kinetic model were relatively smaller than those of the pseudo-first-order kinetic model. This indicated that the pseudo-second-order model provided the best fit for the kinetic data at 25, 50, 100, and 200 ( $\text{mg L}^{-1}$ ) MB concentrations and MB adsorption on the Nb/Mo substituted magnetite samples followed the pseudo-second-order kinetic model.

Figure 4.48 shows the MB ( $100 \text{ mg L}^{-1}$ ) adsorption behavior over the synthesized catalysts. From the figure, the adsorption data fitted well to the pseudo-second order model.

Table 4.16: The calculated parameters of the pseudo-first and pseudo-second order kinetic models with associated  $R^2$  and  $Err$  (%) for the MB adsorption onto synthesized catalysts at various MB concentrations

Samples	Kinetic model	Parameters	$C_0$ (mg L <sup>-1</sup> )			
			25	50	100	200
Fe <sub>2.79</sub> Nb <sub>0.0249</sub> Mo <sub>0.094</sub> O <sub>4</sub>	Pseudo-first	$k_1$ (s <sup>-1</sup> )	0.048	0.047	0.062	0.054
		$q_{e,cal}$ (mg g <sup>-1</sup> )	15.21	16.59	18.09	19.87
		$R^2$	0.881	0.913	0.901	0.997
		Err (%)	15.68	17.44	13.53	20.28
	Pseudo-second	$k_2$ (mg g <sup>-1</sup> s <sup>-1</sup> )	0.009	0.009	0.012	0.021
		$q_{e,cal}$ (mg g <sup>-1</sup> )	16.05	17.45	18.80	20.32
		$R^2$	0.997	0.998	0.999	0.999
		Err (%)	3.29	2.78	2.11	0.46
Fe <sub>2.79</sub> Nb <sub>0.049</sub> Mo <sub>0.089</sub> O <sub>4</sub>	Pseudo-first	$k_1$ (s <sup>-1</sup> )	0.031	0.044	0.057	0.064
		$q_{e,cal}$ (mg g <sup>-1</sup> )	15.78	17.93	19.55	22.74
		$R^2$	0.964	0.946	0.947	0.994
		Err (%)	28.4	20.22	16.53	16.41
	Pseudo-second	$k_2$ (mg g <sup>-1</sup> s <sup>-1</sup> )	0.011	0.010	0.012	0.016
		$q_{e,cal}$ (mg g <sup>-1</sup> )	16.72	18.76	20.24	23.31
		$R^2$	0.998	0.999	0.999	0.999
		Err (%)	3.29	2.58	1.45	0.26
Fe <sub>2.79</sub> Nb <sub>0.099</sub> Mo <sub>0.073</sub> O <sub>4</sub>	Pseudo-first	$k_1$ (s <sup>-1</sup> )	0.043	0.052	0.056	0.056
		$q_{e,cal}$ (mg g <sup>-1</sup> )	17.13	20.37	21.36	24.67
		$R^2$	0.949	0.935	0.969	0.941
		Err (%)	20.92	17.36	18.27	18.59
	Pseudo-second	$k_2$ (mg g <sup>-1</sup> s <sup>-1</sup> )	0.011	0.010	0.015	0.014
		$q_{e,cal}$ (mg g <sup>-1</sup> )	17.89	21.14	21.93	25.32
		$R^2$	0.999	0.999	0.999	0.999
		Err (%)	2.49	2.17	0.88	1.35
Fe <sub>2.79</sub> Nb <sub>0.149</sub> Mo <sub>0.032</sub> O <sub>4</sub>	Pseudo-first	$k_1$ (s <sup>-1</sup> )	0.051	0.062	0.065	0.066
		$q_{e,cal}$ (mg g <sup>-1</sup> )	18.26	22.83	25.51	27.31
		$R^2$	0.952	0.895	0.883	0.938
		Err (%)	17.06	11.80	12.91	14.95
	Pseudo-second	$k_2$ (mg g <sup>-1</sup> s <sup>-1</sup> )	0.010	0.007	0.009	0.011
		$q_{e,cal}$ (mg g <sup>-1</sup> )	19.08	23.92	26.45	28.09
		$R^2$	0.999	0.998	0.999	0.999
		Err (%)	2.03	2.57	1.92	1.05
Fe <sub>2.79</sub> Nb <sub>0.171</sub> Mo <sub>0.023</sub> O <sub>4</sub>	Pseudo-first	$k_1$ (s <sup>-1</sup> )	0.051	0.062	0.068	0.068
		$q_{e,cal}$ (mg g <sup>-1</sup> )	21.41	25.1	27.67	29.61
		$R^2$	0.921	0.917	0.931	0.943
		Err (%)	18.47	13.82	15.07	13.84
	Pseudo-second	$k_2$ (mg g <sup>-1</sup> s <sup>-1</sup> )	0.011	0.009	0.009	0.010
		$q_{e,cal}$ (mg g <sup>-1</sup> )	22.12	26.04	28.57	30.49
		$R^2$	0.999	0.999	0.999	0.999
		Err (%)	1.81	1.58	1.27	0.86



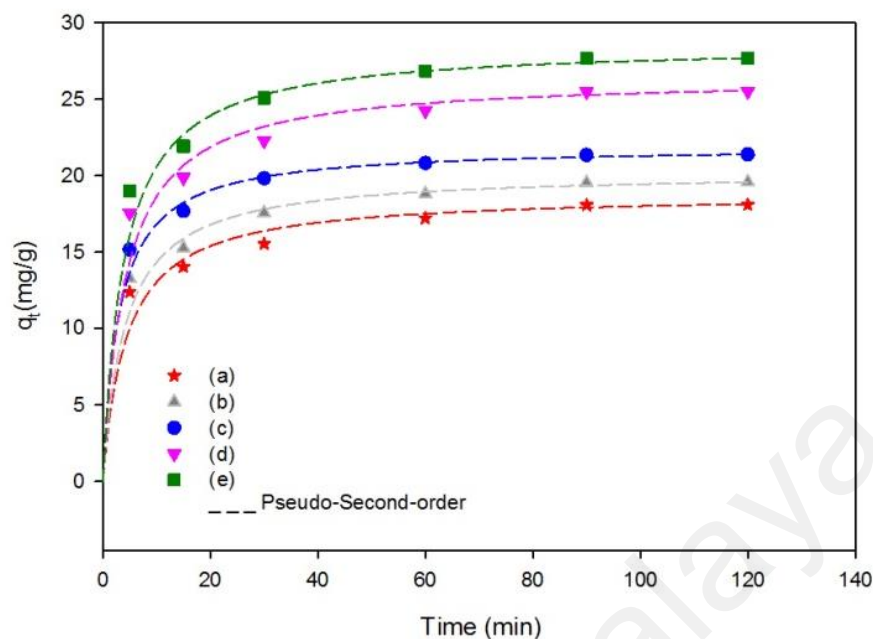


Figure 4.48: Pseudo-Second-order kinetics for adsorption of MB ( $100 \text{ mg L}^{-1}$ ) onto (a)  $\text{Fe}_{2.79}\text{Nb}_{0.0249}\text{Mo}_{0.094}\text{O}_4$ , (b)  $\text{Fe}_{2.79}\text{Nb}_{0.049}\text{Mo}_{0.089}\text{O}_4$ , (c)  $\text{Fe}_{2.79}\text{Nb}_{0.099}\text{Mo}_{0.073}\text{O}_4$ , (d)  $\text{Fe}_{2.79}\text{Nb}_{0.149}\text{Mo}_{0.032}\text{O}_4$  and (e)  $\text{Fe}_{2.79}\text{Nb}_{0.171}\text{Mo}_{0.023}\text{O}_4$  samples

#### 4.10.2. Degradation kinetics

In order to determine the Fenton oxidation rate of MB, experiments carried out by using modified magnetite samples and  $\text{H}_2\text{O}_2$  at neutral condition. Undoubtedly, a multipart process is contributed in overall decolorization. MB removal relied on adsorption on the catalyst prior to  $\text{H}_2\text{O}_2$  addition and initiating the Fenton degradation reaction. Accordingly, overall decolorization resulted from several processes mainly the adsorption of MB on the surface of solid catalyst and MB degradation by hydroxyl radicals generated through  $\text{Fe}_{3-x-y}\text{Nb}_x\text{Mo}_y\text{O}_4/\text{H}_2\text{O}_2$  system. On this basis, the catalyst and dye solution stirred for 2 h to achieve the adsorption equilibrium. It is supposed that the removal rate of MB is directly proportional to MB concentration in aqueous solutions, the concentration of the catalyst and the amount of surface  $\cdot\text{OH}$  radicals. Therefore, a second-order reaction can describe the degradation of MB. Since, the amount of catalyst and surface  $\cdot\text{OH}$  were considered constant, the decolorization rate

would expect to follow pseudo-first-order kinetics mechanism. In previous studies on kinetics of MB oxidation using other transition metal substituted magnetite samples, the oxidation kinetics followed either zero-order (Liang et al., 2012a; Magalhães et al., 2007; Yang et al., 2009) or pseudo-first-order kinetics models (Liang et al., 2013a). Accordingly, both zero-order and pseudo-first-order kinetic models were used to explore the degradation rate parameters using the following equations (Eqs. 4-23 and 4-24):

$$C_0 - C_t = k_0 t \quad (4-23)$$

$$-\ln\left(\frac{C_t}{C_0}\right) = k_1 t \quad (4-24)$$

where  $C_0$  and  $C_t$  are the MB concentrations ( $\text{mg L}^{-1}$ ) at the initial time and reaction time  $t$ ,  $k_0$  and  $k_1$  are zero-order rate constant ( $\text{mg L}^{-1} \text{min}^{-1}$ ) and pseudo-first-order rate constant ( $\text{min}^{-1}$ ). The  $k_0$  and  $k_1$  constants were obtained from the slope of the straight lines by plotting  $C_0 - C_t$  and  $-\ln(C_t/C_0)$  as a function of time  $t$ , through regression. Data on the rate constants ( $k_1$  and  $k_2$ ) and regression ( $R^2$ ) values of both the studied models for  $\text{Fe}_{3-x}\text{Nb}_x\text{O}_4$ ,  $\text{Fe}_{3-x}\text{Mo}_x\text{O}_4$  and  $\text{Fe}_{3-x-y}\text{Nb}_x\text{Mo}_y\text{O}$  samples are presented in Tables 4.17, 4.18 and 4.19, respectively.

In  $\text{Fe}_{3-x}\text{Nb}_x\text{O}_4$  samples (Table 4.17), from the rate constants and  $R^2$  values, it can be concluded that the decolorization process was fittingly described by pseudo-first order kinetic model. Figure 4.49 shows the Pseudo-first order kinetics for Fenton degradation of MB catalyzed by by  $\text{Fe}_{2.79}\text{Nb}_{0.19}\text{O}_4$  sample. It was observed that the experimental data for all MB concentrations fitted well with the Pseudo-first-order kinetics.

Table 4.17: The calculated parameters of the zero and pseudo-first order kinetic models with associated  $R^2$  for Fenton oxidation of MB catalyzed by  $\text{Fe}_{2.79}\text{Nb}_{0.19}\text{O}_4$  samples

MB concentration ( $\text{mg L}^{-1}$ )	Kinetic Model			
	Zero order		Pseudo-first order	
	$k_0$ ( $\text{mg L}^{-1} \cdot \text{min}^{-1}$ )	$R^2$	$k_1$ ( $\text{min}^{-1}$ )	$R^2$
100	0.2383	0.9573	0.0123	0.9898
50	0.1283	0.7944	0.0223	0.9739
25	0.0412	0.8569	0.0308	0.9377

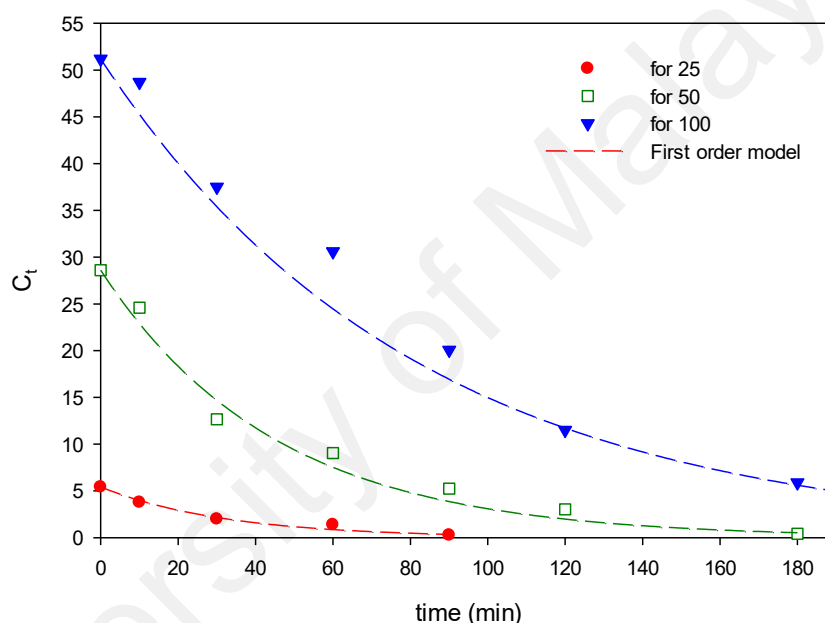


Figure 4.49: Pseudo-first order kinetic for MB degradation through heterogeneous Fenton reaction catalyzed by  $\text{Fe}_{2.79}\text{Nb}_{0.19}\text{O}_4$  samples

On the other hand, based on the calculated values of  $R^2$  in Table 4.18, for all the  $\text{Fe}_{3-x}\text{Mo}_x\text{O}_4$  samples, the zero order kinetic model provided the best fit to the experimental kinetic data (Fig. 4.50). It means that the oxidation reaction rate using Mo-substituted magnetite samples was independent of the reactants concentrations. Furthermore, the reaction rate constants were the highest for the  $\text{Fe}_{2.62}\text{Mo}_{0.21}\text{O}_4$  sample followed by  $\text{Fe}_{2.79}\text{Mo}_{0.13}\text{O}_4$ ,  $\text{Fe}_{2.89}\text{Mo}_{0.069}\text{O}_4$  and  $\text{Fe}_{2.94}\text{Mo}_{0.028}\text{O}_4$ .

Table 4.18: The calculated parameters of the zero and pseudo-first order kinetic models with associated  $R^2$  for Fenton oxidation of MB catalyzed by  $\text{Fe}_{3-x}\text{Mo}_x\text{O}_4$  samples

Sample	Kinetic Model			
	Zero order		Pseudo-first order	
	$k_0$	$R^2$	$k_1$	$R^2$
$\text{Fe}_{2.94}\text{Mo}_{0.028}\text{O}_4$	0.1508	0.9885	0.0071	0.9742
$\text{Fe}_{2.89}\text{Mo}_{0.069}\text{O}_4$	0.1656	0.9965	0.0101	0.8838
$\text{Fe}_{2.79}\text{Mo}_{0.13}\text{O}_4$	0.1803	0.9928	0.0109	0.9015
$\text{Fe}_{2.62}\text{Mo}_{0.21}\text{O}_4$	0.2071	0.9901	0.0251	0.8837

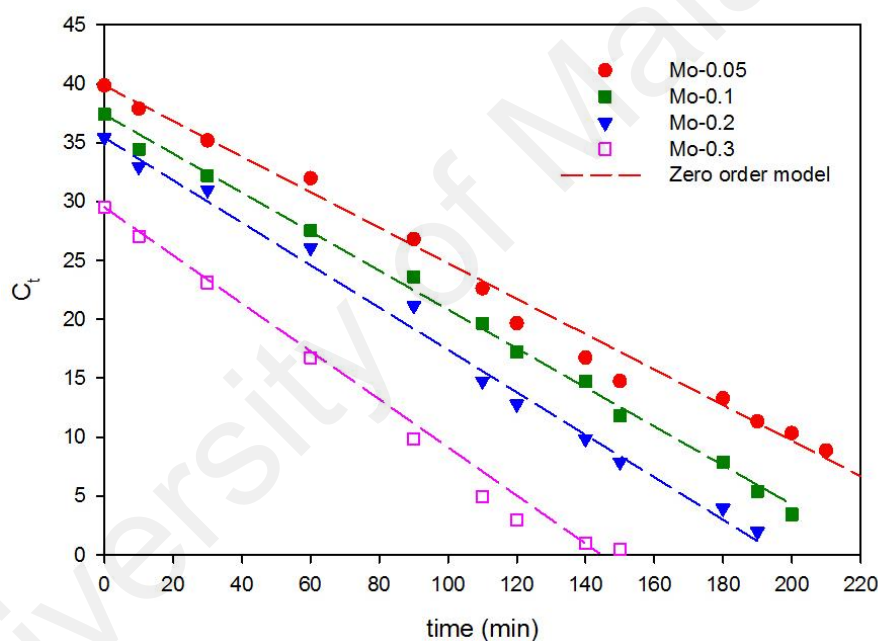


Figure 4.50: Zero order kinetics for MB degradation through heterogeneous Fenton reaction catalyzed by  $\text{Fe}_{3-x}\text{Mo}_x\text{O}_4$  samples

Table 4.19 presents the data on the rate constants and regression ( $R^2$ ) values of both the studied models for  $\text{Fe}_{3-x-y}\text{Nb}_x\text{Mo}_y\text{O}_4$  samples. Although the rate constants of zero-order kinetics were relatively higher than that of the pseudo-first-order kinetics,  $R^2$  values of the pseudo-first-order model of all the samples were closer to one ( $R^2 > 0.99$ ) when compared to the  $R^2$  value of the zero-order kinetics model. The results showed that pseudo-first-order kinetics model well described the experimental data that was in

agreement with Nb substituted magnetite samples. Figure 4.51 shows the Pseudo-first order kinetics for Fenton degradation of MB catalyzed by  $\text{Fe}_{3-x-y}\text{Nb}_x\text{Mo}_y\text{O}_4$  samples. It was observed that the experimental data fitted well with the Pseudo-first-order kinetics.

Furthermore, the degradation rate increased at lower concentrations of MB due to a larger ratio of active sites to probe molecules. The inter-comparison amongst the studied catalysts showed that decolorization rate increased as the amount of imported Nb+Mo of the samples increased. For instance, the rate of MB degradation using  $\text{Fe}_{2.79}\text{Nb}_{0.171}\text{Mo}_{0.023}\text{O}_4$  samples was about 20% higher than the  $\text{Fe}_{2.79}\text{Nb}_{0.0249}\text{Mo}_{0.094}\text{O}_4$  samples with 39% lower Nb+Mo content. This indicated that MB oxidation process was promoted by Nb+Mo content of catalysts that could be attributed to the increase in adsorption and active sites on the samples by increasing Nb/Mo, as explained earlier.

Table 4.19: The calculated parameters of the zero and pseudo-first order kinetic models with associated  $R^2$  for Fenton oxidation of MB catalyzed by  $\text{Fe}_{3-x-y}\text{Nb}_x\text{Mo}_y\text{O}_4$  samples

Sample	Kinetic model	Parameter	MB Concentration ( $\text{mg L}^{-1}$ )		
			50	100	200
$\text{Fe}_{2.79}\text{Nb}_{0.0249}\text{Mo}_{0.094}\text{O}_4$	Pseudo-first order	$k_1$	0.0299	0.0157	0.0105
		$R^2$	0.9960	0.9970	0.9850
	Zero order	$k_0$	0.0428	0.0266	0.0167
		$R^2$	0.9840	0.9770	0.9830
$\text{Fe}_{2.79}\text{Nb}_{0.049}\text{Mo}_{0.089}\text{O}_4$	Pseudo-first order	$k_1$	0.0301	0.0162	0.0114
		$R^2$	0.9920	0.9930	0.9930
	Zero order	$k_0$	0.0575	0.0266	0.0167
		$R^2$	0.9820	0.9900	0.9900
$\text{Fe}_{2.79}\text{Nb}_{0.099}\text{Mo}_{0.073}\text{O}_4$	Pseudo-first order	$k_1$	0.0321	0.0171	0.0121
		$R^2$	0.9950	0.9730	0.9820
	Zero order	$k_0$	0.0575	0.0341	0.0293
		$R^2$	0.9690	0.9590	0.9510
$\text{Fe}_{2.79}\text{Nb}_{0.149}\text{Mo}_{0.032}\text{O}_4$	Pseudo-first order	$k_1$	0.0321	0.0181	0.0127
		$R^2$	0.9830	0.9850	0.9770
	Zero order	$k_0$	0.0580	0.0365	0.0303
		$R^2$	0.9730	0.9540	0.9330
$\text{Fe}_{2.79}\text{Nb}_{0.171}\text{Mo}_{0.023}\text{O}_4$	Pseudo-first order	$k_1$	0.0329	0.0201	0.0137
		$R^2$	0.998	0.983	0.981
	Zero order	$k_0$	0.0625	0.0455	0.0346
		$R^2$	0.960	0.981	0.974

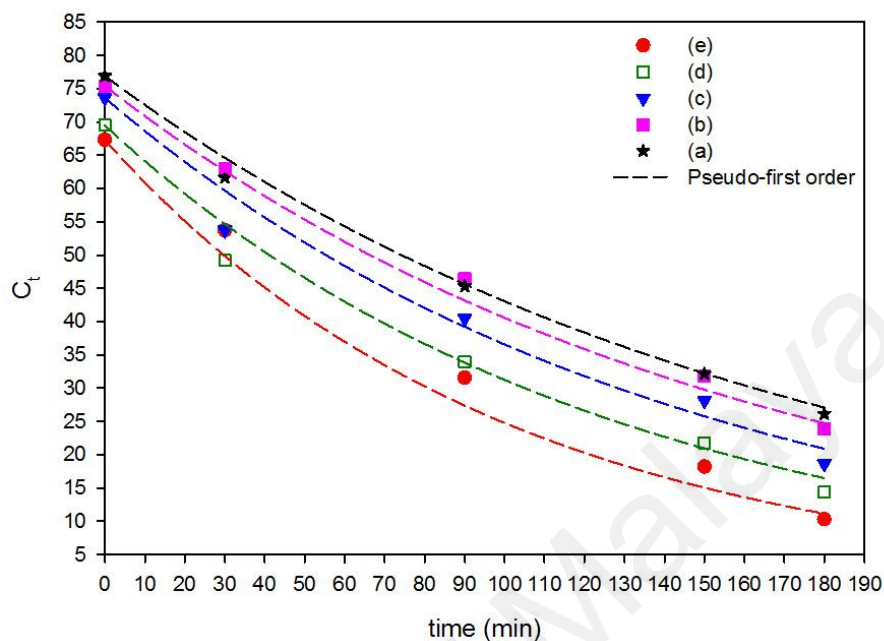


Figure 4.51: Pseudo-first order kinetic for MB degradation through heterogeneous Fenton reaction catalyzed by  $\text{Fe}_{3-x-y}\text{Nb}_x\text{Mo}_y\text{O}_4$  samples

#### 4.11. Single metal vs. co-doped substitutions

In Nb or Mo substituted magnetite samples,  $\text{Fe}_{2.73}\text{Nb}_{0.19}\text{O}_4$  and sample showed highest activities in Fenton-like degradation of MB solution when compared to other synthesized Nb-magnetite samples. On the other hand, in co-doped samples,  $\text{Fe}_{2.79}\text{Nb}_{0.171}\text{Mo}_{0.023}\text{O}_4$  sample showed highest MB adsorption capacity and removal through Fenton reaction in comparison with other combinations. At first sight, it might be concluded that the activity of modified magnetite samples have been more dependent on Nb content rather than that of Mo, mainly due to higher incorporation-maxima of Nb into magnetite than of Mo. Therefore, the sum total Nb+Mo substitution increased with increment in Nb fraction.

However, the comparison of the results for MB adsorption and Fenton reactivity of the samples with  $x=0.2$  of incorporated metals,  $\text{Fe}_{2.73}\text{Nb}_{0.19}\text{O}_4$ ,  $\text{Fe}_{2.79}\text{Mo}_{0.13}\text{O}_4$  and

$\text{Fe}_{2.79}\text{Nb}_{0.171}\text{Mo}_{0.023}\text{O}_4$ , showed that co-doped sample had better performances. Therefore, Mo incorporation has also had positive effects on magnetite performance in Fenton reaction even at minor concentrations. This could be because of the increase in electron mobility in the crystal structure by entering  $\text{Mo}^{4+}/\text{Mo}^{6+}$  cations to the system. In addition, this redox pair entered to  $\text{H}_2\text{O}_2$  decomposition cycle and  $\text{Fe}^{3+}$  reduction reaction and enhanced the Fenton oxidation of MB. It is evident from the results that incorporation of more than one metal into magnetite structure could result in better performances in Fenton oxidation of organic pollutants and proves the opportunity for application of naturally existing magnetite samples with more transition metals in their structure for environmental purification aspects.

## CHAPTER 5: CONCLUSION AND RECOMMENDATIONS

Research on magnetite as a heterogeneous catalyst for Fenton process has been increasing due to its applicability in a wide range of pH, easy separation, reusability and presence of  $\text{Fe}^{2+}$  cations in its octahedral sites. However, magnetite-catalyzed Fenton process has lower reaction rate compared to homogeneous Fenton process. Currently, there are several methods reported in literature to improve magnetite performance in Fenton reaction. Nonetheless, the selected modification method should meet a number of criteria as follows:

- i. Maintaining the main magnetite features: i.e., crystalline structure and magnetic properties.
- ii. Developing a new catalyst using a practicable and affordable method.
- iii. Achieving higher activities in Fenton treatment of recalcitrant contaminants.
- iv. Improving the degradation reaction rate compared to pure magnetite.
- v. Applicable for treating diverse pollutant molecules.
- vi. Maintaining its activity after several recycling.

The most promising method that incorporates the aforementioned criteria is the isomorphic substitution of iron with other transition metal/metals in magnetite structure. In this method, other transition metal/metals replace the structural iron ( $\text{Fe}^{2+}$  and/or  $\text{Fe}^{3+}$ ) in magnetite and brings about some positive changes in its structure and consequently, in its activity in Fenton reaction. However, earlier studies focused mainly on the fourth series of the transition metals, and there is no systematic investigation on the effects of the transition metals from period five. Therefore, the present study focuses on modifying magnetite with transition metals from the fifth period that has capacity to produce robust catalyst with the desired attributes. These include higher adsorption



capacity, efficient activity, higher reaction rate, reusability, and ease of separation. Purposely, these features define an efficient catalytic material for Fenton oxidation of recalcitrant wastewater. Thus, this study highlights the following:

- a. It is possible to synthesize and characterize heterogeneous catalysts based on niobium and/or molybdenum substituted magnetite.
- b. It is possible to enhance the activity of magnetite in Fenton oxidation process by investigating the effects of Nb and/or Mo incorporating in activation of the active sites of magnetite.
- c. It is possible to further improve the activity of these catalysts by introducing external energy sources, ultraviolet and ultrasound, to Fenton oxidation system.
- d. The Nb and/or Mo substituted magnetite samples have the potential to improve the oxidation rate of the pollutants through Fenton reaction.

The study concludes the following:

1. A series of Nb and/or Mo substituted magnetite samples were prepared by co-precipitation method and their characteristics in terms of durability, crystalline phase, morphology, size, surface area and composition and magnetic property were determined.

All the synthesized samples had well-crystalline spinel structure and good magnetic properties. The incorporation of Nb and/or Mo decreased the particle size of the samples and accordingly resulted in larger surface areas compared to pure magnetite sample. Therefore, the adsorption capacity of the modified samples significantly enhanced. The incorporated Nb<sup>4+</sup> and Mo<sup>4+</sup> mainly placed in Fe<sup>3+</sup> and Fe<sup>2+</sup> cations respectively and their surface concentrations increased with the imported metals.

2. Subsequently, the effects of Nb and/or Mo incorporating on the magnetite performance and reactivity for methylene blue adsorption and degradation through Fenton-like experiments were evaluated. Prior to activity evaluation experiments, Fenton oxidation of methylene blue catalyzed by pure magnetite was optimized using Response Surface Methodology (RSM). The effects of the  $\text{H}_2\text{O}_2$  concentration, amount of catalyst, reaction time, and pH of the reaction (variables) on the color, COD and TOC removal efficiencies of magnetite samples (responses) were investigated using a central composite design (CCD). Optimal conditions of  $[\text{H}_2\text{O}_2]_0$ :  $0.2 \text{ mol L}^{-1}$ ,  $[\text{Catalyst}]_0$ :  $1 \text{ g L}^{-1}$ , pH 7 and reaction time: 3 h were chosen and used for Fenton oxidation of MB using all the synthesized samples, thus permitting inter-comparisons.
3. All the modified magnetite samples showed significantly higher activities in degradation and mineralization of methylene blue solutions by Fenton process when compared with pure magnetite. In the  $\text{Fe}_{3-x}\text{Nb}_x\text{O}_4$  ( $x = 0.022, 0.049, 0.099$  and  $0.19$ ) and  $\text{Fe}_{3-x}\text{Mo}_x\text{O}_4$  ( $x = 0.28, 0.069, 0.13$  and  $0.21$ ) groups, the  $\text{Fe}_{2.79}\text{Mo}_{0.21}\text{O}_4$ , and  $\text{Fe}_{2.79}\text{Nb}_{0.19}\text{O}_4$  samples ( $x \approx 0.2$ ) showed the highest activities in Fenton treatment of MB compared to the rest of the samples. Accordingly, the  $\text{Fe}_{3-x-y}\text{Nb}_x\text{Mo}_y\text{O}_4$  samples were prepared through co-precipitation of Nb and Mo with sum total molar fraction of 0.2 ( $x+y=0.2$ ). All the co-doped samples showed exceptional performances in MB degradation and mineralization through Fenton reaction. The total MB degradation and more than 70% of mineralization completed within 180 min using the  $\text{Fe}_{2.79}\text{Mo}_{0.21}\text{O}_4$ ,  $\text{Fe}_{2.79}\text{Nb}_{0.19}\text{O}_4$  and  $\text{Fe}_{2.79}\text{Nb}_{0.171}\text{Mo}_{0.023}\text{O}_4$  samples.
4. The activity of  $\text{Fe}_{2.79}\text{Mo}_{0.13}\text{O}_4$ ,  $\text{Fe}_{2.79}\text{Nb}_{0.19}\text{O}_4$  and  $\text{Fe}_{2.79}\text{Nb}_{0.171}\text{Mo}_{0.023}\text{O}_4$  catalysts were assessed through Fenton reaction combined with ultraviolet and ultrasound irradiations for MB and MO solutions. A significant enhancement in

the degradation efficiency of MB and MO was observed under the influence of UV and US irradiations using the optimized catalysts of each synthesized catalysts ( $\text{Fe}_{2.79}\text{Mo}_{0.13}\text{O}_4$ ,  $\text{Fe}_{2.79}\text{Nb}_{0.19}\text{O}_4$  and  $\text{Fe}_{2.79}\text{Nb}_{0.171}\text{Mo}_{0.023}\text{O}_4$  samples). Amongst the employed catalysts, the  $\text{Fe}_{2.79}\text{Nb}_{0.171}\text{Mo}_{0.023}\text{O}_4$  sample showed the peak adsorption capacity and catalytic activity compared to  $\text{Fe}_{2.79}\text{Mo}_{0.13}\text{O}_4$  and  $\text{Fe}_{2.79}\text{Nb}_{0.19}\text{O}_4$  samples. The main factors that enhanced activity of the synthesized catalysts were:

- a. increased surface adsorption capacity,
  - b. participation of thermodynamically favorable redox pair ( $\text{Nb}^{4+}/\text{Nb}^{5+}$  and/or  $\text{Mo}^{4+}/\text{Mo}^{6+}$ ) in regenerating  $\text{Fe}^{2+}$  from  $\text{Fe}^{3+}$ , and  $\cdot\text{OH}$  radical through  $\text{H}_2\text{O}_2$  decomposition,
  - c. direct MB degradation by surface peroxo-niobium complexes, and
  - d. presence of oxygen vacancies on the surface of catalysts as active sites.
5. The pseudo-second-order model in kinetics described MB adsorption on the surface of the  $\text{Fe}_{3-x-y}\text{Nb}_x\text{Mo}_y\text{O}_4$  samples. In addition, Fenton degradation of MB catalyzed by  $\text{Fe}_{3-x}\text{Mo}_x\text{O}_4$  samples fitted well to zero order model and  $\text{Fe}_{3-x}\text{Nb}_x\text{O}_4$  and  $\text{Fe}_{3-x-y}\text{Nb}_x\text{Mo}_y\text{O}_4$  catalysts best fitted to pseudo-first-order model in kinetics. On the other hand, pseudo-first-order model in kinetics described MB degradation through UV/Fenton and US/Fenton reaction using  $\text{Fe}_{2.79}\text{Mo}_{0.13}\text{O}_4$ ,  $\text{Fe}_{2.79}\text{Nb}_{0.19}\text{O}_4$  and  $\text{Fe}_{2.79}\text{Nb}_{0.171}\text{Mo}_{0.023}\text{O}_4$  samples.
6. All the synthesized samples showed very good stability under the various experimental conditions without significant decrease in their catalytic performances despite reusing for three times.

Conclusively, high adsorption capacity, enhanced degradation efficiency, and negligible leaching of the Nb and Mo ions showed the effectiveness of Nb and/or Mo substituted

magnetite catalysts in treating both synthetic wastewaters (methylene blue and methyl orange) through Fenton process. Therefore, the aim of the study, which was developing high efficient heterogeneous Fenton catalysts for treatment of recalcitrant contaminants, was achieved. Most importantly, this work contributed significantly to the knowledge by systematic identifying appropriate transition metals to be integrated into naturally available magnetite with simple synthesis method, for application as a catalyst, at least for advanced oxidation of selected contaminants. Besides, during this study, seven academic articles were published and the first page of the publications presented.

## **5.2.Recommendations for future work**

The present work aimed at assessing the effects of the incorporating transition metals from period 5 (Nb and Mo) on magnetite structure, adsorption capacity and activity in Fenton reaction. Future studies in this field should address the development of new transition metal-substituted iron oxides to obtain significant leap in activity, while maintaining the magnetic property of the iron oxides for easier separation from reaction medium. In addition, systematic research is required to examine their stability under a wider range of operational conditions to avoid the leaching of these metals into reaction solution and their impact on the environment. However, the recommendations for further understanding and expansion of the current work are as follows:

1. Further studies and comparison on various combinations of two or more transition metals from period 4, 5 or both. This will explore the best combinations for higher degradation efficiencies.
2. Explore other catalyst supports such as clays, activated carbon or zeolite to increase the specific surface area, and adsorption capacity of the samples accordingly.

3. Conduct in-depth surface modification studies that will enhance characteristics of heterogeneous catalysts and their subsequent crucial role for the targeted activity. Surface treatment by  $H_2O_2$  is an example that increases the surface -OH groups.
4. Evaluate various combinations of Fenton reaction with other AOPs, and external energy sources such as electro/Fenton and UV/US/Fenton for increased efficiency of the proposed systems.
5. Additionally, the investigation of the effects of various factors such as wastewater composition on the stability, lexiviation and aging of the catalytic sites of this group of catalysts for longer and efficient use in Fenton treatment of recalcitrant wastewaters are recommended.

## REFERENCES

- Ai, L., Zhang, C., Liao, F., Wang, Y., Li, M., Meng, L., & Jiang, J. (2011). Removal of methylene blue from aqueous solution with magnetite loaded multi-wall carbon nanotube: Kinetic, isotherm and mechanism analysis. *Journal of Hazardous Materials*, 198(0), 282-290.
- Aleboye, A., Daneshvar, N., & Kasiri, M. B. (2008). Optimization of C.I. Acid Red 14 azo dye removal by electrocoagulation batch process with response surface methodology. *Chemical Engineering and Processing: Process Intensification*, 47(5), 827-832.
- Alexander, M. (1975). Environmental and microbiological problems arising from recalcitrant molecules. *Microbial Ecology*, 2(1), 17 -27.
- Alvarez, M., Rueda, E. H., & Sileo, E. E. (2006). Structural characterization and chemical reactivity of synthetic Mn-goethites and hematites. *Chemical Geology*, 231(4), 288-299.
- An, J., Zhu, L., Zhang, Y., & Tang, H. (2013). Efficient visible light photo-Fenton-like degradation of organic pollutants using in situ surface-modified BiFeO<sub>3</sub> as a catalyst. *Journal of Environmental Sciences*, 25(6), 1213-1225.
- Andreozzi, R., Caprio, V., Insola, A., & Marotta, R. (1999). Advanced oxidation processes (AOP) for water purification and recovery. *Catalysis Today*, 53(1), 51-59.
- Arami-Niya, A., Wan Daud, W. M. A., S. Mjalli, F., Abnisa, F., & Shafeeyan, M. S. (2012). Production of microporous palm shell based activated carbon for methane adsorption: Modeling and optimization using response surface methodology. *Chemical Engineering Research and Design*, 90(6), 776-784.
- Arora, R., Chanderia, K., Punjabi, P. B., & Sharma, V. K. (2010). Synthesis, characterization of hydroxyl-Fe-pillared-bentonite and its use in heterogeneous photo-fenton degradation of rose Bengal. *Journal of Chemical and Pharmaceutical Research*, 2( 2), 627-636.
- Ayodele, O. B., Lim, J. K., & Hameed, B. H. (2012). Degradation of phenol in photo-Fenton process by phosphoric acid modified kaolin supported ferric-oxalate catalyst: Optimization and kinetic modeling. *Chemical Engineering Journal*, 197(0), 181-192.
- Babuponnusami, A., & Muthukumar, K. (2012). Advanced oxidation of phenol: A comparison between Fenton, electro-Fenton, sono-electro-Fenton and photo-electro-Fenton processes. *Chemical Engineering Journal*, 183(0), 1-9.
- Bagal, M. V., & Gogate, P. R. (2014). Wastewater treatment using hybrid treatment schemes based on cavitation and Fenton chemistry: A review. *Ultrasonics Sonochemistry*, 21(1), 1-14.

- Baldrian, P., Merhautová, V., Gabriel, J., Nerud, F., Stopka, P., Hruby, M., & Beneš, M. J. (2006). Decolorization of synthetic dyes by hydrogen peroxide with heterogeneous catalysis by mixed iron oxides. *Applied Catalysis B: Environmental*, 66(3-4), 258-264.
- Ballesteros Martín, M. M., Sánchez Pérez, J. A., Casas López, J. L., Oller, I., & Malato Rodríguez, S. (2009). Degradation of a four-pesticide mixture by combined photo-Fenton and biological oxidation. *Water Research*, 43(3), 653-660.
- Batista, A. P. S., & Nogueira, R. F. P. (2012). Parameters affecting sulfonamide photo-Fenton degradation – Iron complexation and substituent group. *Photochemistry and Photobiology A: Chemistry* 232, 8– 13.
- Bautitz, I. R., & Nogueira, R. F. P. (2010). Photodegradation of lincomycin and diazepam in sewage treatment plant effluent by photo-Fenton process. *Catalysis Today*, 151, 94–99.
- Beltran Huarac, J. C. S. a. c. o. M. Z. o. a. M. Z. m. s. c.-s. h. n. U. o. P. R., Mayaguez (Puerto Rico)). ProQuest Dissertations and Theses, , 62. Retrieved from <http://search.proquest.com/docview/822426629?accountid=28930>. (822426629).
- Benkelberg, H.-J., & Warneck, P. (1995). Photodecomposition of Iron(III) Hydroxo and Sulfato Complexes in Aqueous Solution: Wavelength Dependence of OH and SO<sub>4</sub><sup>-</sup> Quantum Yields. *The Journal of Physical Chemistry*, 99(14), 5214-5221.
- Benkelberg, H. J., & Warneck, P. (1995). Photodecomposition of iron (III) hydroxo and sulfato complexes in aqueous solution: wavelength dependence of OH and SO<sub>4</sub> quantum yields. *Physical Chemistry A*, 99, 5214–5221.
- Bernabeu, A., Palacios, S., Vicente, R., Vercher, R. F., Malato, S., Arques, A., & Amat, A. M. (2012). Solar photo-Fenton at mild conditions to treat a mixture of six emerging pollutants. *Chemical Engineering Journal*, 198–199(0), 65-72.
- Bobu, M., Yediler, A., Siminiceanu, I., Zhang, F., & Schulte-Hostede, S. (2012). Comparison of different advanced oxidation processes for the degradation of two fluoroquinolone antibiotics in aqueous solutions. *Journal of Environmental Science and Health, Part A*, 48(3), 251-262
- Bouet, L., Tailhades, P., Rousset, A., Domenichini, B., & Gillot, B. (1992). Mixed valence states of iron and molybdenum ions in MoxFe<sub>3-x</sub>O<sub>4</sub> magnetites and related cation deficient ferrites. *Solid State Ionics*, 52(4), 285-286.
- Bremner, D. H., Carlo, S. D., Chakinala, A. G., & Cravotto, G. (2008). Mineralisation of 2,4-dichlorophenoxyacetic acid by acoustic or hydrodynamic cavitation in conjunction with the advanced Fenton process. *Ultrasonics Sonochemistry*, 15(4), 416-419.
- Büchler, M., Schmuki, P., Böhni, H., Stenberg, T., & Mäntylä, T. (1998). Comparison of the semiconductive properties of p-putter-deposited iron oxides with the passive film on iron. *Journal of Electrochemical Society*, 145(2), 378-385

- Carra, I., Casas López, J. L., Santos-Juanes, L., Malato, S., & Sánchez Pérez, J. A. (2013). Iron dosage as a strategy to operate the photo-Fenton process at initial neutral pH. *Chemical Engineering Journal*, 224(0), 67-74.
- Carvalho, H. W. P., Hammer, P., Pulcinelli, S. H., Santilli, C. V., & Molina, E. F. (2014). Improvement of the photocatalytic activity of magnetite by Mn-incorporation. *Materials Science and Engineering: B*, 181, 64-69.
- Cavalcante, R., Rocha Sandim, L., Bogo, D., Barbosa, A., Osugi, M., Blanco, M., . . . Ferreira, V. (2013). Application of Fenton, photo-Fenton, solar photo-Fenton, and UV/H<sub>2</sub>O<sub>2</sub> to degradation of the antineoplastic agent mitoxantrone and toxicological evaluation. *Environmental Science and Pollution Research*, 20(4), 2352-2361.
- Chamarro, E., Marco, A., & Espulgas, S. (2000). Use of Fenton reagent to improve organic chemical biodegradability. *Water Research*, 35 (4), 1047–1051.
- Chen, C.-Y., Wu, P.-S., & Chung, Y.-C. (2009). Coupled biological and photo-Fenton pretreatment system for the removal of di-(2-ethylhexyl) phthalate (DEHP) from water. *Bioresource Technology*, 100(19), 4531-4534.
- Chun, J., Lee, H., Lee, S.-H., Hong, S.-W., Lee, J., Lee, C., & Lee, J. (2012). Magnetite/mesocellular carbon foam as a magnetically recoverable fenton catalyst for removal of phenol and arsenic. *Chemosphere*, 89(10), 1230-1237.
- Coelho, A., Castro, A. V., Dezotti, M., & Sant'Anna Jr, G. L. (2006). Treatment of petroleum refinery sourwater by advanced oxidation processes. *Journal of Hazardous Materials*, 137(1), 178-184.
- Coker, V. S., Pearce, C. I., Patrick, R. A. D., van der Laan, G., Telling, N. D., Charnock, J. M., . . . Lloyd, J. R. (2008). Probing the site occupancies of Co-, Ni-, and Mn-substituted biogenic magnetite using XAS and XMCD. *American Mineralogist*, 93(7), 1119-1132.
- Comninellis, C., Kapalka, A., Malato, S., Parsons, S. A., Poulios, I., & Mantzavinos, D. (2008). Perspective, Advanced oxidation processes for water treatment: advances and trends for R&D. *Journal of Chemical Technology and Biotechnology*, 83(0), 769–776
- Cornell, R., & Schwertmann, U. (2003). *The iron oxides: structure, properties, reactions, occurrences and uses*: John Wiley & Sons.
- Costa, R. C. C., Lelis, M. d. F. F., Oliveira, L. C. A., Fabris, J. D., Ardisson, J. D., Rios, R. R. V. A., . . . Lago, R. M. (2003). Remarkable effect of Co and Mn on the activity of Fe<sub>3-x</sub>M<sub>x</sub>O<sub>4</sub> promoted oxidation of organic contaminants in aqueous medium with H<sub>2</sub>O<sub>2</sub>. *Catalysis Communications*, 4(10), 525-529.
- Costa, R. C. C., Lelis, M. F. F., Oliveira, L. C. A., Fabris, J. D., Ardisson, J. D., Rios, R. R. V. A., . . . Lago, R. M. (2006). Novel active heterogeneous Fenton system based on Fe<sub>3-x</sub>M<sub>x</sub>O<sub>4</sub> (Fe, Co, Mn, Ni): The role of M<sup>2+</sup> species on the reactivity towards H<sub>2</sub>O<sub>2</sub> reactions. *Journal of Hazardous Materials*, 129(1-3), 171-178.



- da Rocha, O. R. S., Dantas, R. F., Bezerra Duarte, M. M. M., Lima Duarte, M. M., & da Silva, V. L. (2013). Solar photo-Fenton treatment of petroleum extraction wastewater. *Desalination and Water Treatment*, 1-7.
- da Silva, M. R. A., Trovó, A. G., & Nogueira, R. F. P. (2007). Treatment of 1,10-phenanthroline laboratory wastewater using the solar photo-Fenton process. *Journal of Hazardous Materials*, 146(3), 508-513.
- da Silva, S. S., Chiavone-Filho, O., de Barros Neto, E. L., & Nascimento, C. A. O. (2012). Integration of processes induced air flotation and photo-Fenton for treatment of residual waters contaminated with xylene. *Journal of Hazardous Materials*, 199–200(0), 151-157.
- Daneshvar, N., Behnajady, M. A., Khayyat, A. M., Mohammadi, M. S., & Seyed Dorraji. (2008). UV/H<sub>2</sub>O<sub>2</sub> treatment of rhodamine B in aqueous solution: influence of operational parameters and kinetic modeling. *Desalination*, 230, 16–26.
- Dantas, T. L. P., Mendonea, V. P., Jose, H. J., Rodrigues, A. E., & Moreira, R. F. P. M. (2006). Treatment of textile wastewater by heterogeneous Fenton process using a new composite Fe<sub>2</sub>O<sub>3</sub>/carbon. *Chemical Engineering Journal*, 118(1-2), 77-82.
- David R. Lide, e. (2005). *CRC Handbook of Chemistry and Physics*, . Boca Raton, FL.: CRC Press.
- de Freitas Matos, T. A., Nunes Dias, A. L., Di Piazza Reis, A., da Silva, M. R. A., & Matiko Kondo, M. (2012). Degradation of Abamectin Using the Photo-Fenton Process. *International Journal of Chemical Engineering*, 2012, 7.
- De la Cruz, N., Giménez, J., Esplugas, S., Grandjean, D., de Alencastro, L. F., & Pulgarín, C. (2012). Degradation of 32 emergent contaminants by UV and neutral photo-fenton in domestic wastewater effluent previously treated by activated sludge. *Water Research*, 46(6), 1947-1957.
- De Laat, J., & Le, T. G. (2006). Effects of chloride ions on the iron(III)-catalyzed decomposition of hydrogen peroxide and on the efficiency of the Fenton-like oxidation process. *Applied Catalysis B: Environmental*, 66(1–2), 137-146.
- de Lima Perini, J. A., Perez-Moya, M., & Nogueira, R. F. P. (2013). Photo-Fenton degradation kinetics of low ciprofloxacin concentration using different iron sources and pH. *Journal of Photochemistry and Photobiology A: Chemistry*, 259(0), 53-58.
- de Oliveira, I. S., Lilian Viana, Cenira Verona, Vera Lúcia Vargas Fallavena, Carla Maria Nunes Azevedo, & Marçal Pires. (2007). Alkydic resin wastewaters treatment by fenton and photo-Fenton processes. *Journal of Hazardous Materials* 146, 564–568.

- de Souza, W. F., Guimarães, I. R., Oliveira, L. C. A., Giroto, A. S., Guerreiro, M. C., & Silva, C. L. T. (2010). Effect of Ni incorporation into goethite in the catalytic activity for the oxidation of nitrogen compounds in petroleum. *Applied Catalysis A: General*, 381(1–2), 36-41.
- Deng, Y., & Englehardt, J. D. (2007). Electrochemical oxidation for landfill leachate treatment. *Waste Management*, 27(3), 380-388.
- Devi, L. G., Raju, K. S. A., Kumar, S. G., & Rajashekhar, K. E. (2011). Photodegradation of di azo dye Bismarck Brown by advanced photo-Fenton process: Influence of inorganic anions and evaluation of recycling efficiency of iron powder. *Journal of the Taiwan Institute of Chemical Engineers*, 42(2), 341-349.
- Diya'uddeen, B. H., Rahim Pوران, S., Abdul Aziz, A. R., & Wan Daud, W. M. A. (2015). Fenton oxidative treatment of petroleum refinery wastewater: Process optimization and Sludge characterization. *RSC Advances*.
- Doll, T. E., & Frimmel, F. H. (2003). Fate of pharmaceuticals—photodegradation by simulated solar UV-light. *Chemosphere*, 52(10), 1757-1769.
- dos Santos, C. A., Horbe, A. M. C., Barcellos, C. M. O., & Marimon da Cunha, J. B. (2001). Some structure and magnetic effects of Ga incorporation on  $\alpha$ -FeOOH. *Solid State Communications*, 118(9), 449-452.
- Duesterberg, C. K., Cooper, W. J., & Waite, T. D. (2005). Fenton-mediated Oxidation in the Presence and Absence of Oxygen. *Environmental Science & Technology*, , 39(13), 5052–5058.
- Dükkancı, M., Vinatoru, M., & Mason, T. J. (2014). The sonochemical decolourisation of textile azo dye Orange II: Effects of Fenton type reagents and UV light. *Ultrasonics Sonochemistry*, 21(2), 846-853.
- Elmolla, E. S., & Chaudhuri, M. (2009). Degradation of the antibiotics amoxicillin, ampicillin and cloxacillin in aqueous solution by the photo-Fenton process. *J Hazard Mater*, 172(2–3), 1476-1481.
- Elmolla, E. S., & Chaudhuri, M. (2011). Combined photo-Fenton-SBR process for antibiotic wastewater treatment. *Journal of Hazardous Materials*, 192(3), 1418-1426.
- Esteves, A., Oliveira, L. C. A., Ramalho, T. C., Goncalves, M., Anastacio, A. S., & Carvalho, H. W. P. (2008). New materials based on modified synthetic Nb<sub>2</sub>O<sub>5</sub> as photocatalyst for oxidation of organic contaminants. *Catalysis Communications*, 10(3), 330-332.
- Farré, M. J., Doménech, X., & Peral, J. (2006). Assessment of photo-Fenton and biological treatment coupling for Diuron and Linuron removal from water. *Water Research*, 40(13), 2533-2540.

- Farrokhi, M., Mesdaghinia, A. R., Yazdanbakhsh, A. R., & Nasser, S. (2004). Characteristics of Fenton's Oxidation of 2, 4, 6 Trichlorophenol. *Iranian Journal of Environmental Health Science & Engineering*, 1(1), 13-19.
- Faust, B. C., & Hoigne, J. (1990). Photolysis of Fe(III)-hydroxyl complexes as sources of OH radicals in clouds, fog and rain. *Atmospheric Environment*, 24(0), 79-89.
- Franch, M. I., Ayllón, J. A., Peral, J., & Domènech, X. (2004). Fe(III) photocatalyzed degradation of low chain carboxylic acids: implications of the iron salt. *Applied Catalysis B: Environmental*, 50(2), 89-99.
- Francombe, M. H. (1957). Lattice changes in spinel-type iron chromites. *Journal of Physics and Chemistry of Solids*, 3(1-2), 37-43.
- Frontistis, Z., Xekoukoulotakis, N. P., Hapeshi, E., Venieri, D., Fatta-Kassinou, D., & Mantzavinos, D. (2011). Fast degradation of estrogen hormones in environmental matrices by photo-Fenton oxidation under simulated solar radiation. *Chemical Engineering Journal*, 178(0), 175-182.
- Gallared, H., De Leet, J., & Legube, B. (1998). Effect of pH on the oxidation rate of organic compounds by Fe-II/ H<sub>2</sub>O<sub>2</sub> mechanisms and simulation. *New Journal of Chemistry*, 22(3), 263-268.
- Galvão, S. A. O., Mota, A. L. N., Silva, D. N., Moraes, J. E. F., Nascimento, C. A. O., & Chiavone-Filho, O. (2006). Application of the photo-Fenton process to the treatment of wastewaters contaminated with diesel. *Science of The Total Environment*, 367(1), 42-49.
- García-Fernández, I., Polo-López, M. I., Oller, I., & Fernández-Ibáñez, P. (2012). Bacteria and fungi inactivation using Fe<sup>3+</sup>/sunlight, H<sub>2</sub>O<sub>2</sub>/sunlight and near neutral photo-Fenton: A comparative study. *Applied Catalysis B: Environmental*, 121-122(0), 20-29.
- Garrido-Ramírez, E. G., Theng, B. K. G., & Mora, M. L. (2010). Clays and oxide minerals as catalysts and nanocatalysts in Fenton-like reactions - A review. *Applied Clay Science*, 47(3-4), 182-192.
- Glaze WH., Kang JW., & Chapin DH. (1987). The chemistry of water and water treatment processes involving ozone, hydrogen peroxide and ultra-violet radiation. *Ozone Science & Engineering*, 9(0), 335-342.
- Gogate, P. R., & Pandit, A. B. (2004). A review of imperative technologies for wastewater treatment I: oxidation technologies at ambient conditions. *Advances in Environmental Research*, 8(3-4), 501-551.
- Gong, C., & Hart, D. P. (1998). Ultrasound Induced Cavitation and Sonochemical Yields. *Journal of the Acoustical Society of America*, 104.
- Gonzalez-Olmos, R., Martin, M. J., Georgi, A., Kopinke, F.-D., Oller, I., & Malato, S. (2012). Fe-zeolites as heterogeneous catalysts in solar Fenton-like reactions at neutral pH. *Applied Catalysis B: Environmental*, 125(0), 51-58.

- González, O., Sans, C., & Esplugas, S. (2007). Sulfamethoxazole abatement by photo-Fenton: Toxicity, inhibition and biodegradability assessment of intermediates. *Journal of Hazardous Materials*, 146(3), 459-464.
- Guimaraes, I. R., Giroto, A., Oliveira, L. C. A., Guerreiro, M. C., Lima, D. Q., & Fabris, J. D. (2009). Synthesis and thermal treatment of cu-doped goethite: Oxidation of quinoline through heterogeneous fenton process. *Applied Catalysis B: Environmental*, 91(3-4), 581-586.
- Guimarães, I. R., Oliveira, L. C. A., Queiroz, P. F., Ramalho, T. C., Pereira, M., Fabris, J. D., & Ardisson, J. D. (2008). Modified goethites as catalyst for oxidation of quinoline: Evidence of heterogeneous Fenton process. *Applied Catalysis A: General*, 347(1), 89-93.
- Haneda, K., & Morrish, A. H. (1988). Noncollinear magnetic structure of CoFe<sub>2</sub>O<sub>4</sub> small particles. *Journal of Applied Physics*, 63(8), 4258-4260.
- Hanna, K., Kone, T., & Medjahdi, G. (2008). Synthesis of the mixed oxides of iron and quartz and their catalytic activities for the Fenton-like oxidation. *Catalysis Communications*, 9(5), 955-959.
- He, P. J., Zheng, Z., Zhang, H., Shao, L. M., & Tang, Q. Y. (2009). PAEs and BPA removal in landfill leachate with Fenton process and its relationship with leachate DOM composition. *Sci Total Environ*, 407(17), 4928-4933.
- Heng, G. C., Elmolla, E. S., & Chaudhuri, M. (2012). Optimization of Photo-Fenton Treatment of Mature Landfill Leachate. *Journal of Nature Environment and Pollution Technology*, 11, 65-72.
- Hermosilla, D., Cortijo, M., & Huang, C. P. (2009). Optimizing the treatment of landfill leachate by conventional Fenton and photo-Fenton processes. *Science of The Total Environment*, 407(11), 3473-3481.
- Huang, H.-H., Lu, M.-C., & Chen, J.-N. (2001). Catalytic decomposition of hydrogen peroxide and 2-chlorophenol with iron oxides. *Water Research*, 35(9), 2291-2299.
- Huang, W., Brigante, M., Wu, F., Hanna, K., & Mailhot, G. (2012). Development of a new homogenous photo-Fenton process using Fe(III)-EDDS complexes. *Journal of Photochemistry and Photobiology A: Chemistry*, 239(0), 17-23.
- Huang, W., Brigante, M., Wu, F., Hanna, K., & Mailhot, G. (2013). Effect of ethylenediamine-N,N'-disuccinic acid on Fenton and photo-Fenton processes using goethite as an iron source: optimization of parameters for bisphenol A degradation. *Environmental Science and Pollution Research*, 20(1), 39-50.
- Huang, Y.-H., Huang, Y.-J., Tsai, H.-C., & Chen, H.-T. (2010). Degradation of phenol using low concentration of ferric ions by the photo-Fenton process. *Journal of the Taiwan Institute of Chemical Engineers*, 41(6), 699-704.

- Hug, S. J., & Leupin, O. (2003). Iron-catalyzed oxidation of Arsenic(III) by oxygen and by hydrogen peroxide: pH-dependent formation of oxidants in the Fenton reaction. *Environmental Science & Technology*, 37, 4403-4409.
- Jacobs, J. P., Maltha, A., Reintjes, J. G. H., Drimal, J., Ponec, V., & Brongersma, H. H. (1994). The Surface of Catalytically Active Spinels. *Journal of Catalysis*, 147(1), 294-300.
- Jentzsch, T. L., Lan Chun, C., Gabor, R. S., & Lee Penn, R. (2007). Influence of Aluminum Substitution on the Reactivity of Magnetite Nanoparticles. *Physical Chemistry C*, 111, 10247-10253.
- Ji, F., Li, C., Zhang, J., & Deng, L. (2011). Heterogeneous photo-Fenton decolorization of methylene blue over  $\text{LiFe}(\text{WO}_4)_2$  catalyst. *Journal of Hazardous Materials*, 186(2-3), 1979-1984.
- Jiang, J., Bank, J. F., & Scholes, C. (1993). Subsecond time-resolved spin trapping followed by stopped-flow EPR of Fenton reaction products. *Journal of the American Chemical Society*, 115(11), 4742-4746.
- Jordá, L. S.-J., Martín, M. M. B., Gómez, E. O., Reina, A. C., Sánchez, I. M. R., López, J. L. C., & Pérez, J. A. S. (2011). Economic evaluation of the photo-Fenton process. Mineralization level and reaction time: The keys for increasing plant efficiency. *Journal of Hazardous Materials*, 186(2-3), 1924-1929.
- Kavitha, V. & Palanivelu, K. (2004). The role of ferrous ion in Fenton and photo-Fenton processes for the degradation of phenol. *Chemosphere*, 55, 1235-1243.
- Kang, Y. W., & Hwang, K.-Y. (2000). Effects of reaction conditions on the oxidation efficiency in the Fenton process. *Water Research*, 34(10), 2786-2790.
- Karaolia, P., Michael, I., García-Fernández, I., Agüera, A., Malato, S., Fernández-Ibáñez, P., & Fatta-Kassinos, D. (2014). Reduction of clarithromycin and sulfamethoxazole-resistant *Enterococcus* by pilot-scale solar-driven Fenton oxidation. *Science of The Total Environment*, 468-469(0), 19-27.
- Katsumata, H., Kaneco, S., Suzuki, T., Ohta, K., & Yobiko, Y. (2005). Degradation of linuron in aqueous solution by the photo-Fenton reaction. *Chemical Engineering Journal*, 108(3), 269-276.
- Khataee, A. R., Zarei, M., & Moradkhannejhad, L. (2010). Application of response surface methodology for optimization of azo dye removal by oxalate catalyzed photoelectro-Fenton process using carbon nanotube-PTFE cathode. *Desalination*, 258(1-3), 112-119.
- Kim, S. M., & Vogelpohl, A. (1998). Degradation of organic pollutants by the photo-Fenton process. *Chemical Engineering & Technology*, 21(2), 187-191.
- Klamerth, N., Malato, S., Agüera, A., & Fernández-Alba, A. (2013). Photo-Fenton and modified photo-Fenton at neutral pH for the treatment of emerging contaminants

in wastewater treatment plant effluents: A comparison. *Water Research*, 47(2), 833-840.

- Klamerth, N., Miranda, N., Malato, S., Agüera, A., & FernándezAlba, A. R. (2009). Degradation of emerging contaminants at low concentrations in MWTPs effluents with mild solar photoFenton and TiO<sub>2</sub>. *Catalysis Today*, 144, 124–130.
- Klamerth, N., Rizzo, L., Malato, S., Maldonado, M. I., Agüera, A., & Fernández-Alba, A. R. (2010). Degradation of fifteen emerging contaminants at  $\mu\text{g L}^{-1}$  initial concentrations by mild solar photo-Fenton in MWTP effluents. *Water Research*, 44(2), 545-554.
- Klas, S., Dubowski, Y., Pritosiwi, G., Gerth, J., Calmano, W., & Lahav, O. (2011). Extent and mechanism of metal ion incorporation into precipitated ferrites. *Journal of Colloid and Interface Science*, 358(1), 129-135.
- Klavarioti, M., Mantzavinos, D., & Kassinos, D. (2009). Removal of residual pharmaceuticals from aqueous systems by advanced oxidation processes. *Environment International*, 35(2), 402-417.
- Klemenčič, A. K., Balabanič, D., Kompare, B., Krzyk, M., Panjan, J., Bulc, T. G., . . . Holobar, A. (2012 27 May - 2 June ). *Recycling of AOP-Treated Effluents for Reduction of Fresh Water Consumption in Textile and other High Water Volume Consuming Industries*. Paper presented at the BALWOIS, Ohrid, Republic of Macedonia.
- Knapp, J. S., & Bromley-Challoner, K. C. A. (2003). 34 - Recalcitrant organic compounds *Handbook of Water and Wastewater Microbiology* (pp. 559-595). London: Academic Press.
- Kneisel, P., Ciovati, G., Dhakal, P., Saito, K., Singer, W., Singer, X., & Myneni, G. R. (2015). Review of ingot niobium as a material for superconducting radiofrequency accelerating cavities. *Nuclear Instruments and Methods in Physics Research Section A: Accelerators, Spectrometers, Detectors and Associated Equipment*, 774, 133-150.
- Kremer, M. L., & Stein, G. (1959). The catalytic decomposition of hydrogen peroxide by ferric perchlorate. *Transactions of the Faraday Society*, 55(0), 959-973. doi:10.1039/TF9595500959
- Kwan, W. P., & Voelker, B. M. (2003). Rates of Hydroxyl Radical Generation and Organic Compound Oxidation in Mineral-Catalyzed Fenton-like Systems. *Environmental Science & Technology*, 37(6), 1150-1158.
- Lan, Q., Li, F.-b., Sun, C.-x., Liu, C.-s., & Li, X.-z. (2010). Heterogeneous photodegradation of pentachlorophenol and iron cycling with goethite, hematite and oxalate under UVA illumination. *Journal of Hazardous Materials*, 174(1-3), 64-70.

- Lee, C. S., & Joe, Y. H. (2010). Structural and Magnetic Properties of Cu-Substituted Magnetite Studied by Using Mössbauer Spectroscopy. *Journal of the Korean Physical Society*, 56(1), 85-88.
- Lee, H. J., Kim, G., Kim, D. H., Kang, J.-S., Zhang, C. L., Cheong, S.-W., . . . Min, B. I. (2008). Valence states and occupation sites in (Fe,Mn)<sub>3</sub>O<sub>4</sub> spinel oxides investigated by soft x-ray absorption spectroscopy and magnetic circular dichroism. *Journal of Physics: Condensed Matter*, 20.
- Lelis, M. F. F., Porto, A. O., Gonçalves, C. M., & Fabris, J. D. (2004). Cation occupancy sites in synthetic Co-doped magnetites as determined with X-ray absorption (XAS) and Mössbauer spectroscopies. *Journal of Magnetism and Magnetic Materials*, 278(1-2), 263-269.
- Leong, T., Ashokkumar, M., & Kentish, S. (2011). The fundamentals of power ultrasound – a review. *Acoustics Australia*, 39( 2).
- Liang, X., He, Z., Zhong, Y., Tan, W., He, H., Yuan, P., . . . Zhang, J. (2013). The effect of transition metal substitution on the catalytic activity of magnetite in heterogeneous Fenton reaction: In interfacial view. *Colloids and Surfaces A: Physicochemical and Engineering Aspects*(0).
- Liang, X., Zhong, Y., He, H., Yuan, P., Zhu, J., Zhu, S., & Jiang, Z. (2012). The application of chromium substituted magnetite as heterogeneous Fenton catalyst for the degradation of aqueous cationic and anionic dyes. *Chemical Engineering Journal*, 191(0), 177-184.
- Liang, X., Zhong, Y., Zhu, S., He, H., Yuan, P., Zhu, J., & Jiang, Z. (2013). The valence and site occupancy of substituting metals in magnetite spinel structure Fe<sub>3-x</sub>M<sub>x</sub>O<sub>4</sub> (M = Cr, Mn, Co and Ni) and their influence on thermal stability: An XANES and TG-DSC investigation. *Solid State Sciences*, 15(0), 115-122.
- Liang, X., Zhong, Y., Zhu, S., Ma, L., Yuan, P., Zhu, J., . . . Jiang, Z. (2012). The contribution of vanadium and titanium on improving methylene blue decolorization through heterogeneous UV-Fenton reaction catalyzed by their co-doped magnetite. *Journal of Hazardous Materials*, 199-200(0), 247-254.
- Liang, X., Zhu, S., Zhong, Y., Zhu, J., Yuan, P., He, H., & Zhang, J. (2010). The remarkable effect of vanadium doping on the adsorption and catalytic activity of magnetite in the decolorization of methylene blue. *Applied Catalysis B: Environmental*, 97(1-2), 151-159.
- Lin, S.-S., & Gurol, M. D. (1998). Catalytic Decomposition of Hydrogen Peroxide on Iron Oxide: Kinetics, Mechanism, and Implications. *Environmental Science & Technology*, 32(10), 1417-1423.
- Litter, M. I., & Blesa, M. A. (1992). Photodissolution of iron oxides. IV. A comparative study on the photodissolution of hematite, magnetite, and maghemite in EDTA media. *Canadian Journal of Chemistry*, 70, 2502-2510.

- Liu, T., You, H., & Chen, Q. (2009). Heterogeneous photo-Fenton degradation of polyacrylamide in aqueous solution over Fe(III)–SiO<sub>2</sub> catalyst. *Journal of Hazardous Materials*, 162(2–3), 860-865.
- Luna, A. J., Chiavone-Filho, O., Machulek Jr, A., de Moraes, J. E. F., & Nascimento, C. A. O. (2012). Photo-Fenton oxidation of phenol and organochlorides (2,4-DCP and 2,4-D) in aqueous alkaline medium with high chloride concentration. *Journal of Environmental Management*, 111(0), 10-17.
- Magalhães, F., Pereira, M. C., Botrel, S. E. C., Fabris, J. D., Macedo, W. A., Mendonca, R., . . . Oliveira, L. C. A. (2007). Cr-containing magnetites Fe<sub>3-x</sub>Cr<sub>x</sub>O<sub>4</sub>: The role of Cr<sup>3+</sup> and Fe<sup>2+</sup> on the stability and reactivity towards H<sub>2</sub>O<sub>2</sub> reactions. *Applied Catalysis A: General*, 332(1), 115-123.
- Malato, S., Fernández-Ibáñez, P., Maldonado, M. I., Blanco, J., & Gernjak, W. (2009). Decontamination and disinfection of water by solar photocatalysis: Recent overview and trends. *Catalysis Today*, 147(1), 1-59.
- Maldonado, M. I., Passarinho, P. C., Oller, I., Gernjak, W., Fernández, P., Blanco, J., & Malato, S. (2007). Photocatalytic degradation of EU priority substances: A comparison between TiO<sub>2</sub> and Fenton plus photo-Fenton in a solar pilot plant. *Journal of Photochemistry and Photobiology A: Chemistry*, 185(2–3), 354-363.
- Matta, R., Hanna, K., Kone, T., & Chiron, S. (2008). Oxidation of 2,4,6-trinitrotoluene in the presence of different iron-bearing minerals at neutral pH. *Chemical Engineering Journal*, 144(3), 453-458.
- Maximova, N. (2008). Application of the x-ray photoelectron spectroscopy for development of the niobium chemical mechanical process, photomodification of silicon for the field release mass spectrometer, and analysis of the multifunctional oxide heterostructures. (Master), Northeastern University.
- Meeker, R. E. (1965). US Patent No. 3,168,097 2, US Patent.
- Méndez-Arriaga, F., Esplugas, S., & Giménez, J. (2010). Degradation of the emerging contaminant ibuprofen in water by photo-Fenton. *Water Research*, 44(2), 589-595.
- Michael, I., Hapeshi, E., Michael, C., Varela, A. R., Kyriakou, S., Manaia, C. M., & Fatta-Kassinos, D. (2012). Solar photo-Fenton process on the abatement of antibiotics at a pilot scale: Degradation kinetics, ecotoxicity and phytotoxicity assessment and removal of antibiotic resistant enterococci. *Water Research*, 46(17), 5621-5634.
- Micó, M. M., Bacardit, J., Malfeito, J., & Sans, C. (2013). Enhancement of pesticide photo-Fenton oxidation at high salinities. *Applied Catalysis B: Environmental*, 132–133(0), 162-169.
- Miró, P., Arques, A., Amat, A. M., Marin, M. L., & Miranda, M. A. (2013). A mechanistic study on the oxidative photodegradation of 2,6-dichlorodiphenylamine-derived drugs: Photo-Fenton versus photocatalysis with



- a triphenylpyrylium salt. *Applied Catalysis B: Environmental*, 140–141(0), 412-418.
- Mitsika, E. E., Christophoridis, C., & Fytianos, K. (2013). Fenton and Fenton-like oxidation of pesticide acetamiprid in water samples: Kinetic study of the degradation and optimization using response surface methodology. *Chemosphere*, 93(9), 1818-1825.
- Módenes, A. N., Espinoza-Quiñones, F. R., Borba, F. H., & Manenti, D. R. (2012). Performance evaluation of an integrated photo-Fenton – Electrocoagulation process applied to pollutant removal from tannery effluent in batch system. *Chemical Engineering Journal*, 197, 1-9.
- Molina, R., Segura, Y., Martínez, F., & Melero, J. A. (2012). Immobilization of active and stable goethite coated-films by a dip-coating process and its application for photo-Fenton systems. *Chemical Engineering Journal*, 203(0), 212-222.
- Monteagudo, J. M., Durán, A., Aguirre, M., & San Martín, I. (2011). Optimization of the mineralization of a mixture of phenolic pollutants under a ferrioxalate-induced solar photo-Fenton process. *Journal of Hazardous Materials*, 185(1), 131-139.
- Monteagudo, J. M., Durán, A., Culebradas, R., San Martín, I., & Carnicer, A. (2013). Optimization of pharmaceutical wastewater treatment by solar/ferrioxalate photo-catalysis. *Journal of Environmental Management*, 128(0), 210-219.
- Monteagudo, J. M., Durán, A., Martín, I. S., & Aguirre, M. (2010). Effect of light source on the catalytic degradation of protocatechuic acid in a ferrioxalate-assisted photo-Fenton process. *Applied Catalysis B: Environmental*, 96(3–4), 486-495.
- Moura, F. C. C., Araujo, M. H., Costa, R. C. C., Fabris, J. D., Ardisson, J. D., Macedo, W. A. A., & Lago, R. M. (2005). Efficient use of Fe metal as an electron transfer agent in a heterogeneous Fenton system based on Fe<sup>0</sup>/Fe<sub>3</sub>O<sub>4</sub> composites. *Chemosphere*, 60(8), 1118-1123.
- Mulazzani, Q. G., D'Angelantonio, M., Venturi, M., Hoffman, M. Z., & Rodgers, M. A. J. (1986). Interaction of formate and oxalate ions with radiation-generated radicals in aqueous solution. Methylviologen as a mechanistic probe. *Journal of Physical Chemistry A*, 90, 5347-.
- Munoz, M., de Pedro, Z. M., Casas, J. A., & Rodriguez, J. J. (2015). Preparation of magnetite-based catalysts and their application in heterogeneous Fenton oxidation – A review. *Applied Catalysis B: Environmental*, 176–177(0), 249-265.
- Muthukumari, B., Selvam, K., Muthuvel, I., & Swaminathan, M. (2009). Photoassisted hetero-Fenton mineralisation of azo dyes by Fe(II)–Al<sub>2</sub>O<sub>3</sub> catalyst. *Chemical Engineering Journal*, 153, 9–15.

- Navalon, S., Alvaro, M., & Garcia, H. (2010). Heterogeneous Fenton catalysts based on clays, silicas and zeolites. *Applied Catalysis B: Environmental*, 99(1–2), 1-26.
- Neyens, E., & Baeyens, J. (2003). A review of classic Fenton's peroxidation as an advanced oxidation technique. *J Hazard Mater*, 98(1–3), 33-50.
- Nguyen, T. D., Phan, N. H., Do, M. H., & Ngo, K. T. (2011). Magnetic Fe<sub>2</sub>MO<sub>4</sub> (M:Fe, Mn) activated carbons: Fabrication, characterization and heterogeneous Fenton oxidation of methyl orange. *Journal of Hazardous Materials*, 185(2-3), 653-661.
- Nichela, D. A., Berkovic, A. M., Costante, M. R., Juliarena, M. P., & García Einschlag, F. S. (2013). Nitrobenzene degradation in Fenton-like systems using Cu(II) as catalyst. Comparison between Cu(II)- and Fe(III)-based systems. *Chemical Engineering Journal*, 228(0), 1148-1157.
- Nitoi, I., Oncescu, T., & Oancea, P. (2013). Mechanism and kinetic study for the degradation of lindane by photo-Fenton process. *Journal of Industrial and Engineering Chemistry*, 19(1), 305-309.
- Nogueira, K. R. B., Teixeira, A. C. S. C., Nascimento, C. A. O., & Guardani, R. (2008). Use of solar energy in the treatment of water contaminated with phenol by photochemical processes. *Brazilian Journal of Chemical Engineering* 25(04), 671 - 682.
- Nogueira, R. F. P., Silva, M. R. A., & Trovó, A. G. (2005). Influence of the iron source on the solar photo-Fenton degradation of different classes of organic compounds. *Solar Energy*, 79(4), 384-392.
- Ok, H. N., Pan, L. S., & Evans, B. J. (1978). Fe-57 Mossbauer study of chromium-doped magnetite, Fe<sub>3-x</sub>Cr<sub>x</sub>O<sub>4</sub> (0 ≤ x ≤ 0.5) above Verwey transition. *Physical review. B, Condensed matter*, 17, 85–90.
- Oliveira, L. C. A., Gonçalves, M., Guerreiro, M. C., Ramalho, T. C., Fabris, J. D., Pereira, M. C., & Sapag, K. (2007). A new catalyst material based on niobia/iron oxide composite on the oxidation of organic contaminants in water via heterogeneous Fenton mechanisms. *Applied Catalysis A: General*, 316(1), 117-124.
- Oliveira, L. C. A., Lago, R. M., Rios, R. V. R. A., Augusti, R., Sousa, P. P., Mussel, W. N., & Fabris, J. D. (2000). The effect of Mn substitution on the catalytic properties of ferrites. In F. V. M. S. M. Avelino Corma & G. F. José Luis (Eds.), *Studies in Surface Science and Catalysis* (Vol. 130, pp. 2165-2170): Elsevier.
- Oliveira, L. C. A., Ramalho, T. C., Souza, E. F., Gonçalves, M., Oliveira, D. Q. L., Pereira, M. C., & Fabris, J. D. (2008). Catalytic properties of goethite prepared in the presence of Nb on oxidation reactions in water: Computational and experimental studies. *Applied Catalysis B: Environmental*, 83(3–4), 169-176.
- Ortega-Gómez, E., Esteban García, B., Ballesteros Martín, M. M., Fernández Ibáñez, P., & Sánchez Pérez, J. A. (2013). Inactivation of *Enterococcus faecalis* in

simulated wastewater treatment plant effluent by solar photo-Fenton at initial neutral pH. *Catalysis Today*, 209(0), 195-200.

- Ortega-Liévana, M. C., Sánchez-López, E., Hidalgo-Carrillo, J., Marinas, A., Marinas, J. M., & Urbano, F. J. (2012). A comparative study of photocatalytic degradation of 3-chloropyridine under UV and solar light by homogeneous (photo-Fenton) and heterogeneous (TiO<sub>2</sub>) photocatalysis. *Applied Catalysis B: Environmental*, 127(0), 316-322.
- Ortiz de la Plata, G. B., Alfano, O. M., & Cassano, A. E. (2008). Optical properties of goethite catalyst for heterogeneous photo-Fenton reactions: Comparison with a titanium dioxide catalyst. *Chemical Engineering Journal*, 137(2), 396-410.
- Panias, D., Taxiarchou, M., Paspaliaris, I., & Kontopoulos, A. (1996). Mechanisms of dissolution of iron oxides in aqueous oxalic acid solutions. *Hydrometallurgy*, 42(2), 257-265.
- Paparazzo, E. (2006). On the quantitative XPS analysis of Fe<sub>2</sub>O<sub>3</sub> and Fe<sub>1-x</sub>O oxides. *Journal of Electron Spectroscopy and Related Phenomena*, 154(1-2), 38-40.
- Pariante, M. I., Martínez, F., Melero, J. A., Botas, J. Í., Velegraki, T., Xekoukoulotakis, N. P., & Mantzavinos, D. (2008). Heterogeneous photo-Fenton oxidation of benzoic acid in water: Effect of operating conditions, reaction by-products and coupling with biological treatment. *Applied Catalysis B: Environmental*, 85(1-2), 24-32.
- Pearce, C. I., Henderson, C. M. B., Telling, N. D., Patrick, R. A. D., Charnock, J. M., Coker, V. S., . . . van der Laan, G. (2015). Fe site occupancy in magnetite-ulvöspinel solid solutions: A new approach using X-ray magnetic circular dichroism. *American Mineralogist*, 95(4), 425-439. doi:10.2138/am.2010.3343
- Pignatello, J. J. (1992). Dark and photoassisted Fe<sup>3+</sup>-catalyzed degradation of chlorophenoxy herbicides by hydrogen peroxide. *Environmental Science & Technology*, 26(5), 944-951.
- Pignatello, J. J., Oliveros, E., & MacKay, A. (2006). Advanced Oxidation Processes for Organic Contaminant Destruction Based on the Fenton Reaction and Related Chemistry. *Critical Reviews in Environmental Science and Technology*, 36(1), 1-84.
- Platanitis, P., Panagiotou, G. D., Bourikas, K., Kordulis, C., Fierro, J. L. G., & Lycourghiotis, A. (2016). Preparation of un-promoted molybdenum HDS catalysts supported on titania by equilibrium deposition filtration: Optimization of the preparative parameters and investigation of the promoting action of titania. *Journal of Molecular Catalysis A: Chemical*, 412, 1-12.
- Polo-López, M. I., García-Fernández, I., Velegraki, T., Katsoni, A., Oller, I., Mantzavinos, D., & Fernández-Ibáñez, P. (2012). Mild solar photo-Fenton: An effective tool for the removal of Fusarium from simulated municipal effluents. *Applied Catalysis B: Environmental*, 111-112(0), 545-554.

- Prieto-Rodríguez, L., Oller, I., Zapata, A., Agüera, A., & Malato, S. (2011). Hydrogen peroxide automatic dosing based on dissolved oxygen concentration during solar photo-Fenton. *Catalysis Today*, 161(1), 247-254.
- Primo, O., Rivero, M. J., & Ortiz, I. (2008). Photo-Fenton process as an efficient alternative to the treatment of landfill leachates. *Journal of Hazardous Materials*, 153(1-2), 834-842.
- Punzi, M., Mattiasson, B., & Jonstrup, M. (2012). Treatment of synthetic textile wastewater by homogeneous and heterogeneous photo-Fenton oxidation. *Journal of Photochemistry and Photobiology A: Chemistry*, 248(0), 30-35.
- Ramalho, T., Oliveira, L., Carvalho, K., Souza, E., da Cunha, E., & Nazzaro, M. (2009). The molecular basis for the behaviour of niobia species in oxidation reaction probed by theoretical calculations and experimental techniques. *Molecular Physics*, 107(2), 171-179.
- Ramankutty, C. G., & Sugunan, S. (2001a). Surface properties and catalytic activity of ferrosinels of nickel, cobalt and copper, prepared by soft chemical methods. *Applied Catalysis A: General*, 218(1-2), 39-51.
- Ramankutty, C. G., & Sugunan, S. (2001b). Surface properties and catalytic activity of ferrosinels of nickel, cobalt and copper, prepared by soft chemical methods. *Applied Catalysis A: General*, 218(1-2), 39-51.
- Ramankutty, C. G., Sugunan, S., & Thomas, B. (2002). Study of cyclohexanol decomposition reaction over the ferrosinels,  $A_{1-x}C_xFe_2O_4$  (A=Ni or Co and  $x=0, 0.3, 0.5, 0.7$  and 1), prepared by 'soft' chemical methods. *Journal of Molecular Catalysis A: Chemical*, 187(1), 105-117.
- Ravina, M., Campanella, L., & Kiwi, J. (2002). Accelerated mineralization of the drug Diclofenac via Fenton reactions in a concentric photo-reactor. *water research*, 36, 3553-3560.
- Robbins, M., Wertheim, G. K., Sherwood, R. C., & Buchanan, D. N. E. (1971). Magnetic properties and site distributions in the system  $FeCr_2O_4-Fe_3O_4(Fe^{2+}Cr_{2-x}Fe_x^{3+}O_4)$ . *Journal of Physics and Chemistry of Solids*, 32(3), 717-729.
- Rodríguez, E., Fernández, G., Ledesma, B., Álvarez, P., & Beltrán, F. J. (2009). Photocatalytic degradation of organics in water in the presence of iron oxides: Influence of carboxylic acids. *Applied Catalysis B: Environmental*, 92(3-4), 240-249.
- Rodríguez, E. M., Núñez, B., Fernández, G., & Beltrán, F. J. (2009). Effects of some carboxylic acids on the Fe(III)/UVA photocatalytic oxidation of muconic acid in water. *Applied Catalysis B: Environmental*, 89(1-2), 214-222.
- Rusevova, K., Kopinke, F.-D., & Georgi, A. (2012). Nano-sized magnetic iron oxides as catalysts for heterogeneous Fenton-like reactions - influence of Fe(II)/Fe(III) ratio on catalytic performance. *Journal of Hazardous Materials*(0).

- Saghafinia, M. S., Emadian, S. M., & Vossoughi, M. (2011). Performances Evaluation of Photo-Fenton Process and Sonolysis for the Treatment of Penicillin G Formulation Effluent. *Procedia Environmental Sciences*, 8(0), 202-208.
- Santos-Juanes, L., Sánchez, J. L. G., López, J. L. C., Oller, I., Malato, S., & Sánchez Pérez, J. A. (2011). Dissolved oxygen concentration: A key parameter in monitoring the photo-Fenton process. *Applied Catalysis B: Environmental*, 104(3-4), 316-323.
- Shafeeyan, M. S., Wan Daud, W. M. A., Houshmand, A., & Arami-Niya, A. (2012). The application of response surface methodology to optimize the amination of activated carbon for the preparation of carbon dioxide adsorbents. *Fuel*, 94(0), 465-472.
- Shemer, H., Kaçar Kunukcu, Y., & Linden, K. G. (2006). Degradation of the pharmaceutical Metronidazole via UV, Fenton and photo-Fenton processes. *Chemosphere*, 63 (2), 269-276.
- Shukla, P., Wang, S., Sun, H., Ang, H.-M., & Tadé, M. (2010). Adsorption and heterogeneous advanced oxidation of phenolic contaminants using Fe loaded mesoporous SBA-15 and H<sub>2</sub>O<sub>2</sub>. *Chemical Engineering Journal*, 164, 255-260.
- Silva, A. C., Cepera, R. M., Pereira, M. C., Lima, D. Q., Fabris, J. D., & Oliveira, L. C. A. (2011). Heterogeneous catalyst based on peroxo-niobium complexes immobilized over iron oxide for organic oxidation in water. *Applied Catalysis B: Environmental*, 107(3-4), 237-244.
- Silva, A. C., Oliveira, D. Q. L., Oliveira, L. C. A., Anastácio, A. S., Ramalho, T. C., Lopes, J. H., . . . Torres, C. E. R. (2009). Nb-containing hematites Fe<sub>2-x</sub>Nb<sub>x</sub>O<sub>3</sub>: The role of Nb<sup>5+</sup> on the reactivity in presence of the H<sub>2</sub>O<sub>2</sub> or ultraviolet light. *Applied Catalysis A: General*, 357(1), 79-84.
- Silva, A. M. T., Zilhão, N. R., Segundo, R. A., Azenha, M., Fidalgo, F., Silva, A. F., . . . Teixeira, J. (2012). Photo-Fenton plus Solanum nigrum L. weed plants integrated process for the abatement of highly concentrated metalaxyl on waste waters. *Chemical Engineering Journal*, 184(0), 213-220.
- Simunovic, M., Kusic, H., Koprivanac, N., & Bozic, A. L. (2011). Treatment of simulated industrial wastewater by photo-Fenton process: Part II. The development of mechanistic model. *Chemical Engineering Journal*, 173(2), 280-289.
- Sirtori, C., Zapata, A., Gernjak, W., Malato, S., Lopez, A., & Agüera, A. (2011). Solar photo-Fenton degradation of nalidixic acid in waters and wastewaters of different composition. Analytical assessment by LC-TOF-MS. *Water Research*, 45(4), 1736-1744.
- Sirtori, C., Zapata, A., Oller, I., Gernjak, W., Agüera, A., & Malato, S. (2009). Decontamination industrial pharmaceutical wastewater by combining solar photo-Fenton and biological treatment. *Water Research*, 43(3), 661-668.

- Stevens, L., Williams, K., Han, W. Y., Drage, T., Snape, C., Wood, J., & Wang, J. (2013). Preparation and CO<sub>2</sub> adsorption of diamine modified montmorillonite via exfoliation grafting route. *Chemical Engineering Journal*, 215–216(0), 699–708.
- Stoner, E. C., & Wohlfarth, E. P. (1948). A Mechanism of Magnetic Hysteresis in Heterogeneous Alloys.
- Sugimoto, T., & Matijević, E. (1980). Formation of uniform spherical magnetite particles by crystallization from ferrous hydroxide gels. *Journal of Colloid and Interface Science*, 74(1), 227–243.
- Sun, J.-H., Sun, S.-P., Fan, M.-H., Guo, H.-Q., Lee, Y.-F., & Sun, R.-X. (2008). Oxidative decomposition of p-nitroaniline in water by solar photo-Fenton advanced oxidation process. *Journal of Hazardous Materials*, 153, 187–193.
- Sun, S.-P., Zeng, X., & Lemley, A. T. (2013). Nano-magnetite catalyzed heterogeneous Fenton-like degradation of emerging contaminants carbamazepine and ibuprofen in aqueous suspensions and montmorillonite clay slurries at neutral pH. *Journal of Molecular Catalysis A: Chemical*, 371(0), 94–103.
- Sun, S.-P., Zeng, X., Li, C., & Lemley, A. T. (2014). Enhanced heterogeneous and homogeneous Fenton-like degradation of carbamazepine by nano-Fe<sub>3</sub>O<sub>4</sub>/H<sub>2</sub>O<sub>2</sub> with nitrilotriacetic acid. *Chemical Engineering Journal*, 244(0), 44–49.
- Sun, Z.-X., Su, F.-W., Forsling, W., & Samskog, P.-O. (1998). Surface Characteristics of Magnetite in Aqueous Suspension. *Journal of Colloid and Interface Science*, 197(1), 151–159.
- Suslick, K. S., Didenko, Y., Fang, M. M., Hyeon, T., Kolbeck, K. J., McNamara, W. B., . . . Wong, M. (1999). Acoustic cavitation and its chemical consequences. *Philosophical Transactions of the Royal Society A: Mathematical, Physical and Engineering Sciences*, 357, 335–353.
- Tamimi, M., Qourzal, S., Barka, N., Assabbane, A., & Ait-Ichou, Y. (2008). Methomyl degradation in aqueous solutions by Fenton's reagent and the photo-Fenton system. *Separation and Purification Technology*, 61(1), 103–108.
- Tang, W. Z., & Huang, C. P. (1996). 2,4-dichlorophenol oxidation kinetics by Fenton's reagent. *Environmental Technology*, 17(12), 1371–1378.
- Teixeira, A. C. S. C., Mendes, L., Stollar, G., Guardani, R., & Nascimento, C. A. O. d. (2005). Photo-fenton remediation of wastewaters containing agrochemicals. *Brazilian Archives of Biology and Technology*, 48, 207–218.
- Tolman, C. A., & Barton, D. H. R. (1993). *The Activation of Dioxygen and Homogeneous Catalytic Oxidation*. Plenum Press, New York: Springer US.

- Trovo', A. G., Pupo Nogueira, R. F., Agu'era, A., Fernandez-Alba, A. R., & Malato, S. (2011). Degradation of the antibiotic amoxicillin by photo-Fenton process - Chemical and toxicological assessment. *Water Research*, 45(3), 1394-1402.
- Usman, M., Faure, P., Hanna, K., Abdelmoula, M., & Ruby, C. (2012a). Application of magnetite catalyzed chemical oxidation (Fenton-like and persulfate) for the remediation of oil hydrocarbon contamination. *Fuel*, 96(0), 270-276.
- Usman, M., Faure, P., Ruby, C., & Hanna, K. (2012b). Remediation of PAH-contaminated soils by magnetite catalyzed Fenton-like oxidation. *Applied Catalysis B: Environmental*, 117-118(0), 10-17.
- Vargas, A. M. M., Cazetta, A. L., Kunita, M. H., Silva, T. L., & Almeida, V. C. (2011). Adsorption of methylene blue on activated carbon produced from flamboyant pods (*Delonix regia*): Study of adsorption isotherms and kinetic models. *Chemical Engineering Journal*, 168(2), 722-730.
- Vilar, V. J. P., Moreira, F. C., Ferreira, A. C. C., Sousa, M. A., Gonçalves, C., Alpendurada, M. F., & Boaventura, R. A. R. (2012). Biodegradability enhancement of a pesticide-containing bio-treated wastewater using a solar photo-Fenton treatment step followed by a biological oxidation process. *Water Research*, 46(15), 4599-4613.
- Walling, C. (1975). Fenton's reagent revisited. *Accounts of Chemical Research*, , 8(4), 125-131.
- Wang, J. L., & Xu, L. J. (2011). Advanced Oxidation Processes for Wastewater Treatment: Formation of Hydroxyl Radical and Application. *Critical Reviews in Environmental Science and Technology*, 42(3), 251-325.
- Wang, X., Liu, C., Li, X., Li, F., & Zhou, S. (2008). Photodegradation of 2-mercaptobenzothiazole in the  $\gamma$ -Fe<sub>2</sub>O<sub>3</sub>/oxalate suspension under UVA light irradiation. *Journal of Hazardous Materials*, 153(1-2), 426-433.
- Wang, Y., Liang, J. B., Liao, X. D., Wang, L.-s., Loh, T. C., Dai, J., & Ho, Y. W. (2010). Photodegradation of Sulfadiazine by Goethite-Oxalate Suspension under UV Light Irradiation. *Industrial & Engineering Chemistry Research*, 49, 3527-3532.
- Watts, R., & Teel, A. (2006). Treatment of Contaminated Soils and Groundwater Using ISCO. *Practice Periodical of Hazardous, Toxic, and Radioactive Waste Management*, 10(1), 2-9.
- Wei, G., Liang, X., He, Z., Liao, Y., Xie, Z., Liu, P., . . . Zhang, J. (2015). Heterogeneous activation of Oxone by substituted magnetites Fe<sub>3-x</sub>M<sub>x</sub>O<sub>4</sub> (Cr, Mn, Co, Ni) for degradation of Acid Orange II at neutral pH. *Journal of Molecular Catalysis A: Chemical*, 398(0), 86-94.
- Wenk, J., von Gunten, U., & Canonica, S. (2011). Effect of Dissolved Organic Matter on the Transformation of Contaminants Induced by Excited Triplet States and the Hydroxyl Radical. *Environmental Science & Technology*, 45, 1334-1340.

- Xavier, S., Gandhimathi, R., Nidheesh, P. V., & Ramesh, S. T. (2013). Comparison of homogeneous and heterogeneous Fenton processes for the removal of reactive dye Magenta MB from aqueous solution. *Desalination and Water Treatment*, 1-10.
- Xia, M., Chen, C., Long, M., Chen, C., Cai, W., & Zhou, B. (2011). Magnetically separable mesoporous silica nanocomposite and its application in Fenton catalysis. *Microporous and Mesoporous Materials*, 145(1-3), 217-223.
- Xing, M.-y., Deng, C., Godefroid, B., & Jian. (2006). Treatment of pharmaceutical wastewater containing recalcitrant compounds in a Fenton-coagulation process *Journal of Environmental Sciences*, 18(3), 459-463.
- Xue, X., Hanna, K., & Deng, N. (2009a). Fenton-like oxidation of Rhodamine B in the presence of two types of iron (II, III) oxide. *Journal of Hazardous Materials*, 166(1), 407-414.
- Xue, X., Hanna, K., Despas, C., Wu, F., & Deng, N. (2009b). Effect of chelating agent on the oxidation rate of PCP in the magnetite/H<sub>2</sub>O<sub>2</sub> system at neutral pH. *Journal of Molecular Catalysis A: Chemical*, 311(1-2), 29-35.
- Yamashita, T., & Hayes, P. (2008). Analysis of XPS spectra of Fe<sup>2+</sup> and Fe<sup>3+</sup> ions in oxide materials. *Applied Surface Science*, 254(8), 2441-2449.
- Yang, B., Tian, Z., Zhang, L., Guo, Y., & Yan, S. (2015). Enhanced heterogeneous Fenton degradation of Methylene Blue by nanoscale zero valent iron (nZVI) assembled on magnetic Fe<sub>3</sub>O<sub>4</sub>/reduced graphene oxide. *Journal of Water Process Engineering*, 5(0), 101-111.
- Yang, S., He, H., Wu, D., Chen, D., Liang, X., Qin, Z., . . . Yuan, P. (2009). Decolorization of methylene blue by heterogeneous Fenton reaction using Fe<sub>3-x</sub>Ti<sub>x</sub>O<sub>4</sub> (0 ≤ x ≤ 0.78) at neutral pH values. *Applied Catalysis B: Environmental*, 89(3-4), 527-535.
- Yang, S., He, H., Wu, D., Chen, D., Ma, Y., Li, X., . . . Yuan, P. (2009). Degradation of Methylene Blue by Heterogeneous Fenton Reaction Using Titanomagnetite at Neutral pH Values: Process and Affecting Factors. *Industrial & Engineering Chemistry Research*, 48, 9915–9921.
- Yeh, C. K.-J., Hsu, C.-Y., Chiu, C.-H., & Huang, K.-L. (2008). Reaction efficiencies and rate constants for the goethite-catalyzed Fenton-like reaction of NAPL-form aromatic hydrocarbons and chloroethylenes. *Journal of Hazardous Materials*, 151(2–3), 562-569.
- Yip, A. C. K., Lam, F. L. Y., & Hu, X. (2005). Chemical-vapor-deposited of copper on acidactivated bentonite clay as an applicable heterogeneous catalyst for the photo Fenton-like oxidation of textile organic pollutants. *Industrial & Engineering Chemistry Research*, 44, 7983–7990.



- Yuan, B., Li, X., Li, K., & Chen, W. (2011). Degradation of dimethyl phthalate (DMP) in aqueous solution by UV/Si-FeOOH/H<sub>2</sub>O<sub>2</sub>. *Colloids and Surfaces A: Physicochemical and Engineering Aspects*, 379, 157-162.
- Zapata, A., Oller, I., Rizzo, L., Hilgert, S., Maldonado, M. I., Sánchez-Pérez, J. A., & Malato, S. (2010). Evaluation of operating parameters involved in solar photo-Fenton treatment of wastewater: Interdependence of initial pollutant concentration, temperature and iron concentration. *Applied Catalysis B: Environmental*, 97(1-2), 292-298.
- Zaror, C., Segura, C., Mansilla, H., Mondaca, M., & González, P. (2008). Effect of temperature on Imidacloprid oxidation by homogeneous photo-Fenton processes. *Water Science and Technology*, 58(1), 259-265.
- Zhang, Y., & Pagilla, K. (2010). Treatment of malathion pesticide wastewater with nanofiltration and photo-Fenton oxidation. *Desalination*, 263(1-3), 36-44.
- Zhang, Y., Yang, M., Dou, X.-M., He, H., & Wang, D.-S. (2005). Arsenate Adsorption on an Fe-Ce Bimetal Oxide Adsorbent: Role of Surface Properties. *Environmental Science & Technology*, 39(18), 7246-7253.
- Zhao, X.-K., Yang, G.-P., Wang, Y.-J., & Gao, X.-C. (2004). Photochemical degradation of dimethyl phthalate by Fenton reagent. *Photochemistry and Photobiology A: Chemistry*, 161, 215-220.
- Zhong, Y., Liang, X., He, Z., Tan, W., Zhu, J., Yuan, P., . . . He, H. (2014). The constraints of transition metal substitutions (Ti, Cr, Mn, Co and Ni) in magnetite on its catalytic activity in heterogeneous Fenton and UV/Fenton reaction: From the perspective of hydroxyl radical generation. *Applied Catalysis B: Environmental*, 150-151(0), 612-618.
- Zhong, Y., Liang, X., Tan, W., Zhong, Y., He, H., Zhu, J., . . . Jiang, Z. (2013). A comparative study about the effects of isomorphous substitution of transition metals (Ti, Cr, Mn, Co and Ni) on the UV/Fenton catalytic activity of magnetite. *Journal of Molecular Catalysis A: Chemical*, 372(0), 29-34.
- Zhong, Y., Liang, X., Zhong, Y., Zhu, J., Zhu, S., Yuan, P., . . . Zhang, J. (2012). Heterogeneous UV/Fenton degradation of TBBPA catalyzed by titanomagnetite: Catalyst characterization, performance and degradation products. *Water Research*, 46(15), 4633-4644.
- Zhou, H., & Smith, D. W. (2002). Advanced technologies in water and wastewater treatment. *Environmental Engineering and Science*, 1(0), 247-264

## LIST OF APPENDIXES

### Appendix A: LIST OF PUBLICATIONS AND PAPERS PRESENTED

#### Academic articles

1. **Shima Rahim Pouran**, Abdul Aziz Abdul Raman, Wan Mohd Ashri Wan Daud, “Review on the application of modified iron oxides as heterogeneous catalysts in Fenton reactions”, *Journal of Cleaner Production*, Impact Factor: 3.84, 64 (2014), Pages 24-35.
2. **Shima Rahim Pouran**, Abdul Aziz Abdul Raman, Wan Mohd Ashri Wan Daud, “Review on the main advances in photo-Fenton oxidation system for recalcitrant wastewaters”, *Journal of Industrial and Engineering Chemistry*, Impact Factor: 3.51, 21 (2015), Pages 53-69.
3. **Shima Rahim Pouran**, Abdul Aziz Abdul Raman, Wan Mohd Ashri Wan Daud, Shahaboddin Shamsirband, “Estimation of the effect of catalyst physical characteristics on Fenton-like oxidation efficiency using adaptive neuro-fuzzy computing technique”, *Measurement*, Impact Factor: 1.48, 59 (2015), 314-328.
4. **Shima Rahim Pouran**, Abdul Aziz Abdul Raman, Wan Mohd Ashri Wan Daud, Zaidi Embong, “Niobium substituted magnetite as a strong heterogeneous Fenton catalyst for wastewater treatment”, *Applied Surface Science*, Impact Factor: 2.71, 351 (2015), 175-187.
5. **Shima Rahim Pouran**, Abdul Aziz Abdul Raman, Wan Mohd Ashri Wan Daud, Mohammad Saleh Shafeeyan, “Effects of niobium and molybdenum

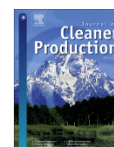
impregnation on adsorption capacity and Fenton catalytic activity of magnetite” *RSC Advances*, Impact Factor: 3.84, 5 (106), 87535-87549.

6. **Shima Rahim Pوران**, Abdul Aziz Abdul Raman, Wan Mohd Ashri Wan Daud, Mohammad Saleh Shafeeyan, “Ultrasound and UV Assisted Fenton Treatment of Recalcitrant Wastewaters using Transition Metal Substituted Magnetite Nanoparticles” *Chemosphere*, Impact Factor: 3.34, (2016), Under review.
7. B.H. Diya’uddeen, **Shima Rahim Pوران**, Abdul Aziz Abdul Raman, S.M. Nashwan, Wan Mohd Ashri Wan Daud, M.G. Shaaban, “Hybrid of Fenton and sequencing batch reactor for petroleum refinery wastewater treatment”, *Journal of Industrial and Engineering Chemistry*, Impact Factor: 3.51, 25 (2015), 186-191.
8. B.H. Diya’uddeen, **Shima Rahim Pوران**, Abdul Aziz Abdul Raman, Wan Mohd Ashri Wan Daud, “Fenton oxidative treatment of petroleum refinery wastewater: process optimization and sludge characterization”, *RSC Advances*, Impact Factor: 3.84, 5 (2015), 68159-68168.

## Conference Proceeding

1. Shima Rahim Pouran, Abdul Aziz Abdul Raman, Wan Mohd Ashri Wan Daud, “Review on Biodegradability enhancement of refractory effluents using photo-Fenton oxidation system”, International conference on civil engineering, Tabriz/Iran, 2013.
2. Shima Rahim Pouran, Abdul Aziz Abdul Raman, Wan Mohd Ashri Wan Daud, “Methylene blue decolorization using homogeneous and heterogeneous Fenton oxidation systems: a comparative study”, fifth International Conference on Environment, Penang/Malaysia, 2015.

University of Malaya



## Review

## Review on the application of modified iron oxides as heterogeneous catalysts in Fenton reactions

Shima Rahim Pouran<sup>1</sup>, Abdul Aziz Abdul Raman\*, Wan Mohd Ashri Wan Daud<sup>2</sup>

Chemical Engineering Department, Faculty of Engineering, University of Malaya, 50603 Kuala Lumpur, Malaysia

## ARTICLE INFO

## Article history:

Received 6 March 2013  
 Received in revised form  
 31 August 2013  
 Accepted 10 September 2013  
 Available online 18 September 2013

## Keywords:

Heterogeneous catalyst  
 Transition metal substituted iron oxide  
 Redox pairs  
 Oxygen vacancies

## ABSTRACT

Heterogeneous Fenton reaction is an advanced oxidation process which has gained wide spread acceptance for higher removal efficiency of recalcitrant organic contaminants under wide range of pH compared to homogeneous reactions. Conventionally, iron oxides are used as heterogeneous catalysts for Fenton oxidation system because of their abundance, easy separation and lower cost. This paper reviews the substitution of iron in an iron oxide with other transition metals as a mean to improve the properties of the iron oxide towards higher performance for contaminant degradation. Several studies have reported enhanced performance resulted from this substitution based on two possible mechanisms. First is the conjugation of redox pairs of iron species and imported active ion in hydroxyl radical production cycle. Second: the generation of oxygen vacancies as active sites on the surface of catalyst via adjustments for unequal charge substitutions. This class of catalysts is anticipated to work effectively for treatment of various recalcitrant wastewaters using Fenton oxidation system. Subsequently, the stability of the produced catalyst needs to be examined under various experimental conditions to prevent the adverse effects of transition metals on the receiving environment.

© 2013 Elsevier Ltd. All rights reserved.

## 1. Introduction

Water pollution abatement and treatment of wastewaters carrying recalcitrant contaminants have been major issues for decades. Recalcitrant compounds are generally of high molecular weight and hydrophobic in nature. It poses high resistance to microbiological degradation (Alexander, 1975) and may not be degraded readily by biological treatment methods. Large number of pharmaceutical and agrochemical compounds are recalcitrant. Discharge of these recalcitrant compounds to the environment even in small quantities may eventually lead to accumulate in ecosystem (Knapp and Bromley-Challoner, 2003). Many of recalcitrant compounds are

capable to directly or indirectly affect living organisms including human being. Some examples are revelation of antibiotic-resistant bacteria (Walter and Vennes, 1985), interfering the human endocrine system (Bredhult et al., 2007) and oxidative stress on fish (Laville et al., 2004). To prevent their adverse effects, the attempt should encompass minimisation of recalcitrant wastewaters from industries (Klemeš et al., 2012) as well as enhancement in treatment technologies such as advanced oxidation processes (AOPs). AOPs have been applied for degradation and mineralisation of organic pollutants such as phenolic compounds (Babuponnusami and Muthukumar, 2011; Ortiz de la Plata et al., 2010), pharmaceuticals (Valcárcel et al., 2012), agrochemicals (Silva et al., 2012) landfill leachate (Rocha et al., 2011) and also for feasible and enhanced treatment of decentralised wastewaters (Chong et al., 2012). These processes were found to be environmentally sustainable if the process energy consumption was low (Chatzisymeon et al., 2013). Fenton process is a strong oxidation system amongst advanced oxidation processes and has been successfully put into use for removal of recalcitrant organic contaminants (Ortiz de la Plata et al., 2010; Rocha et al., 2011). This process is known as the reaction between hydrogen peroxide as an oxidant and iron ions as a catalyst to produce highly active species, mainly non-selective \*OH radicals with oxidation potential of 2.8 V (Haber and Weiss, 1934), as shown in Equations (1) and (2) (Pignatello et al., 2006):

*Abbreviations:* AOPs, advanced oxidation processes; AV\*, anion vacancies; BET, Brunauer-Emmett-Teller; C, Carbon; CA, chelating agents; CMCD, carboxymethyl-β-cyclodextrin; DMP, dimethyl phthalate; EDTA, Ethylene diamine tetraacetic acid; MB, methylene blue; MIMS, membrane introduction mass spectrometry; \*OH, hydroxyl radical; PCP, pentachlorophenol; SSA, surface area per unit mass;  $t_{1/2}$ , half-lives; T, tesla; TMSIO, transition metal substituted iron oxide; TNT, 2,4,6-trinitrotoluene; TOC, Total organic carbon; UV-Vis, Ultraviolet-visible light region.

\* Corresponding author. Tel.: +60 3 79675313, +60 3 79675300; fax: +60 3 79675319

*E-mail addresses:* [rahimpouran@yahoo.com](mailto:rahimpouran@yahoo.com) (S. Rahim Pouran), [rsnazrin@gmail.com](mailto:rsnazrin@gmail.com), [azizraman@um.edu.my](mailto:azizraman@um.edu.my) (A.A. Abdul Raman), [ashri@um.edu.my](mailto:ashri@um.edu.my) (W.M.A. Wan Daud).

<sup>1</sup> Tel.: +60 3 796 75206; fax: +60 3 796 75319.

<sup>2</sup> Tel.: +60 3 79675297; fax: +60 3 79675319.

0959-6526/\$ – see front matter © 2013 Elsevier Ltd. All rights reserved.  
<http://dx.doi.org/10.1016/j.jclepro.2013.09.013>



ELSEVIER

Contents lists available at ScienceDirect

Journal of Industrial and Engineering Chemistry

journal homepage: [www.elsevier.com/locate/jiec](http://www.elsevier.com/locate/jiec)

## Review

## Review on the main advances in photo-Fenton oxidation system for recalcitrant wastewaters

Shima Rahim Pouran<sup>1</sup>, A.R. Abdul Aziz\*, Wan Mohd Ashri Wan Daud<sup>2</sup>

Chemical Engineering Department, Faculty of Engineering, University of Malaya, 50603 Kuala Lumpur, Malaysia

## ARTICLE INFO

## Article history:

Received 10 February 2014  
 Received in revised form 5 May 2014  
 Accepted 5 May 2014  
 Available online 12 May 2014

## Keywords:

Biodegradability enhancement  
 Chelating agents  
 Modified Fenton  
 Non-biodegradable wastewater

## ABSTRACT

This paper reviews the main advances in photo-Fenton oxidation treatment for recalcitrant wastewaters. This oxidation method is able to produce biodegradable intermediates and mineralize such pollutants effectively when the main operational conditions are at optimum level. However, cost of the process is one of the main limitations. Several strategies have been put in practice to minimize cost and improve photo-Fenton efficiency primarily through application of heterogeneous catalysts and/or chelating agents. In addition, cost can be further reduced by applying solar energy and integrating biological treatment technologies in the treatment process.

© 2014 The Korean Society of Industrial and Engineering Chemistry. Published by Elsevier B.V. All rights reserved.

## Contents

1. Introduction	53
2. Fenton-based reactions	54
3. Homogeneous vs. Heterogeneous systems	56
4. Application to recalcitrant streams	57
4.1. Pharmaceuticals	57
4.2. Agrochemicals	58
4.3. Petroleum refinery plants	59
4.4. Leachate from landfills	60
5. Effects of main operational conditions	61
5.1. Probe molecule	61
5.2. Fenton reagents	62
5.3. pH	63
5.4. Temperature	63
5.5. Other factors	63
5.5.1. Composition of reaction medium	63
5.5.2. Chelating agents	64
6. Cost evaluation	65
7. Conclusion	66
Acknowledgements	66
References	67

\* Corresponding author. Tel.: +60 3 79675300; fax: +60 3 79675319.

E-mail addresses: [rahimpooran@yahoo.com](mailto:rahimpooran@yahoo.com) (S. Rahim Pouran), [azizraman@um.edu.my](mailto:azizraman@um.edu.my), [rshazrin@gmail.com](mailto:rshazrin@gmail.com) (A.R. Abdul Aziz), [ashri@um.edu.my](mailto:ashri@um.edu.my) (W.M.A. Wan Daud).

<sup>1</sup> Tel.: +60 3 796 75206; fax: +60 3 796 75319.

<sup>2</sup> Tel.: +60 3 79675297; fax: +60 3 79675319.

<http://dx.doi.org/10.1016/j.jiec.2014.05.005>

1226-086X/© 2014 The Korean Society of Industrial and Engineering Chemistry. Published by Elsevier B.V. All rights reserved.

## 1. Introduction

The rapid global economic growth has resulted in clean water crisis and environmental pollution since industrial revolution. Literature indicate an increasing trend in generation of wastewaters with recalcitrant characteristics from the many activities of



## Estimation of the effect of catalyst physical characteristics on Fenton-like oxidation efficiency using adaptive neuro-fuzzy computing technique



Shima Rahim Pouran<sup>a</sup>, A.R. Abdul Aziz<sup>a,\*</sup>, Wan Mohd Ashri Wan Daud<sup>a</sup>, Shahaboddin Shamshirband<sup>b,c,\*</sup>

<sup>a</sup> Chemical Engineering Department, Faculty of Engineering, University of Malaya, 50603 Kuala Lumpur, Malaysia

<sup>b</sup> Department of Computer System and Technology, Faculty of Computer Science and Information Technology, University of Malaya, 50603 Kuala Lumpur, Malaysia

<sup>c</sup> Department of Computer Science, Chalous Branch, Islamic Azad University (IAU), 46615-397 Chalous, Iran

### ARTICLE INFO

#### Article history:

Received 10 August 2014

Received in revised form 11 September 2014

Accepted 19 September 2014

Available online 28 September 2014

#### Keywords:

Adaptive neuro-fuzzy system (ANFIS)

Adsorption capacity

Central composite design

Heterogeneous Fenton treatment

### ABSTRACT

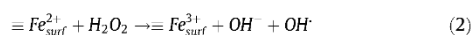
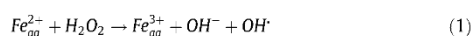
Catalyst size, which determines surface area, is one of the major factors in catalytic performance. In this study, response surface methodology (RSM) and an adaptive neuro-fuzzy inference system (ANFIS) were applied to quantify the effects of physical characteristics of magnetite on Fenton-like oxidation efficiency of methylene blue. For this purpose, two magnetite samples (M and N) were used and characterized by XRD, BET surface area, particle size analyzer and FE-SEM. Central composite design (CCD) was applied to design the experiments, develop regression models, optimize and evaluate the individual and interactive effects of five independent variables: H<sub>2</sub>O<sub>2</sub> and catalyst concentrations, pH, reaction time (numeric factors) and the type of catalyst (categorical factor). For each categorical factor, three quadratic models were developed regarding target responses: decolorization (Y<sub>MB</sub>), COD (Y<sub>COD</sub>) and TOC (Y<sub>TOC</sub>) removal efficiencies (%). The quadratic models were estimated by CCD and ANFIS methodologies. ANFIS was implemented using Matlab/Simulink and the performances were investigated. ANFIS models performed better for catalyst N compared to catalyst M, for color, COD and TOC separately. On contrary, it performed better for catalyst M compared to catalyst N, for combinations of color, COD and TOC. The obtained RMSE and R<sup>2</sup> for the ANFIS networks show the effectiveness of catalyst N compared to catalyst M in Fenton oxidation process.

© 2014 Elsevier Ltd. All rights reserved.

### 1. Introduction

Fenton oxidation process is an effective advanced treatment technology for degradation of a wide range of organic contaminants [6,26]. In this process, the reaction between

H<sub>2</sub>O<sub>2</sub> and Fe<sup>2+</sup> ions in an acidic solution produces highly oxidative species, mainly hydroxyl radicals, based on Eq. (1) [17]:



This oxidation system is highly efficient in terms of organic contaminant removal with relatively less operational cost and under ambient conditions of temperature and pressure [13]. However, in homogeneous Fenton

\* Corresponding authors. Tel.: +60 03 79675300 (office) (A.R. Abdul Aziz). Address: Department of Computer System and Technology, Faculty of Computer Science and Information Technology, University of Malaya, 50603 Kuala Lumpur, Malaysia. Tel.: +60 146266763 (S. Shamshirband).

E-mail addresses: [azizraman@um.edu.my](mailto:azizraman@um.edu.my) (A.R. Abdul Aziz), [shamshirband@um.edu.my](mailto:shamshirband@um.edu.my) (S. Shamshirband).

<http://dx.doi.org/10.1016/j.measurement.2014.09.060>  
0263-2241/© 2014 Elsevier Ltd. All rights reserved.



ELSEVIER

Contents lists available at ScienceDirect

Applied Surface Science

journal homepage: [www.elsevier.com/locate/apsusc](http://www.elsevier.com/locate/apsusc)

## Niobium substituted magnetite as a strong heterogeneous Fenton catalyst for wastewater treatment



Shima Rahim Pouran<sup>a,1</sup>, A.R. Abdul Aziz<sup>a,\*</sup>, Wan Mohd Ashri Wan Daud<sup>a,2</sup>,  
Zaidi Embong<sup>b,3</sup>

<sup>a</sup> Chemical Engineering Department, Faculty of Engineering, University of Malaya, 50603 Kuala Lumpur, Malaysia

<sup>b</sup> Faculty of Science, Technology and Human Development, University Tun Hussein Onn Malaysia, 86400 Johor, Malaysia

### ARTICLE INFO

#### Article history:

Received 11 March 2015  
Received in revised form 14 May 2015  
Accepted 21 May 2015  
Available online 29 May 2015

#### Keywords:

Fenton-like reaction  
Heterogeneous catalyst  
Mineralization  
Transition metal substituted magnetite

### ABSTRACT

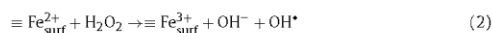
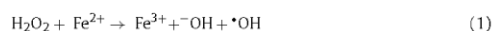
In this study, a series of Nb substituted magnetites;  $\text{Fe}_{3-x}\text{Nb}_x\text{O}_4$  ( $x = 0.0, 0.022, 0.049, 0.099, \text{ and } 0.19$ ) were prepared and characterized by XRD, BET surface area, TEM, VSM, XPS, and chemical experiments. The magnetite inverse spinel structure and magnetic property were maintained in all the synthesized samples. A significant decrease in crystal size ( $\approx$ two times) and increase in specific surface area ( $\approx$ three times) were observed with increased Nb content, resulting in higher adsorption capacity of the samples. In addition, the reactivity of the synthesized samples was examined through degradation of methylene blue solution using Fenton-like reaction. It was found that the incorporation of niobium significantly improved the degradation of methylene blue of which total MB removal was achieved within 180 min at higher molar ratios of Nb ( $x = 0.19$ ). This could be attributed to the generated oxygen vacancies on the surface of catalysts, the contribution of the introduced Nb cations in Fenton oxidation cycle for regeneration of  $\text{Fe}^{2+}$  cations, and increase in adsorption capacity of the samples due to larger surface area. The MB degradation through  $\text{Fe}_{2.79}\text{Nb}_{0.19}\text{O}_4/\text{H}_2\text{O}_2$  system was well described by the pseudo-first-order equation in kinetics. All samples showed good stability under the studied pH conditions. The amount of niobium leached was not detectable in neutral and basic solutions and the samples could be reused in oxidation process for several times without a significant decrease in their catalytic efficiency. The results proved that incorporation of niobium into magnetite significantly improved the characteristics and effectiveness of the heterogeneous catalyst for Fenton treatment of recalcitrant effluents.

© 2015 Elsevier B.V. All rights reserved.

### 1. Introduction

Fenton oxidation process is a potent catalytic reaction used for environmental remediation. In this iron catalyzed Haber–Weiss reaction, hydroxyl radicals ( $\cdot\text{OH}$ ) are generated in situ through decomposition of hydrogen peroxide (Eq. 1). Hydroxyl radicals are highly active ( $E_{\text{ox}} = 2.8 \text{ V}$ ) and capable to destroying almost all organic pollutants unselectively. Recently, the homogeneous ferrous ion is replaced with heterogeneous iron compounds in Fenton oxidation (Eq. 2) mainly because of their easy separation, applicability for a wide range of pH, feasibility for repeated use and elimination of ferric hydroxide sludge [1]. This is specifically

reported for magnetite [ $(\text{Fe}^{3+})_{\lambda}(\text{Fe}^{2+}\text{Fe}^{3+})_{\text{oc}}\text{O}_4$ ] that has shown better performances due to presence of  $\text{Fe}^{2+}$  cations in its structure which is responsible for initiating  $\text{H}_2\text{O}_2$  activation in Fenton oxidation [2,3]. However, magnetite application in Fenton reaction in its pure form is restricted due to its lower oxidation rate compared to soluble iron in homogeneous Fenton reaction [4,5]. In this regard, recent studies have focused on various modifications in magnetite structure to improve the adsorption and degradation of organic pollutants through Fenton reaction [6]. Application of chelating agents [2,7], pillared clays, activated carbon, and alumina as support to increase the adsorption capacity of the magnetite [8,9] and introduction of other transition metal/metals into the magnetite structure [3,10] are number of examples, so far reported in literature. Amongst them, transition metal substituted magnetite has been introduced as a promising Fenton catalyst for treatment of recalcitrant wastewater.



\* Corresponding author. Tel.: +60 3 79675300; fax: +60 3 79675319.

E-mail addresses: [rahimpooran@yahoo.com](mailto:rahimpooran@yahoo.com) (S. Rahim Pouran), [azizraman@um.edu.my](mailto:azizraman@um.edu.my), [raja.shazrin@gmail.com](mailto:raja.shazrin@gmail.com) (A.R. Abdul Aziz), [ashri@um.edu.my](mailto:ashri@um.edu.my) (W.M.A. Wan Daud), [zembong@gmail.com](mailto:zembong@gmail.com) (Z. Embong).

<sup>1</sup> Tel.: +60 3 79675206; fax: +60 3 79675319.

<sup>2</sup> Tel.: +60 3 79675297; fax: +60 3 79675319.

<sup>3</sup> Tel.: +60 7 4537962; fax: +60 7 4536051.



Cite this: *RSC Adv.*, 2015, 5, 87535

## Effects of niobium and molybdenum impregnation on adsorption capacity and Fenton catalytic activity of magnetite†

Shima Rahim Pوران, A. R. Abdul Aziz,\* Wan Mohd Ashri Wan Daud and Mohammad Saleh Shafeeyan

In the present study, a number of modified magnetite samples were prepared by impregnating magnetite with Nb and Mo ( $\text{Fe}_{3-x-y}\text{Nb}_x\text{Mo}_y\text{O}_4$ ,  $x + y = 0.2$ ). The characteristics of the samples in terms of durability, crystalline phase, morphology, size, surface area and composition, and magnetic property were determined. Subsequently, the effect of Nb and Mo incorporation on adsorption capacity of magnetite and its activity in heterogeneous Fenton oxidation of methylene blue was investigated. The amount of MB adsorbed on the synthesized samples increased considerably, mainly due to the increase in their specific surface area. In addition, the presence of Nb and Mo significantly improved degradation of MB, especially at higher contents of Nb + Mo. About 90% of MB ( $100 \text{ mg L}^{-1}$ ) and 46% of TOC were removed under the studied conditions. MB adsorption and Fenton degradation using synthesized samples were well described by pseudo-second-order and pseudo-first-order equations in kinetics, respectively. The samples demonstrated good durability and insignificant loss of performance in three consecutive experiments. The obtained results verified that Nb and Mo co-incorporation could effectively improve magnetite properties towards higher adsorption and remarkable activity in heterogeneous Fenton process at neutral condition.

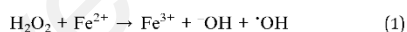
Received 5th August 2015  
Accepted 29th September 2015

DOI: 10.1039/c5ra15660b

www.rsc.org/advances

### 1. Introduction

Iron is the fourth most abundant element in the Earth's crust and is widely used. Besides numerous benefits, the demand for iron for environmental purification purposes, such as adsorbent or involved in degradation reactions, is in a rising trend. One of the commonly known treatment methods that utilize iron salts as the catalyst is the Fenton reaction, which produces highly oxidative species, *i.e.* hydroxyl radicals from  $\text{H}_2\text{O}_2$  decomposition (eqn (1)). This process offers several advantages over conventional methods, such as simple equipment, high removal efficiency within a short reaction time, and complete oxidation and mineralization of pollutants to innocuous byproducts under suitable operating conditions.<sup>1</sup>



Chemical Engineering Department, Faculty of Engineering, University of Malaya, 50603 Kuala Lumpur, Malaysia. E-mail: rahimpooran@yahoo.com; azizraman@um.edu.my; ashri@um.edu.my; ms.shafeeyan@gmail.com; Fax: +60 3 796 75319; Tel: +60 3 796 75206; +60 3 796 75300; +60 3 796 75297

† Electronic supplementary information (ESI) available. See DOI: 10.1039/c5ra15660b

Despite the fact that homogeneous Fenton oxidation is highly efficient in the treatment of recalcitrant effluents in acidic conditions, it encounters several limitations such as dependency on pH, sludge generation at non-acidic conditions and irrecoverable catalyst.<sup>2,3</sup> This has brought about the idea of the use of heterogeneous iron compounds in Fenton reaction (eqn (2)). The intrinsic convenience of iron minerals, such as natural prevalence, simple magnetic separation and low cost, makes them valuable candidates for this purpose. There have been extensive studies on application of iron minerals in Fenton treatment of polluted soil and water.<sup>4-7</sup> Iron oxides can operate at neutral pH without generation of ferric sludge and can be recovered and reused in Fenton reaction. However, several researchers have explored the lower reaction rate of iron oxide catalyzed Fenton when compared to homogeneous reaction.<sup>8,9</sup> Consequently, many of the recent researches have focused on modification of iron oxide's structure to improve their performances over several applications. The most reported studies in the literature for higher adsorption capacity of iron compounds deal with supported iron oxides on various materials such as silica,<sup>10,11</sup> activated carbon,<sup>12</sup> alumina<sup>13</sup> and clays.<sup>14,15</sup> With respect to catalytic activity in Fenton reaction, surface modification of iron oxides through treatment by  $\text{H}_2$  or  $\text{H}_2\text{O}_2$  (ref. 16 and 17) and incorporation of transition metals into iron oxides have recently been extensively reported in literature.<sup>18-20</sup>



## Hybrid of Fenton and sequencing batch reactor for petroleum refinery wastewater treatment



B.H. Diya'uddeen<sup>a,b,1</sup>, Shima Rahim Pouran<sup>b,2</sup>, A.R. Abdul Aziz<sup>b,\*</sup>, S.M. Nashwan<sup>c,3</sup>,  
Wan Mohd Ashri Wan Daud<sup>b,4</sup>, M.G. Shaaban<sup>c,5</sup>

<sup>a</sup> National Research Institute for Chemical Technology, PMB 1052 Zaria, Nigeria

<sup>b</sup> Department of Chemical Engineering, Faculty of Engineering, University of Malaya, Kuala Lumpur, Malaysia

<sup>c</sup> Department of Civil Engineering, Faculty of Engineering, University of Malaya, Kuala Lumpur, Malaysia

### ARTICLE INFO

#### Article history:

Received 17 June 2014

Received in revised form 15 October 2014

Accepted 18 October 2014

Available online 29 October 2014

#### Keywords:

Advanced oxidation process  
Biodegradability enhancement  
Hybrid system  
Zero-valent iron

### ABSTRACT

The treatment of high-strength petroleum refinery effluent (PRE) with  $[BOD_5]/[COD]_0 = 0.14$  was investigated using combined Fenton–sequencing batch reactor (SBR). The effect of  $[H_2O_2]:[COD]_0$  molar ratio on biodegradability enhancement was investigated. Fenton optimal conditions were:  $[H_2O_2]:[COD]_0$  of 6,  $[H_2O_2]:[Fe^{2+}]$  of 10 and  $pH = 3.0$  that could remove 76.5%, 45% and 96% of COD, TOC and phenol and increased biodegradability ratio to 0.37. The pretreated PRE subjected to SBR for one single cycle of 10 h. The results revealed the effectiveness of hybrid Fenton–SBR system in treating PRE where the complete treatment of the PRE was attained by this system.

© 2014 The Korean Society of Industrial and Engineering Chemistry. Published by Elsevier B.V. All rights reserved.

### Introduction

Petroleum refinery effluent (PRE) is a refractory wastewater consisting of complex aromatics, organic and inorganic constituents [1]. These wastewaters are generated in large volumes as a consequence of high water consumption during the refining process [2]. Based on the available figures of crude oil exploration for 2009 (84 million barrels per day (mbpd)), an estimated volume of 33.6 mbpd of PRE is generated globally [1]. PRE typically contains high concentrations of hazardous aromatic pollutants and aliphatic compounds which are similar to crude oil [3]. Phenolic compounds are of the main constituents of PRE that are considered as priority pollutants due to their high toxicity and harmful effects

on human health and the environment [1]. In face of recent strict global regulations and legislation on pollution control, the need for efficient water treatment technologies becomes paramount. There are abundant literature reports on treatment technologies of this category of wastewater, namely coagulation–flocculation [4–6], adsorption [7] and membrane [8,9]. However, these methods do not mineralize wastewaters but generate huge amount of sludge and require adsorbent regeneration. In addition, in the case of membrane technology, frequent fouling renders the method unattractive. In contrast to the enumerated conventional processes, biological systems appear suitable as they offer the merit of cost effective degradation of organic effluent. However, the robustness and effectiveness of biological treatment of PRE is retarded due to high and varied composition of organic loads [10]. Biological treatment partially degrades organic matter, generates sludge and requires longer reaction time [11]. The prolonged reaction time is associated with the degradation of recalcitrant aromatic component of PRE as longer oxidation time is required to destroy the aromatic ring due to the stability of the bonds [12]. These limitations of the biological systems in treating recalcitrant wastewaters have been a subject of discussion in a number of cited literature [1,13]. Accordingly, modification of several conventional biological systems has been reported and sequencing batch reactor (SBR) is a notable system among them. In this system, the wastewater treatment process is based on the principles of the activated sludge process and has been successfully employed in

\* Corresponding author. Postal address: Chemical Engineering Department, Faculty of Engineering, University of Malaya, 50603 Kuala Lumpur, Malaysia. Tel.: +60 3 79675313; fax: +60 3 79675300.

E-mail addresses: [diyauddeen.bh@narict.ng.org](mailto:diyauddeen.bh@narict.ng.org) (B.H. Diya'uddeen), [rahimpouran@yahoo.com](mailto:rahimpouran@yahoo.com) (S. Rahim Pouran), [azizraman@um.edu.my](mailto:azizraman@um.edu.my), [rshazrin@gmail.com](mailto:rshazrin@gmail.com) (A.R. Abdul Aziz), [nashwan\\_alhasso@yahoo.com](mailto:nashwan_alhasso@yahoo.com) (S.M. Nashwan), [ashri@um.edu.my](mailto:ashri@um.edu.my) (W.M.A. Wan Daud), [ghazaly@um.edu.my](mailto:ghazaly@um.edu.my) (M.G. Shaaban).

<sup>1</sup> Tel.: +234 8036517771; fax: +234 69334835.

<sup>2</sup> Tel.: +60 3 796 75206; fax: +60 3 796 75319.

<sup>3</sup> Tel.: +60 1 29356591; fax: +60 370675319.

<sup>4</sup> Tel.: +60 3 79675297; fax: +60 3 79675319.

<sup>5</sup> Tel.: +60 3 79675202; fax: +60 3 79555781.

<http://dx.doi.org/10.1016/j.jiec.2014.10.033>

1226-086X/© 2014 The Korean Society of Industrial and Engineering Chemistry. Published by Elsevier B.V. All rights reserved.

Cite this: *RSC Adv.*, 2015, 5, 68159

## Fenton oxidative treatment of petroleum refinery wastewater: process optimization and sludge characterization

B. H. Diya'uddeen,<sup>ab</sup> Shima Rahim Pouran,<sup>a</sup> A. R. Abdul Aziz<sup>\*a</sup> and W. M. A. W. Daud<sup>a</sup>

Sludge generation is one of the major concerns in Fenton treatment of recalcitrant wastewaters. In this work, mineralization (reduction of Dissolved Organic Carbon (DOC)) of petroleum refinery effluent (PRE) and the accompanying sludge generated in treating PRE was investigated. The mineralization level of 53% at optimum conditions produced 0.16 L of wet sludge per litre of wastewater. Further investigation of the sludge properties was conducted to assess the ease of handling and potential reuse of the sludge. For this purpose, sludge generated at studied conditions exceeding 30% DOC reduction were characterized by sludge volume index (SVI), sludge settling rates ( $V_s$ ) and volumes of settled sludge within the first 30 minutes (SSV<sub>30</sub>). High  $V_s$  ( $\approx 0.16$  cm s<sup>-1</sup>) and low SVI (<100 mL g<sup>-1</sup>) and SSV<sub>30</sub> (<50 min s<sup>-1</sup>) values indicated that the sludge has good settling and compaction properties. The results confirmed that the sludge generated could be managed systematically with appropriate operating conditions.

Received 2nd May 2015  
Accepted 4th August 2015

DOI: 10.1039/c5ra08079g

www.rsc.org/advances

### 1. Introduction

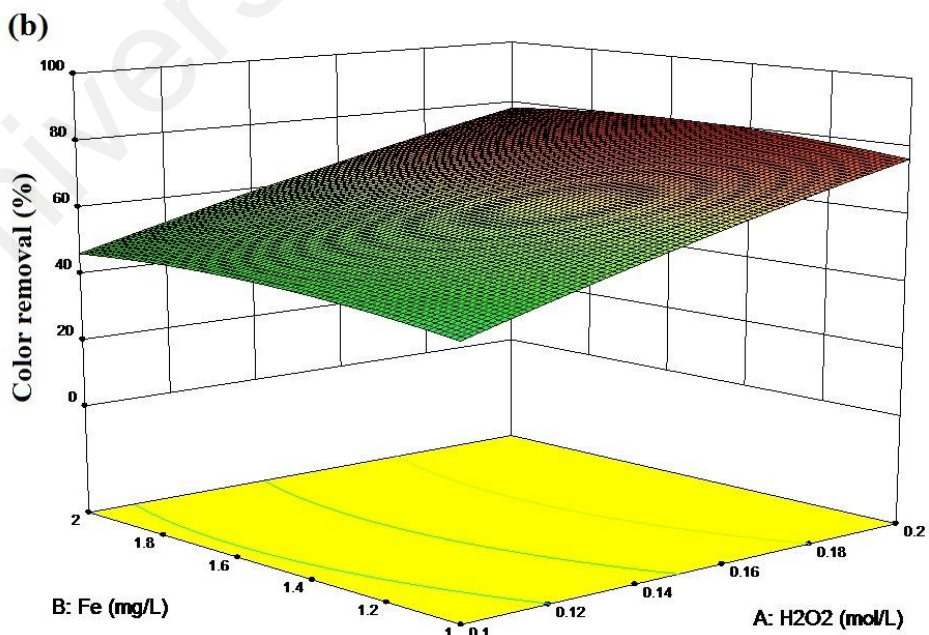
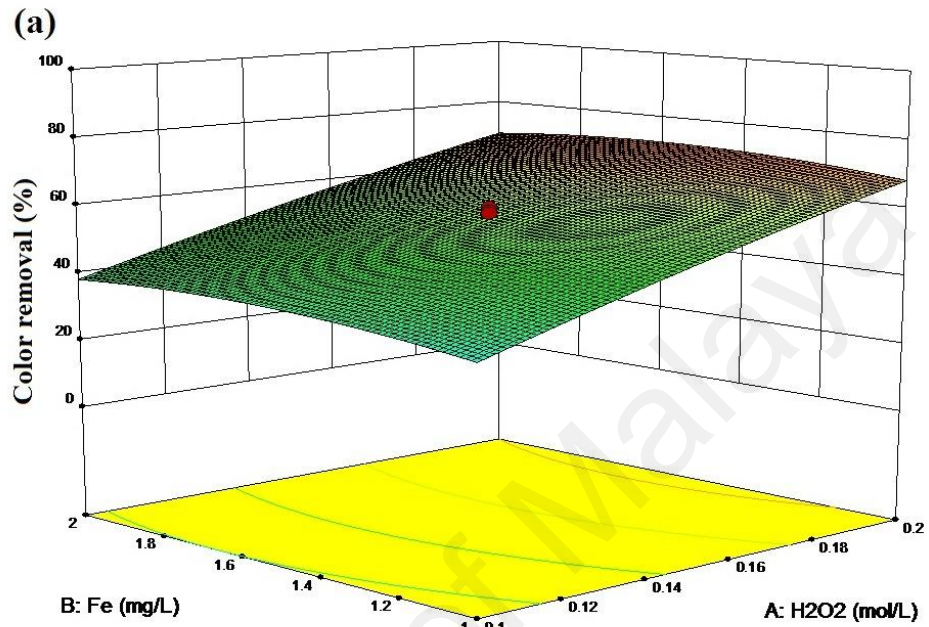
Petroleum refinery effluent (PRE) contains hundreds of various organic pollutants ranging from aliphatic to aromatic compounds. Many of these compounds resist microbial degradation and are not treatable biologically. This results in low biodegradability of this wastewater due to high Chemical Oxygen Demand (COD) and low Biochemical Oxygen Demand (BOD<sub>5</sub>).<sup>1-3</sup> Generally, the organic compounds present in PRE are carcinogenic which causes considerable damage to the ecosystem and human health.<sup>4,5</sup> Disposal of improperly treated PRE into water-bodies results in decreased algae productivity and depleted oxygen level in receiving water bodies which affect the food chain.<sup>6-8</sup> The environmental concern of these discharges is related to their large volume, high toxicity and lack of biodegradability.<sup>1,9</sup>

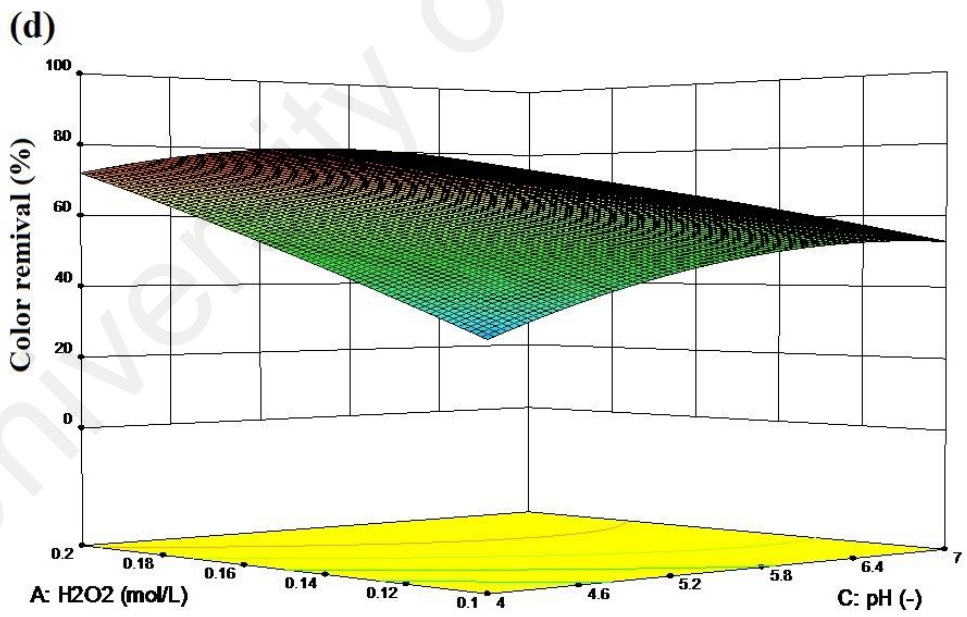
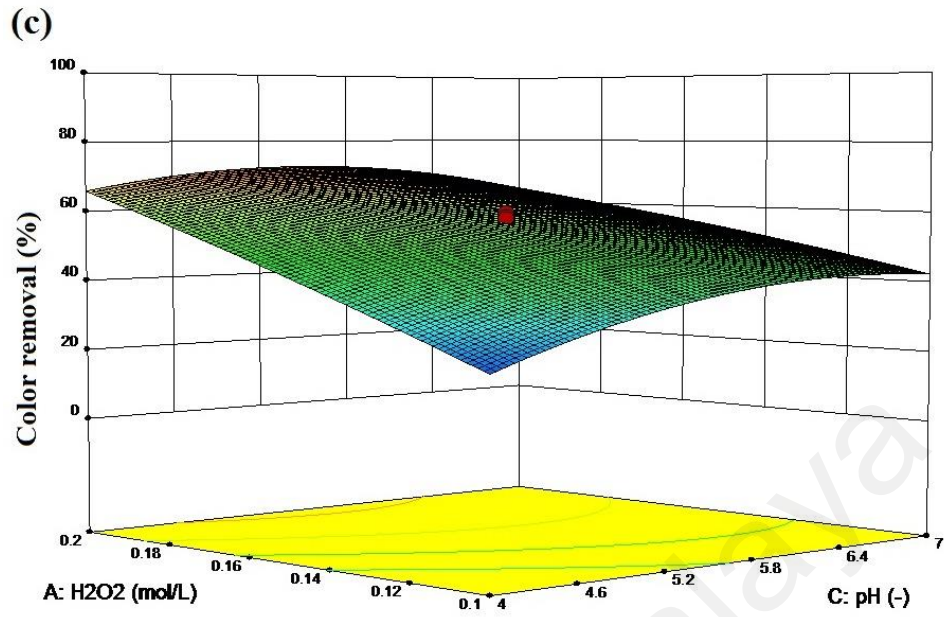
A critical review of the processes currently adopted for treatment of PRE shows that these methods are bedevilled with many problems.<sup>2</sup> The primary drawbacks that are associated with these treatment methods are (i) inability to mineralize contaminants;<sup>10</sup> (ii) phase transfer of contaminants from one medium to another; (iii) generation of a large amount of sludge; (iv) low treatment efficiencies and (v) slow reaction rates.<sup>11,12</sup> In

this regard, Fenton oxidation, an advanced oxidation process (AOPs), that generates highly aggressive hydroxyl radicals ( $\cdot\text{OH}$ ) through catalytic decomposition of hydrogen peroxide by iron species is expected to offer better treatment efficiencies. Literature is replete with the equations governing Fenton oxidation.<sup>13-15</sup> In this oxidation system: the reagents are easy to handle, the treatment process is relatively inexpensive, the reactors are simple and minimal control and operation are required.<sup>16,17</sup> A large number of studies have used this strong oxidative method for treatment of sludge<sup>18</sup> and various industrial wastewaters.<sup>13,19,20</sup> However, based on the articles that have been reviewed, literature on Fenton oxidative treatment of PRE is scarce.<sup>2</sup> Recently, our group has reported the feasibility of Fenton oxidative mineralisation of this wastewater, omitting the pre-treatment stage<sup>17</sup> and in another study, assessed the effectiveness Fenton process in treatment of PRE when combined with a sequencing batch reactor.<sup>21</sup> However, generation of ferric hydroxide sludge at pH above 4.0 is an environmental and economic issue associated with this process. Several strategies such as recycling as a coagulant, using in construction or industry or disposing through land filling<sup>22</sup> that have been used for sewage sludge management can be studied for this iron-containing sludge to address this matter. In addition, Fenton sludge can be used as a base material for goethite production<sup>23,24</sup> which is a potential heterogeneous catalyst for water purification.<sup>25</sup> Though, the characteristics of the generated sludge in terms of settling and compaction should be identified under the influence of initial carbon load of the wastewater and the amount of Fenton reagents utilized in the treatment system. Considering that a typical PRE is recalcitrant,

<sup>a</sup>Department of Chemical Engineering, Faculty of Engineering, University of Malaya, 50603 Kuala Lumpur, Malaysia. E-mail: rahimpooran@yahoo.com; azizranan@um.edu.my; ashri@um.edu.my; Fax: +60 3 796 75319, +60 3 796 7561, +60 3 79675300; Tel: +60 3 796 75206, +60 3 796-75233, +60 3 79675297, +60 3 79675313  
<sup>b</sup>National Research Institute for Chemical Technology, PMB 1052, Zaria, Nigeria. E-mail: diyauddeen.bh@narict.ng.org; Fax: +234 69334835; Tel: +234 8036517771

**Appendix B: The response surface plot of the (1) decolorization, (2) COD and (3) TOC removal efficiencies (%)**





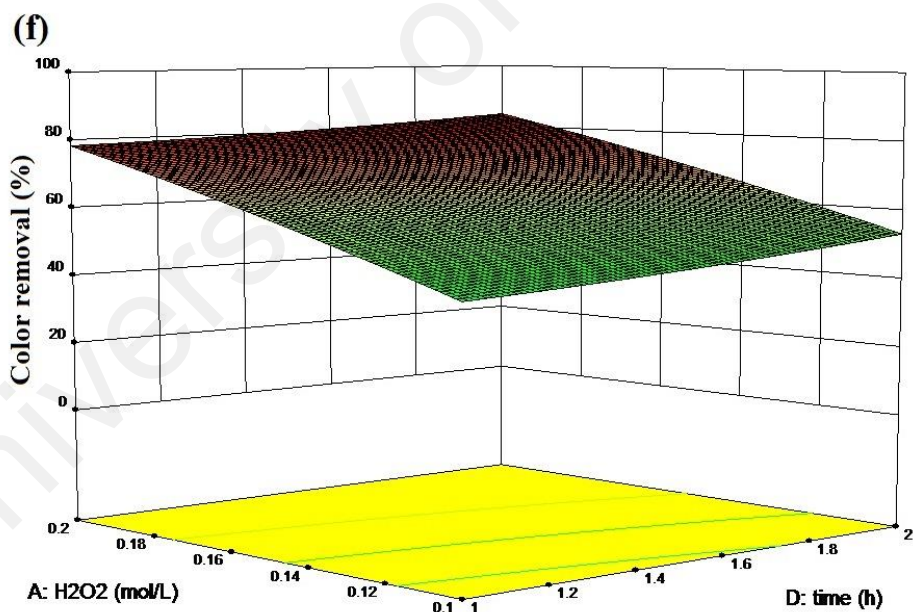
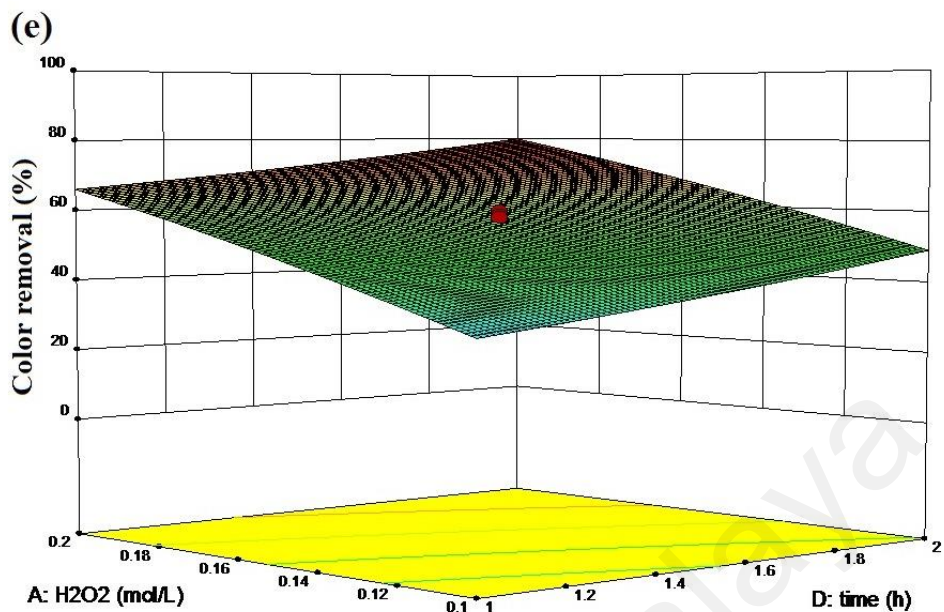
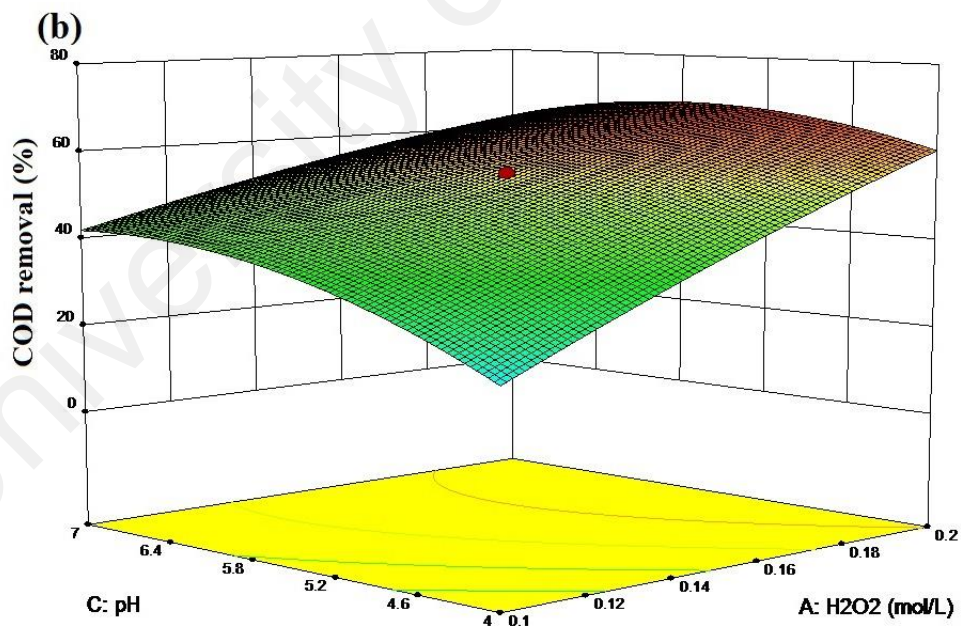
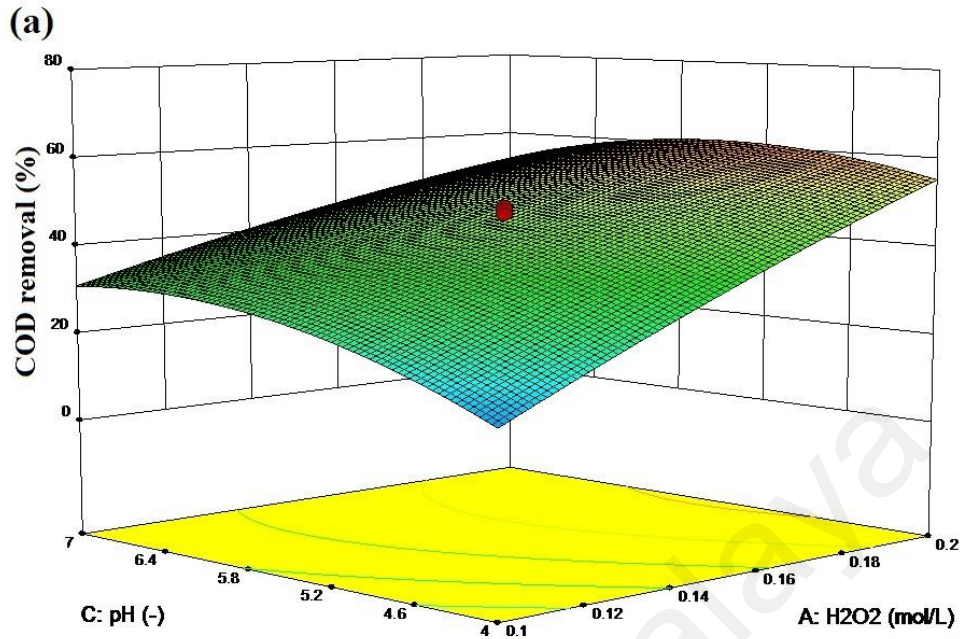
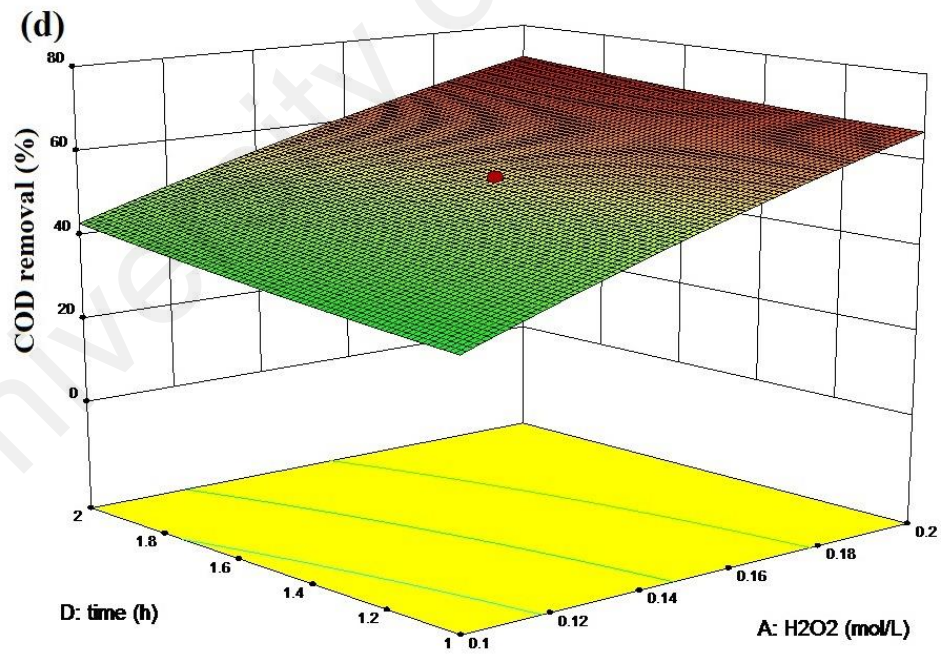
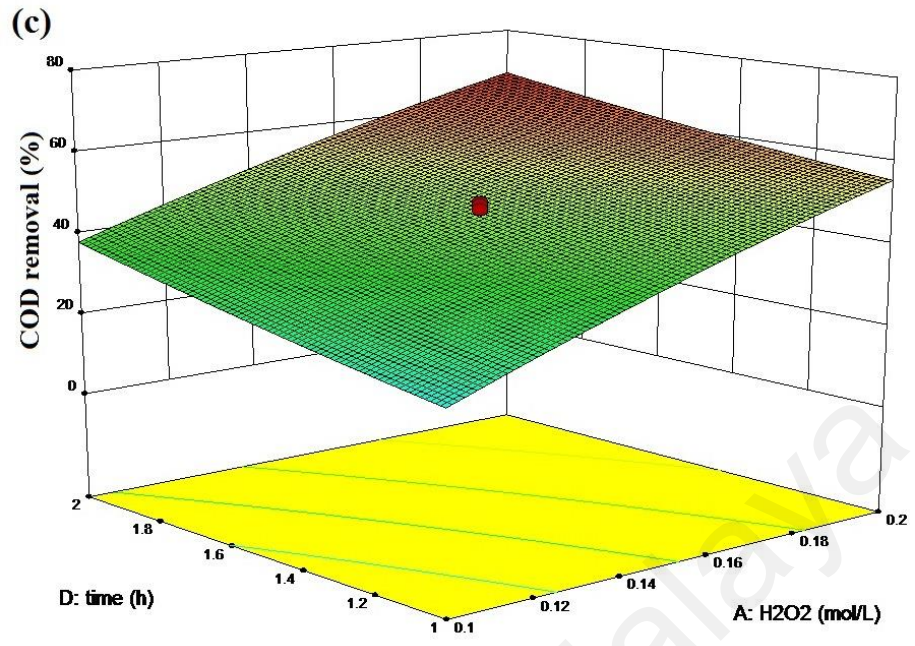


Figure A.B1: The response surface plot of the decolorization efficiency (%) as a function of AB, AC and AD effects for the magnetite sample (a)(c)(e) M and (b)(d)(f) N







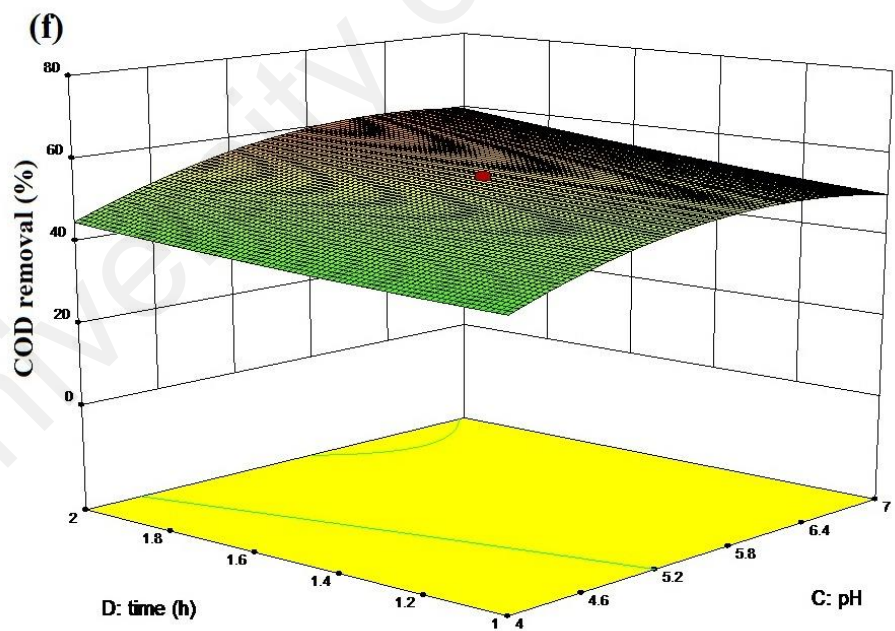
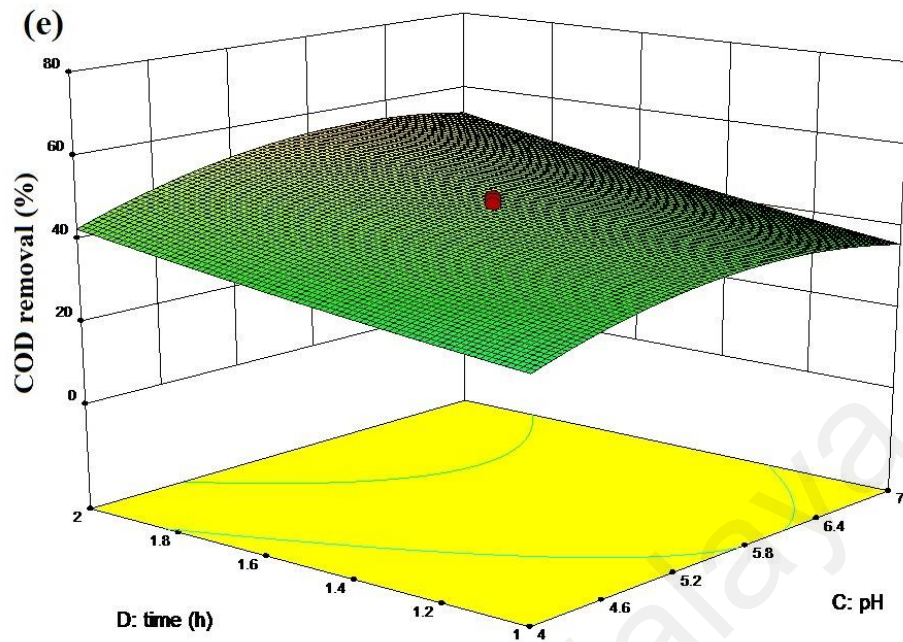
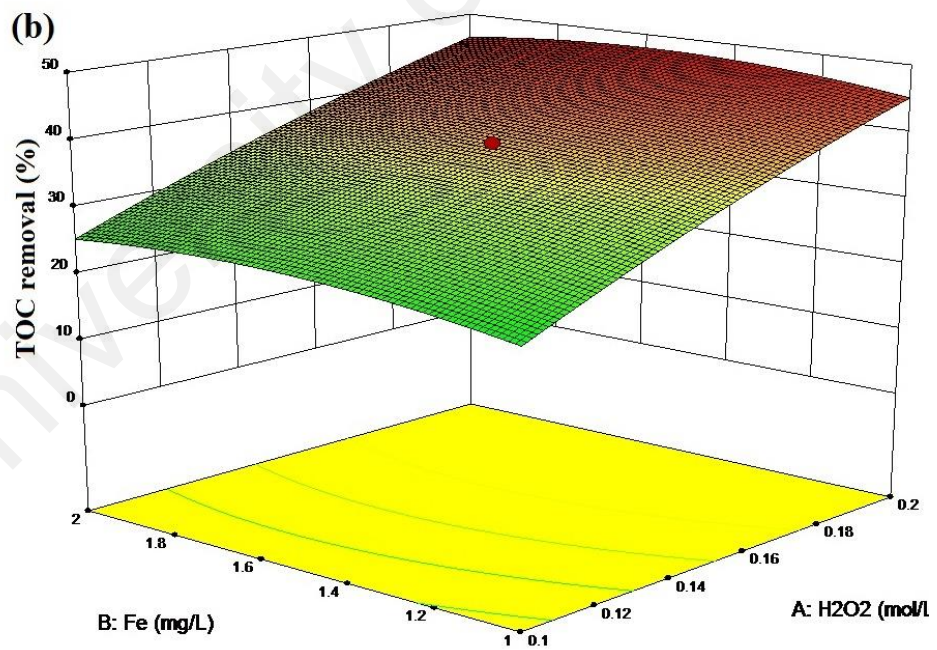
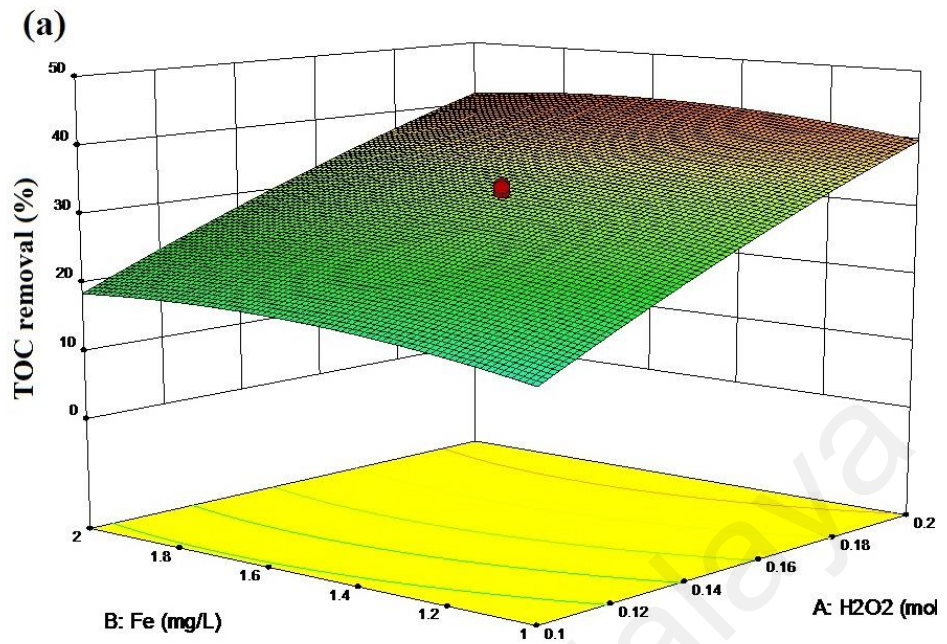
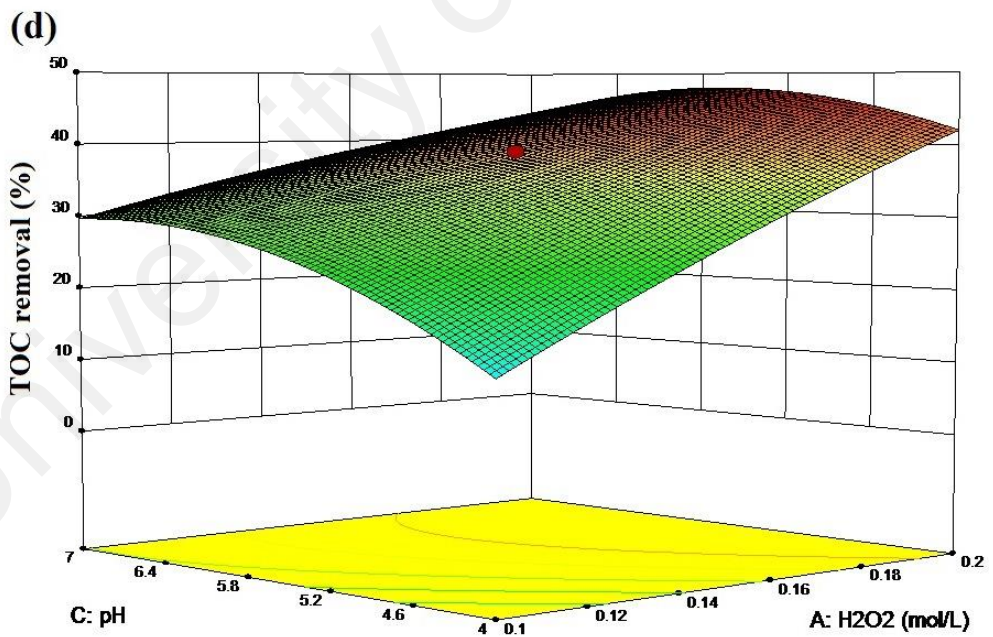
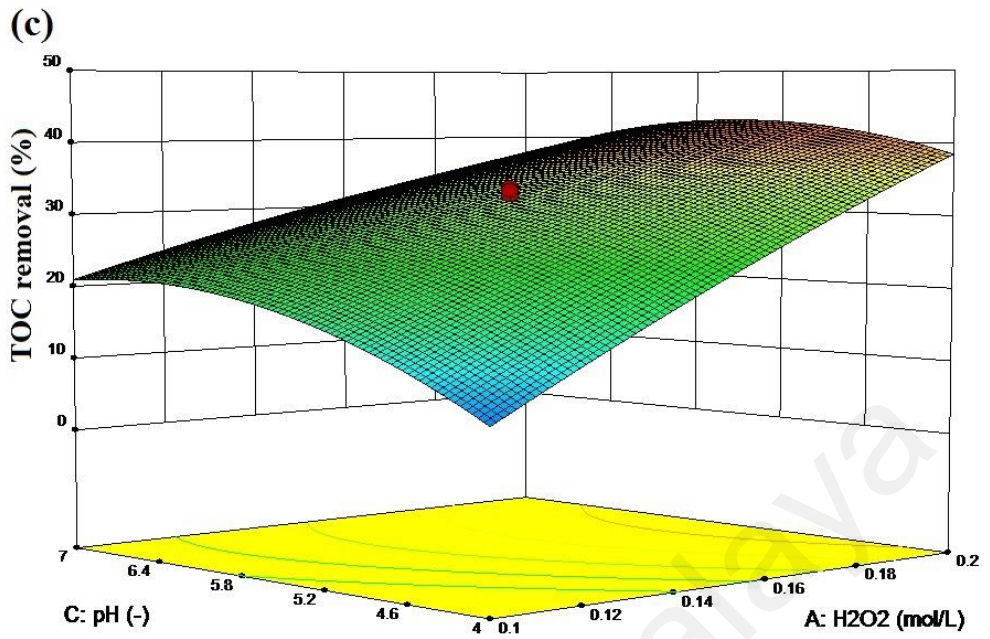


Figure A.B2: The response surface plot of COD removal efficiency (%) as a function of AC, AD and CD effects for the magnetite samples (a)(c) M and (b)(d) N





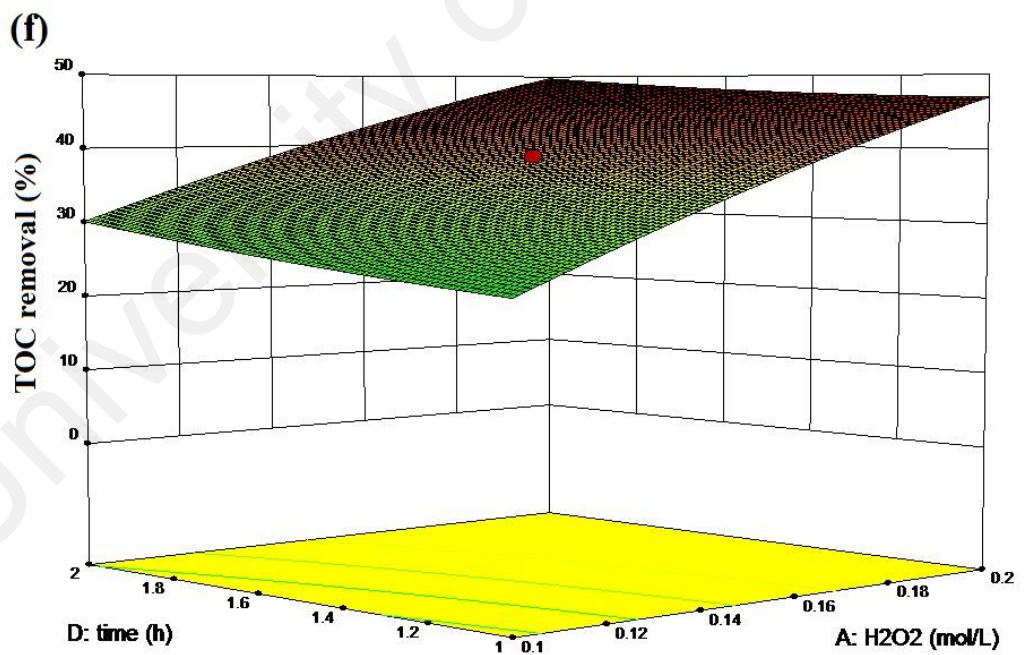
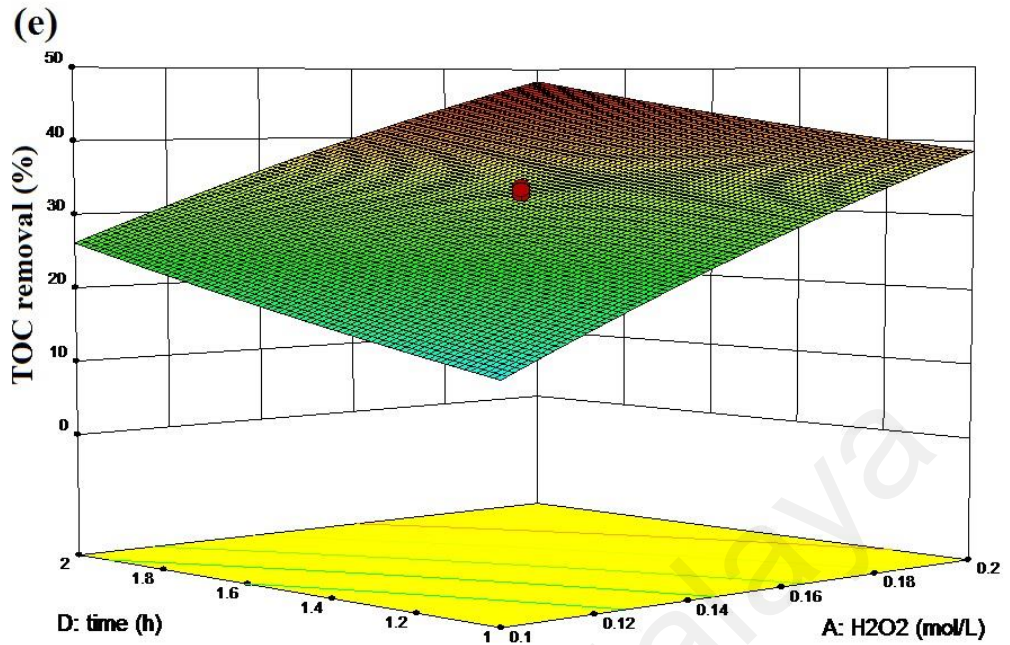
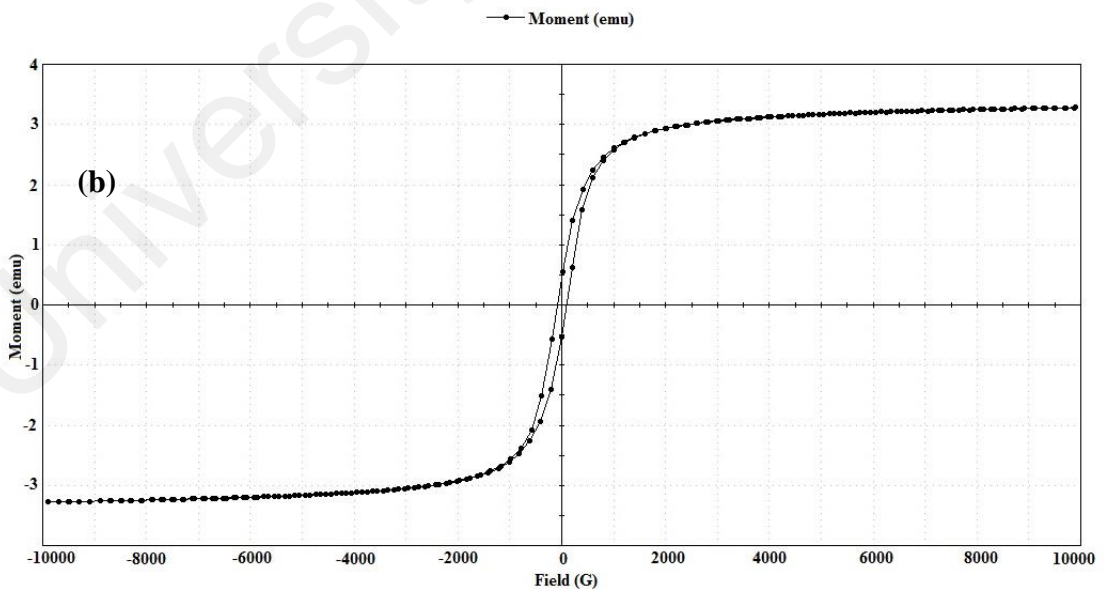
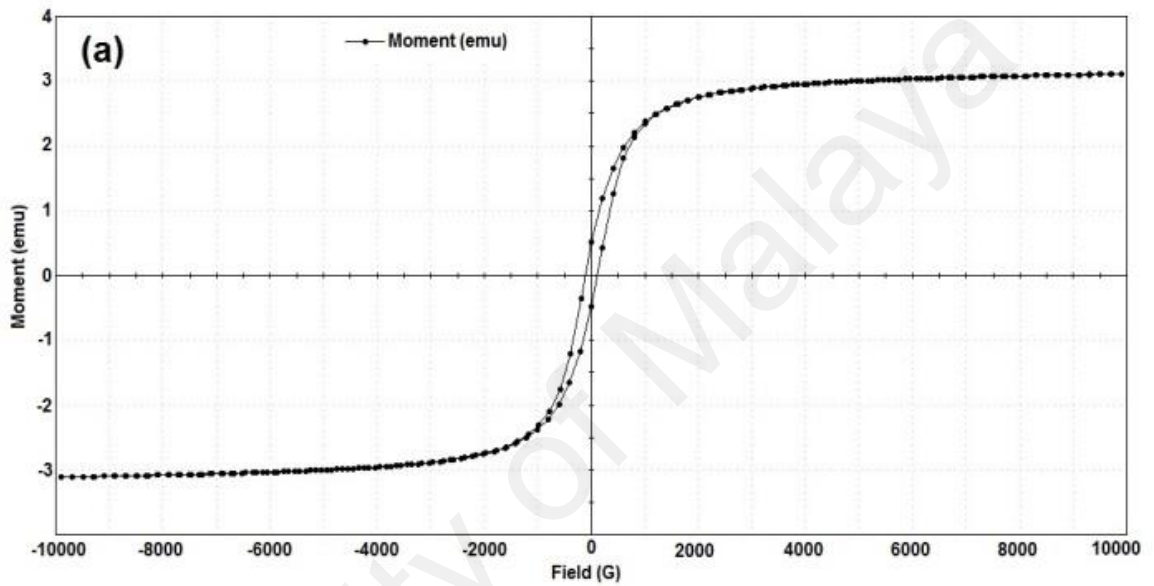
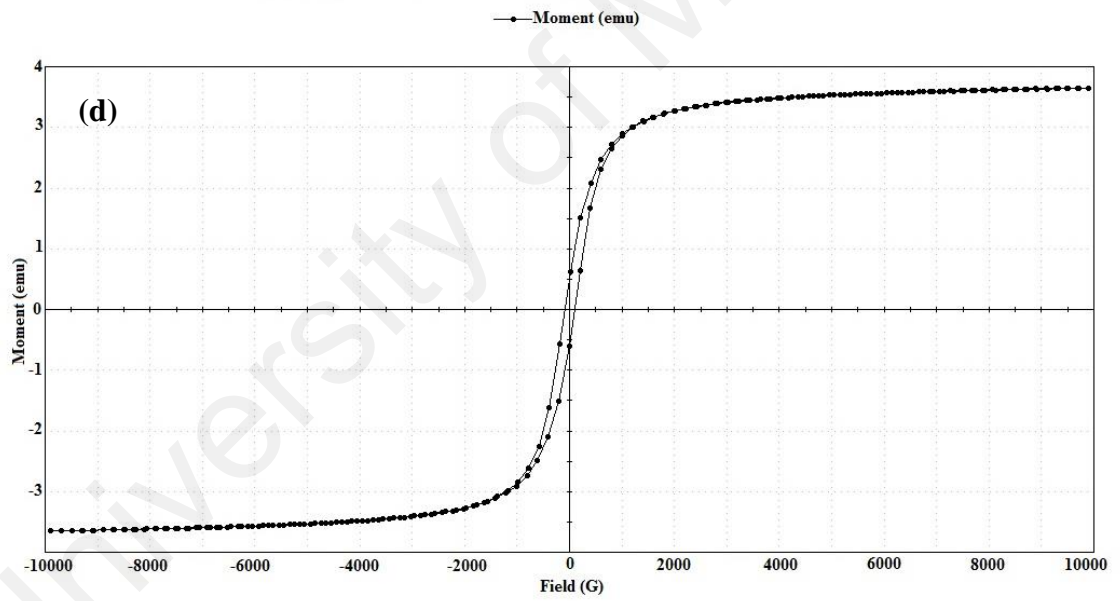
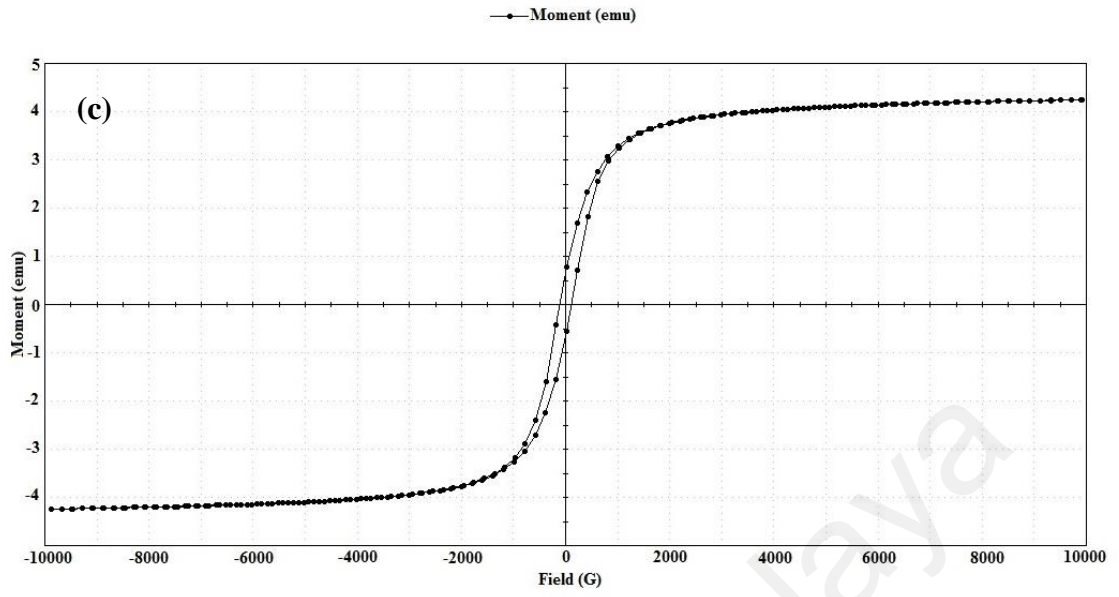


Figure A.B3: The response surface plot of TOC removal efficiency (%) as a function of AB, AC and AD effects for the magnetite samples (a)(c) M and (b)(d) N

### Appendix C: Hysteresis loops for $\text{Fe}_{3-x-y}\text{Nb}_x\text{Mo}_y\text{O}_4$ samples

- (a)  $\text{Fe}_3\text{O}_4$  (b)  $\text{Fe}_{2.79}\text{Nb}_{0.0249}\text{Mo}_{0.094}\text{O}_4$ , (c)  $\text{Fe}_{2.79}\text{Nb}_{0.049}\text{Mo}_{0.089}\text{O}_4$ , (d)  $\text{Fe}_{2.79}\text{Nb}_{0.099}\text{Mo}_{0.073}\text{O}_4$ , (e)  $\text{Fe}_{2.79}\text{Nb}_{0.149}\text{Mo}_{0.032}\text{O}_4$  and (f)  $\text{Fe}_{2.79}\text{Nb}_{0.171}\text{Mo}_{0.023}\text{O}_4$  samples





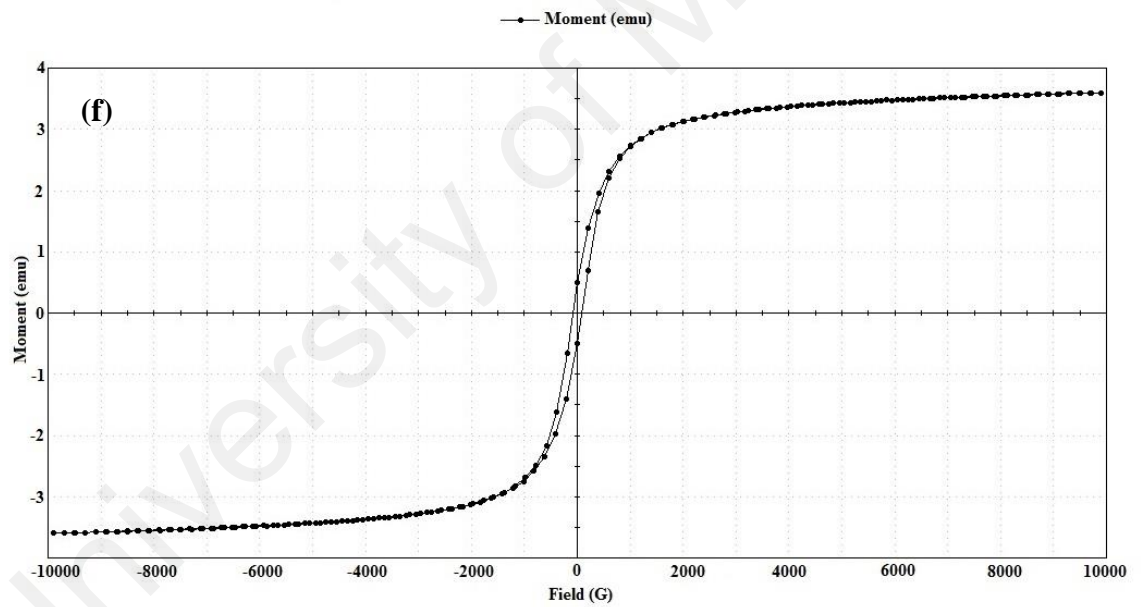
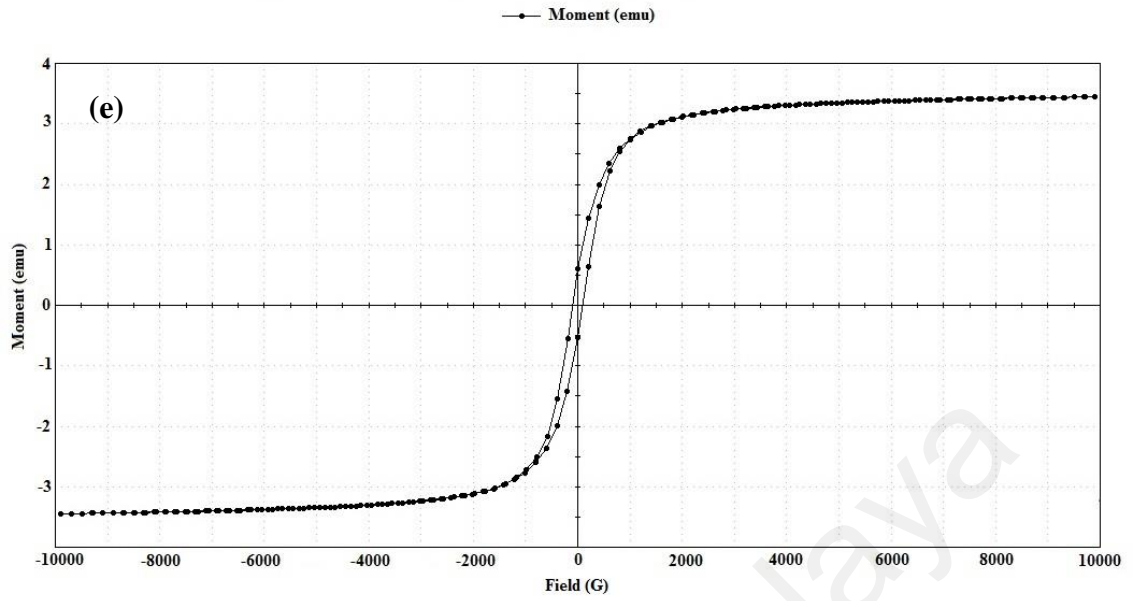


**Fig. A.C** Hysteresis loops for (a)  $\text{Fe}_3\text{O}_4$  (b)  $\text{Fe}_{2.79}\text{Nb}_{0.0249}\text{Mo}_{0.094}\text{O}_4$ , (c)  $\text{Fe}_{2.79}\text{Nb}_{0.049}\text{Mo}_{0.089}\text{O}_4$ , (d)  $\text{Fe}_{2.79}\text{Nb}_{0.099}\text{Mo}_{0.073}\text{O}_4$ , (e)  $\text{Fe}_{2.79}\text{Nb}_{0.149}\text{Mo}_{0.032}\text{O}_4$  and (f)  $\text{Fe}_{2.79}\text{Nb}_{0.171}\text{Mo}_{0.023}\text{O}_4$  samples